UNIVERSITY OF LONDON

LAMINAR FLOW ALONG CORNERS HAVING ARBITRARILY LARGE TRANSVERSE CURVATURE

by

ADIL HADI RIDHA

B.Sc. (Eng.)

A Thesis submitted for the Degree of Doctor of Philosophy in the Faculty of Engineering in the University of London

1978

Department of Mechanical Engineering

University College London

ABSTRACT

Theoretical and experimental studies of the behaviour of flows in streamwise corners have hitherto been confined to corners formed by intersecting planes (sharp corners). The new work presented here concerns situations where the region of intersection is replaced by a symmetrical surface of finite curvature which smoothly joins the planes (radiused corner). The curved surface is chosen to be invariant with respect to the streamwise coordinate and asymptotes to a flat plate within a distance from the symmetry plane of the same order as the boundary layer thickness. A new analytical formulation of the equations of motion is developed to handle the problem along such corners and is of considerable generality. It contains the sharp corner geometry as a special case and is applicable to corners of angles greater or less than 180^{o}.

Numerical solutions are obtained for corners of included angle from 45^{o} to 315^{o} and include results for sharp and radiused corners. The agreement between an existing exact solution for the 90^{o} sharp corner and the corresponding results given here is excellent. The only other solutions available for sharp corners of angles different from 90^{o} are inexact as is shown.

Results obtained from measurements of the flow along a rectangular radiused corner are given and when compared with the theoretical results show fair qualitative agreement although at any point within the boundary layer the experimental flow velocity is somewhat higher than predicted.

ACKNOWLEDGEMENTS

The author is indebted to Dr. W. H. Barclay, lecturer in the Department of Mechanical Engineering, University College London, who suggested the problem investigated in this text. His valuable discussions, sound constructive criticisms, and above all, his friendly attitude, patience and encouragement were of great help in making this work possible.

The assistance of the Departmental Workshop staff in the design and making of the corner model is gratefully appreciated.

The author wishes to express his thanks to the Iraqi Ministry of Oil without whose financial support this research would not have been concluded.

The help and encouragement extended to the author by his friends and colleagues made this work more interesting and enjoyable.

Finally, the author renders his sincere thanks to Ms Ketty Shoet for typing the thesis.

CONTENTS

NOTATION

Important symbols used in the text are given below. All symbols are defined where they first appear.

A, A'	constants
$\vec{A}$	a (dummy) vector
A^i	($i = 1,2,3$) contra-varient component of $\vec{A}$
$A(i)$	physical component of $\vec{A}$
A_n, B_n, C_n	see equations (2.41)
a, b	constants in the transformation of ξ^3 into ζ
B, B'	constants
C_r	wall curvature
$\bar{C}_r$	$= R_e^{-\frac{1}{2}} C_r$
c	$\cos \lambda$
c^*	$\cos \lambda^*$
D, D^*, E, E^* F^*, G	see equation (2.66)
d	diameter of hot-wire
d'	a length scale characterizing corner geometry, equation (4.5)
f	Blasius function, equation (2.45)
g_{ij}	metric tensors, equation (2.4)
$H(\eta)$	a function related to crossflow velocity w^*, equation (2.62d)
h	step-size in the finite difference formulation
h'	Coefficient of heat transfer
J	Jacobian of coordinate transformation, equation (2.5)
k	thermal conductivity

L, ℓ', ℓ	length scales
M	number of mesh planes in the ξ^3 direction in the finite difference formulation
m	exponent for the free stream variation, equation (2.16)
N	number of mesh planes in the ξ^2 direction
N_u	$= h' d/k$, Nusselt number
p	pressure, equation (2.17a)
p	pressure
$\bar{p}_0, \bar{p}_1, \bar{p}_2, \ldots$	coefficients of p in expansion of $R_e^{-\frac{1}{2}}$, equation (2.14)
R_ℓ	$= \ell U_\infty/\nu$
R_e	$= L U_\infty/\nu$, Reynolds number
R_x	$= U_\infty x^1/\nu$, local Reynolds number
R_{ex}	$= 2U_\infty x^1/\nu$, local Reynolds number
r_o, r	radius of curvature at symmetry plane
r'	radius of curvature
s	$\sin \lambda$
s^*	$\sin \lambda^*$
$\tilde{s}$	defined at p. 65
$\bar{s}$	$= d'/\ell'$, equation (4.6)
t	distance from symmetry plane in mm
U_∞	free-stream velocity in zero-pressure gradient
$U(\bar{x}^1)$	$= U_\infty \bar{x}^{1\,m}$
u, v, w	velocities in directions ξ^1, ξ^2, ξ^3
$\tilde{u}_o$	$U_\infty/10$
V	voltage across the hot-wire
V_o	voltage across the hot-wire in still air
v^1, v^2, v^3	contra-variant components of velocity vector
v_1, v_2, v_3	co-variant components of velocity vector

$v(1)$, $v(2)$, $v(3)$	physical components of velocity vector, equation (2.12)
v^*, w^*	crossflow velocities in rectangular cartesian coordinates
$\bar{v}^1$, $\bar{v}^2$, $\bar{v}^3$	non-dimensional velocities, equation (2.14)
$\bar{v}_2$, $\bar{v}_3$	non-dimensional variables, equations (2.14)
x^1, x^2, x^3	non-orthogonal curvilinear coordinates
$\bar{x}^1$, $\bar{x}^2$, $\bar{x}^3$	non-dimensional coordinates, equation (2.14)
y^1, y^2, y^3	rectangular cartesian coordinates
α , σ	quantities related to u, v and w
β	$\lim_{\xi^2 \to \infty} (\xi^2 f' - f)$
β_o	$= \beta \cos \lambda^*$
δ	two-dimensional boundary layer thickness
λ	defined at p. 40
λ^*	defined at p. 50
ϵ	constant
η	a dummy (boundary layer) coordinate
μ	viscosity
ν	kinematic viscosity
ρ	density
ξ^1, ξ^2, ξ^3	curvilinear coordinates, equation (2.17a)
φ , ψ	variables related to u, v, w, equation (2.17a)
ψ^*	$= \psi - c^* \xi^3 f'$
Ω	non-dimensional streamwise vorticity in the ξ^i (i = 1, 2, 3), coordinate system variables, equation (2.33)
θ	a quantity related to streamwise vorticity, equations (2.17a, c)
θ^*	$= \theta - \frac{1}{c^*} \xi^3 f''$
$\omega(1)$	physical component of the vorticity in direction x^1
Γ_{λ_c}	$= (\xi^1 R_\ell)^{-1}$, defined at p. 108

ζ transformed independent variable, equation (2.64)

ζ_{max} maximum value of ζ in the numerical scheme

ξ^2_{max} maximum value of ξ^2 in the numerical scheme

τ_{w_c} wall shear stress in the corner layer

τ_{w_∞} wall shear stress in the two-dimensional region

$$\kappa = \frac{\partial \lambda}{\partial \xi^3}$$

$$\Delta = \frac{\partial^2}{(\partial x^1)^2} + \frac{1}{\cos^2\lambda}\left[\frac{\partial^2}{(\partial x^2)^2} - 2\sin\lambda\,\frac{\partial^2}{\partial x^2 \partial x^3} + \frac{\partial^2}{(\partial x^3)^2} - \frac{C_\tau}{\cos\lambda}\frac{\partial}{\partial x^2} + C_\tau\frac{\sin\lambda}{\cos\lambda}\frac{\partial}{\partial x^3}\right]$$

$$\overline{\nabla}^2 = \frac{1}{\cos^2\lambda}\left[\frac{\partial^2}{(\partial \bar{x}^2)^2} - 2\sin\lambda\,\frac{\partial^2}{\partial \bar{x}^2 \partial \bar{x}^3} + \frac{\partial^2}{(\partial \bar{x}^3)^2} - \frac{\overline{C}_\tau}{\cos\lambda}\frac{\partial}{\partial \bar{x}^2} + \frac{\sin\lambda}{\cos\lambda}\overline{C}_\tau\frac{\partial}{\partial \bar{x}^3}\right]$$

$$\nabla^2 = \frac{1}{\cos\lambda}\left[\frac{\partial^2}{(\partial \xi^2)^2} - 2\sin\lambda\,\frac{\partial^2}{\partial \xi^2 \partial \xi^3} + \frac{\partial^2}{(\partial \xi^3)^2} - \frac{\kappa}{\cos\lambda}\frac{\partial}{\partial \xi^2} + \frac{\kappa\sin\lambda}{\cos\lambda}\frac{\partial}{\partial \xi^3}\right]$$

$$\nabla^{*2} = \frac{\partial^2}{(\partial \xi^2)^2} - 2\sin\lambda^*\,\frac{\partial^2}{\partial \xi^2 \partial \xi^3} + \frac{\partial^2}{(\partial \xi^3)^2}$$

$$\overline{\nabla}^* = \frac{1}{\cos\lambda}\left[\frac{\partial^2}{(\partial \xi^2)^2} - 2\zeta_1\sin\lambda\frac{\partial^2}{\partial \xi^2 \partial \zeta} + \zeta_1^2\frac{\partial^2}{\partial \zeta^2} + \frac{\kappa\sin\lambda}{\cos\lambda}\zeta_1\frac{\partial}{\partial \zeta} - \frac{\kappa}{\cos\lambda}\frac{\partial}{\partial \xi^2}\right]$$

$$\zeta_1 = \frac{\partial \zeta}{\partial \xi^2}$$

$$\zeta_2 = \frac{\partial^2 \zeta}{(\partial \xi^2)^2}$$

Superscripts

i, j, k etc.	denote the contra-variant component of a vector
'	a prime denotes differentiation with respect to ξ^2
-	denote non-dimentional quantities when used with variables in the x^i coordinate system
^	denotes coefficients of expansions for large ξ^2 when used with v and w

Subscripts

1, 2, 3,..etc.	refers to order of expansions when used with flow variables $u, v, \varphi, \theta, \psi, w$.
i, j, k etc.	indicate co-variant component of a vector
$'_i$	denotes partial differentiation with respect to ξ^i
$;_i$	denotes co-variant derivatives in the x^i co-ordinate.

CHAPTER 1

INTRODUCTION

1.1 General remarks on the corner flow problem

The laminar boundary layer flow along corners formed by joining two quarter-infinite thin flat plates at their side edges has attracted considerable attention, particularly in the case of an internal right-angle corner, (see Fig. (1.1)). In every case the leading edges are coplaner and the joining line of the corner ('corner line') is parallel to the undisturbed free stream. In the vicinity of the corner line there exists an inherently three-dimensional flow region arising from the mutual interaction of the boundary layers on the plates. This problem is now one of the classic problems in the mechanics of fluids, and its treatment has provided a valuable background against which to treat the flow in a wider category of corner geometry, one new example of which will be the subject of the present work.

The presence of the three-dimensional region in the vicinity of the join does not require that the corner be mathematically sharp in the above sense but will exist, as will become apparent later, if the infinite curvature at the corner line is replaced by a joining surface of maximum curvature of $O(R_e^{\frac{1}{2}})$ or greater. This condition of course includes the infinite curvature as a special case.

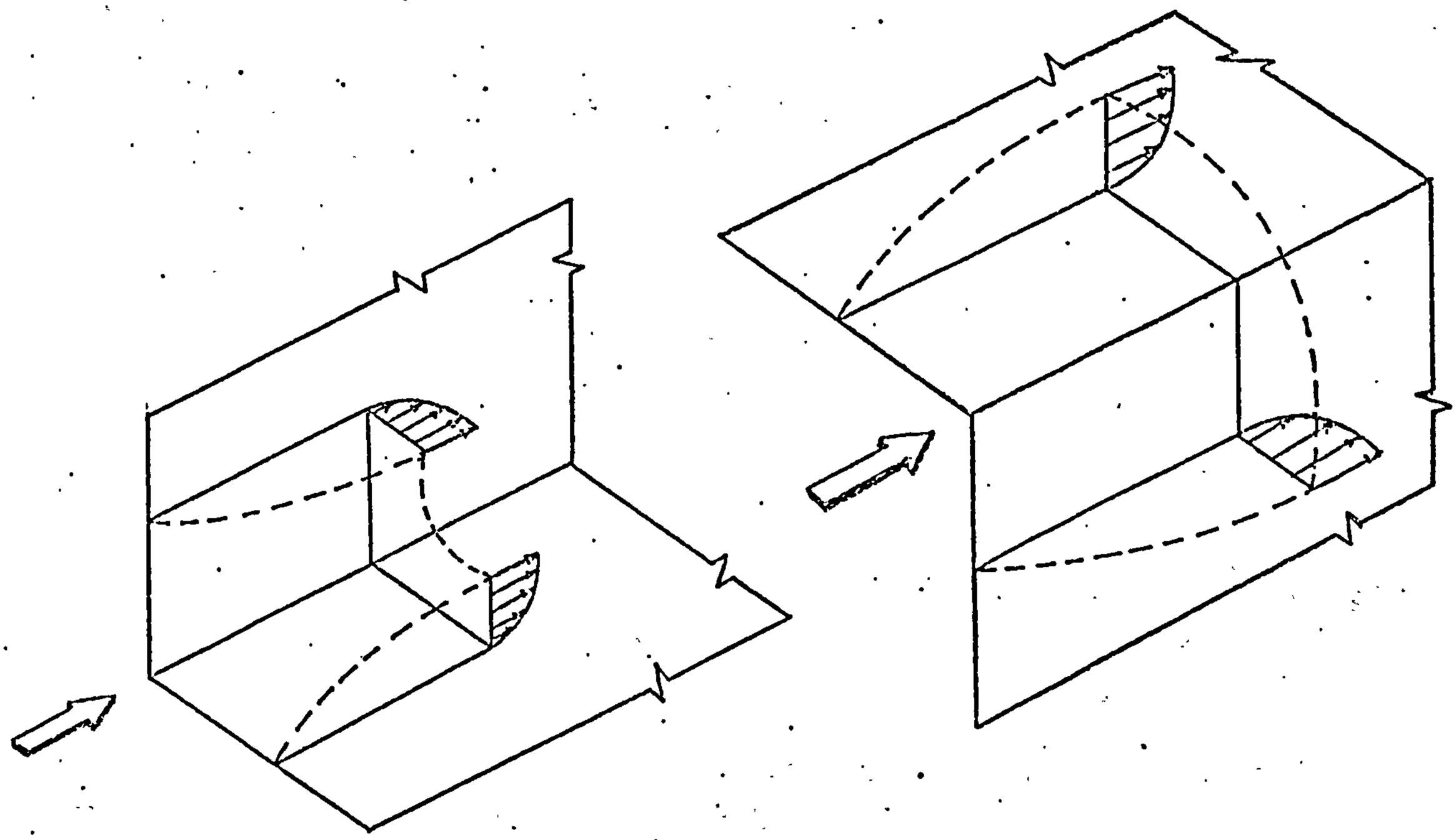

Fig. (1.1). Corner flow configuration.
(a) Flow along an internal corner.
(b) Flow along an external corner.

Apart from its greater generality, a solution to the problem of flow along a corner of finite transverse curvature ('radiused' corner) is of more immediate practical value since 'sharp' corners are rarely found in important flow systems. Corners having a finite curvature on the other hand are of common occurrence in engineering, notably in the blade spaces of turbomachinery.

The problem to be treated in this work is the laminar incompressible flow along geometrically symmetrical streamwise corners of arbitrary transverse curvatures and arbitrary angles, but with no streamwise curvature variation. The analysis is applicable to a wide variety of corner shapes, examples of which are shown in Fig. (1.2). It is important,

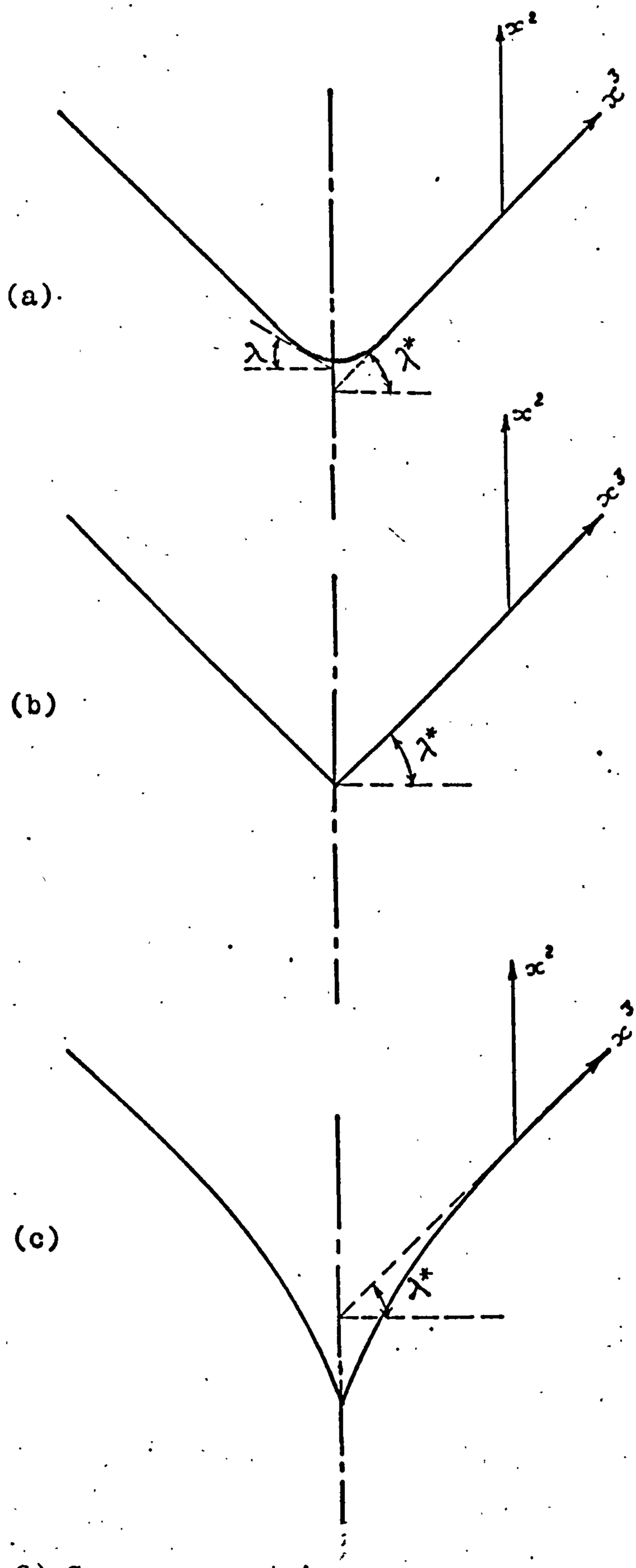

Fig.(1.2) Corner geometries ;
(a) radiused corner, (b) sharp corner, (c) sharp-profiled corner.

however, to note that the analysis is limited to shapes which asymptote to plane surfaces within a distance of $O(R_e^{-\frac{1}{2}})$ from the plane of symmetry.

One of the anticipated advantages of the radiused corner is an improvement in the stability of the flow. It is easy to show that for an internal sharp corner the wall shear stress vanishes at the corner line. Zero wall shear stress is a characteristic of the flow at separation in two-dimensional problems and by inference vanishing shear stress in the sharp corner is a warning that the flow may be in only a marginally stable condition. This is borne out experimentally [1] where it is found that the flow near the corner line will separate in the presence of a seemingly arbitrarily small adverse pressure gradient. This behaviour of the flow is a direct consequence of the infinite curvature and the effect of a finite curvature will therefore be to produce a non-zero shear stress with consequent improvement in the stability of the flow. This is confirmed in the present work.

The work to be presented here consists of two parts; analytical and experimental. The analytical part deals with incompressible boundary layer flow along radiused and sharp corners of arbitrary angle (internal and external corners).

The experimental programme is mainly that of traversing with a hot-wire anemometer a rectangular radiused corner of maximum curvature (at the symmetry line) of 0.1 mm^{-1}. Velocity profile development is calculated from these traverses and compared with the corresponding theoretical results.

1.2 Review of some literature on corner flow

To the author's knowledge, the literature available on corner flow is confined to sharp corners. Somewhat detailed treatments have been accorded to different parts of the literature by previous workers notably by Zamir [2], Barclay [3] and El-Gamal [4]. This review deals mainly with publications of relevance to the present work.

Two properties of the corner boundary layer need re-emphasizing prior to looking at individual attempts to solve the problem it poses. The first is the inherent three-dimensionality of the flow which requires the involvement of the equation of motion for each coordinate direction. The second is that the three dimensional region extends only to a distance of $O(R_e^{-\frac{1}{2}})$ from the plane of symmetry. Past failure to recognize one or both of these characteristics has resulted in incorrect solutions, some of which are discussed below.

The first attempted solution appears to have been by Loitsianskii [5] who considered the case of a rectangular sharp corner by using an adaptation of the momentum integral method which was well established in the treatment of two-dimensional flows. Later, with Bolshakov, Loitsianiskii [6] generalized his work to deal with corners of angles less than 180^o. Both works failed to satisfy the conditions stated above.

Carrier [7] made the first attempt to satisfy the boundary layer equations for the corner flow when considering the case of a 90^o sharp corner. He used only the streamwise

momentum and continuity equations augmented by an assumption concerning the relationship amongst the three components of the velocity vector. The solution was consistent with physical expectation but the question of the importance of the omitted crossflow equations remained.

Dowdell [8], under Carrier's supervision, attempted to resolve the matter by finding a solution satisfying all the equations of motion. He treated the case of an internal sharp corner of arbitrary angle with zero pressure gradient. The four equations of motion were reduced to two fourth order equations by introducing two stream functions satisfying the continuity equation identically and eliminating the pressure terms by cross-differentiation and subtraction of the cross-flow equations. Using an iterative scheme the resulting equations were solved numerically subject to the correct boundary conditions. Dowdell's results for a 90^{o} corner were only very slightly different from Carrier's solution and consequently the latter's approach, though inexact, was assumed to yield satisfactory results.

Rubin, in association with Pal and Grossman, has since shown, [9] [10] [11], that Carrier's, and consequently Dowdell's solutions were grossly in error. Rubin left unanswered the reason for the near coincidence of Dowdell's and Carrier's solutions where, as we have noted, Dowdell used all the equations of motion and the correct boundary conditions. El-Gamal [4] on considering this point, found that Dowdell had omitted, presumably by oversight, two terms from the vorticity equation as a result of which his solution satisfied only the continuity and streamwise momentum

equations as in Carrier's method.

In his first paper [9], Rubin demonstrated that the "boundary layer in a corner can be represented by four distinct regions" as depicted in Fig. (1.3a). I represents the region where the flow is potential to $O(R_e^{-\frac{1}{2}})$. In regions II and III the usual two-dimensional boundary layer equations apply to $O(R_e^{-\frac{1}{2}})$ but with three dimensional effects arising from the mutual interaction of the respective boundary layers through the potential flow region. Finally there is region IV, the 'corner layer', in which the flow is essentially three-dimensional and here nothing short of the complete set of boundary layer equations is required for the solution.

Having made this distinction, Rubin used the method of matched asymptotic expansion in a systematic formulation of the flow problem for a 90° sharp corner. This was in manner similar to an earlier treatment by Stewartson [12] of the flow near the side-edge of a quarter infinite flat plate.

Rubin has clarified the mechanism of the interaction between the boundary layers in regions II and IV and derived the correct boundary conditions for all the flow variables in region IV. He found that as $\zeta \longrightarrow \infty$ the crossflow velocity component w parallel to the wall y = 0 is given by

$$w = U_\infty \left(\frac{2U_\infty x}{\nu}\right)^{1/2} \beta f''(\eta) \int_0^\eta \frac{\beta - \tau}{f''(\tau)} d\tau \qquad (1.1)$$

where f is the Blasius function, a prime denotes differentiation with respect to η and $\beta = \lim_{\eta \to \infty} (\eta f' - f)$. This constitutes one of the boundary conditions on region IV as

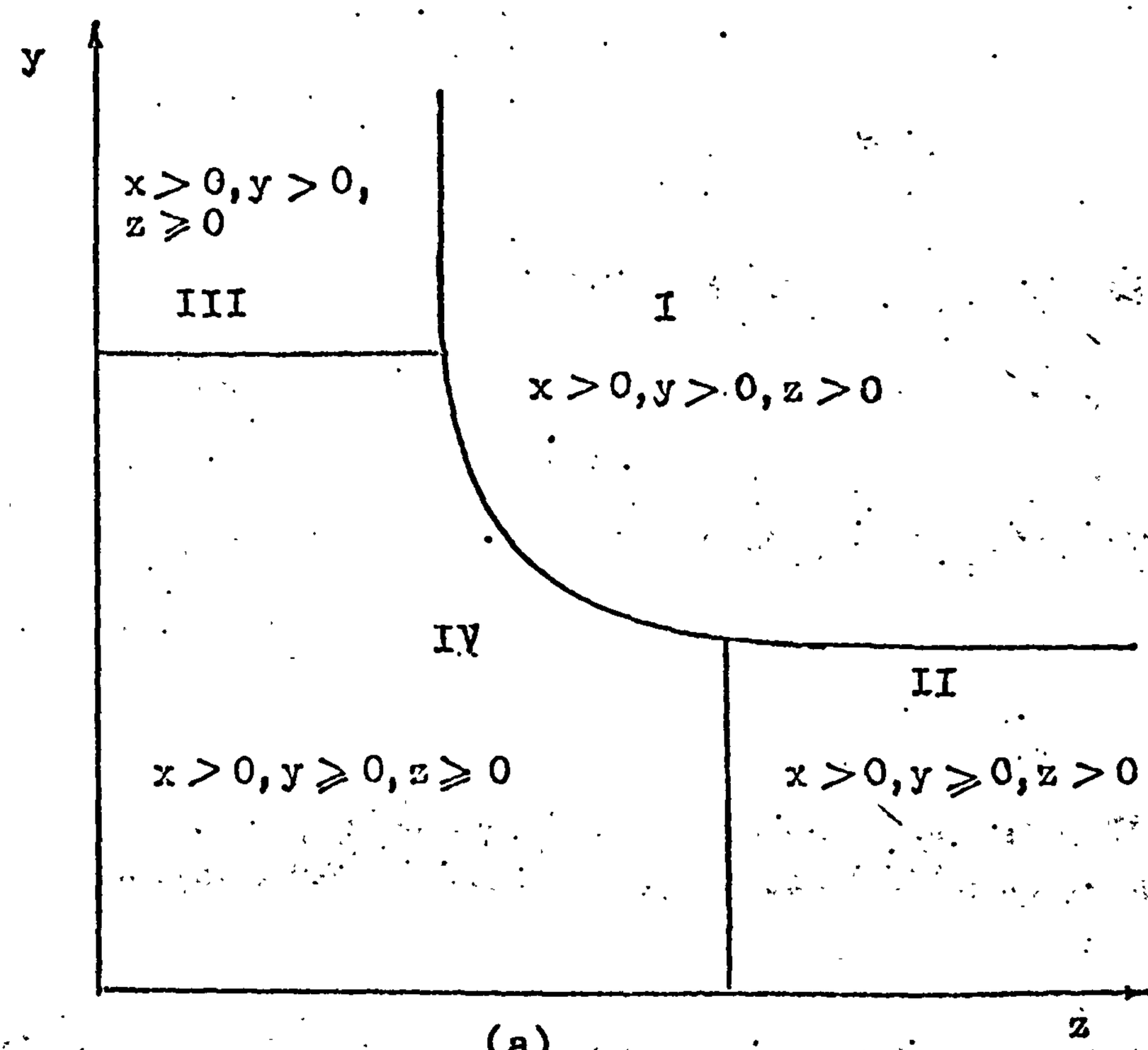

(a)

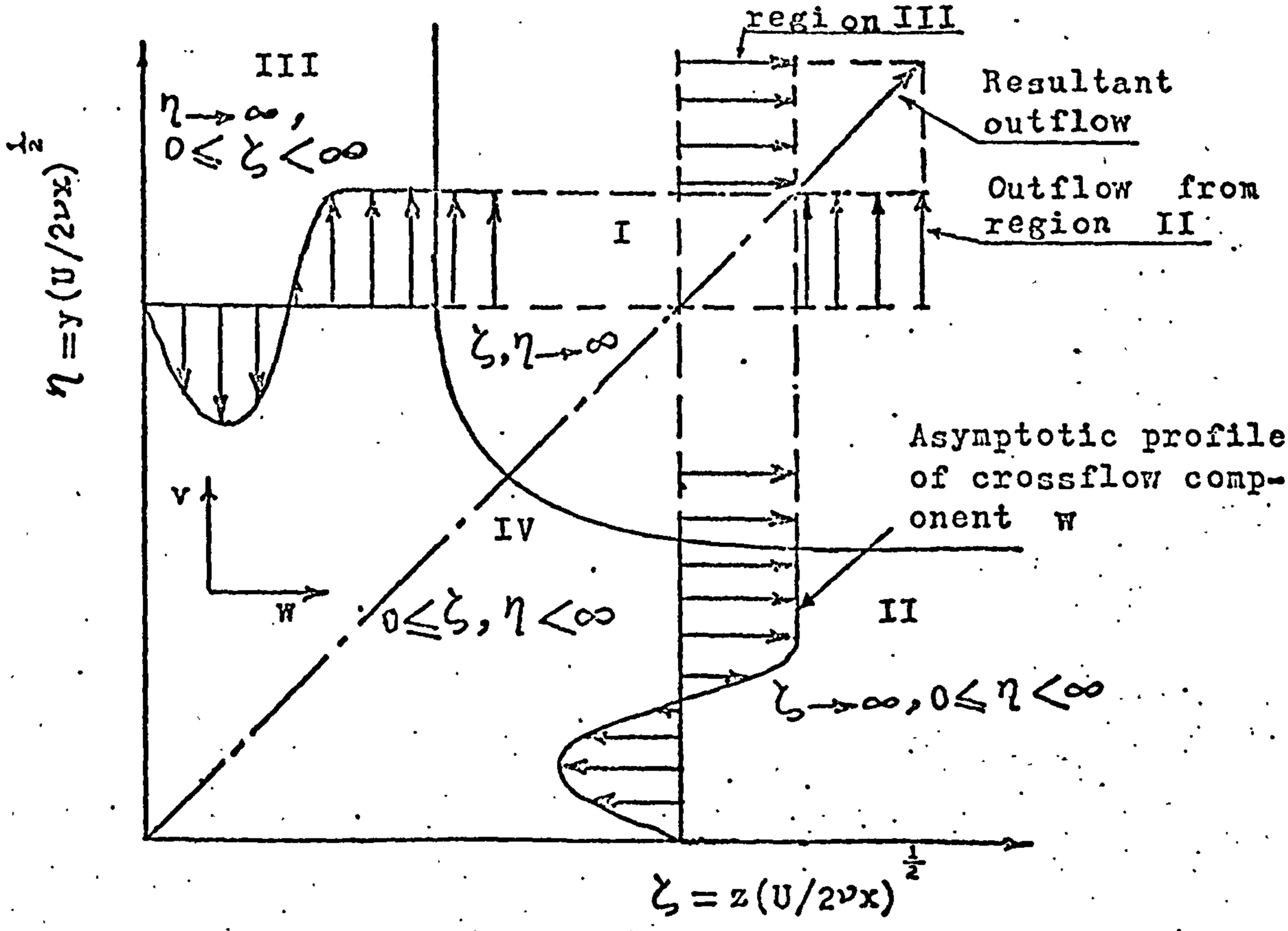

(b)

Fig.(1.3) Corner flow geometry.

$\zeta \longrightarrow \infty$ but in the numerical solution necessary for region IV the boundary had to be set at finite and small values of $\zeta (\zeta \approx 15 \equiv \zeta_{max}, say)$. Preliminary computations indicated that the corner layer flow variables did not decay exponentially but only algebraically into regions II and III and that it was incorrect to apply (1.1) at finite values of ζ_{max}. Pal and Rubin [10] then investigated the asymptotic behaviour of the corner layer region and found that all flow variables decay algebraically into the boundary layer (regions II and III) while only the streamwise velocity and vorticity decay exponentially into the potential flow region. Using this analysis, Rubin and Grossman [11] produced a numerical solution for the corner layer in a bounded domain. As remarked above their results showed that Carrier's solution was substantially in error. This can be seen in Fig. (1.4) which shows the results for streamwise velocity profiles in the symmetry plane.

Although Rubin and his colleagues produced the most rigorous analysis to date for the corner problem, he was not the first to find the correct matching requirements for regions II and IV (and, III and IV). These were earlier established by Pearson [13] who utilized the symmetry of the problem to arrive at an equation essentially the same as equation (1.1). Pearson failed to recognize the algebraic decay, however, and this resulted in a solution which was numerically incorrect (see Fig. (1.4)).

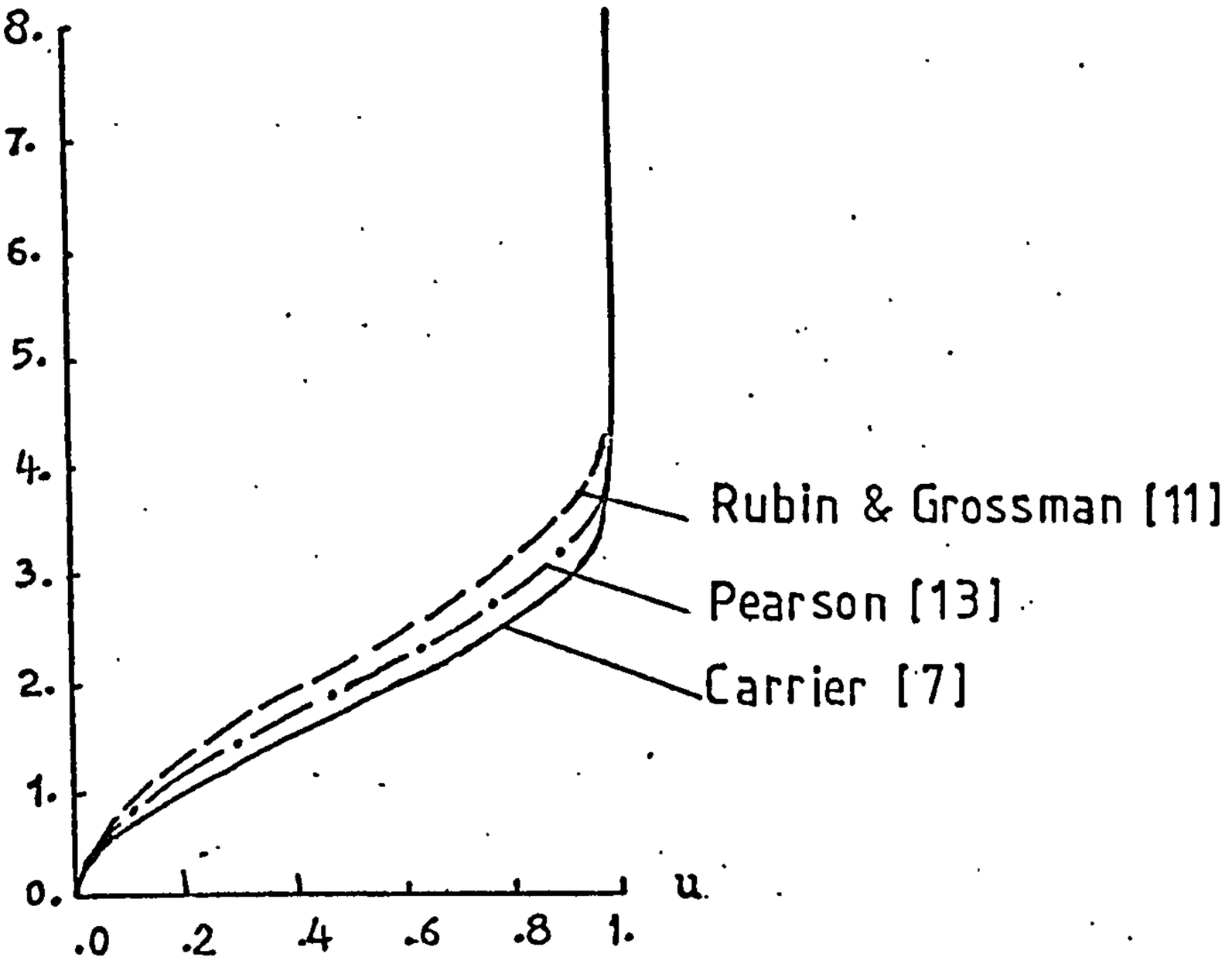

Fig. (1.4). Streamwise velocity in symmetry plane.

An alternative method of treating the problem posed by the algebraically decaying crossflow is due to Ghia [14]. Starting with Rubin's equations and boundary conditions he transformed them in terms of the new independent variables N and S where

$$N = \frac{\eta}{C + \eta} \quad , \quad S = \frac{\zeta}{C + \zeta}$$

and C is a constant. In this way the quarter infinite domain bounded by the symmetry plane $\eta = \zeta$ and the wall $\eta = 0$ is mapped onto the finite region $0 \leqslant N, S \leqslant 1$. Dependent variables which were unbounded as η or ζ becomes large were readily transformed to remove this inconvenience. The new set of equations with their boundary conditions were then solved numerically by an alternating direction implicit (ADI) scheme throughout $0 \leqslant N, S \leqslant 1$.

The crossflow velocity results were found to compare well with Rubin and Grossman's results in general trend but differ by a maximum of about 10% near the peak value at $\eta=\zeta=0.4$.

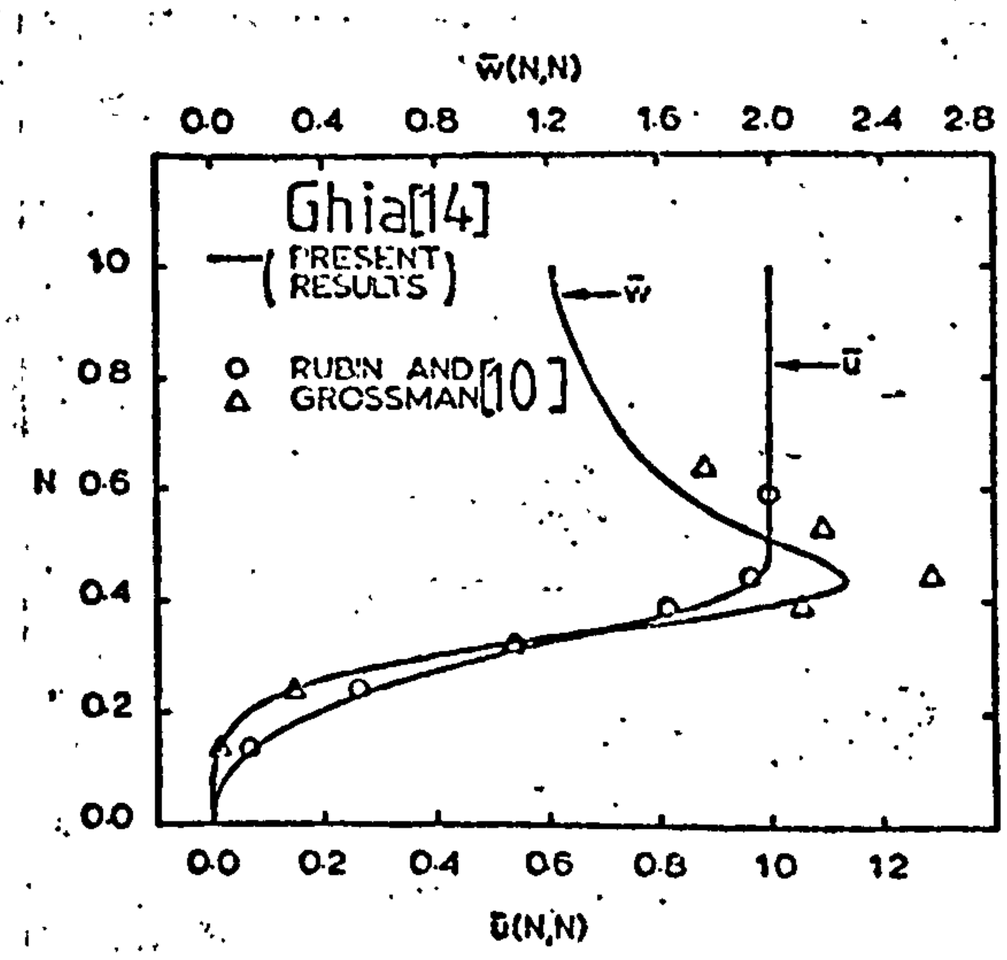

Velocities along symmetry line of infinite corner.

Fig. (1.5) Streamwise velocity $\bar{u}$ and crossflow velocity $\bar{w}$ in symmetry plane (reference [14]).

Fig. (1.5) is taken from reference [14] and shows the cross-flow velocity $\bar{w}$ and the streamwise velocity $\bar{u}$ from Ghia's and Rubin and Grossman's solution for the symmetry plane. In the (N,S) coordinate used in that figure agreement between the solution for $\bar{u}$ seems excellent. On request Professor Ghia kindly sent the present writer a copy of his numerical results. These [15], together with Rubin and Grossman's results for $\bar{u}$ in the symmetry plane are re-plotted in the convential boundary layer coordinate η in Fig. (1.6). In this coordinate the agreement is still fair but the difference in the two solutions is made clearer. The reasons for this difference are given in Ghia's paper in the course of explaining the corresponding differences in the cross-flow velocities. He reported that when solving the problem

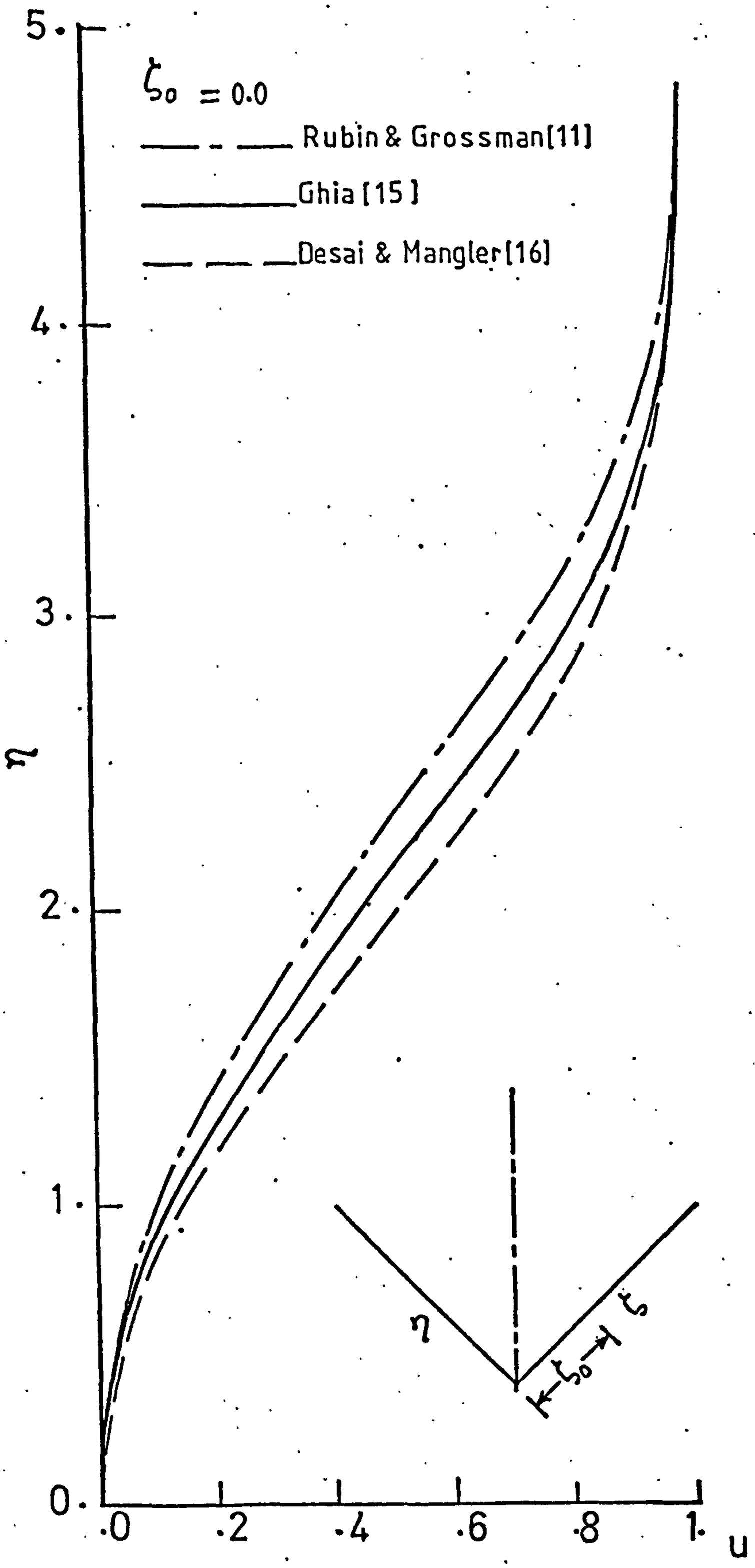

Fig.(1.6) Streamwise velocity in symmetry plane.

in a finite region using the asymptotic series arrived at by Pal and Rubin [10], it was found that the solution was influenced by ζ_{max} . Ghia concluded that because of the algebraic asymptotic behaviour of the solution, it should be more accurate to place the asymptotic boundary conditions at $\zeta_{max} \longrightarrow \infty$. In view of Ghia's method of solution, and the remarks made above, his solution is taken as the reference for comparison with the present author's results in the case of a rectangular sharp corner.

The sharp corner has also been dealt with by Desai and Mangler [16] who analysed the problem for a corner of arbitrary angle. Their solution for the streamwise velocity component in the symmetry plane is shown in Fig. (1.6). They assumed similarity from the outset but within this limitation they have expressed the boundary layer equations in a general curvilinear coordinate system, (ξ^1, ξ^2, ξ^3). Coordinate ξ^1 is parallel to the streamwise direction and ξ^2, ξ^3 coordinates lie in the planes ξ^1 = constant. ξ^2 and ξ^3 are stretched in the usual boundary layer sense.

The particular system chosen for the corner problem is

$$\left.\begin{aligned} x^1 &= \xi^1 = x \quad , \text{say} \\ x^2 &= \xi^2 \cos\beta \sqrt{\frac{\nu x}{U_\infty}} \\ x^3 &= \left[\left(\cos\beta + \frac{2}{\pi}\sin\beta\right)\xi^3 + \frac{2}{\pi}(\sin\beta)\,\xi^2 \tan^{-1}(\xi^2/\xi^3)\right]\sqrt{\frac{\nu x}{U_\infty}} \end{aligned}\right\} \quad (1.2)$$

and is shown in Fig. (1.7), where (x^1, x^2, x^3) form a rectangular Cartesian system with origin on the symmetry plane at the leading edge. U_∞ and ν are the free stream velocity and kinematic

Fig.(1.7) Sketch of the general co-ordinate system .
From Desai and Mangler [16] .

Fig.(1.8) Flow in the cross plane.
From Desai and Mangler [16].

viscosity respectively.

Desai and Mangler subdivided the flow into regions similar to the model used by Rubin. Fig. (1.8) is taken from the paper by Desai and Mangler to show this subdivision.

The solution for a 90^{o} corner was significantly different from that obtained by Rubin and Grossman [11] and Ghia [14] particularly for the crossflow velocity vector at $\xi^2 \longrightarrow \infty$. In Desai and Mangler's solution the crossflow component parallel to the wall is zero, i.e. the flow is strictly two dimensional in the region $\xi^2 \longrightarrow \infty$. This contrasts with Pearson's [13] and Rubin's [11] results equation (1.1). The vanishing crossflow component parallel to the wall as $\xi^2 \longrightarrow \infty$ amounts to an assumption by Desai and Mangler. They assumed that $\xi^2 \longrightarrow \infty$ corresponded to the physical coordinate x^2 being large (where indeed the velocity component in question would vanish). This is not so of course. The proper matching condition is to be applied when $\xi^2 \longrightarrow \infty$ with $|x^2|$ fixed and arbitrarily small. In this vicinity the boundary layer is subjected to the outflow from the boundary layer on the wall at $\xi^2 \longrightarrow -\infty$. This gives rise to a secondary shear layer which results in the velocity distribution equation (1.1). This point is clarified in Fig. (1.3b).

A related contributory factor affecting the results for the 90^{o} corner is the different condition imposed in each case, on the crossflow velocity vector in the potential region. As the potential region is approached in a direction parallel to the symmetry plane the magnitude of the crossflow velocity vector attains a constant value to $O(R_e^{-\frac{1}{2}})$ which is

analogous to the situation of flow over a semi-infinite flat plate. This condition is common to Pearson's, Rubin's and Desai and Mangler's solutions. However, since the vorticity is also zero here, it follows that the magnitude of the crossflow velocity vector must be the same throughout the potential region and from symmetry that the direction of the vector must be parallel to the symmetry plane (Fig. (1.3b)). In consequence the crossflow velocity vector may be determined by the solution to the boundary layer flow at $\xi^2 \longrightarrow \infty$ *. Desai and Mangler used only the weaker condition that the rate of change of the crossflow vector with respect to ξ^3 was zero at $\xi^2 \longrightarrow \infty$. The consequences of this for the solution are described in some detail in Appendix (A).

These are defects in an otherwise valuable work. Desai and Mangler have derived the boundary layer equations in a general curvilinear coordinate system and the equations may be used to treat a wide variety of three-dimensional problems where similarity can be assumed.

Zamir [2] [17] derived equations for the boundary layer in a general three-dimensional curvilinear coordinate system prior to analysing the corner flow problem. These equations are of some utility but unfortunately not for the purpose intended in consequence of some defects in the analysis. To clarify these it is necessary to consider the analysis in some detail.

Zamir's derivation commences from consideration of the tensor representation of energy per unit volume of a fluid

---

* An alternative but equivalent approach is used to arrive at this result in Chapter 2 , pp. 55-56.

element in motion.

$$F^{ij} = \begin{Bmatrix} \rho u^1 u^1 + g^{11} p - \tau^{11} & \rho u^1 u^2 - \tau^{12} & \rho u^1 u^3 - \tau^{13} & \rho u^1 \\ \rho u^2 u^1 - \tau^{21} & \rho u^2 u^2 + g^{22} p - \tau^{22} & \rho u^2 u^3 - \tau^{23} & \rho u^2 \\ \rho u^3 u^1 - \tau^{31} & \rho u^3 u^2 - \tau^{32} & \rho u^3 u^3 + g^{33} p - \tau^{33} & \rho u^3 \\ \rho u^1 & \rho u^2 & \rho u^3 & \rho \end{Bmatrix} \quad (1.3)$$

where ρ denotes density, P the pressure and u^k is the contravarient component of the velocity vector,

$$u^k = \frac{d\xi^k}{dt}$$

where ξ^k is a general curvilinear coordinate system (ξ^1, ξ^2, ξ^3) and t is a time coordinate $\xi^4 = t$.

$$\tau^{ij} = \mu \left(g^{ik} u^j_{,k} + g^{\ell j} u^i_{,\ell} \right)$$

where a comma before a subscript indicates covarient differentiation and μ is the coefficient of viscosity.

Zamir assumed that in terms of the physical components of the velocity the following hold

$$g_{11} u^1 u^1 \gg g_{22} u^2 u^2 , g_{33} u^3 u^3 \quad (1.4)$$

having specified ξ^1 as the streamwise coordinate, and

$$\frac{\partial u^i}{\partial S_i} \gg \frac{\partial u^i}{\partial S_j} \quad (i=1,2,3), \ (j=1,3) \quad (1.5)$$

where $dS_j = \sqrt{g_{jj}}\, d\xi^j$ is the line element along ξ^j.

Assumptions (1.4) and (1.5) were directly applied (i.e. without an order of magnitude comparison with other terms) to the energy tensor (1.3). This resulted in

$$C^{ij} = \begin{matrix} \rho u^1 u^1 + g^{11} p & \rho u^1 u^2 - \mu g^{22} \frac{\partial u^1}{\partial \xi^2} & \rho u^1 u^3 & \rho u^1 \\ \rho u^2 u^1 - \mu g^{22} \frac{\partial u^1}{\partial \xi^2} & g^{22} p & 0 & \rho u^2 \\ \rho u^3 u^1 & 0 & g^{33} p & \rho u^3 \\ \rho u^1 & \rho u^2 & \rho u^3 & \rho \end{matrix} \qquad (1.6)$$

to represent the energy tensor in a boundary layer flow. Incompressible steady flow was considered and an orthogonal curvilinear coordinate system was adopted. The continuity and the streamwise equations were then obtained from $C^{1j}_{,j} = 0$ and $C^{4j}_{,j} = 0$ (j=1,2,3,4) which lead to

$$u^1 \frac{\partial u^1}{\partial \xi^1} + u^2 \frac{\partial u^1}{\partial \xi^2} + u^3 \frac{\partial u^1}{\partial \xi^3} + g^{11} \left(\frac{1}{2} \frac{\partial g_{11}}{\partial \xi^1} u^1 u^1 + \frac{\partial g_{11}}{\partial \xi^2} u^1 u^2 + \frac{\partial g_{11}}{\partial \xi^3} u^1 u^3 \right) + g^{11} \frac{1}{\rho} \frac{\partial p}{\partial \xi^1} = \nu g^{22} \left(\frac{\partial^2 u^1}{(\partial \xi^2)^2} + \frac{\partial u^1}{\partial \xi^2} \left(\frac{3}{2} g^{11} \frac{\partial g_{11}}{\partial \xi^2} + \frac{1}{2} g^{33} \frac{\partial g_{33}}{\partial \xi^2} - \frac{1}{2} g^{22} \frac{\partial g_{11}}{\partial \xi^2} \right) \right) \qquad (1.7)$$

$$\frac{\partial u^1}{\partial \xi^1} + \frac{\partial u^2}{\partial \xi^2} + \frac{\partial u^3}{\partial \xi^3} + u^1 \left(\frac{1}{2} g^{11} \frac{\partial g_{11}}{\partial \xi^1} + \frac{1}{2} g^{22} \frac{\partial g_{22}}{\partial \xi^1} + \frac{1}{2} g^{33} \frac{\partial g_{33}}{\partial \xi^1} \right) + u^2 \left(\frac{1}{2} g^{11} \frac{\partial g_{11}}{\partial \xi^2} + \frac{1}{2} g^{22} \frac{\partial g_{22}}{\partial \xi^2} + \frac{1}{2} g^{33} \frac{\partial g_{33}}{\partial \xi^2} \right) + u^3 \left(\frac{1}{2} g^{11} \frac{\partial g_{11}}{\partial \xi^3} + \frac{1}{2} g^{22} \frac{\partial g_{22}}{\partial \xi^3} + \frac{1}{2} g^{33} \frac{\partial g_{33}}{\partial \xi^3} \right) = 0 \qquad (1.8)$$

where $\nu = \mu/\rho$.

Equations (1.7) and (1.8) were tested for cases where changes in ξ^3 vanish. This test was taken to verify that these equations were applicable to three-dimensional problems when the solid surface, over which the boundary layer developed, was highly curved or discontinuous in the lateral direction.

The following coordinate system was introduced to describe a sharp right-angled corner

$$\left.\begin{aligned} \xi^1 = x \quad , \xi^2 = \frac{yz}{y+z} \quad , \xi^3 = (y^3 - z^3)^{1/3} \quad ; \\ g_{11} = 1 \quad , g_{22} = \frac{(y+z)^4}{y^4+z^4} \quad , \quad g_{33} = \frac{(y^3-z^3)^{4/3}}{y^4+z^4} \end{aligned}\right\} \quad (1.9)$$

where (x,y,z) are coordinates in a cartesian reference frame with the x axis along the corner line as shown in Fig. (1.9). On substituting (1.9) into (1.7) and (1.8) the following equations were obtained

$$u\frac{\partial u}{\partial \xi^1} + \frac{(y^4+z^4)^{1/2}}{(y+z)^2} v\frac{\partial u}{\partial \xi^2} + \frac{(y^4+z^4)^{1/2}}{(y^3-z^3)^{2/3}} w\frac{\partial u}{\partial \xi^3} + \frac{1}{\rho}\frac{\partial P}{\partial \xi^1} = \nu\left[\frac{(y^4+z^4)}{(y+z)^4}\frac{\partial^2 u}{(\partial \xi^2)^2} - \left(\frac{2y^2z^2}{(y+z)(y^4+z^4)} + \frac{2(y^3-z^3)^2}{(y+z)^3(y^4+z^4)}\right)\frac{\partial u}{\partial \xi^2}\right] , \quad (1.10)$$

$$\frac{\partial u}{\partial \xi^1} + \frac{(y^4+z^4)^{1/2}}{(y+z)^2}\frac{\partial v}{\partial \xi^2} + \frac{(y^4+z^4)^{1/2}}{(y^3-z^3)^{2/3}}\frac{\partial w}{\partial \xi^3} - \frac{2y^2z^2(y+z)}{(y^4+z^4)^{3/2}} v - \frac{2yz(y^3-z^3)}{(y^4+z^4)^{3/2}} w = 0 \quad (1.11)$$

where u,v,w are the physical components of velocity along ξ^1, ξ^2, ξ^3 respectively.

Fig.(1.9) Zamir's co-ordinate system,equn. (1.9).

Zamir considered equations (1.10) and (1.11) in the plane of symmetry where

$$y = z;\ w = 0;\ \xi^2 = y/2 = z/2,\ \xi^3 = 0 \qquad (1.12)$$

and put

$$S = y\sqrt{2} = z\sqrt{2} = \xi^2 2\sqrt{2}$$

He argued that $\partial w/\partial \xi^3 = 0$ at the plane of symmetry since its coefficient (in equation (1.11)) was infinite. Substituting (1.12) and $\partial w/\partial \xi^3 = 0$ into (1.10) and (1.11), he produced

$$u\frac{\partial u}{\partial x} + v\frac{\partial u}{\partial S} + \frac{1}{\rho}\frac{\partial P}{\partial x} = \nu\left(\frac{\partial^2 u}{\partial S^2} - \frac{2}{S}\frac{\partial u}{\partial S}\right) \qquad (1.13a)$$

$$\frac{\partial u}{\partial x} + \frac{\partial v}{\partial S} - \frac{2}{S}v = 0 \qquad (1.13b)$$

In his second paper [18], Zamir considered the solution of equations (1.13) with a pressure gradient implied by a free stream velocity U(x), given by

$$U(x) = Ax^n \qquad (1.14)$$

where A and n are constants. He found that only solutions for $n > 1/3$ could be computed. In a further paper [19], Zamir produced a numerical solution for the case n = 1/3 and showed that the equations were very sensitive to the numerical technique used.

Equations (1.13) have been criticized by Tokuda [20] who showed that there exists a system of eddies near the apex of a rectangular sharp corner and that these equations fail to account for such eddies. Tokuda consequently concluded that Zamir's equations were incorrect in the plane of symmetry. Zamir [19] has replied to the criticism and disagreement remains as to the correctness of Zamir's method.

The matter may however be resolved in the following direct manner and it is clear that Zamir's analysis lacks the rigour necessary for the corner problem.

(i) Equations (1.10) and (1.11) are singular in the plane of symmetry. The Jacobian J of the transformation, equations (1.9), is

$$J \equiv \frac{\partial(x,y,z)}{\partial(\xi^1,\xi^2,\xi^3)} = \frac{(y+z)^2(y^3-z^3)^{2/3}}{(y^4+z^4)}$$

$$= 0 \qquad \text{at} \qquad y = z$$

and by definition is a singular condition for the coordinate system at y = z. A consequence of this is the indeterminacy of the underlined term in equation (1.10) at y = z (i.e. the term takes the form 0/0). Zamir dropped this term in the course of obtaining equation (1.13a). There is still less justification for dropping the underlined term in equation (1.11). This term becomes infinite at y = z. Zamir deleted the term for that very reason - an infinite term is physically unrealizable and therefore $\partial w/\partial \xi^3$ must be zero, and although this merely makes the term indeterminate, Zamir assumed it to be zero*.

(ii) Assumption (1.4) was incorrectly used in deriving C^{ij} from F^{ij}. For example, in element F^{22}, u^2u^2 was deleted as negligible compared to u^1u^1 in element F^{11}. This is an invalid procedure. The order of magnitude comparison should only be made to the

---

* In trying to prove that $\partial w/\partial \xi^3 = 0$ Zamir attempted to derive from first principles the continuity equation (1.13b) for an elemental volume at the symmetry plane but unfortunately the derivation involved the implicit assumption that $\partial w/\partial \xi^3 = 0$ and therefore defeated its purpose.

component parts of the same element or to the terms belonging to the same equation.

(iii) Assumption (1.5) is untenable in general, and is applied in the manner used for assumption (1.4). $\partial u^1/\partial S_2 \gg \partial u^1/\partial S_3$ is true only when the coordinate surface S_2 = constant and the isovels of u in the surface S_1 = constant coincide (or nearly so). Insofar as Zamir later chose a coordinate system that may have satisfied this condition the assumption is admissible. It is nevertheless incorrect to neglect, a priori, the terms $\partial u^i/\partial S_j$ (i,j=2,3) as Zamir did. The consequence of doing so (and this illustrates also the defect in the use of assumption (1.4)) are brought out on considering the momentum equation in the ξ^3 direction which is

$$c^{3j}_{,j} = 0 \qquad (j = 1,2,3,4)$$

$$u^1 \frac{\partial u^3}{\partial \xi^1} + u^3 \Big(\underline{\frac{\partial u^1}{\partial \xi^1} + \frac{1}{2}\Big(g^{11}\frac{\partial g_{11}}{\partial \xi^1} + g^{22}\frac{\partial g_{22}}{\partial \xi^1} + g^{33}\frac{\partial g_{33}}{\partial \xi^1}\Big)u^1}\Big)$$

$$+ g^{33}\frac{\partial g_{33}}{\partial \xi^1}u^1u^3 + \frac{1}{\rho}\frac{\partial}{\partial \xi^3}(g^{33}P) + \frac{1}{2\rho}\Big(g^{11}\frac{\partial g_{11}}{\partial \xi^3} + g^{22}\frac{\partial g_{22}}{\partial \xi^3}$$

$$+ 2g^{33}\frac{\partial g_{33}}{\partial \xi^3}\Big)g^3P - \frac{1}{2}\frac{g^{33}}{\rho}\Big((\rho u'u' + Pg'')\frac{\partial g_{11}}{\partial \xi^3} + g^{22}\frac{\partial g_{22}}{\partial \xi^3}P\Big) = 0 \qquad (1.15)$$

for an incompressible steady flow and orthogonal coordinate system. The most obviously defective feature of equation (1.15) is the absence of any viscous term. Secondly the underlined term would vanish if assumption (1.4) was used correctly. A proper derivation of equation (1.15) introduces terms which complement the underlined terms to form the L.H.S. of the continuity equation (1.8) and therefore sum to zero.

The flow along a corner poses an essentially three-dimensional problem and there can be no streamwise plane (i.e. a plane containing the free stream velocity vector) in which the flow is independent of the conditions prevailing in adjacent planes. The flow in the symmetry plane must be, and is, affected by what happens at the solid boundaries, e.g. suction [4]. Zamir's analysis is only applicable to flow problems where streamwise vorticity contribution is negligible and cannot therefore be used to treat a problem like that of the corner flow.

Zamir [2] [21] also produced an extensive set of experimental results for the flow along a right-angled sharp corner. The leading edge of the model was streamlined in shape like that of the front half of a zero-camber aerofoil. The results showed a pronounced bulge in the isovels of the streamwise velocity across the plane of symmetry. This behaviour is markedly different from that obtained by Rubin and Grossman [11]. Fig. (1.10) is taken from reference [20] to illustrate the difference in the two results. Recently El-Gamal [4] determined experimentally the development of the flow along a sharp rectangular corner and his results are quite different from those obtained by Zamir. El-Gamal's experimental results are in much better agreement with the theoretical solution by Rubin (and Ghia) and in particular show no sign of the distortions in the isovels found by Zamir. Fig. (1.11) shows a typical velocity profile in the symmetry plane from Zamir's and El-Gamal's experiments.

The different experimental results are possibly due to the leading edge forms used in each case. Zamir used a profiled leading edge whereas El-Gamal's model incorporated

Fig.(1.10) Streamwise isovels.
(Taken from ref. [20]).

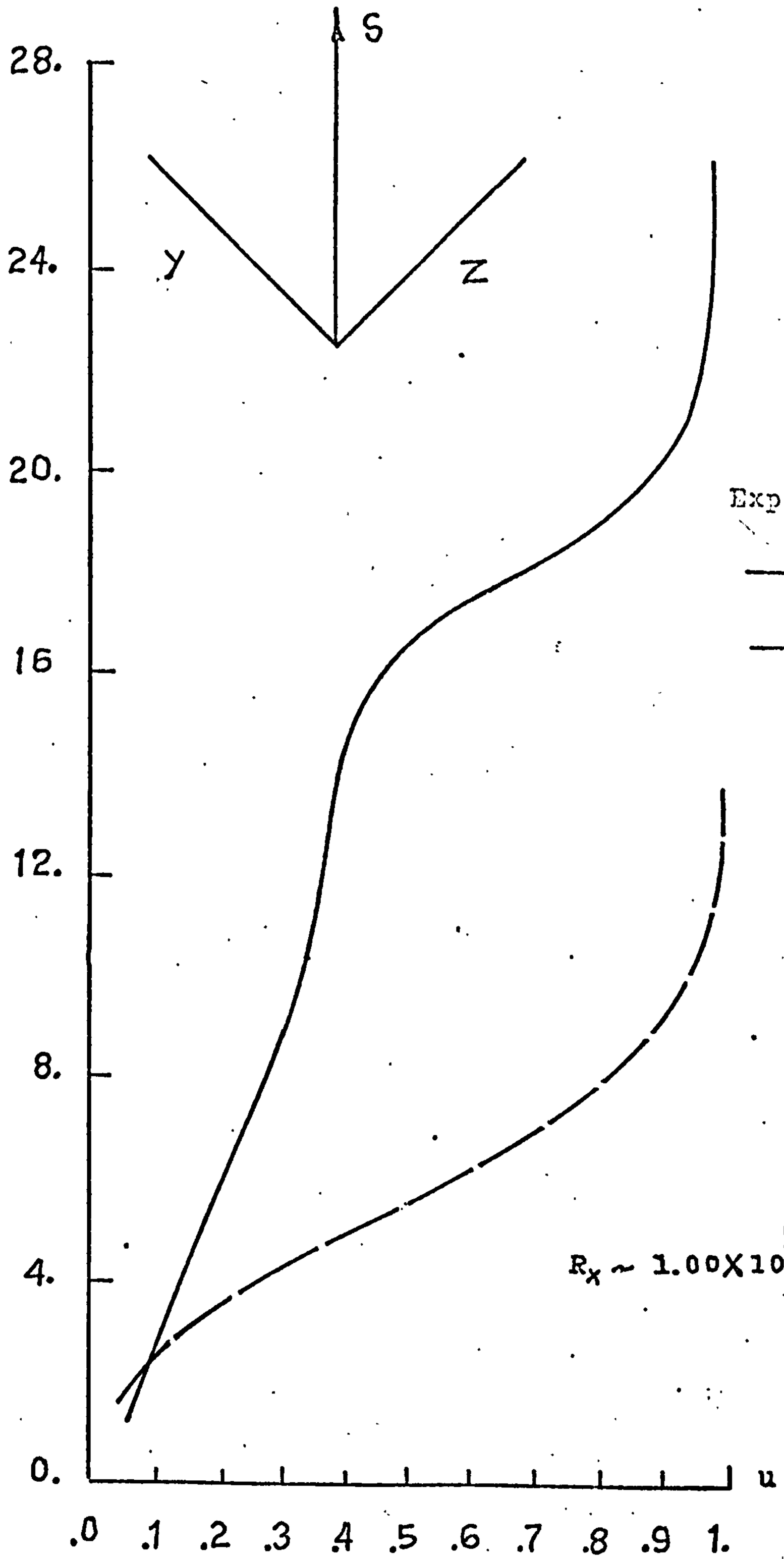

Fig.(1.11) Streamwise velocity in symmetry plane.

a knife edge form.

El-Gamal's work was a preliminary to studying the effect of wall suction on the flow along a sharp rectangular corner. His theoretical analysis is of some interest although of no direct importance to the present work. He considered two kinds of suction distribution. The first was independent of the streamwise coordinate and the second varied in proportion to $R_x^{-\frac{1}{2}}$. In each case the flow was characterized by a dimensionless suction parameter. For small values of the parameter solutions were obtained by perturbing the equation of motion about the zero suction (i.e. Rubin's) solution. For large values of the suction parameter asymptotic solutions were obtained. In regions corresponding to regions II and III of Fig. (1.3) El-Gamal found the exact solution for the cross-flow for all values of the suction parameter.

The perturbation solution for small and large values of the parameter had no overlap domain and this prompted him to re-consider Carrier's approximate method as a device for joining the two solutions. This proved to be extremely satisfactory. As the suction parameter is increased the coupling between the streamwise vorticity and momentum equations is weakened and the defect of Carrier's solution, i.e. disregard of the streamwise vorticity equation, is of smaller importance. Indeed for large values of the suction parameter Carrier's method of solution produces results in excellent agreement with the asymptotic solution. This is a rather pleasing re-valuation of the first boundary layer approach to the corner problem.

Weinberg [22] produced results for what is perhaps the nearest example so far to the flow along a radiused corner. In the course of his study of the compressible flow along a 90^{o} sharp corner he conducted calculations for incompressible flow along a corner having a fillet placed across its apex as in Fig. (1.12). η and ζ are the stretched coordinates.

In discussing his results, Weinberg concluded that so long as the fillet remained small compared to the corner layer dimension its effect on the flow structure was local. The work to be presented here confirms this. Fig. (1.13) is taken from reference [22] to show the effect of the fillet, for $\zeta_{0} = 1.6$, on the isovels of the streamwise velocity.

Apart from Weinberg's work, the literature so far considered deals only with corners which can be characterized by the intersection of two planes (i.e. sharp corners). The absence of any literature on the more immediately important problem of the flow along a radiused corner is a primary motive for the work now to be considered.

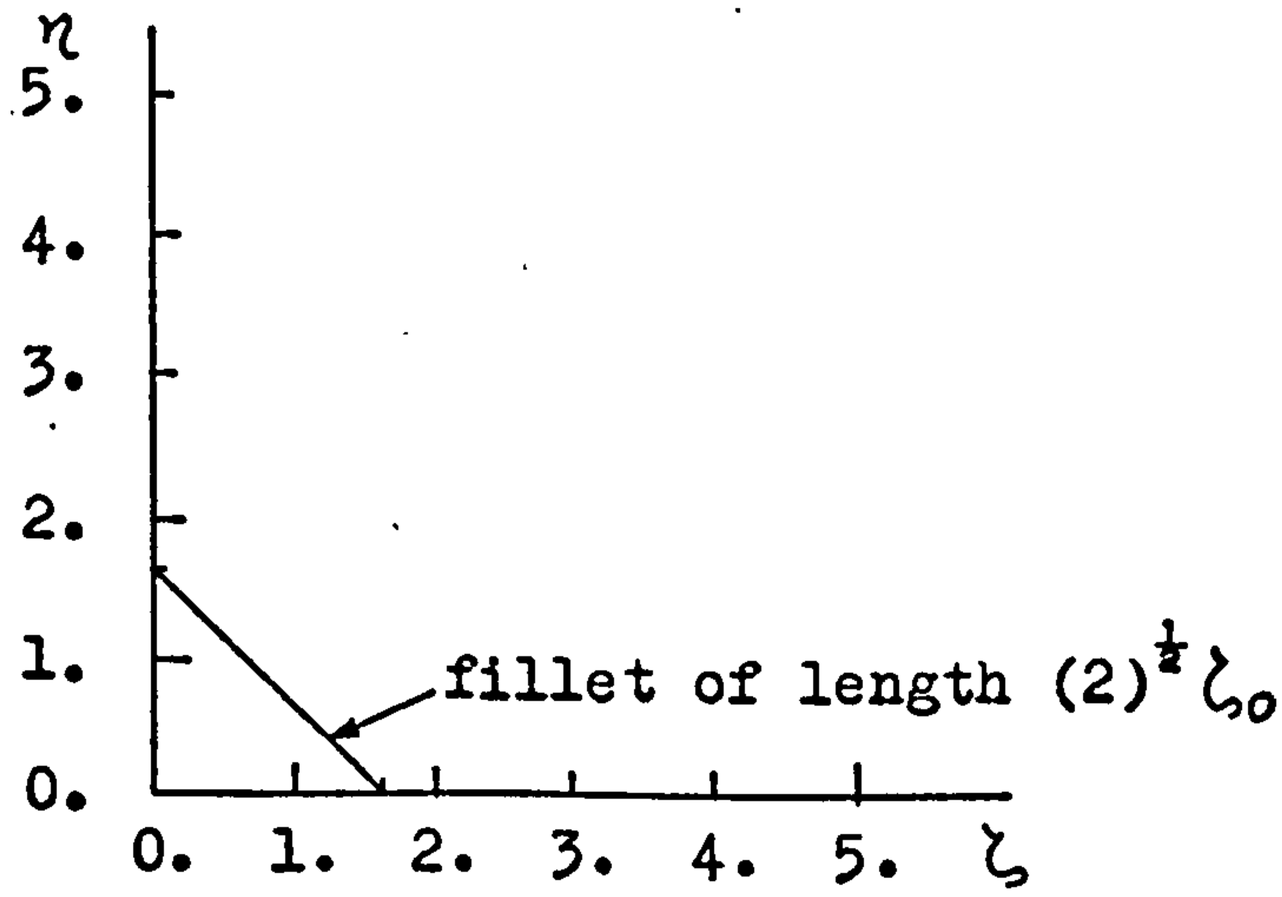

Fig. (1.12) Fillet geometry.

Fig.(1.13) Streamwise isovels , from Weinberg [22].

CHAPTER 2

THEORETICAL ANALYSIS

2.1 Introduction

The analysis of the radiused corner flow problem is most conveniently attempted in the framework of a curvilinear coordinate system in which one of the coordinate surfaces coincides with the solid surface of the corner. It is desirable that such a system assumes a cartesian form far away from the symmetry plane because of the convenience this provides in treating the boundary layer into which the corner layer asymptotes. In this chapter the Navier-Stokes and continuity equations are expressed with respect to such a reference frame and then developed into a boundary layer form which is found to be of the non-similar type. A further approximation, justifiable a posteriori, reduces these equations to a form of the local non-similar type whose solution is found to be independent of the local Reynolds number but depends on another parameter referred to as the 'corner parameter' which is defined in Chapter 4.

The boundary conditions are then derived and it is found that the conditions for the corner layer as it asymptotes into the boundary layer are dependent only on the corner angle (i.e. they do not depend on the curvature of the corner).

2.2 Choice of coordinate system

The radiused corner constitutes a developable surface for which the following coordinate system is suitable

$$\left.\begin{aligned} y^1 &= x^1 \\ y^2 &= x^2 + \int_o^{x^3} \sin\lambda \, dx^3 \\ y^3 &= \int_o^{x^3} \cos\lambda \, dx^3 \end{aligned}\right\} \qquad (2.1)$$

y^i (i = 1,2,3) is an orthogonal cartesian coordinate system and x^1 is a non-orthogonal curvilinear coordinate system. Both systems have the same origin. λ is the angle measured from the axis y^3 to the tangent to the curve described by $x^2 = 0$, in the y^2-y^3 plane as shown in Fig. (2.1). The angle λ is chosen as a function of x^3 only.

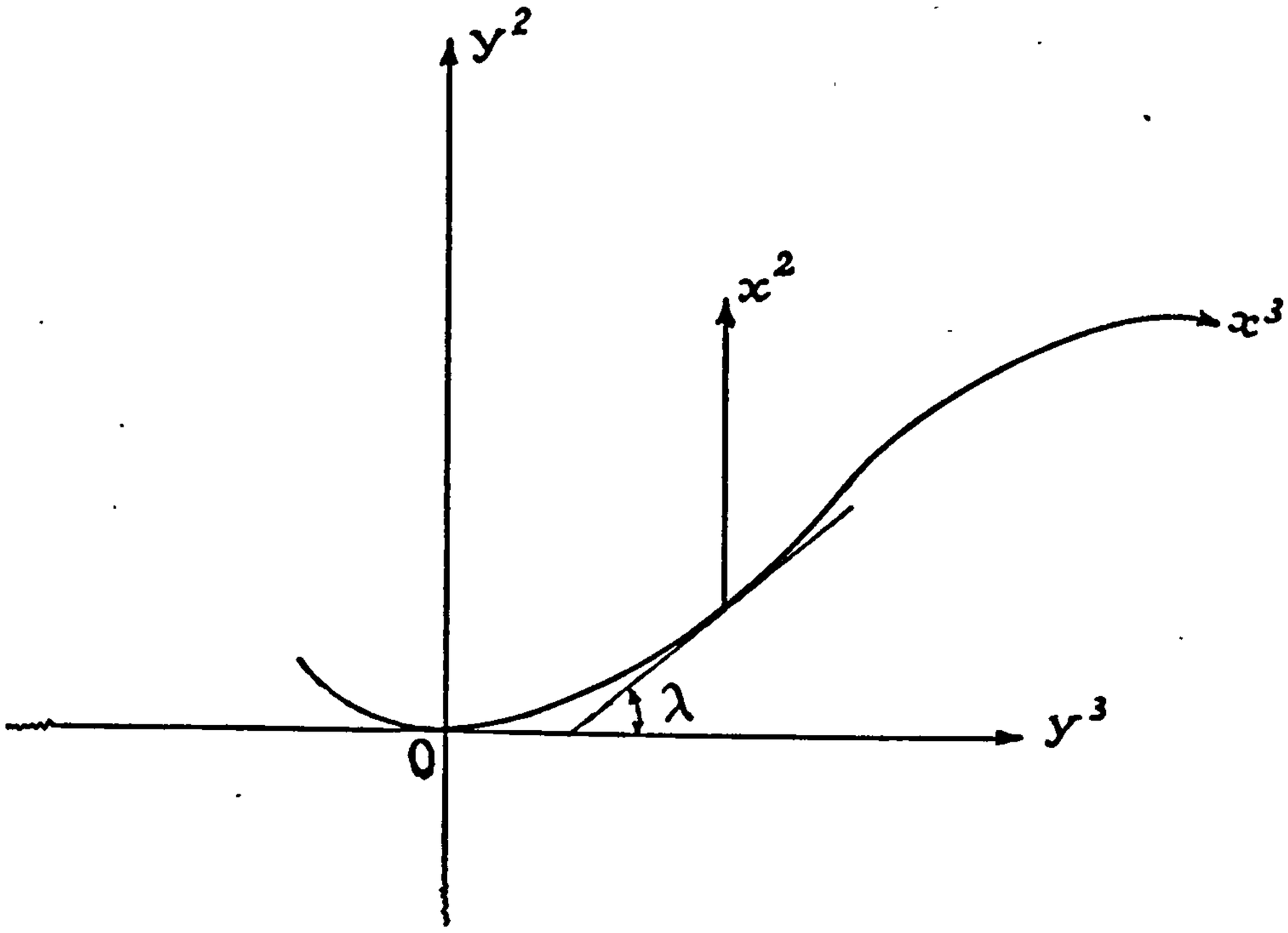

Fig. (2.1). Sketch of coordinate system, equn. (2.1).

The transformation (2.1) is defined by

$$dy^i = \ell^i_j \, dx^j \quad (i,j = 1,2,3) \qquad (2.2)$$

where the components ℓ^i_j are

$$\left.\begin{aligned} \ell^1_1 &= 1 & \ell^1_2 &= 0 & \ell^1_3 &= 0 \\ \ell^2_1 &= 0 & \ell^2_2 &= 1 & \ell^2_3 &= \sin\lambda \\ \ell^3_1 &= 0 & \ell^3_2 &= 0 & \ell^3_3 &= \cos\lambda \end{aligned}\right\} \quad (2.3)$$

The metric tensor g_{ij} is defined by

$$g_{ij} = \sum_{k=1}^{k=3} \ell^k_i \, \ell^k_j$$

and therefore has the components

$$\left.\begin{aligned} g_{11} &= 1 & g_{12} &= 0 & g_{13} &= 0 \\ & & g_{22} &= 1 & g_{23} &= \sin\lambda \\ & & & & g_{33} &= 1 \end{aligned}\right\} \quad (2.4)$$

The Jacobian of the transformation is

$$J = \ell^2_2 \, \ell^3_3 - \ell^2_3 \, \ell^3_2 = \sqrt{g_{22}g_{33} - (g_{23})^2}$$

i.e. $J = \cos\lambda \qquad (\cos\lambda \neq 0)$. (2.5)

2.3 Boundary layer equations

Consider a laminar steady flow of an incompressible viscous fluid along a developable surface as described by $x^2 = 0$. Let the origin of the coordinate system x^1 be at the leading edge and the free stream velocity be in the positive direction of x^1.

If v^i and v_i are respectively the contra-and co-variant components of the velocity vector in the direction of x^1, then the Navier-Stokes equations can be expressed as [23]

$$v^j v_{i;j} = -\frac{1}{\rho} p_{;i} + \nu \, g^{ik} v_{i;jk} \quad (2.6)$$

where a semi-colon before subscript i denotes covarient differentiation in the x^i direction, p is the pressure and ν is the kinematic viscosity. The continuity equation is

$$v^i_{;i} = 0 \qquad (2.7)$$

Written fully in the x^i coordinate system the three components of equations (2.6) are

$$v^1\frac{\partial v_1}{\partial x^1} + v^2\frac{\partial v_1}{\partial x^2} + v^3\frac{\partial v_1}{\partial x^3} = -\frac{1}{\rho}\frac{\partial p}{\partial x^1} + \nu\Delta v_1 \qquad (2.8a)$$

$$v^1\frac{\partial v_2}{\partial x^1} + v^2\frac{\partial v_2}{\partial x^2} + v^3\frac{\partial v_2}{\partial x^3} = -\frac{1}{\rho}\frac{\partial p}{\partial x^2} + \nu\Delta v_2 \qquad (2.8b)$$

$$v^1\frac{\partial v_3}{\partial x^1} + v^2\frac{\partial v_3}{\partial x^2} + v^3\left(\frac{\partial v_3}{\partial x^3} - C_r\cos\lambda\, v^2\right) = -\frac{1}{\rho}\frac{\partial p}{\partial x^3} +$$

$$+ \nu\Big\{\Delta v_3 + 2C_r\frac{\sin\lambda}{\cos^2\lambda}\frac{\partial v_2}{\partial x^2} - \frac{2C_r}{\cos^3\lambda}\frac{\partial v_2}{\partial x^3} -$$

$$- 2C_r\frac{\sin^2\lambda}{\cos^3\lambda}\frac{\partial v_3}{\partial x^2} + 2C_r\frac{\sin\lambda}{\cos^3\lambda}\frac{\partial v_3}{\partial x^3} -$$

$$-\frac{1}{\cos^2\lambda}\left[2\frac{C_r^2\sin\lambda}{\cos^2\lambda} + \frac{\partial}{\partial x^3}\left(\frac{C_r}{\cos\lambda}\right)\right]v_2 + \frac{1}{\cos^2\lambda}\left[2\frac{C_r^2\sin\lambda}{\cos^2\lambda} + \frac{\partial}{\partial x^3}\left(\frac{\sin\lambda}{\cos\lambda}C_r\right)\right]v_3\Big\} \qquad (2.8c)$$

where

$$\Delta = \frac{\partial^2}{(\partial x^1)^2} + \frac{1}{\cos^2\lambda}\left[\frac{\partial^2}{(\partial x^2)^2} - 2\sin\lambda\frac{\partial^2}{\partial x^2\partial x^3} + \frac{\partial^2}{(\partial x^3)^2}\right.$$

$$\left. - \frac{C_r}{\cos\lambda}\frac{\partial}{\partial x^2} + C_r\frac{\sin\lambda}{\cos\lambda}\frac{\partial}{\partial x^3}\right] \qquad (2.8d)$$

and the continuity equation is

$$\frac{\partial v^1}{\partial x^1} + \frac{\partial v^2}{\partial x^2} + \frac{\partial v^3}{\partial x^3} - C_r\frac{\sin\lambda}{\cos\lambda}v^3 = 0 \quad . \qquad (2.9)$$

Here C_r refers to the wall curvature and is given by

$$C_r = \frac{d\lambda}{dx^3} \tag{2.10}$$

The physical components of a tensor are

$$\begin{aligned} A(i) &= \sqrt{g_{ii}}\, A^i \\ &= \sqrt{g_{ii}}\, g^{ij} A_j \qquad \text{(no sum on i)} \end{aligned} \tag{2.11}$$

where A(i) is the physical components in the direction x^i of the vector $\vec{A}$. Accordingly the physical components of the velocity vector are

$$\left.\begin{aligned} v(1) &= \sqrt{g_{11}}\, v^1 = v^1 \\ v(2) &= \sqrt{g_{22}}\, v^2 = v^2 \\ v(3) &= \sqrt{g_{22}}\, v^3 = v^3 \end{aligned}\right\} \tag{2.12}$$

since $g_{11} = g_{22} = g_{33} = 1$ from expression (2.4), i.e. in this coordinate system there is no distinction between physical and contra-variant components. The covariant components in terms of the physical quantities are obtained from the relationship

$$v_i = g_{ij}\, v^j$$

Using (2.4) and (2.12) they are

$$\left.\begin{aligned} v_1 &= v(1) \\ v_2 &= v(2) + g_{23}\, v(3) \\ v_3 &= g_{23}\, v(2) + v(3) \end{aligned}\right\} \tag{2.13}$$

To derive the boundary layer equations it is convenient to express equations (2.8) and (2.9) in a non-dimensional form.

Let U_∞ be a typical velocity, L be a typical length and $R_e = LU_\infty/\nu \gg 1$ be the Reynolds number of the flow. Considering situations where the lateral curvature is of $O(R_e^{\frac{1}{2}})$ the following new variables are introduced,

$$\left.\begin{aligned}
&\bar{x}^1 = x^1/L \quad , \quad \bar{x}^2 = R_e^{1/2}\, x^2/L \quad , \quad \bar{x}^3 = R_e^{1/2}\, x^3/L \\
&\bar{v}^1 = v_{(1)}/U_\infty \quad , \quad \bar{v}^2 = R_e^{1/2}\, v_{(2)}/U_\infty \quad , \quad \bar{v}^3 = R_e^{1/2}\, v_{(2)}/U_\infty \\
&\bar{v}_2 = R_e^{1/2}\, v_2/U_\infty \quad , \quad \bar{v}_3 = R_e^{1/2}\, v_3/U_\infty \\
&p = \rho U_\infty^2 (\bar{p}_0 + R_e^{-1/2}\bar{p}_1 + R_e^{-1}\bar{p}_2 + \cdots) \quad , \quad \bar{C}_r = R_e^{-1/2} C_r L .
\end{aligned}\right\} \tag{2.14}$$

Substitution of (2.14) in (2.8), (2.9) and retaining only the lowest order terms in $R_e^{\frac{1}{2}}$ in each equation gives the following boundary layer equations

$$\bar{v}^1 \frac{\partial \bar{v}^1}{\partial \bar{x}^1} + \bar{v}^2 \frac{\partial \bar{v}^1}{\partial \bar{x}^2} + \bar{v}^3 \frac{\partial \bar{v}^1}{\partial \bar{x}^3} = - \frac{d\bar{p}_0}{d\bar{x}^1} + \bar{\nabla}^2 \bar{v}^1 \tag{2.15a}$$

$$\bar{v}^1 \frac{\partial \bar{v}_2}{\partial \bar{x}^1} + \bar{v}^2 \frac{\partial \bar{v}_2}{\partial \bar{x}^2} + \bar{v}^3 \frac{\partial \bar{v}_2}{\partial \bar{x}^3} = - \frac{\partial \bar{p}_1}{\partial \bar{x}^2} + \bar{\nabla}^2 \bar{v}_2 \tag{2.15b}$$

$$\begin{aligned}
&\bar{v}^1 \frac{\partial \bar{v}_3}{\partial \bar{x}^1} + \bar{v}^2 \frac{\partial \bar{v}_3}{\partial \bar{x}^2} + \bar{v}^3 \left(\frac{\partial \bar{v}_3}{\partial \bar{x}^3} - \bar{v}^2 \bar{C}_r \cos\lambda \right) \\
&\qquad = - \frac{\partial \bar{p}_2}{\partial \bar{x}^3} + \bar{\nabla}^2 \bar{v}_3 + 2 \frac{\bar{C}_r}{\cos^3\lambda} \Big[\\
&\qquad \sin\lambda \frac{\partial \bar{v}_2}{\partial \bar{x}^2} - \frac{\partial \bar{v}_2}{\partial \bar{x}^3} - \sin^2\lambda \frac{\partial \bar{v}_3}{\partial \bar{x}^2} + \sin\lambda \frac{\partial \bar{v}_3}{\partial \bar{x}^3} \Big] - \frac{1}{\cos^2\lambda} \Big[2 \frac{\sin\lambda}{\cos^2\lambda} \bar{C}_r^2 + \\
&\qquad + \frac{\partial}{\partial \bar{x}^3} \Big(\frac{\bar{C}_r}{\cos\lambda} \Big) \Big] \bar{v}_2 + \frac{1}{\cos^2\lambda} \Big[2 \frac{\sin\lambda}{\cos^2\lambda} \bar{C}_r^2 + \\
&\qquad + \frac{\partial}{\partial \bar{x}^3} \Big(\frac{\sin\lambda}{\cos\lambda} \bar{C}_r \Big) \Big] \bar{v}_3
\end{aligned} \tag{2.15c}$$

and

$$\frac{\partial \bar{v}^1}{\partial \bar{x}^1} + \frac{\partial \bar{v}^2}{\partial \bar{x}^2} + \frac{\partial \bar{v}^3}{\partial \bar{x}^3} - \frac{\sin\lambda}{\cos\lambda} \bar{C}_r \bar{v}^3 = 0 \tag{2.15d}$$

where

$$\bar{\nabla}^2 = \frac{1}{\cos^2\lambda}\left[\frac{\partial^2}{(\partial\bar{x}^1)^2} - 2\sin\lambda\frac{\partial^2}{\partial\bar{x}^1\partial\bar{x}^3} + \frac{\partial^2}{(\partial\bar{x}^3)^2} - \frac{\bar{C}_r}{\cos\lambda}\frac{\partial}{\partial\bar{x}^2} + \frac{\sin\lambda}{\cos\lambda}\bar{C}_r\frac{\partial}{\partial\bar{x}^3}\right]$$

and $d\bar{p}_o/dx^1$ is found from (2.15a) at $\bar{x}^2 \longrightarrow \infty$ where the free stream velocity distribution is assumed known. Here we consider a particular free stream velocity $U(\bar{x}^1)$ defined by

$$U(\bar{x}^1) = U_\infty\ \bar{x}^{1\,m} \qquad (2.16)$$

where m is a constant. From equation (2.15a) and the requirement that $\lim_{\bar{x}^2\to\infty} \bar{v}^1 = U(\bar{x}^1)/U_\infty$ we have

$$\frac{d\bar{p}_o}{d\bar{x}^1} = -\bar{v}^1\frac{\partial\bar{v}^1}{\partial\bar{x}^1} \qquad \text{at } \bar{x}^2 \longrightarrow \infty$$

whence $\dfrac{d\bar{p}_o}{d\bar{x}^1} = -\dfrac{m}{\bar{x}^1}\left(\dfrac{U(\bar{x}^1)}{U_\infty}\right)^2$.

The variables (2.14) were found helpful in keeping the development of the equations clear but the final equations are most conveniently expressed in terms of the following variables

$$\left.\begin{aligned} &\xi^1 = (2R_e)^{-1/2}(\bar{x}^1)^{-\frac{m+1}{2}}, \quad \xi^2 = \frac{\bar{x}^2}{\sqrt{2}}\bar{x}^{1\frac{m-1}{2}}, \quad \xi^3 = \frac{\bar{x}^3}{\sqrt{2}}\bar{x}^{1\frac{m-1}{2}} \\ &u = (\bar{x}^1)^{-m}\bar{v}^1, \quad \varphi = J[(1-m)\xi^2 u - v], \quad \psi = J[(1-m)\xi^3 u - w] \\ &\theta = \frac{1}{J}\left(\sigma_{,2} - \alpha_{,3} + \xi^3 k\cos\lambda\ (1-m)u\right), \quad P = 2\bar{p}_2(\bar{x}^1)^{-m+1} \end{aligned}\right\} \qquad (2.17a)$$

where a comma before a subscript i (i=1,2,3) refers to partial differentiation with respect to ξ^i ,

e.g. $\theta_{,i} = \dfrac{\partial\theta}{\partial\xi^i}$, and

$$
\left.
\begin{aligned}
v &= \sqrt{2}\,(\bar{x}^1)^{-\frac{m-1}{2}}\,\bar{v}^2 \\
w &= \sqrt{2}\,(\bar{x}^1)^{-\frac{m-1}{2}}\,\bar{v}^3 \\
\alpha &= (1-m)(\xi^2 + \xi^3 \sin\lambda)u - \sqrt{2}(\bar{x}^1)^{\frac{m-1}{2}}\bar{v}_2 = \frac{1}{J}(\varphi + \psi\sin\lambda) \\
\sigma &= (1-m)(\xi^2\sin\lambda + \xi^3)u - \sqrt{2}(\bar{x}^1)^{\frac{m-1}{2}}\bar{v}_3 = \frac{1}{J}(\varphi\sin\lambda + \psi) \\
\kappa &= \sqrt{2}\,\bar{C}_f\,(\bar{x}^1)^{\frac{-m+1}{2}} \quad .
\end{aligned}
\right\} \qquad (2.17b)
$$

The flow variable θ is related to the streamwise vorticity* $\omega(1)$ by

$$
\omega(1) = \frac{U_\infty}{2L}\,(\bar{x}^1)^{m-1}\left\{\frac{(1-m)}{J}\left[(\xi^2\sin\lambda + \xi^3)u_{,2} - (\xi^2 + \xi^3\sin\lambda)u_{,3}\right] - \theta\right\} . \qquad (2.17c)
$$

All dependent variables in (2.17) except κ and λ are function of ξ^1, ξ^2 and ξ^3. By definition

$$
\lambda \equiv \lambda(x^3/\ell) \qquad (2.18a)
$$

where ℓ is a length scale characterizing the body surface geometry. In terms of the new variables

$$
\lambda \equiv \lambda\left(\frac{\xi^3}{\xi^1 R_\ell}\right) \qquad (2.18b)
$$

where $R_\ell = (\ell/L)\,R_e(\bar{x}^1)^m$. Consequently

$$
\left.
\begin{aligned}
&\frac{d\lambda}{d\bar{x}^1} = 0 = (m-1)\,\xi^3\,\lambda_{,3} - (m+1)\xi^1\lambda_{,1} \\
&\text{and} \\
&\lambda_{,3} = \kappa \quad .
\end{aligned}
\right\} \qquad (2.19)
$$

---

* The physical component $\omega(i)$ of the vorticity vector is defined by

$$
\omega(i) = \sqrt{g_{ii}}\,\omega^i = \sqrt{g_{ii}}\,\frac{\epsilon^{ijk}}{J}\,v_{k,j}
$$

where
$$
\epsilon^{ijk} = \begin{cases} 0, & \text{if any of i,j,k are the same} \\ 1, & \text{if ijk is an even permutation of 123} \\ -1, & \text{if ijk is an odd permutation of 123.} \end{cases}
$$

On substituting expressions (2.17) into equations (2.15) we get

$$\nabla^2 u + \varphi u_{,2} + \psi u_{,3} + 2mc(1-u^2) = -c(m+1)\xi^1 u u_{,1} \qquad (2.21a)$$

$$(\varphi/c)\alpha_{,2} + (\psi/c)\alpha_{,3} - k\xi^3(1-m)u\psi + \xi^1(1+m)u\alpha_{,1} - \xi^1\xi^3 s_{,1}(1-m^2)u^2 -$$

$$-(1-m^2)(\xi^2+s\xi^3)u^2 + 2m(1-m)(\xi^2+s\xi^3) = -P_{,2} + \frac{1}{c}(\theta_{,3} - s\theta_{,2}) +$$

$$+ \frac{\xi^3 k(1-m)}{c} u_{,3} + \xi^1(1+m)u_{,12} - 2mu_{,2} \qquad (2.21b)$$

$$(\varphi/c)\sigma_{,2} + (\psi/c)\sigma_{,3} - k(\psi/c)\varphi + (1-m)k\xi^3 u\varphi - (1-m^2)(\xi^3+s\xi^2)u^2$$

$$+ (1+m)\xi^1\sigma_{,1}u + 2m(1-m)(s\xi^2+\xi^3) = -P_{,3} +$$

$$+ \frac{1}{c}(s\theta_{,3} - \theta_{,2}) + (1+m)\xi^1 u_{,13}$$

$$+ \frac{k\xi^3(1-m)}{c} u_{,2} - 2mu_{,3} \qquad (2.21c)$$

$$\varphi_{,2} + \psi_{,3} = (2c - k\xi^3 s(1-m))u -$$

$$-(1+m)\xi^1 c\, u_{,1} \qquad (2.21d)$$

where s and c denotes $\sin\lambda$ and $\cos\lambda$ respectively and the differential operator ∇^2 reads

$$\nabla^2 = \frac{1}{c}\left[\frac{\partial^2}{(\partial\xi^2)^2} - 2s\frac{\partial^2}{\partial\xi^2\partial\xi^3} + \frac{\partial^2}{(\partial\xi^3)^2}\right.$$

$$\left. - \frac{k}{c}\frac{\partial}{\partial\xi^2} + \frac{ks}{c}\frac{\partial}{\partial\xi^3}\right].$$

The pressure gradient terms $P_{,2}$ and $P_{,3}$ are eliminated by cross differentiation of equations (2.21b) and (2.21c) and subtracting the results to give

$$\nabla^2\theta + \varphi\theta_{,2} + \psi\theta_{,3} + 2u\left[(c - m\xi^3 c_{,3})\theta + m(1-m)\xi^3 \kappa c\, u + \right.$$

$$\left. + (1-m)(2\xi^2\xi^3\kappa c m - (1+m)(s\xi^2 + \xi^3))u_{,2} + ((\xi^2 + s\xi^3) - (\xi^3)^2 c\kappa)(1-m^2)u_{,3}\right]$$

$$=$$

$$c(1+m)\xi^1(\theta u_{,1} - u\theta_{,1}) + \xi^1(1+m)(u_{,3}\alpha_{,1} - u_{,2}\sigma_{,1}) + (1-m^2)\xi^1\xi^3\kappa c\, u u_{,1}$$

$$+ 2m(1-m)\xi^3\kappa c - \frac{(1-m)}{c^2}(s_{,3} + \xi^3 s_{,33} - 2\xi^3\kappa c_{,3})u_{,3} +$$

$$+ \frac{(1-m)\xi^3\kappa}{c}(u_{,22} - u_{,33}) \qquad (2.22a)$$

which is complemented by

$$c\theta = \frac{1}{c}(s\varphi_{,2} + \psi_{,2}) - \frac{1}{c}(\varphi_{,3} + s_{,3}\psi + s\psi_{,3}) +$$

$$+ \frac{c_{,3}}{c^2}(\varphi + s\psi) + \xi^3\kappa c(1-m)u \qquad (2.22b)$$

by definition (see equations (2.17)).

Equations (2.21a), (2.21d) and (2.22) govern completely the boundary layer development for a viscous incompressible fluid flowing over a developable surface characterized by a lateral curvature of $O(R_e^{\frac{1}{2}})$ at some finite value of ξ^3. The equations are evidently non-similar because they contain the stretched streamwise coordinate ξ^1 explicitly, and implicitly in κ and λ (equations (2.18b) and (2.19)). The difficulty associated with the non-similarity is that an exact solution to the equations requires an integration in the streamwise direction from a solution known at a particular value of ξ^1 in the region where $C_r \equiv O(R_e^{\frac{1}{2}})$. This solution promises to be extremely difficult to realise and even if obtained would still leave a problem prohibitive in computational terms. Fortunately the equations are not completely

intractable. By reformulation of the explicit ξ^i derivatives in terms of implicit and explicit components, the problem is greatly simplified by neglecting the explicit components (which are the primary source of trouble) while still retaining a non-similar character to the equations in the implicit components. The consequences of this simplification can be verified a posteriori.

The method is to regard $\xi^1 A,1$ as negligible compared to terms containing A where A refers to u,v or w. For example it is assumed that

$$\left.\begin{aligned} &\left|zCu - \xi^3 k S(1-m))\, u\right| \gg \left|(1+m)C\xi^1 u,_1\right| \quad \text{in (2.21d)} \\ &\text{and} \\ &\left|((\xi^2+S\xi^3) - (\xi^3)^2 Ck)\, u,_3\right| \gg \left|\xi^3 kC\xi^1 u,_1\right| \quad \text{in (2.22a).} \end{aligned}\right\} \quad (2.23)$$

The effects of the assumption on φ are deduced from its definition as given in expressions (2.17):

$$\begin{aligned} \xi^1 \varphi,_1 &= -\frac{(1-m)}{(1+m)}\xi^3 (\ln C),_3\, \varphi + C\xi^1[(1-m)\xi^2 u,_1 - v,_1] \\ &\approx -\frac{(1-m)}{(1+m)}\xi^3 (\ln C),_3\, \varphi \,. \end{aligned} \quad (2.24a)$$

Similarly

$$\left.\begin{aligned} \xi^1 \psi,_1 &\approx -\frac{(1-m)}{(1+m)}\xi^3 (\ln C),_3\, \psi \\ \xi^1 \alpha,_1 &\approx -\frac{(1-m)}{(1+m)}\xi^3 k\, \psi \\ \xi^1 \sigma,_1 &\approx -\frac{(1-m)}{(1+m)}\xi^3 k\, \varphi \\ \xi^1 \theta,_1 &\approx \left(\frac{1-m}{1+m}\right)\Big[\xi^3 (\ln C),_3\, \theta + \frac{1}{C}\xi^3 k(\psi,_3 - \varphi,_2) + \\ &\qquad + \frac{1}{C}(k + \xi^3 k,_3)\psi - \frac{1}{C}\xi^3 (S,_3 + \xi^3 S,_{33})(1-m)u\Big]. \end{aligned}\right\} \quad (2.24b)$$

Evidently the assumption entails no drastic change to the non-similarity in the governing equations as this manifests itself through the presence of λ and κ $(= \lambda_{,3})$ The final form of the boundary layer equations to be used in what follows is therefore

$$\nabla^2 u + \phi u_{,2} + \psi u_{,3} + 2mc(1-u^2) = 0 \qquad (2.25a)$$

$$\nabla^2\theta + \varphi\theta_{,2} + \psi\theta_{,3} + u\Big\{\Big[2(c - m\xi^3 c_{,3}) + (1-m)\xi^3 c(\ln c)_{,3}\Big]\theta$$

$$+ (1-m)\xi^3\big[2mkc - s_{,3} - \xi^3 s_{,33}\big]u + 2\big(\xi^2 + s\xi^3 - (\xi^3)^2 s_{,3}\big)X$$

$$X(1-m^2)u_{,3} + 2\big[2\xi^2\xi^3 kcm - (1+m)(s\xi^2 + \xi^3)\big](1-m)u_{,2} +$$

$$+ \xi^3 k(\psi_{,3} - \varphi_{,2}) + (k + \xi^3 k_{,3})\psi\Big\} + (1-m)\xi^3 k(\psi u_{,3} - \varphi u_{,2}) -$$

$$- 2m(1-m)\xi^3 kc + \frac{(1-m)}{c^2}\big(s_{,3} + \xi^3 s_{,33} - 2\xi^3 k c_{,3}\big)u_{,3} +$$

$$+ \frac{(1-m)}{c^2}\xi^3 k\,(u_{,33} - u_{,22}) = 0 \qquad (2.25b)$$

$$\varphi_{,2} + \psi_{,3} - (2c - (1-m)\xi^3 k s)u = 0 \qquad (2.25c)$$

$$s\varphi_{,2} + \psi_{,2} - (\varphi_{,3} + s_{,3}\psi + s\psi_{,3}) + (\ln c)_{,3}(\varphi + s\psi)$$

$$+ \xi^3 k c^2(1-m)u - c^2\theta = 0 \,. \qquad (2.25d)$$

2.4 Flow along a corner

2.4.1 Corner geometry

The corner is defined by specifying the behaviour of λ subject to satisfying.

(i) symmetry with respect to $x^3 = 0$,

(ii) $\lambda \longrightarrow$ constant $= \lambda^*$ (say) asymptotically within a distance of $O(R_e^{-\frac{1}{2}})$ from $x^3 = 0$.

For example for the configuration shown in Fig. (1.2a) we have

$$\left.\begin{array}{lll} \text{at} \quad x^3/\ell = 0 & & \lambda = 0, \\ \text{as} \quad x^3/\ell \longrightarrow \bar{x}\text{, where } \bar{x} \text{ is large but finite,} & & \lambda \longrightarrow \lambda^*, \\ \text{as} \quad x^3/\ell \longrightarrow -\bar{x} & & \lambda \longrightarrow -\lambda^*, \\ \text{and} \quad \left.\frac{d\lambda}{dx^3}\right|_{x^3=0} \equiv O(R_e^{\frac{1}{2}}) & . & \end{array}\right\} \quad (2.26)$$

λ^* defines the corner angle λ_c by

$$\lambda_c = \pi - 2\lambda^* \quad . \qquad (2.27)$$

2.4.2 Equations of motion in zero pressure gradient

An important case of corner flow is that for which the streamwise pressure gradient is zero and attention henceforth is confined to this situation. The governing equations are obtained directly from equations (2.25) on putting m = 0 and are

$$\nabla^2 u + \varphi u_{,2} + \psi u_{,3} = 0 \qquad (2.28a)$$

$$\begin{aligned} \nabla^2\theta + \varphi\theta_{,2} + \psi\theta_{,3} + u\{ & c(2+\xi^3(\ln c)_{,3})\theta - \\ & -\xi^3(s_{,3}+\xi^3 s_{,33})u + 2(\xi^2 + s\xi^3 - (\xi^3)^2 s_{,3})u_{,3} - \\ & -2(s\xi^2+\xi^3)u_{,2} + \xi^3\kappa(\psi_{,3}-\varphi_{,2}) + (\kappa+\xi^3\kappa_{,3})\psi\} + \\ & + \xi^3\kappa(\psi u_{,3} - \varphi u_{,2}) + \frac{1}{c^2}(s_{,3}+\xi^3 s_{,33} - 2\xi^3\kappa c_{,3})u_{,3} + \\ & + \frac{1}{c^2}\xi^3\kappa(u_{,33} - u_{,22}) = 0 \end{aligned} \qquad (2.28b)$$

$$\varphi_{,2} + \psi_{,3} - (2c - \xi^3\kappa s)u = 0 \qquad (2.28c)$$

$$\begin{aligned} s\varphi_{,2} + \psi_{,2} - (\varphi_{,3} + s_{,3}\psi + s\psi_{,3}) + (\ln c)_{,3}(\varphi + s\psi) \\ + \xi^3\kappa c^2 u - c^2\theta = 0 \quad . \end{aligned} \qquad (2.28d)$$

Utilizing the symmetry in the problem equations (2.28) are to be solved in the domain $0 \leqslant (\xi^2, \xi^3) < \infty$ subject to the boundary conditions derived in the following section.

2.4.3 Boundary conditions

(i) Conditions on the wall ($\xi^2 = 0$)

The no slip condition requires that

$$\left.\begin{aligned} \xi^2 = 0 \;;\; u = v = w = 0 \\ \text{i.e.} \qquad \varphi = \psi = 0 \end{aligned}\right\} \qquad (2.29a)$$

and from the defining equation (2.28d)

$$\theta = \frac{1}{c^2}\,\psi_{,2} \qquad (2.29b)$$

since $\varphi_{,2} = 0$ from the continuity equation, (2.28c).

(ii) Conditions on the symmetry plane ($\xi^3 = 0$)

The physical components v(1) and v(2) of the velocity vector are symmetric with respect to geometric symmetry plane ($y^3 = 0$) whereas v(3) and the streamwise vorticity $\omega(1)$ are anti-symmetric, i.e.

$$y^3 = 0; \quad \frac{\partial v(1)}{\partial y^3} = \frac{\partial v(2)}{\partial y^3} = v(3) = \omega(1) = 0 \qquad (2.30)$$

In terms of the variables involved in (2.17) these conditions are

$$\left.\begin{aligned} \xi^3 = 0; \qquad u_{,3} - s\,u_{,2} &= 0 \\ \varphi_{,3} - s\,\varphi_{,2} - \frac{c_{,3}}{c}\varphi + s\,c\,u &= 0 \\ \psi &= 0 \\ \theta &= 0 \;. \end{aligned}\right\} \qquad (2.31a)$$

A pre-condition for the validity of equations (2.31a) is that the coordinate system itself is continuous at the symmetry plane but the equations are otherwise completely general. For the radiused corner defined in (2.26) the symmetry conditions (2.31a) become

$$\left.\begin{aligned} \xi^3 = 0 \;; \qquad & u_{,3} = \varphi_{,3} = 0 \\ & \psi = \theta = 0 \\ \text{since} \qquad & \sin\lambda = \lambda = 0 \quad . \end{aligned}\right\} \qquad (2.31b)$$

The case of a sharp corner (infinite curvature at $\xi^3 = 0$) is easily dealt with by using, for example, the coordinate system shown in Fig. (2.2a). Referred to this system the boundary conditions (2.31a) apply directly.

For the more usual sharp corner (see Fig. (2.2b)) formed by intersecting plane walls the curvature of the surfaces ξ^2 = const. vanishes and the boundary conditions become

$$\left.\begin{aligned} \xi^3 = 0 \;; \qquad & u_{,3} - s\,u_{,2} = 0 \\ & \varphi_{,3} - s\,\varphi_{,2} + s\,c\,u = 0 \\ & \psi = \theta = 0 \quad . \end{aligned}\right\} \qquad (2.31c)$$

These results remind us that it is not necessary, if sometimes convenient, that the coordinate system is symmetric with respect to the physical plane of symmetry. Equations (2.31a) represent the condition that the flow is symmetrical about the plane $y^3 = 0$ and provided they are satisfied the precise form of the continuous coordinate system in which they are expressed is, to that extent, unimportant.

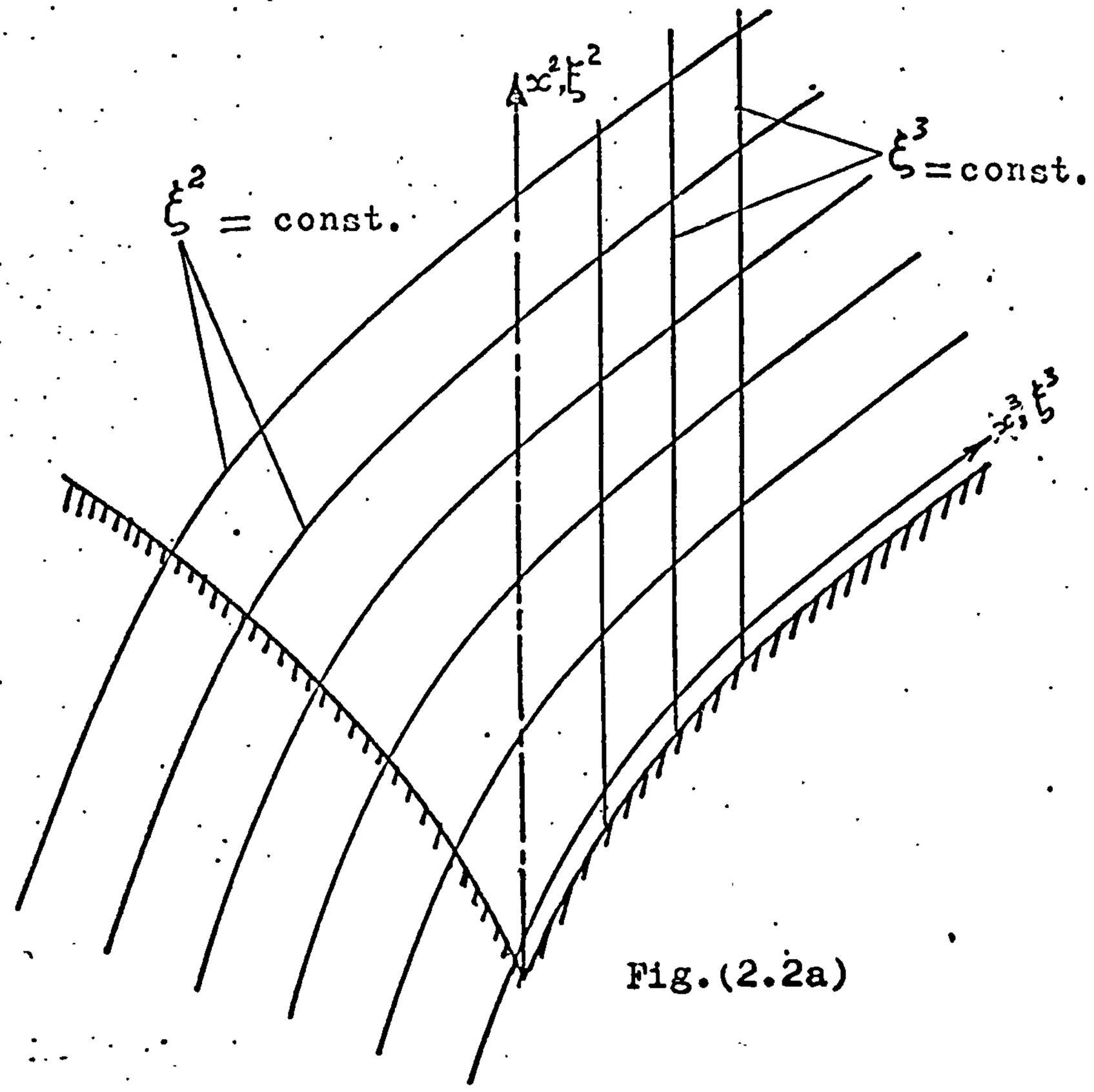

Fig.(2.2a)

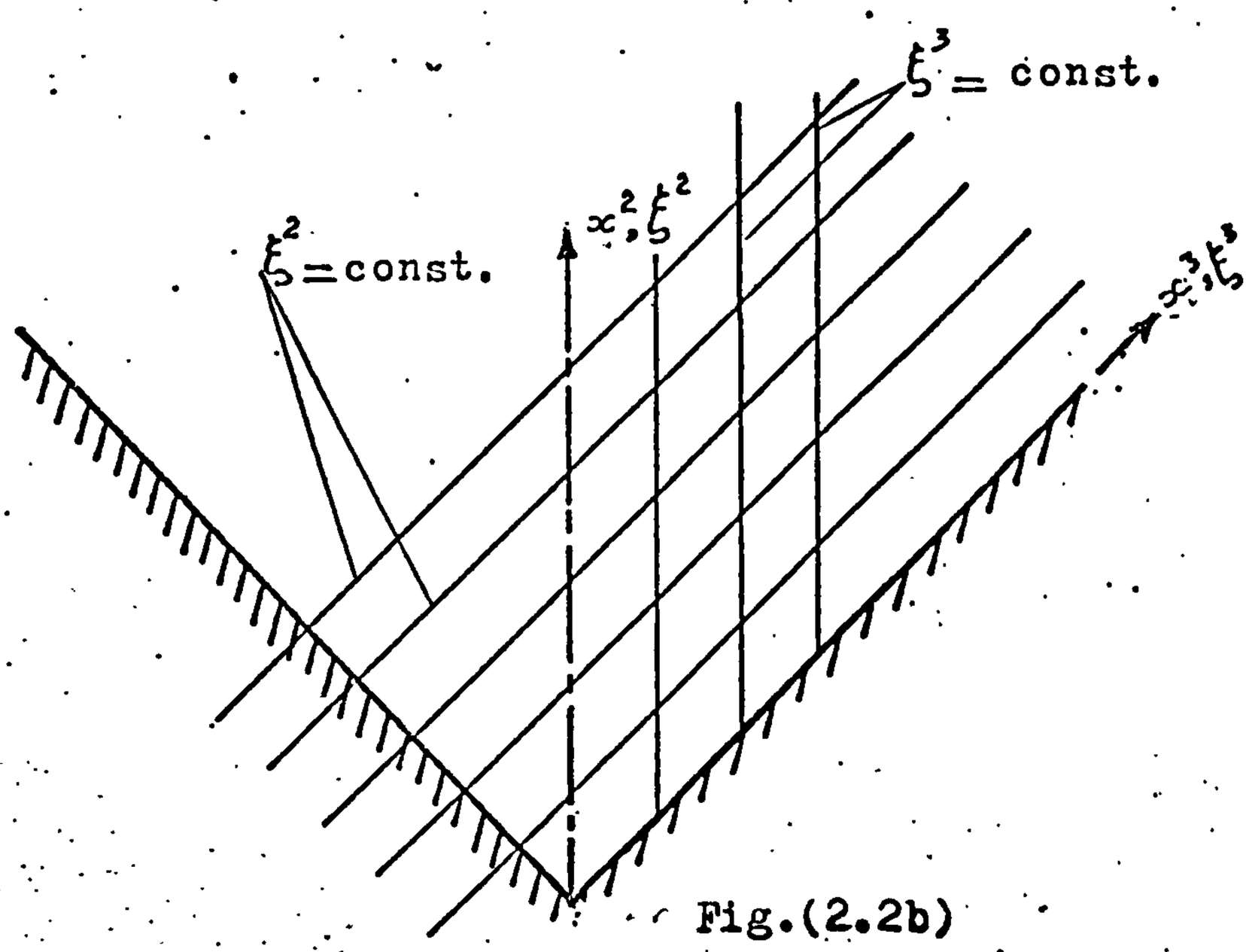

Fig.(2.2b)

Fig.(2.2) Co-ordinate systems used to treat sharp corner flow problems.

(iii) Conditions in the potential region ($\xi^2 \to \infty$)

As $\xi^2 \to \infty$, the streamwise velocity approaches its free stream value and the vorticity vanishes, i.e.

$$\left.\begin{aligned} &\xi^2 \to \infty \;;\; u \sim 1 \\ &\theta \sim 0 \text{ (see equation (2.17c))}. \end{aligned}\right\} \quad (2.32)$$

The conditions on φ and ψ at $\xi^2 \to \infty$ are less obvious but are nonetheless simply obtained from the requirement that the cross flow velocity vector becomes invarient (to $O(R_e^{-\frac{1}{2}})$) with respect to ξ^2 in this limit. In the absence of a streamwise pressure gradient this is the only physically acceptable condition. Consequently, in the present coordinate system the velocity components must also be independent of ξ^2 as $\xi^2 \to \infty$.

The variation in v and w with respect to ξ^3 when $\xi^2 \to \infty$ are found as follows:-

The continuity equation and the vorticity definition in terms of the velocity components u,v,w are

$$\left.\begin{aligned} -\xi^2 u_{,2} - \xi^3 u_{,3} + v_{,2} + \tfrac{1}{c}(cw)_{,3} &= 0 \\ -\Omega c + (w + s v)_{,2} - (v + s w)_{,3} &= 0 \end{aligned}\right\} \quad (2.33)$$

where $\Omega = \dfrac{2x^1}{U_\infty}\,\omega(1)$.

In the limit as $\xi^2 \to \infty$;

$$u_{,2} = u_{,3} = v_{,2} = w_{,2} = \Omega = 0$$

whence

$$(cw)_{,3} = 0$$

and

$$(v+sw)_{,3} = 0$$

i.e.

$$\left.\begin{aligned} cw &= \text{const.} \\ v+sw &= \text{const.} \end{aligned}\right\} \qquad (2.34)$$

From the symmetry condition (2.30) we have

$$\xi^2 \longrightarrow \infty, \ \xi^3 = 0; \quad W = 0$$

and since $c \neq 0$ then

$$\xi^2 \longrightarrow \infty; \qquad w = 0 \ (\text{for all } \xi^3 \geqslant 0). \qquad (2.35a)$$

Therefore

$$v = \text{const.} = \beta \quad \text{say, (for all } \xi^3 \geqslant 0). \qquad (2.35b)$$

β is, at present, an unknown constant whose value will be furnished by the need to match with the outflow from the boundary layer as $\xi^3 \longrightarrow \infty$ (Art. (iv) below).

The boundary conditions for φ and ψ now follow from (2.17) and (2.35) as

$$\left.\begin{aligned} \xi^2 \longrightarrow \infty; \qquad \varphi &\longrightarrow c(\xi^2 - \beta) \\ \psi &\longrightarrow c\,\xi^3. \end{aligned}\right\} \qquad (2.36)$$

(iv) <u>Conditions as $\xi^3 \longrightarrow \infty$</u>

These are found from the asymptotic analysis of equations (2.28) as $\xi^3 \longrightarrow \infty$. It is assumed that, for large ξ^3, the dependent flow variables can be represented by the following expansions*

---

* Equations (2.37a) are similar to those used by Pal and Rubin [10], see the following page.

$$\left.\begin{aligned} u &\sim \sum_{n=0}^{\infty} u_n(\xi^2)\,\xi^{3^{-n}}, \qquad \varphi \sim \sum_{n=0}^{\infty} \varphi_n(\xi^2)\,\xi^{3^{-n}}, \\ \theta &\sim \sum_{n=0}^{\infty} \theta_n(\xi^2)\,\xi^{3^{-n+1}}, \qquad \psi \sim \sum_{n=0}^{\infty} \psi_n(\xi^2)\,\xi^{3^{-n+1}}, \end{aligned}\right\} \quad (2.37a)$$

which are complemented by

$$v \sim \sum_{n=0}^{\infty} v_n(\xi^2)\,\xi^{3^{-n}}, \qquad w \sim \sum_{n=1}^{\infty} w_n(\xi^2)\,\xi^{3^{-n+1}}. \quad (2.37b)$$

In general all functions of λ require expansions similar to those in equations (2.37) but the algebraic labour is considerably eased on choosing $\lambda \longrightarrow \lambda^*$ exponentially. The essential physics of the problem, which is the primary interest, is quite unaffected by this convenience. With this choice the equations of motion (2.28) for large ξ^3 (and $\lambda = \lambda^*$) become

$$\nabla^{*2} u + c^* (\varphi u_{,2} + \psi u_{,3}) = 0 \quad (2.38a)$$

$$\nabla^{*2} \theta + c^* (\varphi \theta_{,2} + \psi \theta_{,3}) + 2uc^* [c^* \theta + (\xi^2 + s^* \xi^3) u_{,3} - (s^* \xi^2 + \xi^3) u_{,3}] = 0 \quad (2.38b)$$

$$\varphi_{,2} + \psi_{,3} - 2c^* u = 0 \quad (2.38c)$$

$$(s^* \varphi_{,2} + \psi_{,2}) - (\varphi_{,3} + s^* \psi_{,3}) - c^{*2} \theta = 0 \quad (2.38d)$$

where

$$\nabla^{*2} = \frac{\partial^2}{(\partial \xi^2)^2} - 2s^* \frac{\partial^2}{\partial \xi^2 \partial \xi^3} + \frac{\partial^2}{(\partial \xi^3)^2}$$

and s^*, c^* are respectively $\sin \lambda^*$, $\cos \lambda^*$.

Placing series (2.37a) into equations (2.38) and retaining terms of equal order in ξ^3 gives the following equations

zeroth order

$$u_o'' + c^* \varphi_o u_o' = 0 \qquad (2.39a)$$

$$\theta_o'' + c^* \varphi_o \theta_o' + c^* \psi_o \theta_o + 2 c^* u_o (c^* \theta_o - u_o') = 0 \qquad (2.39b)$$

$$\varphi_o' + \psi_o - 2 c^* u_o = 0 \qquad (2.39c)$$

$$c^{*2} \theta_o - \psi_o' = 0 \qquad (2.39d)$$

nth Order (n=1,2,3,...)

$$u_n'' + c^* \varphi_o u_n' - n c^* \psi_o u_n + c^* u_o' \varphi_n = A_n \qquad (2.40a)$$

$$\theta_n'' + c^* \varphi_o \theta_n' + [c^*(1-n)\psi_o + 2 c^{*2} u_o] \theta_n - 2 c^* u_o u_n' +$$

$$+ 2c^* (c^* \theta_o - u_o') u_n + c^* \theta_o' \varphi_n + c^* \theta_o \psi_n = B_n \qquad (2.40b)$$

$$\varphi_n' - (n-1) \psi_n - 2 c^* u_n = 0 \qquad (2.40c)$$

$$c^{*2} \theta_n - \psi_n' = C_n \qquad (2.40d)$$

where a prime denotes differentiation with respect to ξ^2.

Here,

$$A_n = -(n-2)(n-1) u_{n-2} - 2 s^* (n-1) u_{n-1}' + \\ + c^* \sum_{i=1}^{n-1} [(n-i) \psi_i u_{n-i} - \varphi_i u_{n-i}'] \qquad (2.41a)$$

$$B_n = -(n-2)(n-3) \theta_{n-2} - 2 s^* (n-2) \theta_{n-1}' + \\ + 2 c^* s^* u_o' u_{n-1} + c^* \sum_{i=1}^{n-1} [(n-i-1) \psi_i \theta_{n-i} - \\ - \varphi_i \theta_{n-i}' - 2 c^* u_i \theta_{n-i} + 2 u_i u_{n-i}' + \\ + 2 s^* (n-i) u_{i-1} u_{n-i} + 2 \xi^2 s^* u_{i-1} u_{n-i-1}'] + 2 c^* \xi^2 \sum_{i=1}^{n} (n-i-1) u_{i-1} u_{n-i-1} \qquad (2.41b)$$

and

$$C_n = s^* (n-2) \psi_{n-1} + s^* \varphi_{n-1}' + (n-2) \varphi_{n-2} \quad . \qquad (2.41c)$$

Sums with upper limit less than one in equations (2.41) are defined as zero.

In addition to equations (2.39) and (2.40) one obtains the following complementary equations:-

zeroth order

$$\varphi_o = c^*(\xi^2 u_o - v_o) \qquad (2.42a)$$

$$\psi_o = c^* u_o \qquad (2.42b)$$

nth order

$$\varphi_n = c^*(\xi^2 u_n - v_n) \qquad (2.42c)$$

$$\psi_n = c^*(u_n - w_n) \qquad (2.42d)$$

by substituting (2.37) into (2.17).

The appropriate boundary conditions of the system of equations (2.39), (2.40) and (2.42) are found by placing series (2.37) into boundary conditions (2.29), (2.32), (2.35) and (2.36) to get

$$\left.\begin{aligned} &\xi^2 = 0 \;; \quad u_n = v_n = w_n = \varphi_n = \psi_n = 0 \quad (n=0,1,2,\ldots) \\ &\xi^2 \to \infty \;; \quad u_o = 1 \,, w_1 = 0 \,, \quad \varphi_o = c^*(\xi^2 - \beta), \psi_o = c^* \,, \theta_o = 0 \\ &\qquad\qquad \psi_n = u_n = \varphi_n = w_n = 0 \quad (n=1,2,3,\ldots) \end{aligned}\right\} (2.43)$$

The substitutions $u_o = f'$, $\varphi = c^* f$, which satisfy (2.39c) identically, transforms (2.39a) and its boundary conditions to

$$f''' + c^{*2} f f'' = 0$$

and
$$\left.\begin{aligned} \xi^2 &= 0; \quad f = f' = 0 \\ \xi^2 &\to \infty; \quad f' \to 1 . \end{aligned}\right\} \quad (2.44)$$

This is just the Blasius flat plate problem in an oblique cartesian coordinate system. Its solution is well known and the details are omitted here (see ref. [24], p. 223). The full solution of equations (2.39) are therefore

$$\left.\begin{aligned} u_o &= f' \quad , \quad \varphi_o = c^* f \\ \theta_o &= (1/c^*)\, f'' \quad , \quad \psi_o = c^* f' \end{aligned}\right\} \quad (2.45)$$

and from (2.42)

$$v_o = \xi^2 f' - f. \quad (2.46)$$

Consequently

$$\beta = \lim_{\xi^2 \to \infty} (v_o) = \lim_{\xi^2 \to \infty} (\xi^2 f' - f). \quad (2.47)$$

First order equations (n = 1)

The equations for φ_1 and u_1 are

$$\frac{1}{c^*}\varphi_1''' + c^* f \varphi_1'' - c^* f' \varphi_1' + 2 c^* f'' \varphi_1 = 0$$

$$\varphi_1' - 2 c^* u_1 = 0 \quad , \text{ (since } A_1 = 0\text{)}$$

with $\xi^2 = 0 \quad ; \quad \varphi_1 = 0$

$$\xi^2 \to \infty ; \quad \varphi_1 = 0 .$$

The only possible solution of this system of equations and boundary conditions is $\varphi_1 = u_1 = 0$. Consequently equation (2.40d) yields

$$\theta_1 = \frac{1}{c^{*2}} \psi_1' \quad (2.48)$$

which on substituting in the governing equation for θ_1 gives

$$\frac{1}{c^{*2}}\psi_1''' + f\psi_1'' + 2f'\psi_1' + f''\psi_1 = 2\frac{s^*}{c^*}f''' + 2c^*s^*\xi^2 f'f'' . \quad (2.49)$$

The boundary conditions are

$$\left.\begin{aligned} \xi^2 = 0 \;; \quad \psi_1 = 0 \\ \xi^2 \longrightarrow \infty \;; \quad \psi_1 = 0 \end{aligned}\right\}$$

Equation (2.49) has the closed form solution (see Appendix (B))

$$\psi_1 = -c^{*3}s^*\beta f'' \int_0^{\xi^2} \frac{\eta-\beta}{f''(\eta)}\,d\eta + s^*c^*(\xi^2 f' - f) . \quad (2.50)$$

Placing this result in (2.48) yields

$$\theta_1 = -c^*s^*\beta\left[f''' \int_0^{\xi^2} \frac{\eta-\beta}{f''(\eta)}\,d\eta + (\xi^2-\beta)\right] + \frac{s^*}{c^*}\xi^2 f'' . \quad (2.51)$$

Second order equations (n = 2)

Here,

$$A_2 = B_2 = C_2 = 0 .$$

It can be shown from equations (2.40) and (2.42d) with some algebra that

$$\frac{1}{c^{*2}}w_2''' + (fw_2')' = 0$$

with

$$\left.\begin{aligned} \xi^2 = 0 \;; \quad w_2 = 0 \\ \xi^2 \longrightarrow \infty \;; \quad w_2 = 0 \end{aligned}\right\} \quad (2.52)$$

Like the equation for φ_1 this is a homogeneous problem for which the only possible solution is $w_2=0$. Similarly it is found that $u_2 = \varphi_2 = \theta_2 = 0$. In general for $n \geqslant 2$,

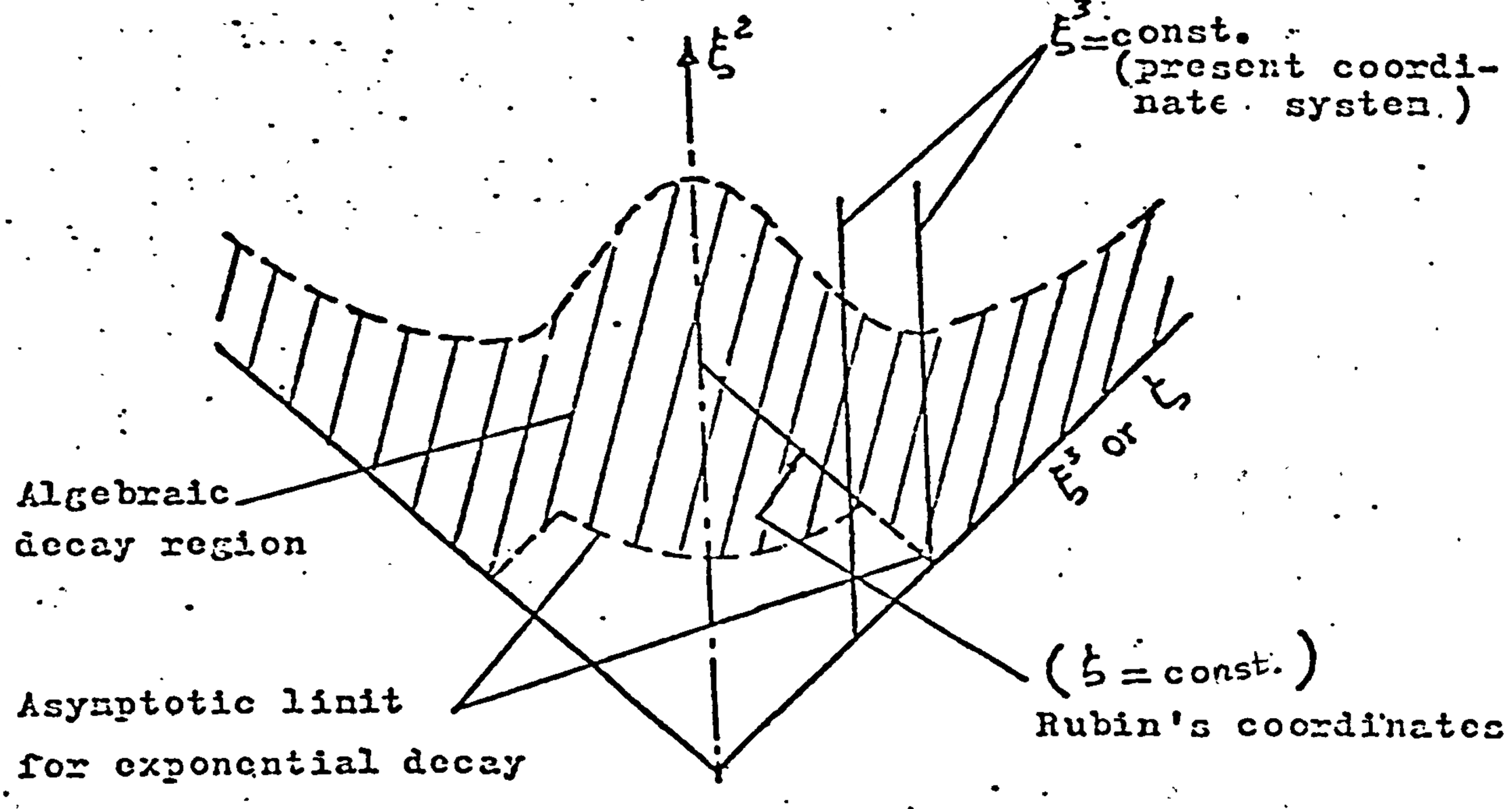

Fig.(2.3) A sketch illustrating the role of co-ordinate systems with respect to algebraic decay of the flow variables.

equations (2.40) have the solutions $U_n = \varphi_n = \psi_n = \theta_n = 0$, and consequently $v_n = w_n = 0$.

The vanishing of the algebraic terms in the crossflow components seems to imply an exponential decay into the boundary layer. This would normally be an eminently satisfactory result since it means that boundary conditions could be applied at moderate values of the coordinates; satisfactorily that is, were it not for the fact that the analysis by Pal and Rubin [10] and the solutions by Rubin and Grossman [11] and Ghia [14] exhibit an algebraic decay that we have been seeking. Evidently the different coordinate systems used play a part in this apparently paradoxical result and their role is illustrated in Fig. (2.3). The algebraically decaying region must necessarily be of a form such as is shown. The consequence for the expansion (2.37) in Rubin's coordinates and the present system is evident. In Rubin's system one boundary is on the symmetry line and the condition there must acknowledge the algebraic decay whereas in the present coordinates the equations to be solved on any ξ^3 line permit the use of a boundary condition in the potential region. Since the assumed series provides no other mechanism for bringing out the algebraic decay, the phenomenon is missed entirely and the results of the series are therefore only valid strictly at $\xi^3 \longrightarrow \infty$.

Knowing that the algebraic decay is there, we may not use equations (2.39)-(2.42) at any finite ξ^3 and practical considerations would appear to preclude their application at infinite ξ^3 without first introducing a transformation to map the infinite range of ξ^3 into the finite range of a

new variable. An alternative way through the difficulty is to seek a series expansion that better represents the flow behaviour at large ξ^3 . The most immediately profitable approach is to employ the mapping scheme and is the alternative used to obtain the numerical results given later. The asymptotic conditions are directly applicable in this situation and collecting them for convenience, they are

$$\left.\begin{aligned} \xi^3 \to \infty\ ; \quad u &= f' \\ \theta &= \frac{1}{c^*}\xi^3 f'' - c^* s^* \beta \left[f'' \int_0^{\xi^2} \frac{\eta-\beta}{f''(\eta)} d\eta + \right. \\ &\qquad \left. + (\xi^2-\beta) \right] + \frac{s^*}{c^*}\xi^2 f' \\ \varphi &= c^* f \\ \psi &= c^*\xi^3 f' - c^{*3} s^* \beta f'' \int_0^{\xi^2} \frac{\eta-\beta}{f''(\eta)} d\eta + s^* c^* (\xi^2 f' - f). \end{aligned}\right\} \quad (2.53)$$

The boundary layer flow along a corner is completely specified by equations (2.28) and boundary conditions (2.29), (2.31), (2.32), (2.36) and (2.53).

The method of solution adopted avoids the need for studying the nature of the decay into the boundary layer, but it is emphasised as a matter of some importance that the decay of the crossflow is algebraic in both ξ^2 and ξ^3 . This is demonstrated by the analysis of the following section.

2.5 Asymptotic decay of the crossflow

To show the algebraically decaying character of the crossflow it is sufficient to consider the flow for ξ^2 large (ξ^3 arbitrary). This simplifies the analysis.

If it is shown that the decay is algebraic in this region then it is algebraic for the corner as a whole and the matter is settled. Consistent with this observation the following series is chosen

$$\left.\begin{aligned} v &= \hat{v}_0 + \frac{1}{t}\hat{v}_1 + \frac{1}{t^2}\hat{v}_2 + \frac{1}{t^3}\hat{v}_3 + O(t^{-4}) \quad , \\ w &= \hat{w}_0 + \frac{1}{t}\hat{w}_1 + \frac{1}{t^2}\hat{w}_2 + \frac{1}{t^3}\hat{w}_3 + O(t^{-4}) \quad . \end{aligned}\right\} \tag{2.54}$$

$\hat{v}_n$ and $\hat{w}_n$ $(n = 0,1,2,..)$ are functions of ζ^3 only and

$t = \zeta^2 + \tilde{s}\,\zeta^3$ for large ζ^2 and arbitrary ζ^3

$$\text{where } \tilde{s} = \begin{cases} +\sin\lambda & \text{for } \lambda^* > 0 \quad (\pi > \lambda_c > 0) \\ -\sin\lambda & \text{for } \lambda^* < 0 \quad (2\pi > \lambda_c > \pi) \, . \end{cases}$$

Equations (2.54) are to be used in conjunction with the continuity equation and streamwise vorticity definition (equations (2.33)).

The series is designed to satisfy the asymptotic conditions:

ζ^3 fixed, $\zeta^2 \to \infty$; $v = \hat{v}_0 \to \beta$ (see equations (2.35))

$w = \hat{w}_0 \to 0$

ζ^2 fixed but large, $\zeta^3 \to \infty$; $v = \hat{v}_0 \to \beta$

$w = \hat{w}_0 \to 0$.

The analytical simplification stems from the fact that for

ζ^2 large ; $u \sim 1$, $\Omega \sim 0$.

whereupon equations (2.33) reduce to the approximation

$$\left.\begin{aligned} v_{,2} + \frac{1}{c}(cw)_{,3} &\sim 0 \\ (w+sv)_{,2} - (sw+v)_{,3} &\sim 0 \,. \end{aligned}\right\} \quad (2.55)$$

Substituting series (2.54) into (2.55) and retaining terms of the same order in t, the following equations are obtained

Zeroth order

$$\left.\begin{aligned} (c\hat{w}_o)_{,3} &= 0 \\ (s\hat{w}_o+\hat{v}_o)_{,3} &= 0 \end{aligned}\right\} \quad (2.56a)$$

First order

$$\left.\begin{aligned} (c\hat{w}_1)_{,3} &= 0 \\ (s\hat{w}_1+\hat{v}_1)_{,3} &= 0 \end{aligned}\right\} \quad (2.56b)$$

Second order

$$\left.\begin{aligned} -\hat{v}_1+\tfrac{1}{c}(c\hat{w}_2)_{,3} &= 0 \\ -(s\hat{v}_1+\hat{w}_1)+(\tilde{s}\,\zeta^3)_{,3}\,(\hat{v}_1+s\hat{w}_1) & \\ -(\hat{v}_2+s\hat{w}_2)_{,3} &= 0 \,. \end{aligned}\right\} \quad (2.56c)$$

The boundary conditions are

$$\left.\begin{aligned} \zeta^3 = 0 \quad ; \ \hat{w}_o = \hat{w}_1 = \hat{w}_2 = 0 \\ \text{and at} \quad \zeta^3 \to \infty \ ; \ \hat{v}_o = \beta \,. \end{aligned}\right\} \quad (2.56d)$$

Equations (2.56a) have the solution $\hat{v}_o = \beta$, $\hat{w} = 0$.

Integrating equations (2.56b) gives

$$\left.\begin{aligned} c\hat{w}_1 &= \text{constant} \\ s\hat{w}_1 + \hat{v}_1 &= \text{constant} \,. \end{aligned}\right\} \quad (2.57)$$

Like equations (2.34), the solution of (2.57) is

$$\hat{v}_1 = \text{constant} \equiv \epsilon \quad , \quad \hat{w}_1 = 0$$

From equations (2.56c) we have by integration

$$\hat{w}_2 = \frac{\epsilon}{c}\left[c^* \zeta^3 + \int_0^{\zeta^3} (c - c^*)\, d\zeta^3\right] \tag{2.58a}$$

and consequently

$$\hat{v}_2 = \epsilon\left[\zeta^3\left(\tilde{s} - s^* - \frac{s}{c}c^*\right) + \int_0^{\zeta^3} (s^* - s)\, d\zeta^3 - \frac{s}{c}\int_0^{\zeta^3} (c - c^*)\, d\zeta^3\right].$$

The constant ϵ can be determined from the numerical solution by using an approach similar to that employed in reference [11] to find the constant encountered on solving the right-angled sharp corner problem.

Terms of higher order in series (2.54) can be determined if desired. The terms obtained however are sufficient to show the algebraic nature of the decay of the crossflow in the ζ^2 and ζ^3 direction.

Series (2.54) while being adequate for its purpose is not the only form that may be used. For example the series

$$v = \hat{v}_0 + \frac{\ln t}{t}\hat{v}_1 + \frac{(\ln t) - 1}{t}\hat{v}_2 + \frac{(2\ln t) - 3}{t^3}\hat{v}_3 + O(t^{-4}) \tag{2.59}$$

and a similar form for w will also yield the solution (2.57) and (2.58). Pal and Rubin [10] showed in an asymptotic analysis for the 90° sharp corner problem that logarithmic terms arise in the fifth and higher order terms in a series solution. The use of equation (2.59) or indeed a linear

combination of (2.54) and (2.59) might suitably anticipate the appearance of logarithmic behaviour. This is a matter of detail only; the algebraic decay is evident whichever series is used.

2.6 Remarks on the asymptotic crossflow velocity w

The crossflow velocity w at $\xi^3 \to \infty$ is found from equations (2.42b,d) and (2.53) together with the definition of ψ to be

$$w = c^{*2} s^* \beta f'' \int_0^{\xi^2} \frac{\eta - \beta}{f''(\eta)} d\eta \quad - \quad s^*(\xi^2 f' - f) \ . \qquad (2.60)$$

This result is a generalization of that derived in references [9] and [13] in the case of a rectangular sharp corner. This can be shown by referring equation (2.60) to an orthogonal cartesian coordinate system where the wall of the corner (at large ξ^3) constitutes one of the coordinate surfaces. If v^* and w^* are respectively the components of the crossflow vector normal and parallel to the wall and η represents the stretched coordinate perpendicular to the wall then we have

$$\left.\begin{aligned} \eta &= \xi^2 \cos \lambda^* \\ v^* &= v \cos \lambda^* \ , \ w^* = w + v \sin \lambda^* \ . \end{aligned}\right\} \qquad (2.61)$$

Substituting (2.61) into (2.46) and (2.60) gives

$$\left.\begin{aligned} v^* &= \eta \ \dot{F}(\eta) \quad - F(\eta) \\ w^* &= \beta_0 \tan \lambda^* \ \ddot{F}(\eta) \int_0^{\eta} \frac{\tau - \beta_0}{\ddot{F}(\tau)} d\tau \end{aligned}\right\} \qquad (2.62a)$$

where $F(\eta)$ is the Blasius function in the new coordinate system, a dot denotes differentiation with respect to η and β_0 is given by

$$\beta_o = \lim_{\eta \to \infty} (\eta \quad \dot{F}(\eta) \qquad - F(\eta)) \tag{2.62b}$$

or, in terms of the ξ^i coordinate system variables, by

$$\beta_o = \beta \cos \lambda^* \ . \tag{2.62c}$$

Equations (2.62) show clearly that the asymptotic cross-flow velocity vector is independent of the wall curvature variations and depends only on the corner angle. For a 90^o corner angle $\lambda^* = 45^o$ and when substituted in (2.62) yields the same crossflow velocity obtained in references [9] and [13].

Throughout the development so far there has been the tacit assumption that $w^*/v^* = 0(1)$ (for $\eta > 0$). It is evident that this condition will be violated for $|\lambda^*|$ in the vicinity of 90^o (corner angle $\lambda_c \sim 0^o$ or 360^o). This points to a changed character in the problem which will require some alternative formulation such as that given to the flow past the side-edge of a quarter infinite flat plate by Stewartson and Howarth [25] and Stewartson [12].

The velocity w^* from (2.62∂) can be written as

$$w^* = \beta_o \tan \lambda^* \quad H(\eta) \ . \tag{2.62d}$$

β_o and $H(\eta)$ are independent of λ^* and $H(\eta)$ is shown in Fig.(2.4). w^* therefore changes sign with λ^*. For example the distribution of w^* for $\lambda^* = -45^o$ is a mirror image of that for $\lambda^* = +45^o$. This remarkable antisymmetry in w^* with respect to λ^* is explained when we understand the controlling influence of the potential flow on the boundary layers.

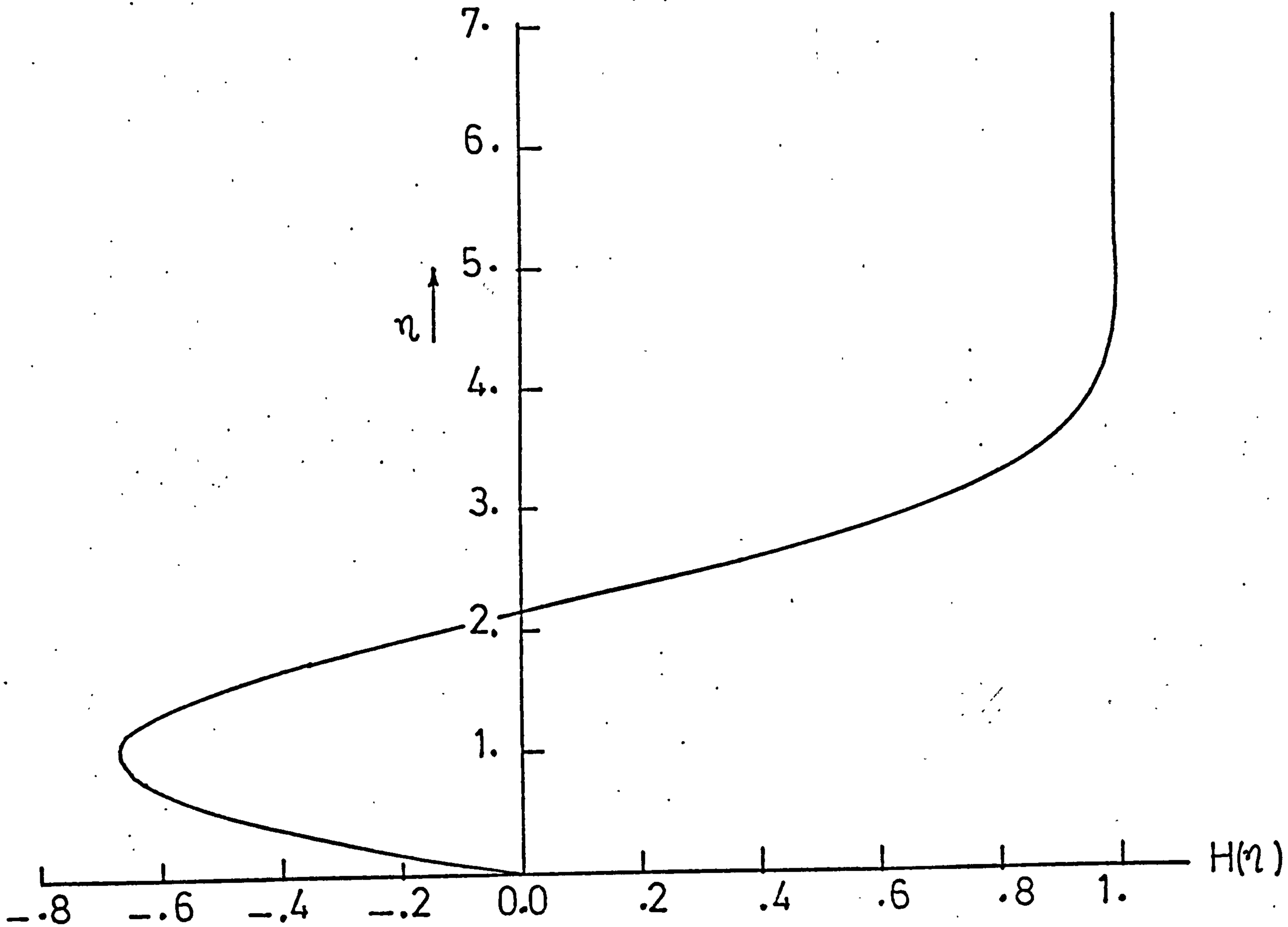

Fig.(2.4)

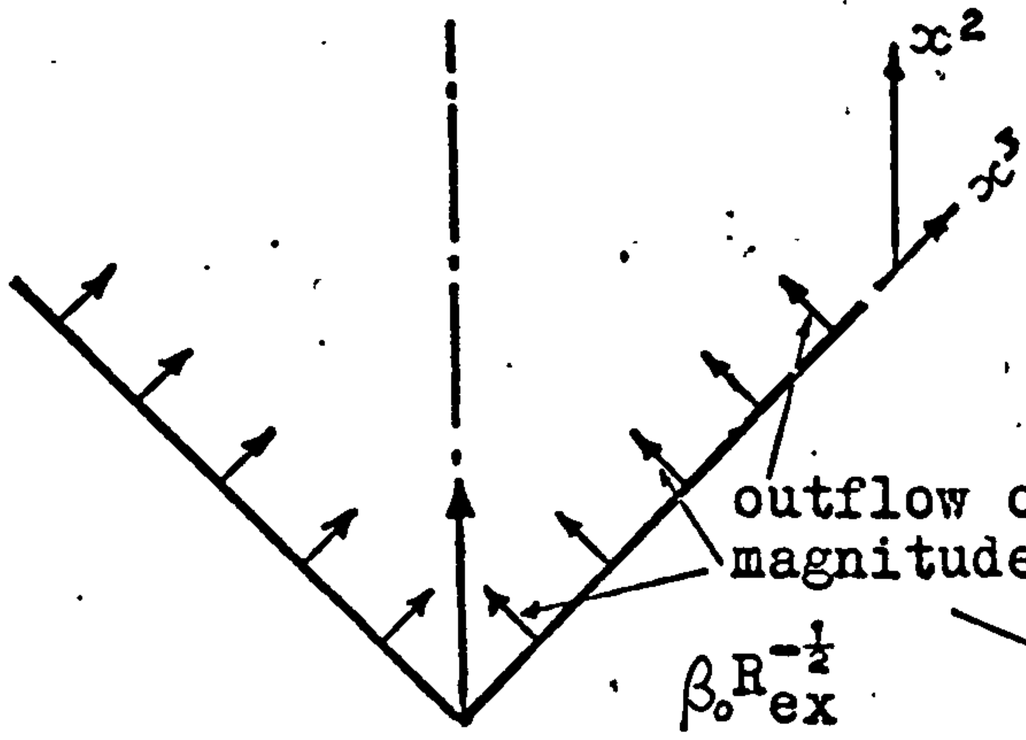

Fig.(2.5a)

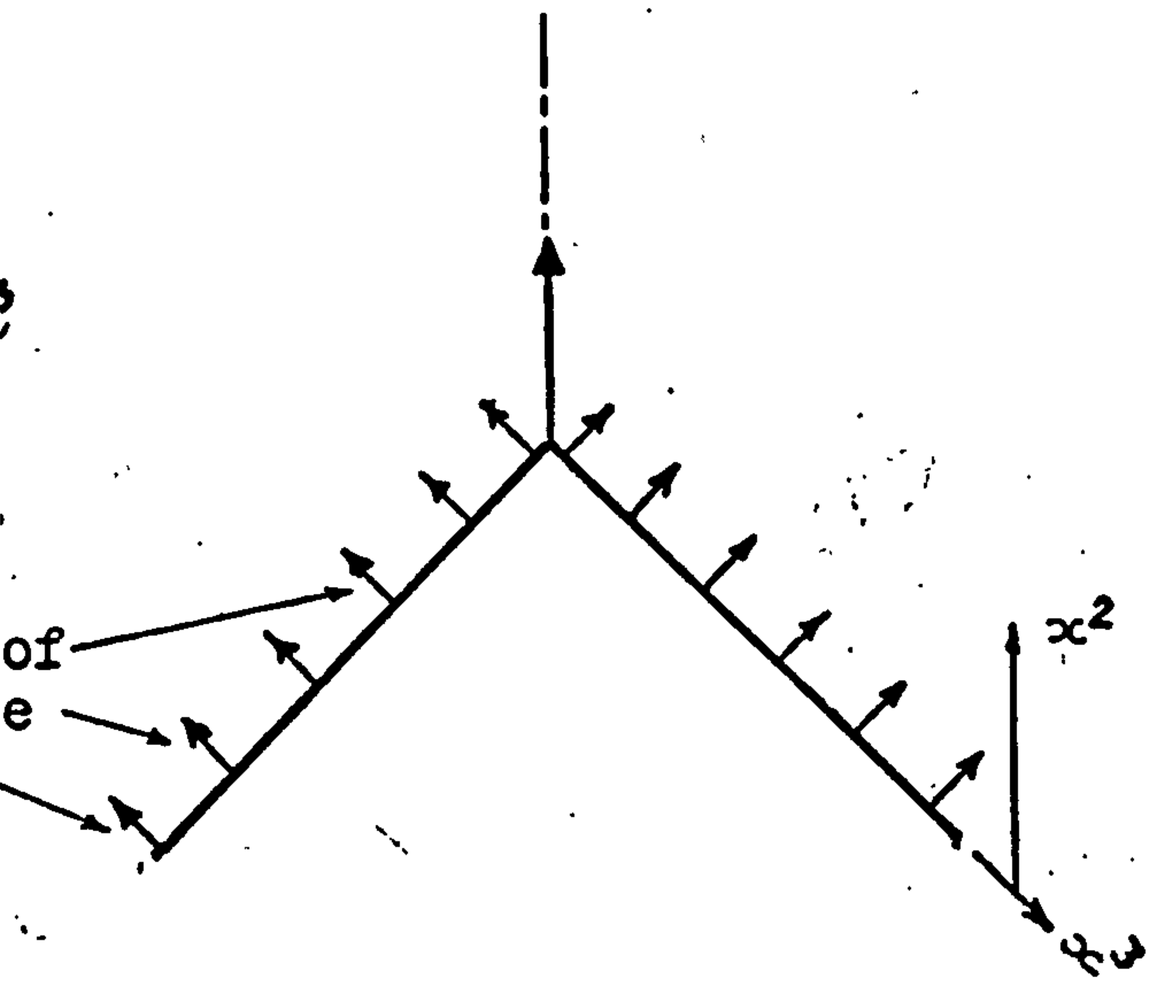

Fig.(2.5b)

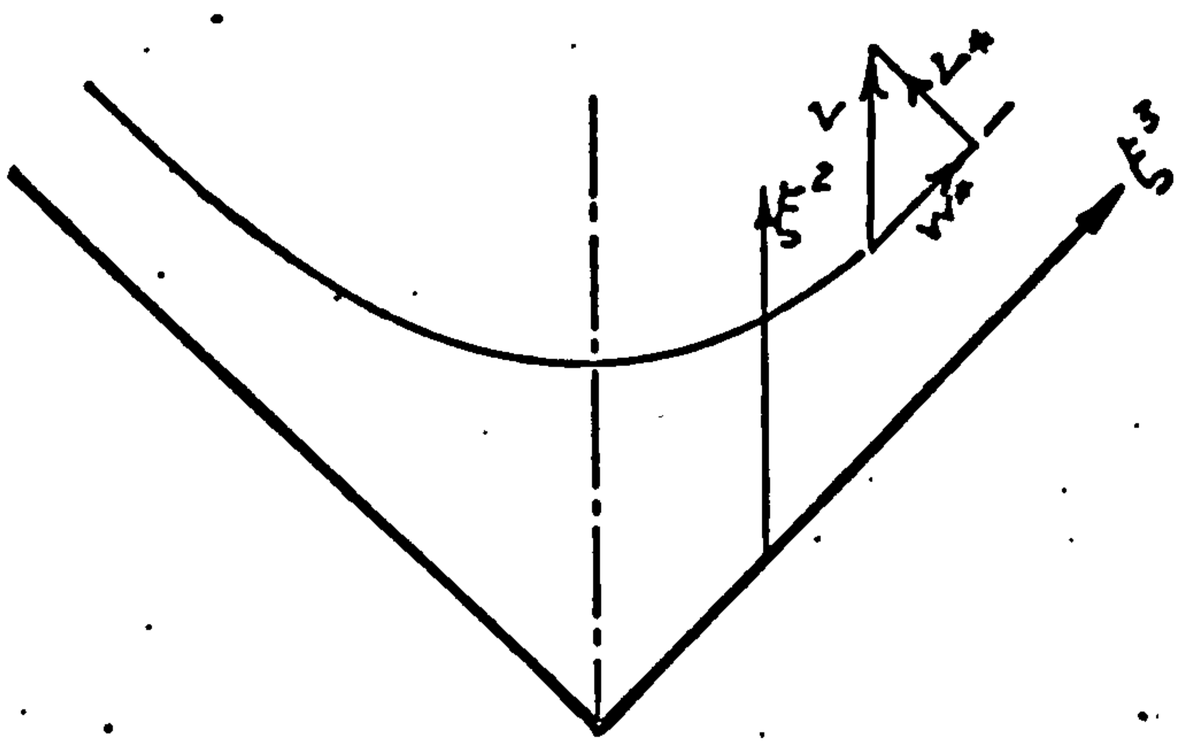

Fig.(2.6a)

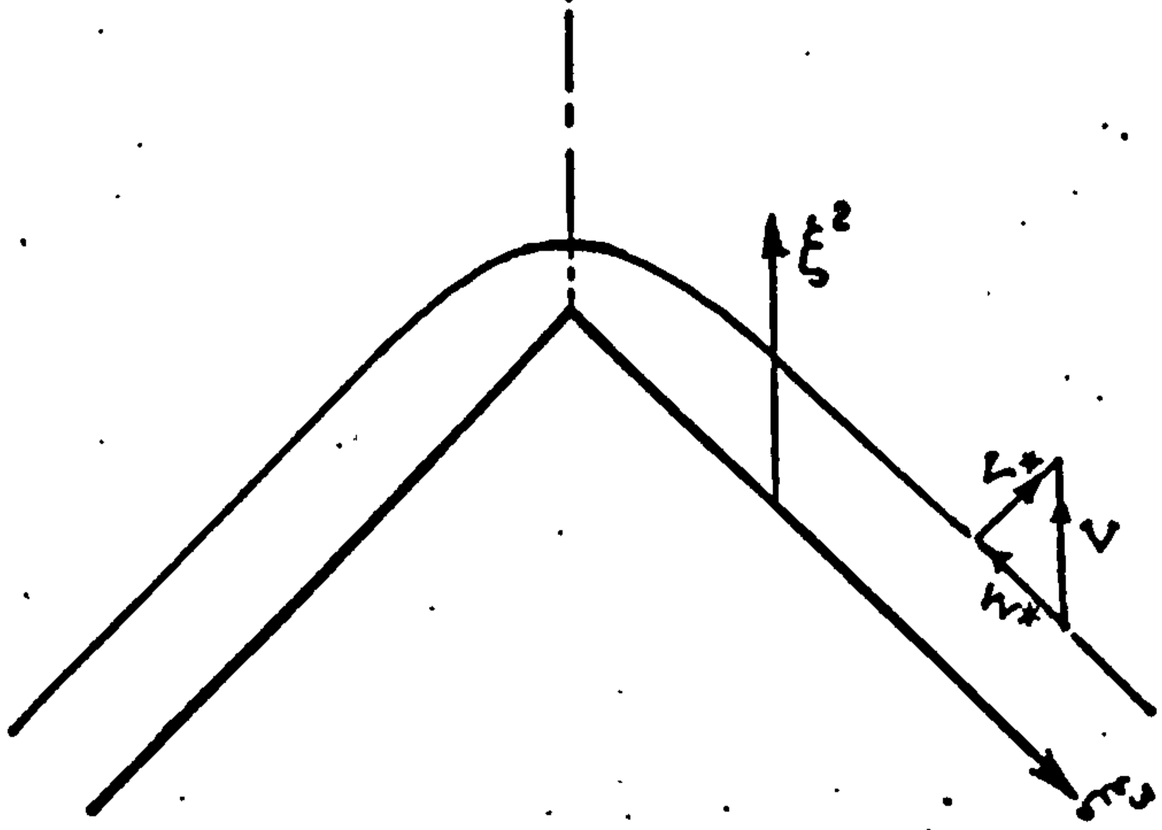

Fig.(2.6b)

The corner layer extends over the region $0 \leq \xi^2, |\xi^3| < \infty$ which in terms of the unstretched physical coordinates is the domain $x^2 = 0^+$, $|x^3| = 0^+$ and matching between the viscous region of the corner flow and the potential flow is to be effected in this vicinity. The potential crossflow solution to $O(R_{ex}^{-\frac{1}{2}})$ has the component $\beta_o R_{ex}^{-\frac{1}{2}}$ normal to the wall at $x^2 = 0^+$, $|x^3| > 0^+$. The resultant of this outflow from each wall in the region $x^2 = 0^+$, $|x^3| = 0^+$ is a vector parallel to the symmetry plane of magnitude $(\beta_o/\cos\lambda^*) R_{ex}^{-\frac{1}{2}}$. This is the potential crossflow controlling the corner layer.

Consider now the cases $\lambda^* = +45^o$ and -45^o. In these, the potential crossflow solution at the 'walls' is indicated in Fig. (2.5). When the vicinity of $x^2 = 0^+$, $|x^3| = 0^+$ is transformed into the region $0 \leq \xi^2 < \infty$, $-\infty \leq \xi^3 < \infty$ the result is shown in Fig. (2.6). The physical component of the potential crossflow parallel to the wall w^* is of the same magnitude but opposite in direction in figures (2.6a) and (2.6b) and illustrates the antisymmetric behaviour of w^* mentioned above.

This method could have been used to arrive at the asymptotic boundary conditions for the corner layer at $\xi^2 \rightarrow \infty$ and $\xi^3 \rightarrow \infty$ directly on knowing $H(\eta)$.

2.7 Method of solution

Equations (2.28c,d) are unsuitable for numerical solution in their present form. It is more convenient to transform these equations into elliptic Poisson-like forms which are generally better suited for numerical treatment by relaxation methods. This is effected by differentiating

both equations with respect to ξ^2 and ξ^3 plus some algebraic work so that

$$\varphi_{,22} + \varphi_{,33} - s\varphi_{,23} - s_{,3}\varphi_{,2} - \left(\frac{c_{,3}}{c}\right)\varphi_{,3} - \left(\frac{c_{,3}}{c}\right)_{,3}\varphi + c^2\theta_{,3} + 2cc_{,3}\theta - (sc_{,3}/c - 2s_{,3})\psi_{,3} - (sc_{,3}/c - s_{,3})\psi - (2c + \xi^3 c_{,3})u_{,2} - \xi^3 c s_{,3} u_{,3} - (cs_{,3} + \xi^3(cs_{,3})_{,3})u = 0 \qquad (2.63a)$$

$$\psi_{,22} + \psi_{,33} + s\varphi_{,22} + \left(\frac{c_{,3}}{c}\right)\varphi_{,2} - s\psi_{,23} - (s_{,3} - sc_{,3}/c)\psi_{,2} - c^2\theta_{,2} + \xi^3 c s_{,3} u_{,2} - (2c + \xi^3 c_{,3})u_{,3} - (3c_{,3} + \xi^3 c_{,33})u = 0 \qquad (2.63b)$$

The numerical solution of equations (2.28a,b) and (2.63a,b) should strictly be effected in the quarter-infinite region $0 \leqslant \xi^2, \xi^3 < \infty$. For this to be done would require variable stretching in both ξ^2 and ξ^3 to map the quarter infinite domain into a finite domain. Interest is particularly directed here at the streamwise velocity component u. This component together with the streamwise vorticity component are known to asymptote to their potential values exponentially fast but considerably more slowly into the boundary layers. It is likely therefore that the boundary at $\xi^2 \to \infty$ can be replaced (as is commonly done in boundary layer problems) by imposing the boundary conditions at a moderate value of ξ^2 (=16 $\equiv \xi^2_{max}$, say) with little effect on the streamwise velocity as has been verified by comparison with known solutions for the special case of the 90^o sharp

corner. To encompass the decay in the flow variables into the boundary layer it was deemed necessary to incorporate the transformation

$$\zeta = \frac{\xi^3}{a + b\xi^3} \tag{2.64}$$

which maps the infinite interval $0 \leqq \xi^3 < \infty$ into $0 \leqq \zeta < 1/b$ where a and b are constants to be chosen. This transformation maps equal intervals in ζ into unequal intervals in ξ^3 with step size in ξ^3 growing as ζ increases. It has the desirable effect of increasing the resolution near $\xi^3 = 0$ where changes with respect to ξ^3 are expected to be most rapid. In this vicinity the interval in ξ^3 is $\sim$ a ζ .

A transformation like (2.64) is applicable only if the dependent variables are bounded for large ξ^3 so that their derivatives with respect to the transformed coordinate become bounded [26,14,16]. It is evident from equations (2.58) that ψ and θ are unbounded with respect to ξ^3 but this difficulty is easily removed by the substitution

$$\left.\begin{aligned} \theta &= \theta^* + \frac{1}{c^*}\xi^3 f'' \\ \psi &= \psi^* + c^* \xi^3 f' \end{aligned}\right\} \tag{2.65}$$

where θ^* and ψ^* are the new dependent variables replacing θ and ψ .

When the new variables ζ , θ^* and ψ^* are introduced, the equations to be solved numerically are

$$\bar{\nabla}^{*2} u + \varphi u_{,2} + D u_{,\zeta} = 0 \tag{2.66a}$$

$$\overline{\nabla}^{*2}\theta^{*} + \varphi\,\theta^{*}_{,2} + D\,\theta^{*}_{,\zeta} + u\Big[c(2+\xi^3(\ln c)_{,3}\theta^{*} -$$

$$-\xi^3(s_{,3}+\xi^3 s_{,33})u + 2\zeta_1(\xi^2+s\xi^3-(\xi^3)^2 s_{,3})u_{,\zeta} -$$

$$-2(s\xi^2+\xi^3)u_{,2} + \xi^3 k(\zeta_1\psi^{*}_{,\zeta}-\varphi_{,2}) + (k+\xi^3 k_{,3})\psi^{*} +$$

$$+ E\Big] + \frac{1}{c^{*}} f''\psi^{*} + \Big(\frac{1}{c^{*}}\xi^3 f''' - \xi^3 k u_{,2}\Big)\varphi + \overline{F}^{*} u_{,\zeta} +$$

$$+\frac{1}{c^2}\xi^3 k(\zeta_1^2 u_{,\zeta\zeta} - u_{,22}) + G = 0 \qquad (2.66b)$$

$$\varphi_{,22} + \zeta_1^2\,\varphi_{,\zeta\zeta} = s\zeta_1\varphi_{,2\zeta} + s_{,3}\varphi_{,2} + \Big(\frac{c_{,3}}{c}\zeta_1+\zeta_2\Big)\varphi_{,\zeta} +$$

$$+\Big(\frac{c_{,3}}{c}\Big)_{,3}\varphi + \zeta_1\Big(\frac{s c_{,3}}{c} - 2s_{,3}\Big)\psi^{*}_{,\zeta} + \Big(\frac{s c_{,3}}{c} - 2s_{,3}\Big)_{,3}\psi^{*} +$$

$$+(2c+\xi^3 c_{,3})u_{,2} + (c s_{,3} + \xi^3(c s_{,3})_{,3})u -$$

$$-\zeta_1 c^2\theta^{*}_{,\zeta} - 2c c_{,3}\theta^{*} + D^{*} \qquad (2.66c)$$

$$\psi^{*}_{,22} + \zeta_1^2\,\psi^{*}_{,\zeta\zeta} = -s\varphi_{,22} - \Big(\frac{c_{,3}}{c}\Big)\varphi_{,2} + s\zeta_1\psi^{*}_{,2\zeta} +$$

$$+(s_{,3} - 2\frac{c_{,3}}{c})\psi^{*}_{,2} - \xi^3 c s_{,3} u_{,2} + \zeta_1(2c+\xi^3 c_{,3})u_{,\zeta} +$$

$$+(3c_{,3}+\xi^3 c_{,33})u + c^2\theta^{*}_{,2} - \zeta_2\psi^{*}_{,\zeta} + E^{*} \qquad (2.66d)$$

where

$$\zeta_1 = \frac{d\zeta}{d\xi^3} \quad , \quad \zeta_2 = \frac{d^2\zeta}{(d\xi^3)^2}$$

$$u_{,\zeta} = \frac{\partial u}{\partial\zeta} \quad , \quad \theta^{*}_{,\zeta} = \frac{\partial\theta^{*}}{\partial\zeta} \qquad etc.$$

$$\overline{\nabla}^{*2} = \frac{1}{c}\Big[\frac{\partial^2}{(\partial\xi^2)^2} - 2s\zeta_1\frac{\partial^2}{\partial\xi^2\partial\zeta} + \zeta_1^2\frac{\partial^2}{\partial\zeta^2} - \frac{k}{c}\frac{\partial}{\partial\xi^2} + \frac{ks}{c}\zeta_1\frac{\partial}{\partial\zeta}\Big]$$

$$D = \zeta_1(\psi^{*} + \xi^3 c^{*} f') + \zeta_2/c$$

$$E = \frac{c}{c^*}\xi^3\left(2 + \xi^3 (\ln c)_{,3}\right) f'' + c^*\xi^3(2k + \xi^3 k_{,3}) f'$$

$$F^* = k\xi^3\zeta_1(\psi^* + c^*\xi^3 f') + \frac{\zeta_{,1}}{c^2}\left(s_{,3} + \xi^3 s_{,33} - 2\xi^3 k c_{,3}\right) +$$

$$+ \frac{1}{c^2}\xi^3\zeta_2 k$$

$$G = \frac{1}{c c^*}\xi^3 f'''' - \left(\frac{2s}{c^* c} + \frac{k}{c^* c^2}\xi^3\right) f''' + \left(\frac{ks}{c^* c^2} + \xi^3 f'\right) f''$$

$$D^* = c^*\left[\left(\frac{s c_{,3}}{c} - 2 s_{,3}\right) + \xi^3\left(\frac{s c_{,3}}{c} - s_{,3}\right)_{,3}\right] f' -$$

$$- \frac{1}{c^*}\left[c^2 + 2 c\, c_{,3}\,\xi^3\right] f'' + \xi^3 c\, s_{,3}$$

$$E^* = \xi^3\left(\frac{c^2}{c^*} - c^*\right) f''' + c^*\left[s + \xi^3\left(s_{,3} - \frac{s c_{,3}}{c}\right)\right] f'' .$$

The boundary conditions in terms of the transformed variables become

$$\left.\begin{aligned} &\xi^2 = 0 \quad ; \\ &u = \varphi = \psi^* = 0 \\ &\theta^* = \frac{1}{c^2}\psi^*_{,2} + \xi^2\left(\frac{c^*}{c^2} - \frac{1}{c^*}\right) f''(0) \quad , \end{aligned}\right\} \qquad (2.67a)$$

$$\left.\begin{aligned} &\zeta = 0, (\xi^3 = 0); \\ &\zeta_1 u_{,\zeta} = s\, u_{,2} \\ &\theta^* = 0 \\ &\zeta_1\varphi_{,\zeta} - s\varphi_{,2} - \frac{c_{,3}}{c}\varphi + s c u = 0 \\ &\psi^* = 0 \quad , \end{aligned}\right\} \qquad (2.67b)$$

$$\left.\begin{aligned} &\xi^2 \to \infty\ ; \\ &\qquad u \sim 1 \\ &\qquad \theta^* \sim 0 \\ &\qquad \varphi \to c(\xi^2 - \beta) \\ &\qquad \psi^* \to \xi^3 (c - c^*) \quad , \end{aligned}\right\} \quad (2.67c)$$

and at

$$\left.\begin{aligned} &\zeta = \frac{1}{b}\ , (\xi^3 \to \infty)\ ; \\ &\qquad u = f' \\ &\qquad \theta^* = -c^* s^* \beta \left[f''' \int_0^{\xi^2} \frac{\eta - \beta}{f''(\eta)} d\eta + (\xi^2 - \beta) \right] + \frac{s^*}{c^*} \xi^2 f'' \\ &\qquad \psi^* = -c^{*3} s^* \beta f'' \int_0^{\xi^2} \frac{\eta - \beta}{f''(\eta)} d\eta + s^* c^* (\xi^2 f' - f) \\ &\qquad \varphi = c^* f \quad . \end{aligned}\right\} \quad (2.67d)$$

Equations (2.66), subject to boundary conditions (2.67), are solved numerically by the Gauss-Seidel iterative method. Details of the numerical scheme are given in App endix (C) and the results are presented and discussed in Chapter 4.

CHAPTER 3

EXPERIMENTAL WORK

3.1 Introduction

The experimental work available for comparison with the results of the theoretical analysis presented in Chapter 2 is limited to 90° and 135° sharp corners. For these two cases El-Gamal [4] and Barclay [3] have obtained what appear to be completely reliable data, sufficient for our purpose, and in the context of the present enquiry there was little merit in repeating or extending their measurements*. These existing works therefore supply the experimental reference data for the sharp corner theory. Of central interest in this report is the flow along a radiused corner and to the writer's knowledge there is no experimental data available for this situation. The experimental phase of the present work has, therefore, been directed towards providing this missing information. Surprisingly, the manufacture of a suitable corner model was a lengthy business stretching over a period of several months. This expense in time precluded the construction of a range of corners covering a variety of angles and different corner root geometry; indeed it became obligatory to carry out the experimental work on a single model. In view of its overwhelming practical importance the corner

---

* El-Gamal's results were obtained in the wind tunnel at University College London, the location for the present work, and in that particular case any new 90° sharp corner test would quite strictly have been a repetition of El-Gamal's work using the same model in the same wind-tunnel.

angle chosen was 90^{o}.

Limiting the experimental work to a single radiused corner is less restrictive than it may at first appear. Together with the sharp corner data we will have data on three markedly different corners to provide what must be an adequate test of a single theory. This view on the adequacy of the programme was in no way influenced by the reflection that every contributor to the experimental data on corner flows known to the writer (references [1,2,3,4, 27]) has confined his attention to a single corner.

3.2 Corner model

3.2.1 Corner profile

The transverse curvature at the corner root is chosen subject to conditions (2.26) and its coordinates are computed in accordance with equations (2.1) on specifying the function to describe $\lambda(x^3)$. Consistent with this $\lambda(x^3)$ is defined by

$$\lambda = \lambda^* \tanh (x^3/\ell) \quad , \lambda^* = 45^{o} \tag{3.1}$$

where ℓ is a length scale related to the wall curvature at $x^3 = 0$ by

$$\left.\begin{aligned} \ell &= \lambda^* / \left(\frac{d\lambda}{dx^3}\right)_{x^3=0} \\ \text{or} \qquad \ell &= \lambda^* r_o \quad , \quad r_o \equiv \left(\frac{d\lambda}{dx^3}\right)_{x^3=0} . \end{aligned}\right\} \tag{3.2}$$

Of the unlimited possibilities for $\lambda(x^3)$, equation (3.1) embodies in the simplest form the required properties of symmetry about $x^3 = 0$ and continuous derivatives everywhere.

The exponentially fast decay of $d\lambda/dx^3$ with increasing $|x^3|$ offered some convenience in the analysis (Chapter 2) and the function $\lambda(x^3)$ itself promised no manufacturing difficulty for the numerically controlled machine to be used in its formation.

The flow situation being studied is such that $r_o = O(R_e^{-\frac{1}{2}})$ but within this constraint there is some freedom to choose the physical size of r_o. In principle the smaller the (non-zero) value for r_o the better, for this would ensure that a single corner would cover the entire range of δ/r_o ratio compatible with the theory (δ is the two-dimensional boundary layer thickness). Sufficiently near to the leading edge δ/r_o would be arbitrarily smaller than unity while at moderate physical distances downstream of the leading edge the ratio would be large enough to constitute a close approximation to a sharp corner. In practice however the choice of r_o must be conditioned by experimental convenience and manufacturing feasibility.

A rational approach to fixing r_o starts with establishing the minumum and maximum thicknesses of two-dimensional boundary layer within which worthwhile measurements of the velocity profile may be made in terms of extent and accuracy of results. The limits will depend on the kind and size of measuring instrument to be used and on the wind-tunnel facility as well as on what is thought to constitute satisfactory coverage of the boundary layer. When the minimum and maximum boundary layer thicknesses are known r_o may then be chosen to give a satisfactory compromise range of δ/r_o ratios centered anywhere we please between the limits δ/r_o

very small and very large.

In the present context an adequate coverage of the boundary profile would at least span the velocity range U_∞ to 0.1 U_∞ and for accuracy the lower value should not be less than the minimum velocity appropriate to the sensitivity of the probe being used. The geometry of the probe fixes its nearest approach (x_o^2) to the wall and if the velocity at this point is to be 0.1 U_∞ , then assuming the Blasius velocity profile, the minimum boundary layer thickness which can be used (condition I) is $\delta = x_o^2 \eta/\eta_o$ where η_o and η are the Blasius coordinates at $u/U_\infty = 0.1$ and, say, 0.99 respectively. The greatest boundary layer thickness is achieved near the trailing edge of the longest corner permitted by the working section of the wind-tunnel and at the lowest air-speed. The maximum boundary layer thickness that can be used (condition II) however is fixed by the condition that 0.1 U_∞ equals the minumum velocity appropriate to the sensitivity of the probe ($\tilde{u}_o$ say). The minimum free stream velocity is then 10 $\tilde{u}_o$ and the corresponding boundary layer thickness is easily calculated. If 10 $\tilde{u}_o$ is less than the minimum steady air-speed available then the latter speed will fix the maximum boundary layer thickness to be used. Provided the maximum boundary layer thickness calculated (condition II) is indeed greater than the minimum thickness calculated (condition I) there is no need to consider the geometry of the probe in the former case or the minimum speed in the latter.

Now choosing the corner length to be the maximum permitted by the test-section, calculations like the above showed that the minimum and maximum two-dimensional boundary

layer thicknesses to be used were approximately 5.0mm and 13.0mm. This small range means that with a single corner model one or both extremes of the ratio δ/r_o must be dropped from the experimental programme. In the present situation the choice of r_o had to be made against the background that large δ/r_o is of great academic interest whereas values of δ/r_o in the vicinity of unity are perhaps of greater practical importance.

In the event the 'choice' was a forced one. Preliminary discussion with the Departmental Workshop staff on the manufacture of the corner showed that the minimum value of r_o consistent with the accurate production of the transverse curvature distribution was 10.0mm. This is at least twice as large as had been hoped for. r_o = 10.0mm was accepted however, since it was within the scope of the theory, although it was anticipated that the three-dimensional flow regime might be less strong than the experimenter would desire.

3.2.2 Model design

The corner was 0.90m long and the width of each corner plate was 200mm. These dimensions were chosen to give the most extensive corner surface compatible with the dimensions of the test-section (1.22m long x 0.61m square). For measurement purpose the lateral extent of the corner layer extends to only three or four two-dimensional boundary layer thicknesses from the symmetry plane and a similar distance adjacent to the edges of the plates is probably also three-dimensional in character. With the thickest boundary layer on the plates therefore, the two-dimensional

y^2 mm	$\lvert y^3 \rvert$ mm
0.0	0.0
0.178	1.889
0.723	3.811
1.562	5.624
2.612	7.326
3.881	8.934
5.077	10.473
6.408	11.966
7.772	13.428
9.156	14.872
10.552	16.304
11.955	17.729
13.363	19.150
14.773	20.568
16.185	21.984

$$x^2 = 0$$

$$y^2 = x^2 + \int_0^{x^3} \sin\lambda \, dx^3$$

$$y^3 = \int_0^{x^3} \cos\lambda \, dx^3$$

$$\lambda = \frac{\pi}{4} \tanh(x^3/\ell)$$

$$\ell = \frac{\pi}{4} r_0 \quad , \qquad r_0 = 10 \text{ mm}.$$

Table (1) Coordinates of the corner profile chosen for the model.

region would be at least 120mm wide.

It was initially envisaged that the transverse curvature of the corner would be created by an end-milling cutter of exactly the required profile. The production of such a cutter is difficult however and the writer was assured that the cost would be unacceptably high. An alternative method which was discarded because of the uncertain accuracy in its results, was to produce an external corner (or edge) having the required profile. This would provide a former on which a metal sheet could be pressed to create the inner surface of the corner. The sheet would then require a rigid supporting framework to maintain its shape. In the opinion of the workshop a more effective method of manufacture was to use a cylindrical cutter driven by the Cincinatti numerically controlled milling machine in the Department. This method was accepted but it brought with it its own particular disadvantages. The cutter spindle was necessarily parallel to the streamwise direction and to ensure an adequate stiffness in the cutting process there was a definite relationship to be satisfied between the cutter diameter and the spindle length which limited the length of the corner that would be cut in a single piece. In other words the smaller the cutter (and hence the spindle) diameter the shorter the cutter spindle must be. This implied that the corner must be made in sections the maximum length of which decreased with the cutter diameter. On consideration it appeared that the best compromise between having a desirable small cutter diameter (i.e. small r_o) and an excessive number of sections to the corner was to take a cutter diameter of 20mm. This gave a maximum streamwise length of approximately

75mm which limited the corner section length to 150mm if the section was milled from both ends in turn. The number of sections would increase very rapidly for smaller cutter diameter. The stiffness per unit length of unit length being proportional to d^4, where d is the spindle diameter, the length of each corner section would reduce as d^4, i.e. a cutter diameter of 10mm would increase the number of corner sections by a factor of 16. As it is, the 0.9m long corner was formed by 6 sections of 150mm length.

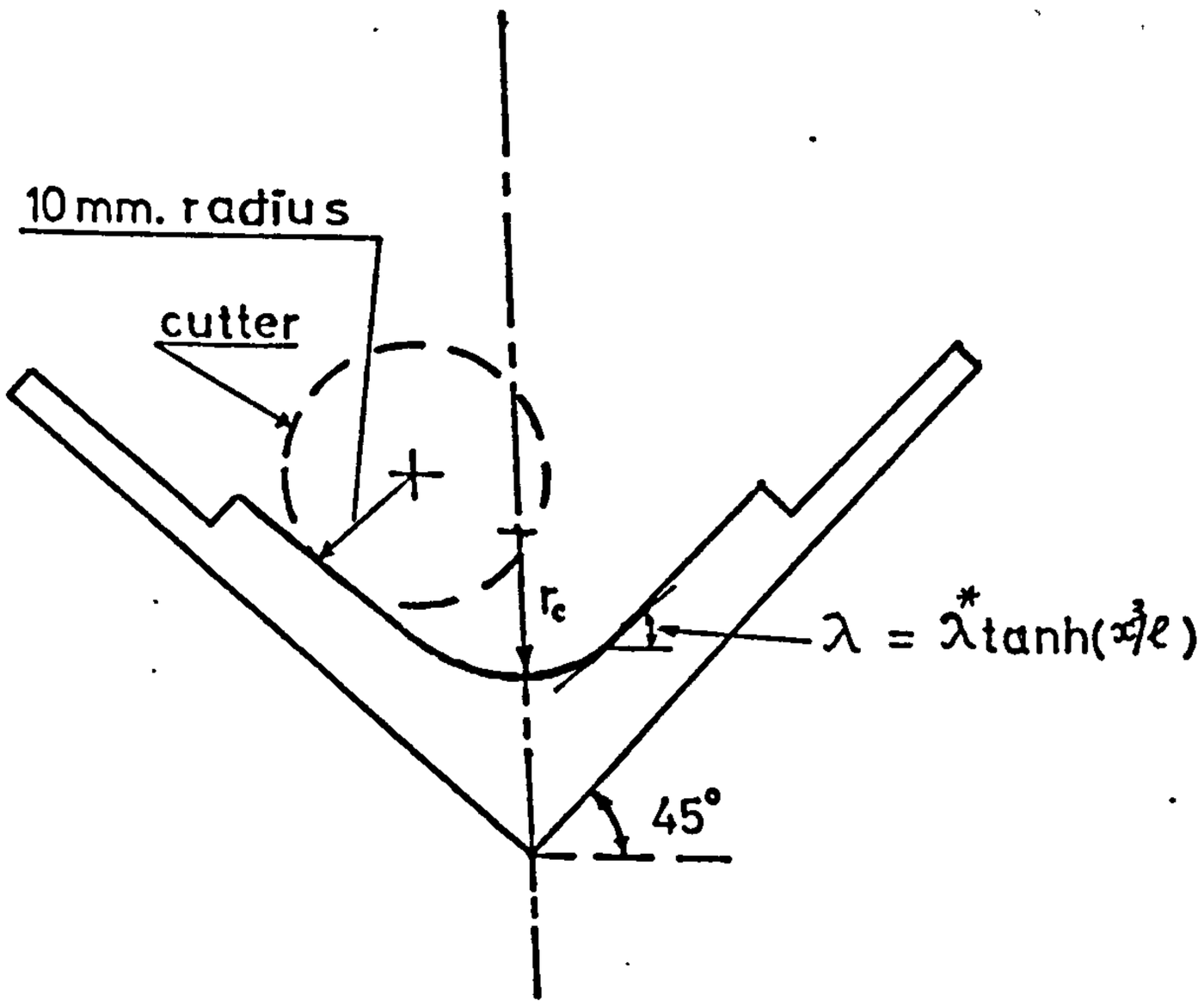

Fig.(3.1)

Each section was milled from a (75 x 75mm) square cross section block of aluminium to the shape shown in Fig. (3.1). The milling machine was a Cincinatti milcron (Cim-x) controlled by an Acramatic 5DX computer to an accuracy of 25 μm. The recesses were milled where the curvature had already asymptoted to zero. This arrangement ensured the smooth joining of two (2.0 x 200.0 x 900.0mm) aluminium flat plates to the blocks after these had been aligned and 'araldited' at the interfaces. The plates

were then securely bolted to the blocks. To this structure an aluminium plate was added to each underside as shown in Fig. (3.2) and bolted via distance pieces to the inner plate. This ensured a rigid construction for the corner. To seal the side and trailing edges aluminium strips of thickness equal to that of the distance pieces were inserted and the edges tightened by bolts. These sealing strips added further stiffness to the corner. All bolts were rendered flush with the plate surfaces.

Previous experiences in regard to the leading edges of the corner models suggested the choice of the knife-edge form and consequently these were adopted. Further, a radiused corner geometry presents a complex and difficult problem with respect to designing and manufacturing a profiled leading-edge and knife-edges are particularly attractive from this particular view point. The angle of the knife-edges was 10^{o}, the chamfer being on the underside of the model. Prior to forming the leading edge the structure of the corner in this vicinity was exactly like that at the trailing edge including the sealing strips. The leading edge was generated separately on the leading corner block, inner and outer plates and the sealing strips. These operations preceded the aralditing of the blocks (mentioned previously) and the final assembly of the corner.

The corner was completed by engraving a hair line on the symmetry line of the corner surface. The engraving was filled with a blue electrically conducting paint and any excess paint was polished off by hand.

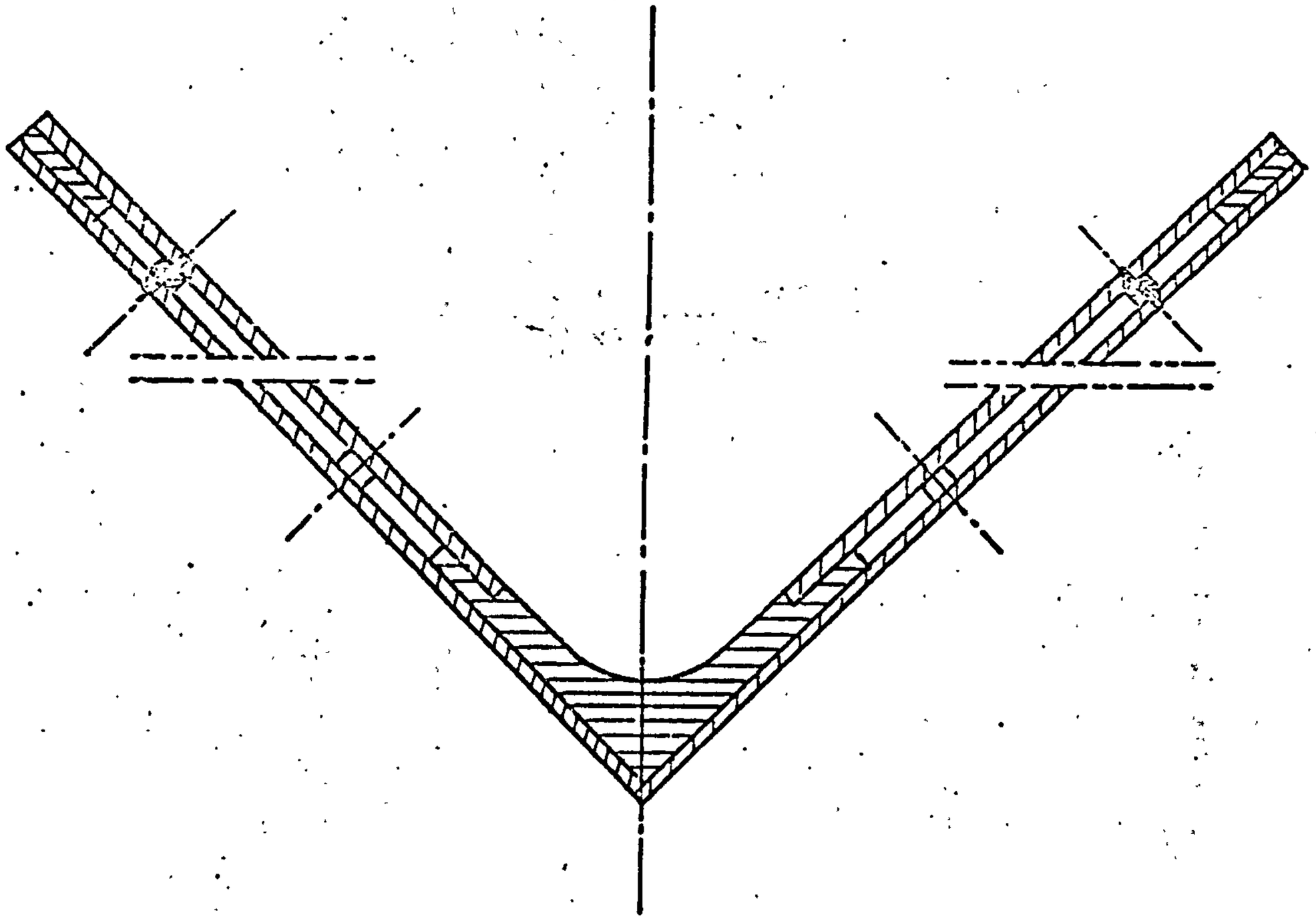

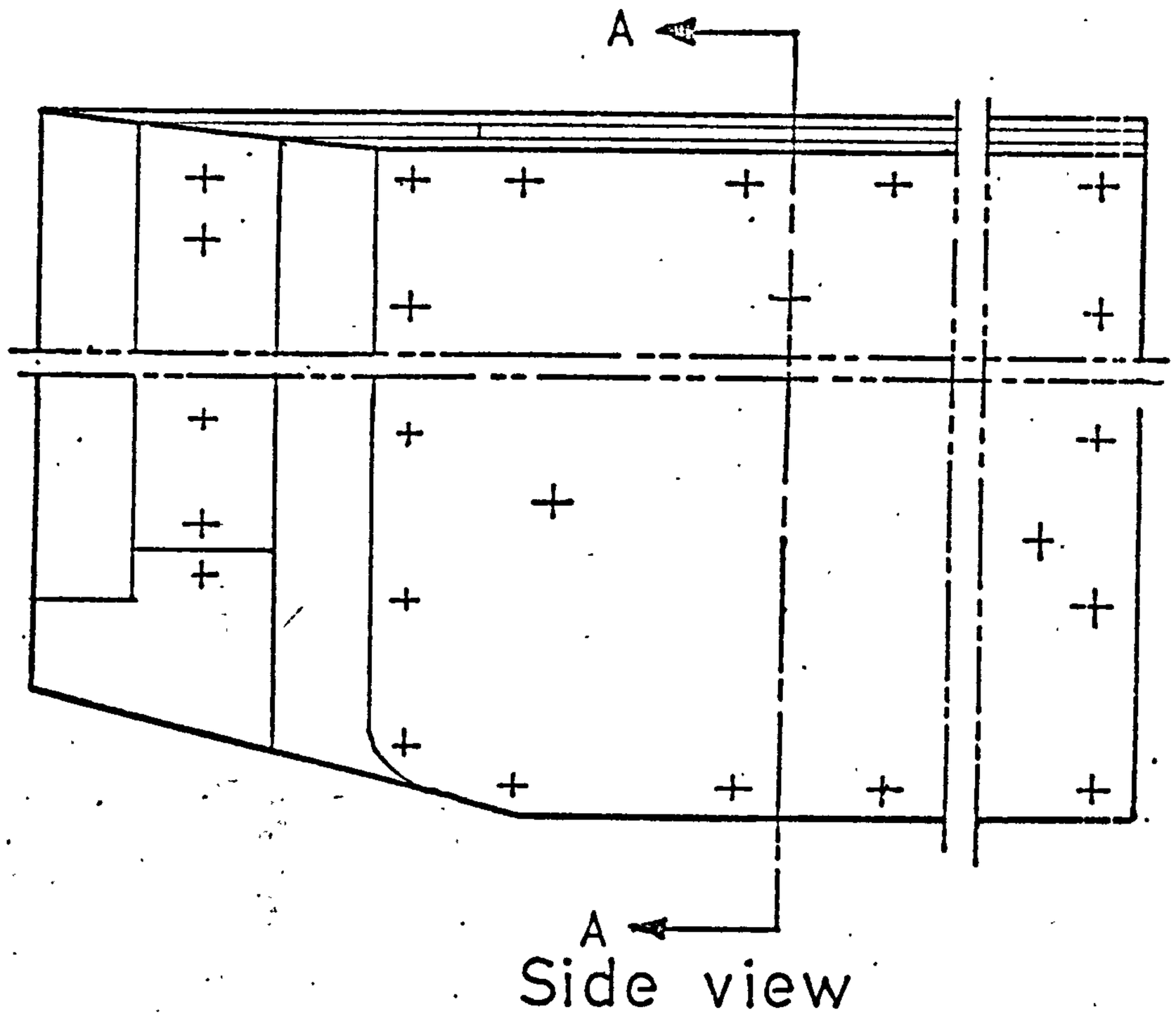

Fig. (3.2) Corner model constructional details (not to scale)

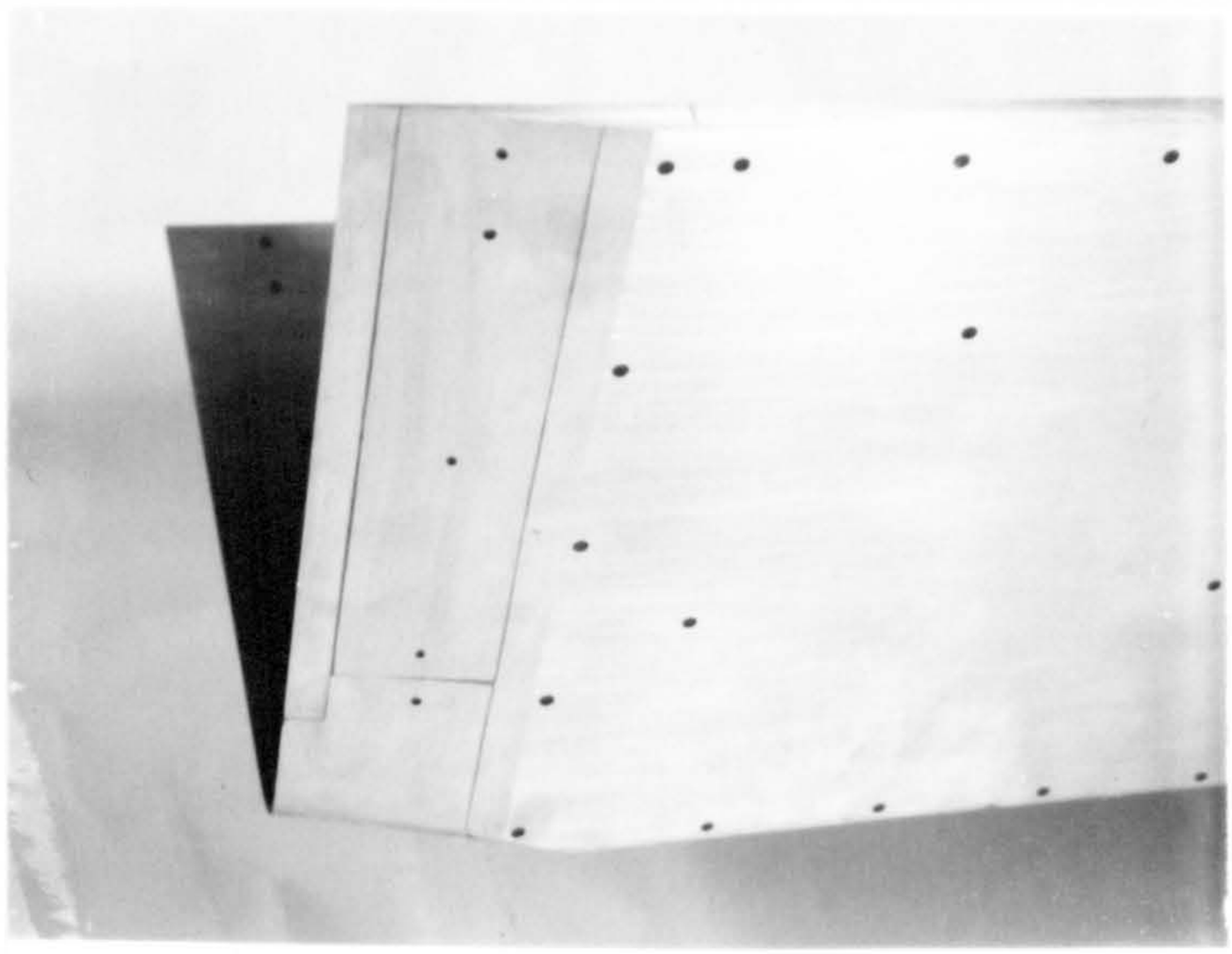

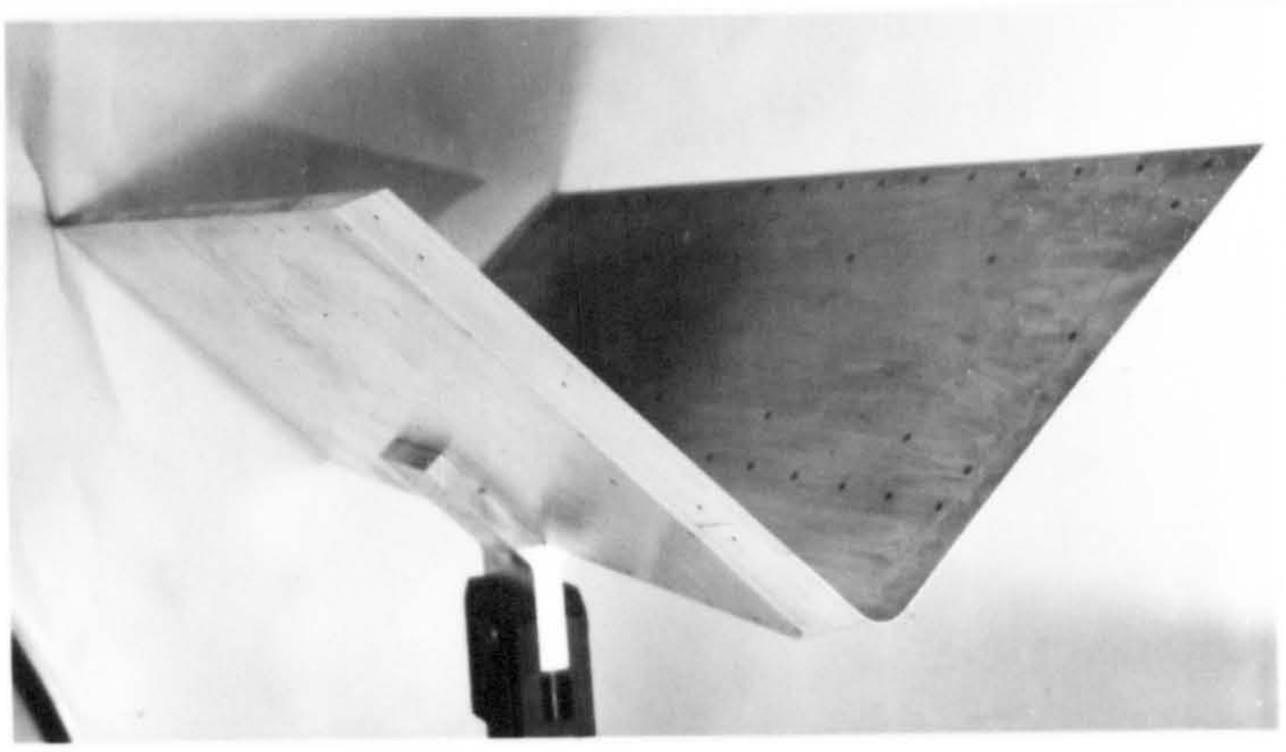

CORNER MODEL

The method of manufacture just outlined resulted in a completely satisfactory model corner, but at a cost which, though unknown, must have been very great. In view of this the writer has again discussed with the technical staff of the Departmental Workshops alternative methods of construction and we are now of the opinion that the use of a spade-cutter instead of a cylindrical-cutter, or an end-cutter would reap the benefits of the last two types without incurring their disadvantages. A spade-cutter has the form shown in the sketch. It is relatively cheaper to manufacture than an end cutter though still somewhat expensive. A spade cutter has the properties of being able to mill the corner profile on any length of the corner without the need for subdivision of the corner into sections. To form a corner it would be advantageous for the life of the spade-cutter if an ordinary end-cutter was first used to generate a first approximation to the required profile and the spade-cutter used only to form the finished surface.

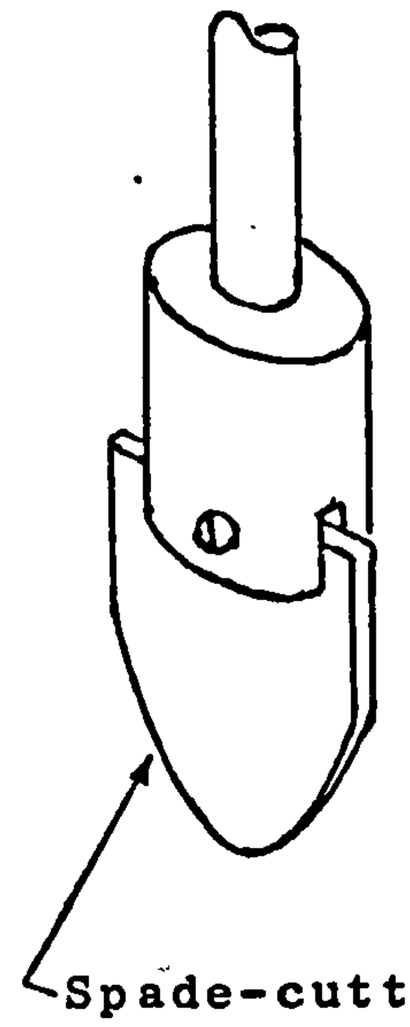

Spade-cutter

3.3 Experimental arrangement and measurements

It has been remarked that the wind-tunnel in which the corner was to be set had already been used by El-Gamal [4] in his study of the flow a long a sharp rectangular corner. The robust support system for that corner was available for the new radiused corner and was therefore used

for this purpose. The situation of the corner with respect to its support and its position within the wind-tunnel were essentially the same as that described by El-Gamal. There is, in fact, very little choice in the rational positioning of a streamwise corner in a wind-tunnel, as witness the very similar arrangements used by Zamir [2], Barclay [3] and El-Gamal.

Fig. (3.3) shows the corner in position. The geometric plane of symmetry of the corner is coincident with the vertical symmetry plane of the wind-tunnel and the leading edge was 0.27m downstream of the inlet plane of the test section; the trailing edge was therefore 0.11m upstream of the exit plane. The lower edge of the corner was nominally 0.2m above the floor of the tunnel.

The corner support system permitted the corner pitch to be varied and the support itself was carried on a turntable set flush with the wind-tunnel floor which allowed very fine adjustment of the yaw angle of the corner. Once a position had been chosen for the corner, a very effective clamp on the pitch mechanism and the worm-wheel drive on the turntable (and removal of the handwheel) rendered the corner immovable. Finally, the support system was encased in thin plywood sheet forming a low drag aerofoil spanning the gap between the underside of the corner and the tunnel floor so that the entire structure within the wind-tunnel formed a rigid corner model offering the minimum of unwanted disturbance to the incident air stream.

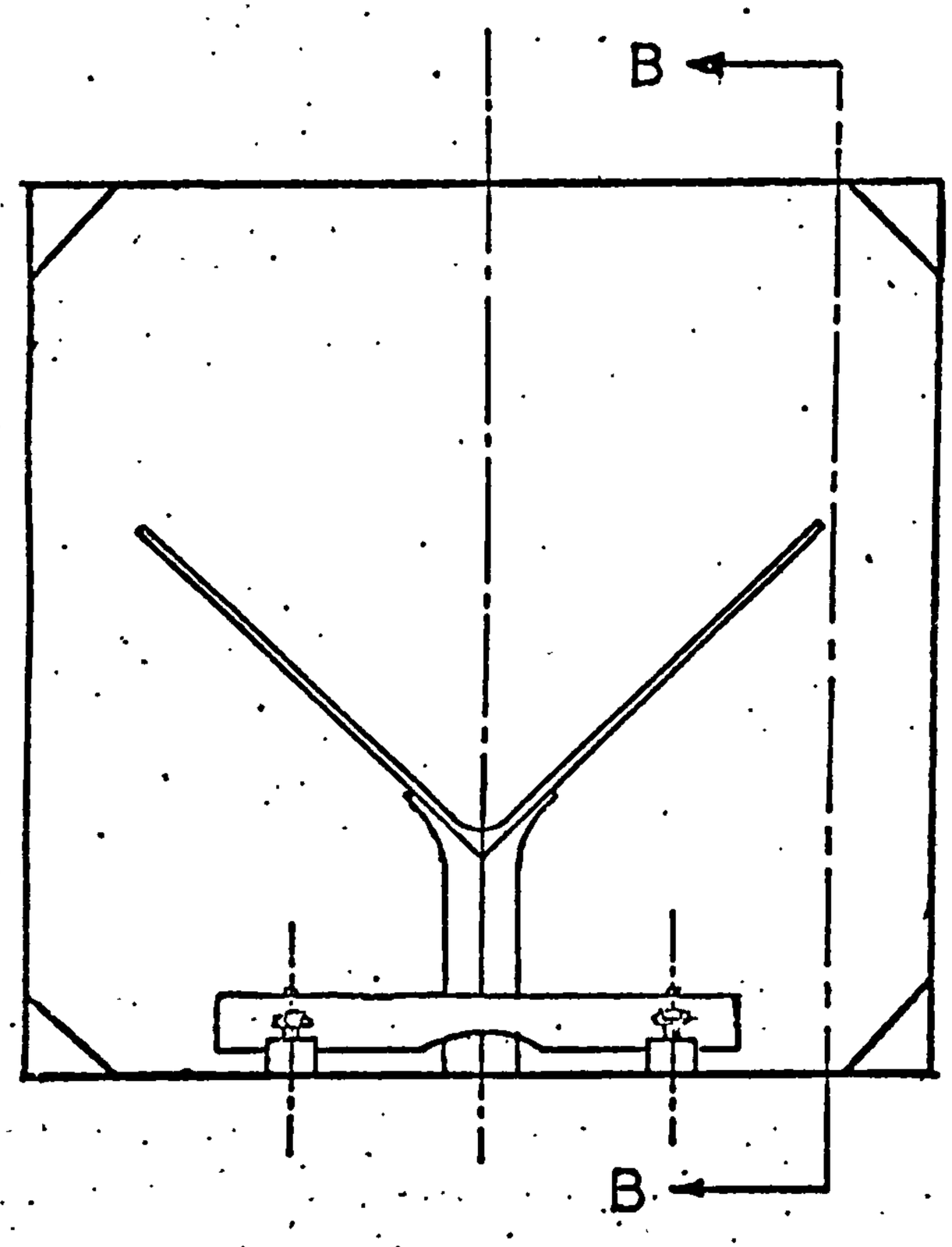

Front view

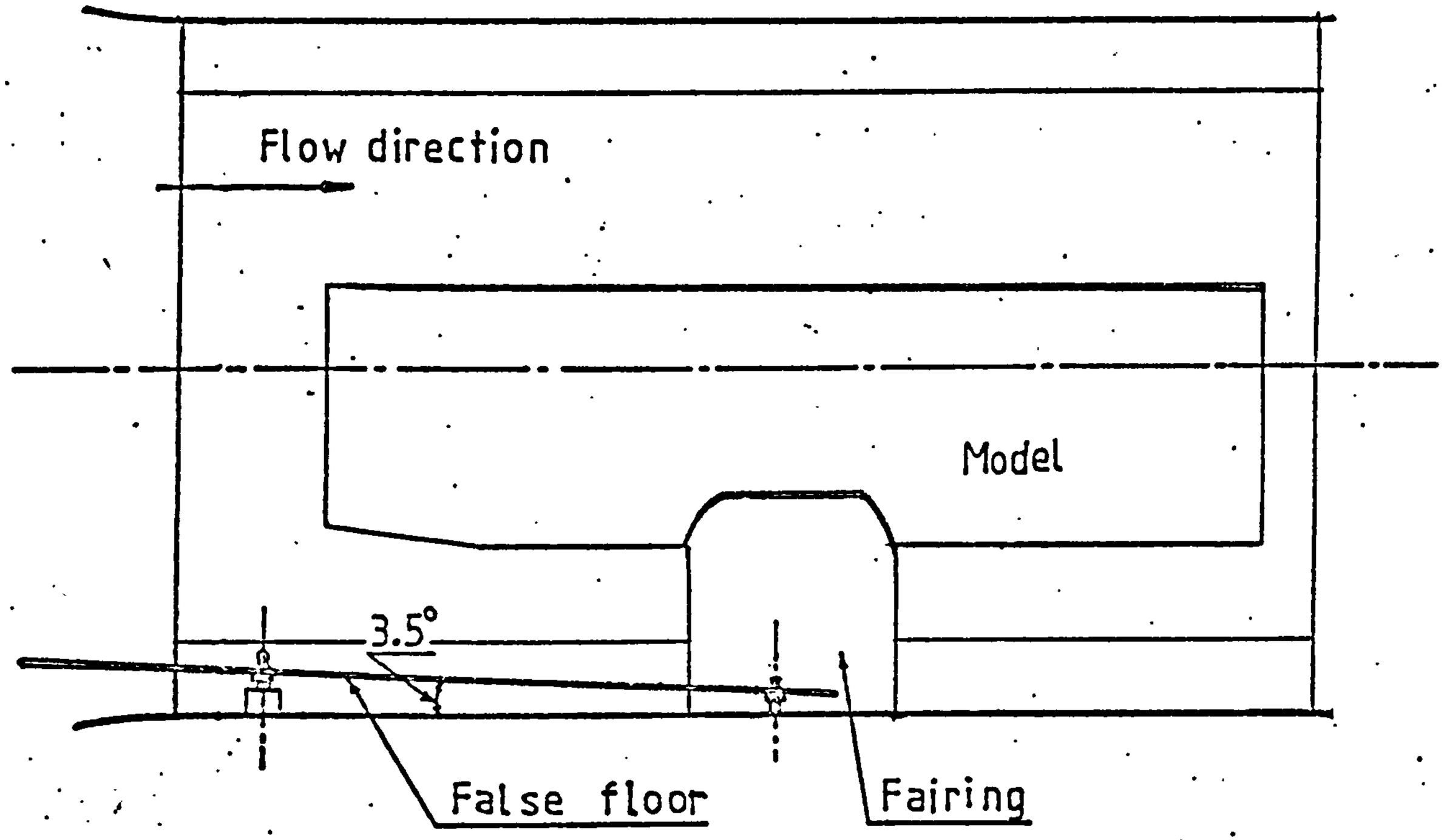

Section (B – B)

Fig. (3.3) Model inside test section and experimental set up.

The flow measuring instrument was a Disa constant temperature hot-wire anemometer with a digital D-C voltmeter, an rms voltmeter and an auxiliary unit incorporating a square signal generator, and high and low pass filters. An oscilloscope was used to help attain a fine adjustment of the anemometer bridge balance and to warn of the presence of turbulence in the flow. The wire probe was of the miniature type (Disa 55A25) having a 5 μm diameter and 1.2mm length. The probe holder is as shown in Fig. (3.4).

The orientation of the probe with respect to the corner wall is a matter for consideration. Zamir [2] and Barclay [3] in their experiments had the wire parallel to the corner wall nearest to the probe. This orientation promises to aggravate the already tedious nature of the three-dimensional traversing (with a manual system) since the wire has to be re-aligned on passing through the symmetry plane. It requires that the wind-tunnel fan be shut down and contrary to expectation the air speed does not always return precisely to its previous value on switching on the fan again. Furthermore, the re-alignment of the wire at the symmetry plane will also require adjustment of the traverse system as well as rotation of wire if the centre point of the wire is eccentric with the axis of the probe holder. The trouble involved at the symmetry plane might be tolerated if the physics of the flow required it, but this is evidently not so. What we are really after is that the wire should be tangent to the isovel and the symmetry of the problem implies that the isovels are horizontal at the symmetry plane and in general are only parallel with the walls in the two-dimensional regions of the flow. In other words a horizontal

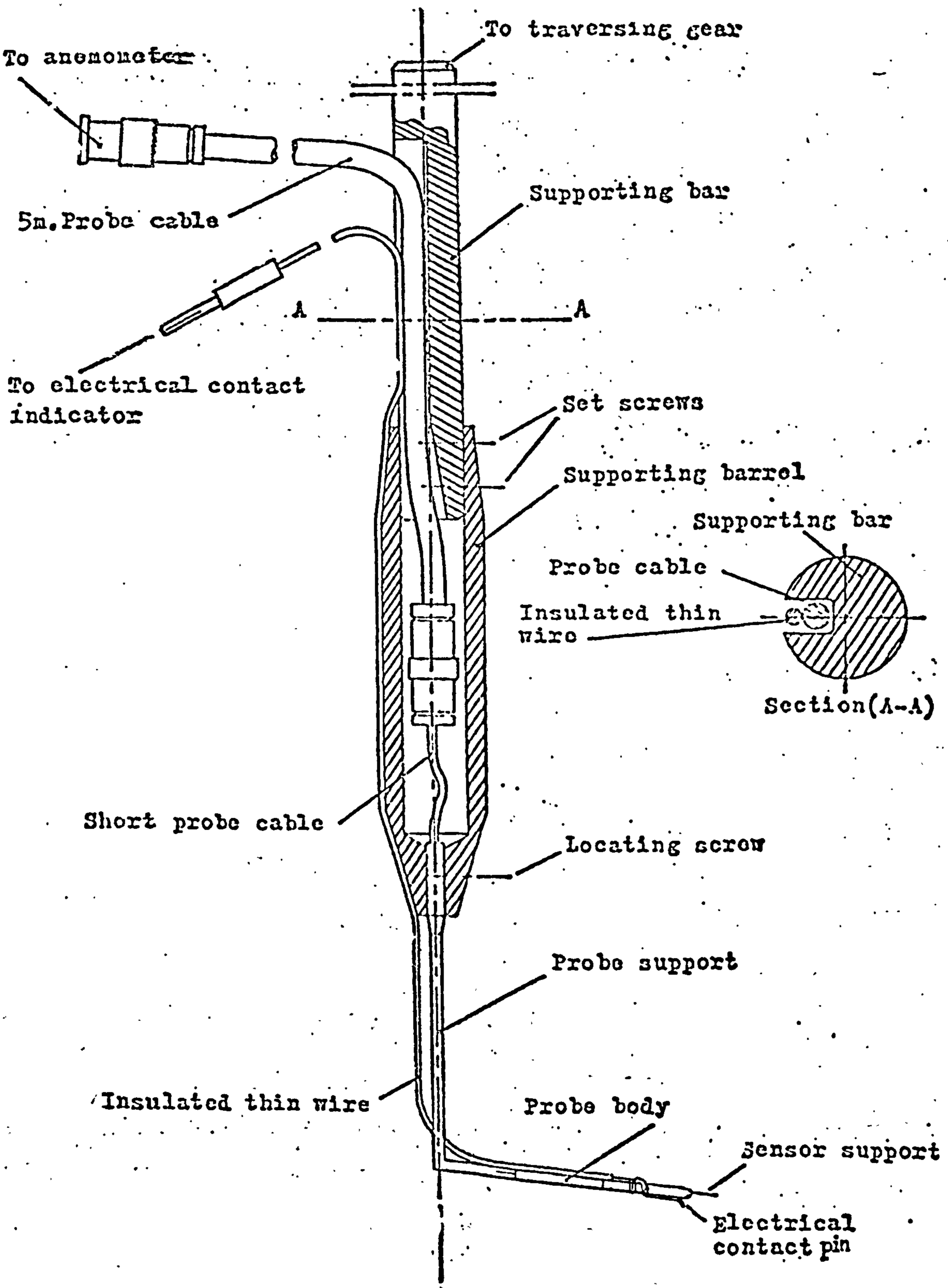

Fig. (3.4) Probe holder construction.

wire is the optimum orientation at the symmetry plane. If a horizontal wire would also prove to be satisfactory in the two-dimensional flow region (i.e. the wire at 45° to the wall) then a horizontal wire would be satisfactory everywhere and this would eliminate the need for the troublesome re-adjustment of the wire every time the symmetry plane was reached. This prompted El-Gamal to carry out measurements in the two-dimensional boundary layers on his corner plates with the wire parallel and at 45° to the walls. The results for the two wire configurations were virtually indistinguishable and showed conclusively that for the Reynolds numbers of interest the horizontal wire was completely satisfactory. It is on the basis of these findings that a horizontal wire was adopted by El-Gamal and in the present work. The use of a single wire orientation is particularly welcome in the present case of a radiused corner since the alternative would seem to involve re-alignment of the wire more than just once in each traverse.

Location of the centre point of the wire with respect to the wall was based on an electric contact being made between a needle point attached to the probe and a point on the plate vertically below the probe axis. Contact was registered by the ignition of a small lamp. The arrangement is shown in Fig. (3.5). It has the advantage that the centre point of the wire is always at the same vertical distance from the wall on establishing electrical contact irrespective of the angle made by the wall with the horizontal wire. The needle point was the end of an ordinary mild steel pin commonly used to fasten sheets of paper together.

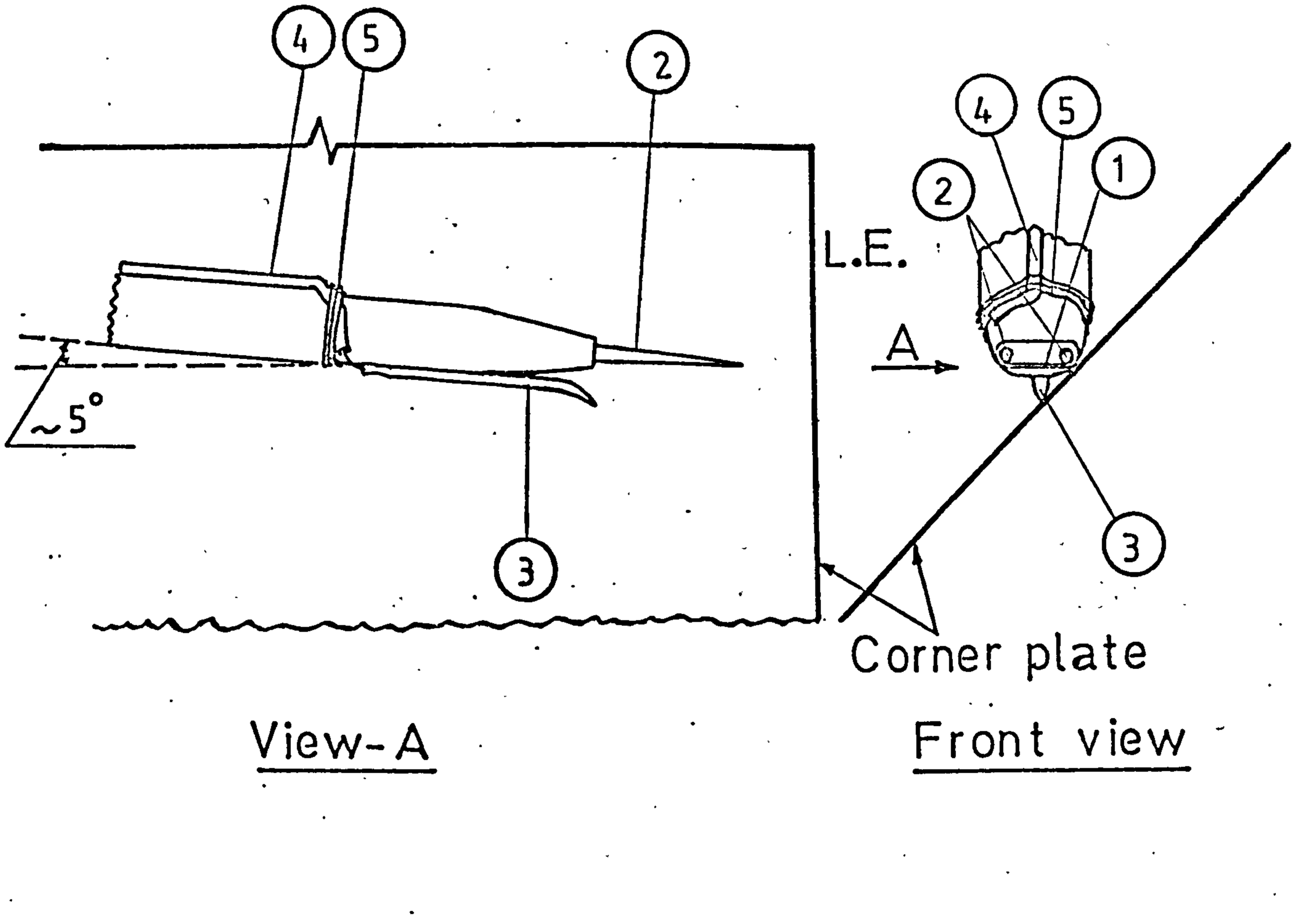

1. 5 μm diameter tungsten wire.
2. Wire support.
3. Electrical contact pin.
4. Thin insulated wire (connected to electrical contact indicator).
5. A cotton thread used to tie item (4) to the body of the hot-wire probe.

Fig.(3.5) Position of the hot-wire probe on making electrical contact between pin and wall.

The body of the pin was flattened for ease of handling when securing it to the probe body by araldite, and the flattened end was tinned to ensure good electrical contact when connected to the electrical lead. The needle point was viewed through a microscope when bonding, to ensure that it lay in the vertical plane containing the probe axis and the centre point of the hot-wire. The position was subsequently checked in a quantitative manner by viewing in a Shadowmaster having a magnification of 40x. After making contact on the flat surface to one side of the symmetry plane and using feeler gauges to measure the clearance between the prong and the wall, the vertical distance from the centre point of the wire was calculated on knowing the length of the wire ($\approx$ 1.2mm). This was repeated on the opposite side of the symmetry plane and any small differences in the feeler gauge readings were eliminated by very small rotation of the probe holder about its vertical axis. While in principle such calculations were only required for one transverse plane, they were nevertheless repeated at every plane for which measurements of velocity were to be made.

In each measuring plane the symmetry line was located by establishing contact with the needle point on the hair line inscribed on the corner, using a magnifying glass for assistance.

Calibration of a hot-wire anemometer is more or less a standard procedure in the context of corner flows and it has been described in detail in references [2], [3] and [4]. The essence of the calibration is to compare the reading on the anemometer with that on a manometer connected

to a standard pitot-static tube when the hot-wire probe and the pitot tube are suitably situated in the wind-tunnel. This is repeated over a wide range of air speeds which, for boundary layer work should particularly include speeds near the lower limit of sensitivity of the pitot tube. The speed is readily calculated from the manometer reading and the calibration for the speed range covered is thereby obtained.

The major advantage of the hot-wire anemometer over the pitot tube is its much greater sensitivity which gives it the potential for measuring accurately very low speeds. Realization of this potential however is dependent on the existence of a reliable calibration method for low speeds lying beyond the range of the pitot tube. One such method is to mount the hot-wire probe in a tube where Poiseuille flow has been established. The velocity profile is known in this condition and knowing the position of the wire with respect to the centreline of the tube and measuring the (steady) volume flow rate (water is used to induce air flow in the tube) the velocity at the wire can be calculated. Since the hot-wire requires frequent calibration this method is unsuitable for wind-tunnel usage. Instead the method to be used is based on the work of Collis and Williams [28] who, developing an earlier result by King [29], showed experimentally that for a constant temperature hot-wire in a constant temperature and density air stream

$$N_u = A + BR_w^n \qquad (3.3)$$

where $N_u = h'd/k$ is the Nusselt number, h' is the coefficient of heat transfer, d is the wire diameter, A and B are

constants and $R_w = U_\infty d/\nu$. Equation (3.3) is valid for $R_w<140$ and in the range $0.02<R_w<44$, n was found to have the value 0.45. For a 5 μm wire diameter and air at 20° C the latter range of R_w corresponds to an air speed range of approximately 0.06 m/s to 131.0 m/s.

For a fluid at constant temperature, the heat transfer rate per unit area is proportional to V^2, where V is the voltage across the hot-wire. This enables equations (3.3) to be rewritten as

$$(V/V_o)^2 = A' + B' U^n \qquad (3.4)$$

where U is the local velocity of the fluid and V_o is the voltage when U is zero.

The relation between $(V/V_o)^2$ and U^n, being linear, is a result of great utility since it provides a reliable means of extrapolating the measured calibration results to much lower speeds. The lowest speed to which the extrapolation is valid is limited to the value where heat transfer by free convection is comparable with that due to forced convection. On the basis of Collis and Williams work [28] Barclay [3] and El-Gamal [4] have worked out that for a 5 μm diameter wire, at 300° C and air at 20° C free convection is unimportant at speeds greater than 0.125 m/s. This speed fixes the minimum permissible free stream speed to 1.25 m/s if the boundary layer profile is to be adequately measured. The minimum free stream speed used here was 1.3 m/s. The speed range of the experiment was therefore always such as to imply the value n = 0.45 when using equation (3.4). The constants A' and B' are obtained by a least square method of fitting equation (3.4) to experimental results. Equation (3.4) was always

found to give an excellent fit to the measured results. See Fig. (3.6).

During the calibration of the hot-wire, the probe and the pitot-static tube were always situated near the axis of the wind tunnel and a small distance ($\sim$ 100-120mm) apart to avoid any possibility of mutual interference. The free-stream in the test section has a very uniform profile and separation of the two sensors (hot-wire and pitot tube) involved no inaccuracy in the calibration.

When the hot-wire is close to a solid boundary heat conduction to the wall may be significant. The reading on the anemometer will then indicate an apparently higher velocity than actually is the case. A correction to the reading may be applied based on the 'still air' correction method used by all previous experimenters on corner flows. The basic assumption in the method is that the forced convection and conduction are independent and that the conduction effect can therefore be determined separately by a calibration carried out when the air in the wind-tunnel is stationary. The effect of conduction to the wall is therefore determined by noting the anemometer reading for different distances of the hot-wire from the wall in 'still air' and subsequently subtracting this from the anemometer reading to arrive at the 'true' value corresponding to the local air speed. The correction is found to be dependent on the geometry of the wall in the vicinity of the wire and this required that the conduction effect be measured in several planes parallel to the symmetry plane. Fig. (3.7) shows the 'still air' correction applied

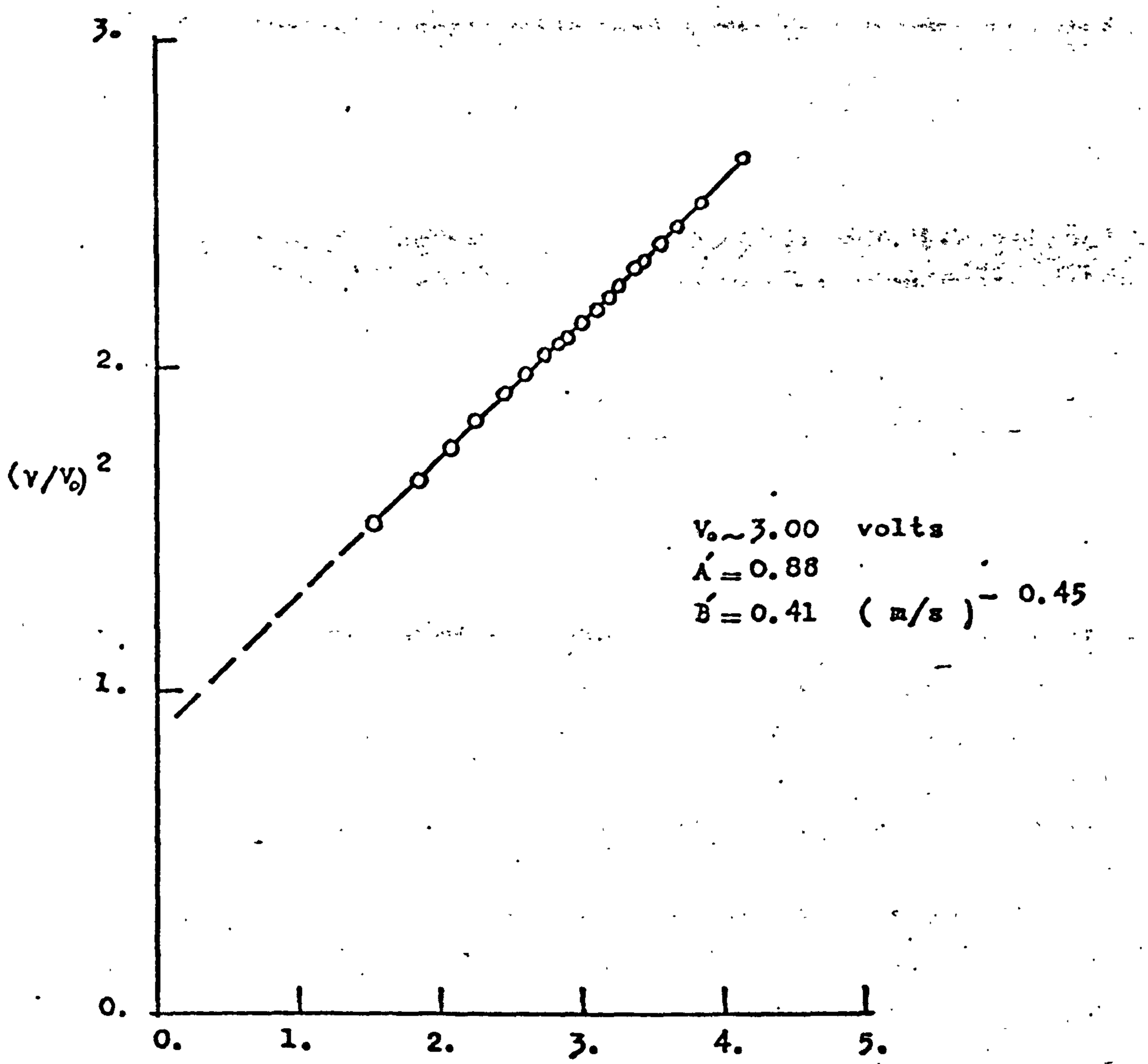

Fig.(3.6) Typical calibration curve for a 5 μm hot-wire probe.

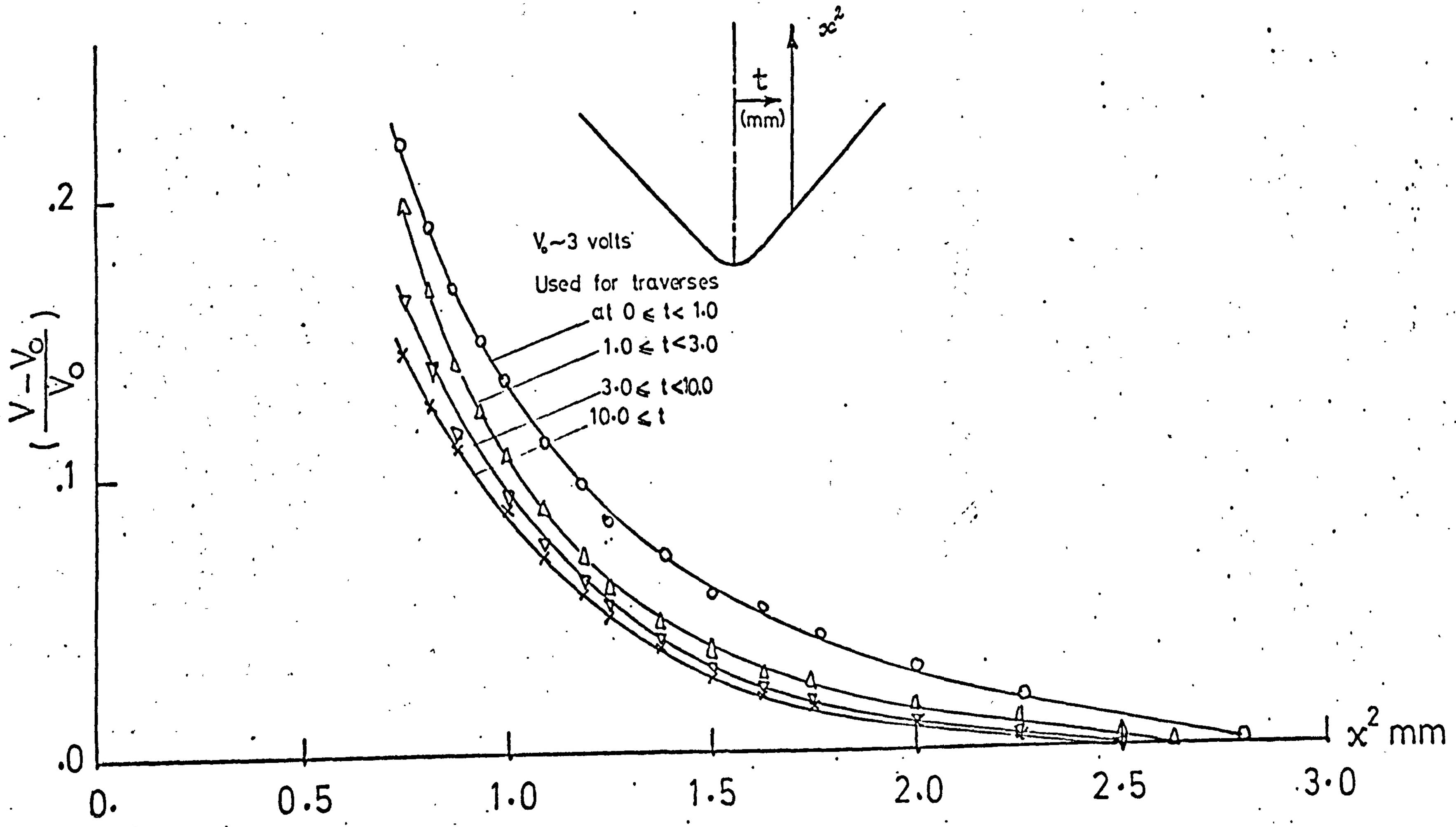

Fig. (3.7) 'Still air' correction for a 5 μm wire probe near the corner walls

in arriving at the experimental results presented in Chapter 4. The voltage ratio $(V-V_o)/V_o$ is plotted against x^2 the distance from the wall to the middle of the wire where V_o is the voltage at sufficiently large distances from the wall for heat-conduction to the wall to be negligible. The four curves shown refer to different distances from the symmetry line and were used according to the scheme indicated in the figure.

The remaining steps in the preparation of the corner in the wind-tunnel were to ensure that the required conditions of zero-pressure gradient laminar flow were established and that the flow was symmetrical about the geometric symmetry plane of the corner.

The conditions sought imply that at sufficient distances from the symmetry plane a Blasius velocity profile should be realized and the satisfactory achievement of such a profile was adopted as the principal criterion that the flow was laminar and the pressure gradient was zero. This is also the criterion used by the other experimenters already mentioned.

The sharp leading-edge was prone to induce turbulence originating at the leading edge near the symmetry plane when the corner was adjusted to give zero streamwise pressure gradient. This was well known from previous experience with sharp leading edges and is apparently caused by all or part of the stagnation line laying on the undersurface of the leading edge. Such a situation can arise from minor non-uniformities in the direction of the free-stream velocity. Given the sharp leading edge one of two alternatives can be

applied. The first is to adjust the geometric incidence of the corner to the point where laminar flow is only just obtained and accept the consequent (favourable) streamwise pressure gradient. The second is to modify artificially the flow direction in the vicinity of the leading edge to ensure that the stagnation line lies everywhere on the upper surface of the corner. The latter alternative is the one adopted here and the particular method is that used by El-Gamal. The arrangement is shown in Fig. (3.3) and consists of a flat wooden plate situated below the corner and with its rounded leading edge about 0.37m upstream of the corner leading edge. The effect of this 'leading edge slat' is to improve the incidence at the inlet to the corner and thereby permit a much closer approach to the Blasius conditions on the plates. The use of a flat plate (rather than, say, a cross-section conforming to the shape of the corner) is justified on the ground that only a local effect in the vicinity of the symmetry plane is required.

Insofar as the induced incidence is moderate and sufficient only to remove the disturbances which caused turbulence its effect will be local to the leading edge and the result for the corner as a whole will be a better realization of the flow which has been modelled theoretically.

With an air speed in the test section of nominally 1.5 m/s a series of experiments was carried out to establish the required flow conditions. These were obtained with the corner model incidence at 0.16^{o} adverse with the 'leading edge slat' at 3.5^{o} adverse incidence (i.e. the configuration shown qualitatively in Fig. (3.3)). The procedure involved

taking measurements on both sides of the symmetry plane in the two-dimensional boundary layers at different streamwise distances and comparing these with the Blasius function. The results and the Blasius function are shown in Figs. (4.62) and (4.63) and their comparison leaves little doubt but that the flow is in the required state, at least as regards zero pressure gradient and laminar nature. The symmetry of the flow about the geometric plane of symmetry was confirmed by measurements taken at several positions along the corner, principally in the plane 0.51 m from the leading edge.

With the corner so arranged, measurements were made throughout the corner in planes 0.165 m, 0.343 m, 0.51 m and 0.805 m from the leading edge. In each plane five vertical traverses were taken on either side of the symmetry plane in addition to two on the symmetry plane itself (i.e. 12 vertical traverses in all at one streamwise station).

A peculiarity of the flow which has been noted by Zamir, Barclay and El-Gamal and was also evident in the course of the present experiments was a sudden and apparently random fluctuations in the velocity. This was manifested in an occasional rapid rise in the level of the trace on the oscilloscope and the readings on the DC and rms voltmeters, but without sign of the high frequency fluctuations indicative of turbulence. This excursion (from the normal situation) lasted for few seconds only ($\sim$10 s), the return to normal being similar to the departure. In this respect it was very much like the behaviour previously reported but the typical time interval between successive occurrences seems to have been smaller than before. The average rate

of occurrences was dependent on the streamwise position of the traverse but near the mid-length of the corner it was usual to encounter this behaviour about once in every vertical traverse, i.e. about once in every 15 minutes. The streamwise dependence was such that the disturbance was more frequent downstream than upstream, perhaps being twice as common near the trailing-edge than at the mid-length and comparatively rare near the leading-edge.

An important aspect of this phenomenon was that it appeared to be confined to the boundary layer or in any event was so mild in the free-stream as to be undetected there.

The increased occurrences of these disturbances relative to previous experiments with a 90° corner may well be due to lower free-stream speeds used in the present case. Goldstein [30, p. 318] has reported that when taking measurements in the laminar flow along a flat plate, a similar random behaviour was found and was attributed to fluctuations in the free stream. Goldstein states that the amplitude of the fluctuations within the boundary layer was several times the amplitude of the fluctuations in the main stream. This may possibly be true in the corner flow although the ratio of boundary layer to free stream fluctuations amplitude must have been very large since, as remarked, fluctuations in the free stream were not detected. Nevertheless it is to be expected that free stream disturbances, if these are indeed the source of the boundary layer fluctuations, are likely to be relatively more pronounced at low tunnel speeds. The flow in the vicinity of the fan is

likely to be in its least steady condition and the upstream propagation of this unsteadiness is the more probable because of the low air speeds. The ratio of velocity fluctuations to mean free-stream speed is also likely to be greater for the same reason.

The phenomenon just described was a factor in choosing the free-stream speed to be used in the experiments where for boundary layer thickness reasons low speed was desirable. The speed chosen was what was thought to be the best compromise between boundary layer thickness and low disturbance rate.

All the results presented in this report were obtained in the disturbance-free flow.

CHAPTER 4

RESULTS AND DISCUSSIONS

4.1. Preliminary

The derived theoretical model of the flow being studied is embodied in equations (2.25). These equations were obtained directly from the somewhat more general formulation, equations (2.21), on assuming that terms explicit in ξ^1 were negligible. This eliminated the rather intractable feature of equations (2.21) without losing the non-similar character of the problem.

To solve equations (2.25) it is necessary to specify the curvature variation of the corner (equation (2.18a))

i.e. $$\lambda = \lambda(x^3/\ell)$$

which in terms of the ξ^i coordinates becomes (equation (2.18b))

$$\lambda = \lambda(\xi^3/\xi^1 R_\ell) \tag{4.1}$$

where $$R_\ell = U_\infty \ell/\nu \ .$$

The important difference in the nature of equations (2.21) and (2.25) becomes particularly clear at this point. To obtain a solution to equations (2.21) at any transverse plane requires the streamwise step-by-step solution from some initial plane whereas equations (2.25) are only paramatically dependent on the quantity $\xi^1 R_\ell$. In other words the solution of equation (2.25) for any plane may be

obtained directly on specifying the value of $\xi^1 R_\ell$ corresponding to that plane.

These remarks are quite general to developable surfaces of large transverse curvature and complying with equations (2.18a). For corner flows, in which we are primarily interested here, it is convenient to define a parameter $\Gamma_{\lambda c}$ by

$$\Gamma_{\lambda c} = (\xi^1 R_\ell)^{-1} \qquad (\lambda_c = \pi - 2\lambda^*). \tag{4.2}$$

$\Gamma_{\lambda c}$ is called the corner parameter. A one parameter family of solutions covers all geometrically similar corners (i.e. corners differing only by a scale factor in their physical dimensions).

The curvature function adopted in this work to describe the radiused corner geometry is

$$\lambda = \lambda^* \tanh(x^3/\ell) \qquad \text{(see equation 3.1)}$$

which transforms according to equation (4.1) to give

$$\lambda = \lambda^* \tanh(\xi^3/\xi^1 R_\ell) = \lambda^* \tanh(\xi^3 \Gamma_{\lambda c}) \tag{4.3}$$

where from equations (3.2), (4.1) and (4.2)

$$\Gamma_{\lambda c} = (\xi^1 R_\ell)^{-1} = \frac{1}{\lambda^* r_0}\left(\frac{2\nu x^1}{U_\infty}\right)^{1/2}. \tag{4.4}$$

$\Gamma_{\lambda c}$ lies in the range $0 \leqslant \Gamma_{\lambda c} \leqslant \infty$ where the limits 0 and ∞ correspond respectively to the flat plate and sharp corner situations. This is evident from equation (4.4).

The generality of the present theoretical analysis with respect to corner configurations may be demonstrated

by solving the corner problem corresponding to the geometry shown in Fig. (1.2c). This more complex geometry still satisfies the conditions of Section 2.4.1, defining the corner geometry. It is sufficient and convenient to specify its shape for $x^3 > 0$ only. Accordingly we may choose

$$\lambda = \lambda' + (\lambda^* - \lambda')\tanh\left(\frac{x^3 - d'}{\ell'}\right) \quad , \quad x^3 > 0^* \qquad (4.5)$$

where λ' is the value of λ at $x^3 = d'$ with ℓ' and d' as scale lengths characterizing the geometry. In terms of the ξ^i coordinate system equation (4.5) may be written as

$$\lambda = \lambda' + (\lambda^* - \lambda')\tanh\left(\frac{\xi^3}{\xi^1 R_{\ell'}} - \bar{s}\right) \qquad (4.6)$$

where $R_{\ell'} = \ell' U_\infty/\nu$ and $\bar{s} = d'/\ell'$. ℓ' is given by

$$\left.\frac{d\lambda}{dx^3}\right|_{x^3=d'} = \frac{\lambda^* - \lambda'}{\ell'} \equiv \frac{1}{r'}$$

$$\text{or} \qquad \ell' = (\lambda^* - \lambda')r' . \qquad (4.7)$$

Therefore $\xi^1 R_{\ell'}$ embodies the new parameters λ' and d' in addition to λ^* and r' (as opposed to λ^* and r' only ($r' \equiv r_o$) in the simpler geometry, equation (3.1), (see equations (4.4))). $\xi^1 R_{\ell'}$ has exactly the same significance as $\xi^1 R_\ell$ in the previous simpler case, being a parameter implying the non-similar character of the flow. For

---

* The curvature is discontinuous at $x^3=0$ and a specification of the complete shape requires two piecewise smooth functions- namely equation (4.5) and an equation for x^3 obtained from equation (4.5) on setting $\lambda' = -\lambda'$ and $d' = -d'$. Equation (4.5) contains as a special case equation (3.1) which represents the geometry mostly used in this work. Equation (3.1) is obtained by setting $\lambda' = 0 = d'$. One consequence of so doing is that the discontinuity at $x^3=0$ disappears and the single function (equation (3.1)) describes the geometry for all x^3.

convenience define

$$\Gamma_{\lambda_c,\lambda_o,\bar{s}} = (\xi^1 R_{\ell'})^{-1} \qquad (4.8)$$

where λ_o is the corner angle at $\xi^3 = 0$.

For want of a better description we shall call the corner described by $\Gamma_{\lambda_c,\lambda_o,\bar{s}}$ a sharp-profiled corner to distinguish it from previous cases, i.e. sharp corners and radiused corners.

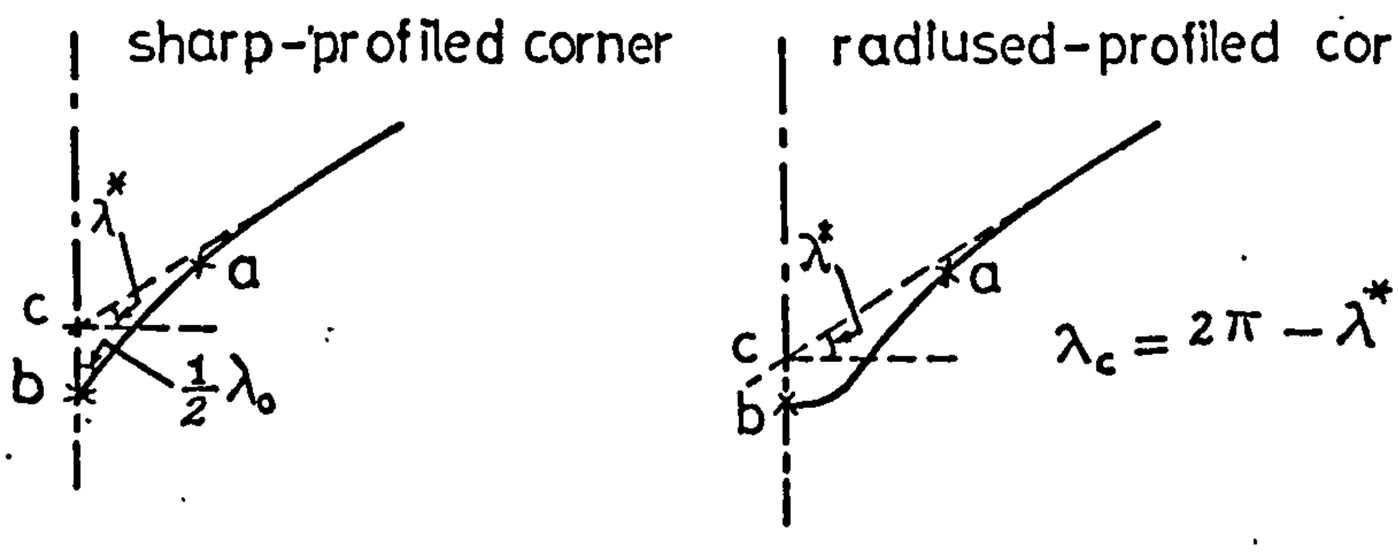

It may be of interest to note that the flow corresponding to the geometry just described is not an asymptotic limit of that along a radiused-profiled corner (see sketch) as is the case with the sharp corner problem which is a limiting form of the radiused corner flow. Nevertheless the flow in both the sharp-profiled and radiused-profiled corners approach the same limit far downstream namely, that along a sharp corner of angle λ_c. In other words, with respect to the boundary layer thickness the points a and b in the sketch coalesce uniformly to become the single point c and the corner will never exhibit the sharp-profiled configuration.

The remarks made so far are with respect to equations (2.25). The flow in zero pressure-gradient is the case being considered here, the equations for this situation being obtained by putting m = 0 in equations (2.25) to give equations (2.28). As described in Chapter 2 equations (2.28) were re-written in terms of the new independent variable $\zeta = \dfrac{\xi^3}{a + b\xi^3}$, (equation (2.64), and the new

dependent variables θ^* and ψ^* defined by equations (2.65). The resulting equations to be solved numerically were equations (2.66) with boundary conditions (2.67). The constants a and b must be chosen prior to computing the solution as must the step-size h and field size (ζ_{max} , ξ^2_{max}). Of these five quantities ζ_{max} and b are uniquely related through equations (2.64) where on letting $\xi^3 \longrightarrow \infty$, $\zeta_{max} = 1/b$. Four parameters remain to be chosen but there is no obvious analytical means for their determination which might suggest them to be arbitrary and yet by some experimental computations, we find that the solution may be dependent on their values. Indeed a solution may be unobtainable for certain choices. On the other hand, the solution to the physical problem being studied is doubtless unique and quite independent of any parameters introduced in the numerical scheme. A rational method for arriving at suitable values for h, a, ζ_{max} and ξ^2_{max} is to seek by trial-and-error methods the combination of values for which changes about those values have the least influence on the solution. This is the method used here and is similar to that adopted by Ghia [14].

All computing was done on the IBM 360 at University College London. The C.P.U. time taken to reach a satisfactory combination of parameters for the different corners treated was in excess of 100 hr. This was so large as to preclude any further experimentation with regard to the mesh interval h used in the computations and as a result this was fixed from the outset at 0.4.

Numerical results for the analytical treatment of the

problem are presented in the following sections together with the results of the experimental work described in Chapter 3. The cases chosen for theoretical solution are corners having angles of 45^{o}, 90^{o}, 135^{o}, 225^{o}, 270^{o} and 315^{o}. These include sharp, radiused and sharp-profiled corners. The theoretical and experimental results obtained are compared amongst themselves and with theoretical and experimental data available in the literature.

4.2 Sharp corners ($\Gamma_{\lambda_c = \infty}$)

After some experimental computations the following choice for the parameters introduced in the numerical scheme was made to satisfy the criterion mentioned above:-

$$\zeta_{max} = 14.4 \qquad (\ b \approx 0.0694)$$
$$\xi^2_{max} = 16.0$$
$$h = 0.4$$
$$a = 0.5 \ .$$

The solution was deemed satisfactory when the difference in the values of u, θ^*, φ and ψ^* from successive iterations was in each case less than 0.0005 everywhere in the domain of integration. A relaxation parameter of 0.5 was found to give the most rapid convergence in most cases and henceforth was used for all computations.

4.2.1 Streamwise velocity

a) $\Gamma_{90} = \infty$

The solution for the streamwise velocity as seen in planes parallel to the symmetry plane is shown in Fig. (4.1).

The figure by itself merits little comment; the profiles are quite smooth and vary in a regular manner to the asymptotic Blasius profile (i.e. at $\zeta^3 = \infty$). Of primary interest is the relationship between this solution and other existing solutions. This matter is discussed presently.

The streamwise velocity profile in the symmetry plane is the characteristic profile of the flow and this is shown separately in Fig. (4.2) along with those from the solutions by Pearson [13], Rubin and Grossman [11] and Ghia [15]. In addition the Blasius profile is included to offer some reference against which to measure the effect of the corner on the one hand and the differences amongst the symmetry plane results on the other. Complete agreement between the results obtained here and those of Ghia is evident and this is generally true throughout the corner as is demonstrated in Fig. (4.3) which depicts the isovels of the streamwise velocity u. In this figure, (4.3), the results of Rubin and Grossman exhibit a slower decay into the side edge boundary layer than do the new results presented here (or those of Ghia [15]). The separation-like character of the profiles in Fig. (4.2) has been pointed out so often in the literature as to require no further comment here.

The reasons believed to cause the differences in the solutions of references [11], [13] and [14, 15], who all have solved the full set of corner layer equations and used the same coordinate system, were outlined in Chapter 1 (see p. 19 and pp. 21-23). Insofar as the explanations are satisfactory, reasons for expecting the present agreement with Ghia's results will simultaneously account for the

differences with the remainder.

In Ghia's solution and in the present case the field of integration was infinite in the ξ^3 direction. The boundary conditions at $\xi^3 = \infty$, on the symmetry plane and everywhere on the wall are equivalent and it must therefore be expected that the solution everywhere near the wall will be virtually the same. In the present solution the boundary conditions for large ξ^2 were applied at finite ξ^2 (=16) whereas in Ghia's integration they were effectively applied at infinity. The streamwise velocity and vorticity, u and Ω decay exponentially fast with increasing ξ^2 while the crossflow velocities v and w do so with algebraic speed. The precise value of ξ^2 at which the boundary conditions are applied would seem to have small importance in the case of u and Ω and we may look for a high degree of correspondence in the results for these variables in the two solutions. This is less likely in the case of the algebraically decaying variables v and w. All of this is exactly as we find it.

A matter of importance of course is how well the theoretical solution agrees with experimental results. This may be assessed from Fig. (4.4) where the streamwise velocity profiles from the present solution and from the measurements by Zamir [2,21] and El-Gamal [4] are shown. Zamir's results contradict any assumption of corner layer similarity whereas El-Gamal's results for the same range of Reynolds numbers are quite different and may even offer some support for the similarity hypothesis.

Zamir's results are particularly remarkable. They represent a physical situation which is quite different from that modelled theoretically but at present one can only speculate on what caused the difference. It may be that the leading edge configuration used was a source of disturbance whose propagation and amplification downstream gave rise to the curious profiles obtained. It is consistent with such a mechanism that the best agreement between experiment and a disturbance free situation should be obtained at the lowest (experimental) Reynolds number which seems to be the case. Zamir's measurements are of considerable interest and importance for they show a completely unexpected behaviour in the corner layer and one that seems to have no counterpart in two-dimensional situations.

The view that these profiles are functions of some extraneous influence and not intrinsic to corner flow is supported by the results of El-Gamal. The latter results are in a better qualitative agreement with the theoretical curve and lie below it. A systematic improvement in this agreement is observed with increasing Reynolds number. El-Gamal believed that there exists an 'entry length' for corner flow which is very much greater than that for flow on a flat plate and this accounts for the apparently developing character of the profiles measured. As an extension of this belief El-Gamal suggested that for a sufficiently large Reynolds number, experimentally measured data would agree with the theoretical solution*. El-Gamal

---

* If El-Gamal's explanation is correct, it is of minor interest to note that transition to turbulent flow may intervene before the development is complete and that in practical situations the theoretical profile may never be realized.

recognized that a laminar flow along a rectangular corner is in a marginally stable condition and as a result may be extremely sensitive to a very small pressure gradient. To answer the question which such a possibility might raise, El-Gamal used his experimental data to construct Fig. (4.5) (taken from his thesis [4]). This figure shows two profiles from the two-dimensional region (obtained for 0.3^{o} favourable and 0.85^{o} adverse corner incidences) and the corresponding profiles for the symmetry plane. The figure also contains the Blasius profile and the symmetry plane profile taken from reference [11]. He compared the differences in the two-dimensional profiles with those in the symmetry plane and concluded that a further improvement in the correspondence between the experimental two-dimensional profile with the Blasius solution would have no significant effect on the experimental profile in the symmetry plane. This was considered to eliminate the possibility of non-zero stream-wise pressure gradient being a cause of the difference between theory and experiment.

Whatever the reason for the difference might prove to be, there seems little cause for questioning the precision of the theoretical analysis. It is much more likely that difficulties of realizing experimentally the idealized theoretical model are sufficient to explain the differences.

This discussion for the 90^{o} corner is of some relevance to the results presented in the following sections.

b) $\Gamma_{135} = \infty$

The results for the 135^{o} sharp corner are shown in

Figs. (4.6) - (4.9). Fig. (4.6) shows the velocity profiles in planes parallel to the symmetry plane and Fig. (4.7) shows the isovels in a transverse plane. The influence of the corner on the velocity distribution for this larger angle is less marked than in the 90^{o} case.

The only theoretical solutions available for the 135^{o} corner problem are those by Barclay [3] and Desai and Mangler [16]. The symmetry plane profiles from these and the present solutions are shown in Fig. (4.8) with the Blasius profile again added for reference. Barclays solution is based on a series method similar to that of Carrier [7] and suffers from the same defects. On the scale of the difference between the Blasius and the symmetry plane profiles, the differences in the three symmetry plane profiles are quite as great as for the 90^{o} corner and have the same origin.

Barclay [3,31] has obtained measurements in the flow along a 135^{o} corner and these are shown in Fig. (4.9) together with the theoretical solution. It is important when comparing data from these two sources to relate them to the corresponding data in the two-dimensional region and the latter are included in the figure for this reason. Barclay is aware [31] that his results are consistent with a small favourable pressure gradient and Desai and Mangler [16] have calculated on the basis of the two-dimensional results that the gradient was equivalent to a free stream velocity distribution given by $v(1) \propto (x^{1})^{0.02}$. Any correction for this would improve in some measure the agreement between experiment and theory. The quantitative effect of the pressure gradient at the symmetry plane is

uncertain but assuming the change would not be less than that in the two-dimensional region the resulting experimental profile would justify confidence in the soundness of the theory. The experimental results make a strong claim for corner layer similarity at this angle and the matter of 'entry length' does not seem to arise here. If such a concept is necessary the 'entry length' would of course be weaker, perhaps very much weaker, at this angle than for a 90^{o} corner.

c) $\Gamma_{45} = \Gamma_{225} = \Gamma_{270} = \Gamma_{315} = \infty$

The symmetry plane profiles for a wide range of corner angles are shown in Fig. (4.10) in which the profiles for the new angles 45^{o}, 225^{o}, 270^{o} and 315^{o} are introduced. The marked variation in the stability of the flow with corner angle is evident. The 180^{o} profile divides the range in two categories characterized respectively by the presence and absence of an inflection point. For corner angles greater than 180^{o} there is no inflection point in the profile. The inflection point appears at the wall in the 180^{o} profile (i.e. the Blasius profile) and moves progressively outward into the flow as the angle is reduced. As anticipated, reduction in the angle of the corner below 90^{o} causes an increasingly rapid thickening in the corner layer but otherwise the flow is characteristically similar to the 90^{o} case. The stability of the flow at this and smaller angles must be very precarious indeed and there may be some doubt as to whether the theoretically determined profiles are likely to be observed experimentally.

For corner angles greater than 180^{o} the character of the flow is typified by the 225^{o} and 270^{o} cases. Figs. (4.11) and (4.12) show the velocity profiles in planes ξ^3 = const., for these angles respectively. The isovels in transverse planes are shown in Figs. (4.13) and (4.13a). They clearly show the thinning of the corner layer as the corner assumes the form of a streamwise edge.

The exceptional profile in Fig. (4.10) is that for $\lambda_c = 315^{o}$ which exhibits a small overshoot in u beyond the asymptotic value 1.0. The reason for this is not clear but may be associated with the fact the velocity reaches unity in a distance from the wall $\xi^2 = 1.6$, which corresponds to only four mesh intervals. In this sense the step size h is very large and it may be that the numerical treatment has difficulty in handling the problem with accuracy.

4.2.2. Crossflow Velocities v and w

The smallness of the crossflow velocity vector makes its direct experimental determination almost impracticable. Its real importance lies in its influence on the streamwise velocity component and it is as a result of a defect in the handling of the crossflow that the solutions by Carrier [7] and by Desai and Mangler [16] were in error. This was discussed in Chapter 1.

The crossflow velocity vector components v and w are computed from equations (2.17a) in conjunction with the definition of ψ^*, equation (2.65), once a converged solution is obtained.

a) $\Gamma_{90} = \infty$

The most significant feature of the crossflow here is the appearance of negative values for the component v in the vicinity of the corner line. This was also found by Ghia [14]. Both Ghia's and the present crossflow results are shown in Fig. (4.14). Here the arrows represent only the direction of the crossflow velocity vector and convergence towards or divergence from a point does not imply the presence of a sink or a source. The similarity between the present results and Ghia's solution is remarkable. It is clearly seen that the crossflow velocity vector is null at two points in the body of the fluid. For reference purposes such points will be called 'zero points'. The first zero point is on the symmetry plane and the other is a small distance from it and near to the wall. Off the symmetry plane and near the wall the crossflow is parallel to the wall and directed towards the symmetry plane; this is consistent with the experimental flow visualization of Zamir and Young [21]. Everywhere else except for a small region near the corner line the flow is outwards and parallel to the symmetry plane.

Tokuda [20], who analysed the Stokes flow region in the vicinity of the corner line of a 90^{o} sharp corner, has predicted the existence of a series of viscous eddies there. The complex structure of the crossflow near the corner line, shown in Fig. (4.14), may be indicative of such a behaviour. If the eddies exist then this fine structure will be missed by a numerical solution employing the step sizes used here. Nevertheless it is extremely doubtful that eddies of such small scale can appreciably influence the bulk of the cross-flow distribution and hence the streamwise velocity component.

A series of profiles of v in planes ξ^3 = constant is shown in Fig. (4.15). The negative values of v indicated in Fig. (4.14) are too small to be plotted in Fig. (4.15). The feature of v illustrated by these profiles is its sensitivity to variation in ξ^3 and taking the profiles at the extremes $\xi^3 = 0$, and $\xi^3 = \infty$ as a measure the difference in the profiles is seen to be very marked indeed.

The profile of the velocity component v in the plane of symmetry is shown in Fig. (4.16) together with the corresponding profiles obtained by Pearson [13], Rubin and Grossman [11] and Ghia [15]. Qualitative agreement among all the results is quite good particularly for ξ^2 less than about 5. The greater differences amongst the profiles as ξ^2 increases beyond 5 are consequences of certain numerical aspects of the problem. The principal of these concerns the placing of the asymptotic boundary conditions. Ghia applied these correctly (see Chapter 1 pp. 20-22). It will be recalled that in the present solution the boundary conditions for large ξ^3 were correctly applied ($\xi^3 = \infty$) but for large ξ^2 they were applied at a finite value ($\xi^2 = 16$) rather than at infinity. Where differences are relatively large ($\xi^2 > 5$) the streamwise velocity component u is virtually uncoupled from the crossflow and is consequently little influenced by the behaviour of v.

Fig. (4.17) shows velocity profiles of the w component of the crossflow velocity vector in planes parallel to the symmetry plane. The results have two curious features. One is the double reversal in the flow direction shown by profile 2. This is in accord with Ghia's results and is found from the computations to be the characteristic shape

for $\xi^3 < 1.738$. The second feature for comment is the undershooting in the case of profile 6. Curve 7 is an analytically exact result (equation (2.60)) and we might expect the profiles to asymptote uni-directionally towards this limiting case, contrary to the results shown. The resolution of this conflict between expectation and results has received a great deal of time consuming attention. As well as varying the several parameters introduced in the numerical scheme, a reformulation of the vorticity condition at the wall was made in an attempt to force the boundary condition at $\xi^3 = \infty$ more strongly on the solution but this resulted eventually in a diverging solution after apparent convergence up to about 1500 iterations. Another device for extending the field size in the ξ^2 direction was tried and is outlined briefly here.

For any of the corner configurations considered in this Chapter it is assumed that u and θ^* attain their asymptotic values at $\xi^2 = 12.0$ (this is well confirmed by the numerical solution) and as a consequence of which equations (2.66a,b) are identically satisfied. It remains now to treat equations (2.66c,d) only for $\xi^2 > 12$. These equations approximate to

$$\varphi_{,22} + \zeta_1^2 \varphi_{,\zeta\zeta} = s\zeta_1 \varphi_{,2\zeta} + s_{,3} \varphi_{,2} + \left(\frac{c_{,3}}{c}\zeta_1 + \zeta_2\right)\varphi_{,\zeta} + \left(\frac{c_{,3}}{c}\right)_{,3}\varphi + \left(\zeta_1 \frac{s c_{,3}}{c} - 2 s_{,3}\right)\psi^*_{,\zeta} + \left(\frac{s c_{,3}}{c} - 2 s_{,3}\right)_{,3}\psi^* + D^* \quad (4.9a)$$

$$\psi^*_{,22} + \zeta_1^2 \psi^*_{,\zeta\zeta} = -s\varphi_{,22} - \left(\frac{c_{,3}}{c}\right)\varphi_{,2} + s\zeta_1 \psi^*_{,2\zeta} + \left(s_{,3} - 2\frac{c_{,3}}{c}\right)\psi^*_{,2} - \left(3 c_{,3} + \xi^3 c_{,3}\right) + E^* . \quad (4.9b)$$

Analogously to the variable ζ, we introduce the new independent variable

$$\eta = \frac{\xi^2}{a' + b'\xi^2} \qquad \text{for} \quad 12 < \xi^2 \leqslant \infty$$

where a' and b' are constants. φ increases indefinitely with ξ^2 and is therefore replaced by the bounded variable φ^* defined by

$$\varphi^* = \varphi - c\, f(\xi^2)$$

The boundary conditions for φ^* are (for $\xi^2 > 12$)

$$\left.\begin{aligned} \zeta &= 0 \quad ; \quad \zeta_1 \varphi^*_{,\zeta} - s\eta_1 \varphi^*_{,\eta} - \frac{c_{,3}}{c}\varphi^* = 0 \\ \zeta &= \zeta_{max} ; \qquad \varphi^* = 0 \\ \eta &= \frac{1}{b'}, (\xi^2 = \infty) ; \qquad \varphi^* = 0 \end{aligned}\right\} \qquad (4.10)$$

where $\eta_1 = \dfrac{\partial \eta}{\partial \xi^2}$ and $\varphi^*_{,\eta} = \dfrac{\partial \varphi^*}{\partial \eta}$.

Equations (2.9) are re-written in terms of η and φ^* and solved simultaneously with equations (2.66). The interface conditions (at $\xi^2 = 12$) are taken from the iterations on system (2.66) and used directly in the approximate equations. This method, though attractive because of the relative simplicity it provides as opposed to transforming the whole of equations (2.66), was unfortunately found to converge rather slowly. More than 3000 iterations were found insufficient for convergence and the attempt to solve the undershoot problem by this scheme was abandoned.

b) $\underline{\Gamma_{135} = \infty}$

Fig. (4.18) pertains to the crossflow velocity vector direction in the corner layer. It resembles very closely

the corresponding plot for the 90^{o} corner, Fig. (4.14), but unlike that case only one zero point exists and this is on the symmetry plane. Evidently the change in angle is responsible and the result is in keeping with expectation since we must have the zero points disappear altogether when the angle is 180^{o}.

The profiles of v and w in planes parallel to the plane of symmetry are shown in Figs. (4.19) and (4.20) respectively. The profiles in both cases are similar in character to their counterparts for the 90^{o} corner. One small but significant difference is the absence of the double reversal in w of the kind noted in the rectangular corner (cf. Fig. (4.17)). Otherwise the discussion for the smaller angle can be carried over to the 135^{o} corner.

c) $\underline{\Gamma_{270} = \infty}$

Fig. (4.21) shows the diagram of the crossflow velocity direction for the 270^{o} corner. In this case the inflow on the symmetry line near the walls extends over a greater length than was found in the previous internal corners and is of greater magnitude. (See curve 1 on Fig. (4.22)).

As a result of the discussion in Section 2.6 it comes as no surprise to find a certain anti-symmetry in the cross-flow near the wall in the 90^{o} and 270^{o} corners. The flow is outward from the symmetry plane in the 270^{o} case but inward in the 90^{o} corner. There is a zero point on the symmetry plane in each case and another zero point similarly disposed just off the symmetry plane. This second zero point in the 270^{o} corner is particularly interesting. The behaviour

of the arrows (Fig. (4.21)) in its vicinity is suggestive of a closed vortex. To illustrate this possibility a scrap view of this region of the flow is also shown in the figure. Added to the scrap view are directions calculated from the computer results for points not used in forming the main diagram. The circle shown on this view represents the author's suggestion of how the flow might be interpreted here, i.e. as a closed vortex. If this might be the case in this, the 270^{o} corner, might it also be true at the similar zero point in the 90^{o} case? Looking again at Fig. (4.14) it is not at all clear that any such interpretation can be placed on the flow.

Profiles of the crossflow components v and w at ξ^3 = constant planes are shown in Figs.(4.22) and (4.23) respectively. The v-component shows a slight overshoot not seen in the internal corner flows but the undershoot in the w component at large ξ^3 is still present (see curve 7, Fig. (4.23)).

To complete the remarks on the crossflow vector, its profile at the symmetry plane (which is simply the component v since w = 0 here) for different angles is shown for comparison purposes in Fig. (4.24).

d) $\Gamma_{45} = \Gamma_{315} = \infty$

The crossflow velocity fields for these two cases are shown in figures (4.25) and (4.26). The crossflow in Fig. (4.25) is more complex than that for $\Gamma_{90} = \infty$. The possibility of a closed vortex in the case of $\Gamma_{270} = \infty$ is strengthened on noting a similar and even more pronounced situation resulting from increasing the angle to 315^{o} (Fig.(4.26)).

The weight of this additional evidence is modified however by the doubt regarding the computational accuracy for $\Gamma_{315} = \infty$, mentioned on page 119 .

4.2.3. .Wall shear stress

The contribution to the wall shear stress from the cross-flow velocity is negligible compared with that from the stream-wise velocity. Consequently the wall shear stress is assumed to be given by

$$\tau_{w_c} = \mu \left. \frac{\partial v(1)}{\partial (x^2 \cos\lambda)} \right|_{x^2=0}$$

or in terms of the corner layer variables

$$\tau_{w_c} = \frac{\rho U_\infty^2}{\cos\lambda} \left(\frac{2 x^1 U_\infty}{\nu} \right)^{-\frac{1}{2}} \left. \frac{\partial u}{\partial \xi^2} \right|_{\xi^2=0} .$$

Denoting the wall shear stress at $\xi^3 = \infty$ by τ_{w_∞} the results are presented in terms of

$$\frac{\tau_{w_c}}{\tau_{w_\infty}} = \frac{\left. \frac{\partial u}{\partial \xi^2} \right|_{\xi^2=0}}{\cos\lambda \left(f''(0)/\cos\lambda^* \right)} \qquad (4.11)$$

where $f''(0)$ is the second derivative of the Blasius function f at $\xi^2 = 0$, (equation (2.44)). For a sharp corner this ratio becomes

$$\frac{\tau_{w_c}}{\tau_{w_\infty}} = \frac{\left. \frac{\partial u}{\partial \xi^2} \right|_{\xi^2=0}}{f''(0)} \qquad (4.12)$$

since $\lambda = \lambda^*$ for $\xi^3 > 0$ in this case.

The results for corners of angles 45^o, 90^o, 135^o, 225^o, 270^o and 315^o are shown in Fig. (4.27) together with the results for the 90^o corner as obtained by Ghia [14,15] added for comparison. The two sets of results for the 90^o case are in close agreement. The figure shows the expected variation in shear stress with increase in λ_c and near the

symmetry plane the shear stress for corners having $\lambda_c >$ 180^o rises to very large (i.e. indeterminately large) values.

An interesting feature noted in the figure is the negative shear observed in the $\Gamma_{45} = \infty$ case. Whether this is a numerical error or a correct prediction of the physical situation is uncertain. Nevertheless it is not inconceivable that a situation of self-induced reverse flow exists here and there is an example of such a situation [32].

The extent of the corner influence might conveniently be defined as the distance from the symmetry plane ξ^3 to the point where $\tau_{w_c}/\tau_{w_\infty} = 0.99$, say. The variation of the wall shear stress with corner angle is evident from the figure.

4.3. Radiused corners ($0 < \Gamma_{\lambda_c} < \infty$)

The choice of values for the parameters ζ_{max}, ξ^2_{max}, h and a to be used in the numerical solution for the radiused corner was conditioned amongst other things by the requirement to provide a large enough number of mesh points on the curved part of the corner for the solution to get a 'grip' on the curvature variation. This is particularly important in the immediate vicinity of the symmetry plane. It is the impossibility of satisfying this requirement that necessitates the special treatment of the shap corner described in Section 2.4.3 (ii) (p. 52). Even in the radiused corner there will be some value of the radius below which it becomes impracticable to provide the necessary coverage over the curved part and simultaneously

have an adequate coverage elsewhere because of limitations in computing time. This difficulty has been encountered in the course of the computations carried out in this work and will be discussed when the results are presented below. Following the criterion described in Section 4.1 the choice of parameter values made for the radiused corner was

$$\zeta_{max} = 12.$$

$$\xi^2_{max} = 16.$$

$$h = 0.4$$

$$a = 0.1 \quad .$$

4.3.1. Streamwise velocity

a) $0 < \Gamma_{90} < \infty$

The streamwise velocity profiles in the symmetry plane are shown in Fig. (4.28) for different values of Γ_{90} together with the profiles for $\Gamma_{90} = \infty$ and $\Gamma_{90} = 0$ (i.e. the sharp rectangular corner and flat plate cases). The profiles vary with Γ_{90} in a smooth, regular manner. The limiting values $\Gamma_{90} = 0$ and ∞ represent special cases which have already been solved by special methods. Solutions for all other values of Γ_{90} are obtained from the general radiused corner formulation. This is limited in its applications to problems that are not too close to the extreme situations of the flat plate and sharp corner. The reasons are different for each extreme.

As Γ_{λ_c} increases the rate of change of the local angle λ with respect to ξ^3 increases. When Γ_{λ_c} becomes very large the numerical methods have difficulty in adequately representing the rapid variation in λ with ξ^3. Fig. (4.29) shows the variation of the local angle λ with ξ^3 in the

important range $0 \leqslant \xi^3 \leqslant 0.51$. This range is covered by 10 mesh planes the first two of which are $\xi^3 = 0.04$ and $\xi^3 = 0.086$. The angle turned between $\xi^3 = 0.0$ and $\xi^3 = 0.04$ and 0.086 must, intuitively, be an important influence on the accurate representation of the curvature and the smaller this increment in λ the better.

Equation (4.3) is

$$\lambda = \lambda^* \tanh(\xi^3 \Gamma_{\lambda_c})$$

from which it is seen that for fixed ξ^3, λ increases exponentially with Γ_{λ_c}. This is also evident in Fig. (4.29). It is quite certain that above some value of Γ_{λ_c} the angle turned through between the symmetry plane and the first few mesh points will be so great as to render the numerical representation of the problem inaccurate in this vicinity.

For Γ_{90} greater than about 15 the calculations were non-convergent, presumably for the reason just given. Some effort was made to improve the result by reducing the mesh size near $\xi^3 = 0$ but for practical reasons this had to be accomplished at the expense of a larger mesh elsewhere and whether or not this negated the effect of the improved coverage near the symmetry line, non-convergence persisted.

For $10 < \Gamma_{90} \leqslant 15$ the solution was virtually stationary and $\Gamma_{90} = 10$ evidently constitutes the upper limit to the combination of radiused corner theory and numerical scheme used here. It is suggested that this is no serious defect in the present work since the difference between the solutions for $\Gamma_{90} = 10$ and $\Gamma_{90} = \infty$ is small enough to permit any reasonable interpolation to be adopted for

intermediate cases with negligible error in conceivable practical situations.

Regarding the opposite extreme where Γ_{90} is very small (<0.2), the solution has proved to be unsatisfactory. In the range $0.2 \geqslant \Gamma_{90} \geqslant 0.15$ the resulting velocity profiles, characteristically lie below the Blasius profile* and increasingly so as Γ_{90} is reduced towards 0.15 below which value no numerical results could be obtained. The reason for this behaviour is rather uncertain. Apart from the ever present possibility that numerical procedures are imperfect (e.g. the choice of ξ^2_{max}, ζ_{max} and a may be unsuitable in this extreme), the likelihood that the theory is reaching its limit of application also suggests itself. A central-requirement for the valid application of the theory developed in this thesis is that the radius of curvature $r_o = 0(\delta)$ or less where $\delta = 5xR_x^{-\frac{1}{2}}$ and $R_x \longrightarrow \infty$ (reference [33], p. 130). In terms of Γ_{90}

$$\delta/r_o = \frac{5\pi}{4\sqrt{2}}\Gamma_{90}$$

from which we have that Γ_{90} should be 0(1) or greater. Normally this is taken to mean that δ/r_o should be finite (perhaps infinite) but not extremely small. $\Gamma_{90} = 0.2$ corresponds to $\delta/r_o = 0.56$ which would seem to lie well within the required range. It is just conceivable that in practice this ratio is rather small and that the application of the theory is limited to larger values of Γ_{90}. However there is no strong indication that this is so any more than that the numerical treatment is in some way responsible for the behaviour noted in this lower range of corner parameter.

---

* That is on the opposite side from the profiles for $\Gamma_{90} > 0.2$.

One possible contributory factor in the context of the present discussion is the omission from the final theoretical formulation of terms such as those exemplified in equation (2.23). It may be thought that these terms assume a greater importance than was recognized, at least for Γ_{90} small. The experimental results on the other hand suggest that this is not so (see Section 4.5, Fig. (4.76)). On theoretical ground also it is doubtful that the omitted terms should be important. They contribute to the non-similar behaviour of the flow, but at or near the extremes $\Gamma_{90} = \infty$ and 0 the flow is virtually similar and these terms will naturally diminish in importance as these limits are approached.

The cause of the dubious behaviour of the solution for small values of the corner parameter remains problematical. Until such times as an unequivocal answer is available it is appropriate that the range of Γ_{90} be truncated to exclude the lower questionable values. In view of the difficulties associated with very large Γ_{90} values, already discussed, the recommended range of application of the radiused corner theory is consequently

$$0.225 \leqslant \Gamma_{90} \leqslant 10.$$

This is a large and practically useful range. The ratio of the extreme values is about 44 but, more importantly, it is shown in Fig. (4.28) that together with the special solutions for $\Gamma_{90} = 0$ and ∞ the solutions presented, effectively provide complete coverage of the entire spectrum of Γ_{90} values.

A solution to the radiused corner theory is dependent on λ_c and Γ_{λ_c} and a discussion of the results will

normally require considering the flow in different planes ξ^3 = constant. The volume of discussion is considerably reduced without essential loss of insight into the effect of the radius if we confine attention to one representative value of the corner parameter Γ_{λ_c}. Such a value is Γ_{λ_c} =3. The variation of the streamwise velocity profile with ξ^3 is shown for Γ_{90} =3 in Fig. (4.30). The corresponding isovels are shown in Fig. (4.31). The behaviour displayed in these figures is exactly as expected and require no comment otherwise.

b) $\Gamma_{270} = 3$

The results are shown in figures (4.32) and (4.33). The symmetry profile of the streamwise velocity u for the case $\Gamma_{270} = \infty$ (sharp external corner) is included in figure (4.32) for the purpose of comparison. As expected this profile lies well below the corresponding profile for Γ_{270}=3 (radiused external corner).

c) $\Gamma_{\lambda_c} = 3$

The effect of λ_c on the solution is illustrated in Fig. (4.34) which shows the profiles for the streamwise velocity component in the symmetry plane. The results are similar to those for the sharp corner (Fig. (4.10)) but they are clearly less susceptible to changes in λ_c.

4.3.2. Crossflow velocities v and w

a) $0 < \Gamma_{90} < \infty$

The crossflow velocity field variations with Γ_{90} are given in figures (4.35) to (4.41). Consistent with the behaviour of the streamwise velocity, the crossflow

varies in a regular fashion from the case $\Gamma_{90} = 0.225$ towards the sharp corner. The situation for $\Gamma_{90} = 7$ and 10 are virtually the same as the asymptotic (i.e. sharp corner) limit.

The flow near the symmetry line is rather complex even for the smallest Γ_{90} (=0.225) and it is here that changes with Γ_{90} are most marked. The principal observation concerns the position of the zero point on the symmetry plane. The zero point is substantially clear of the wall for $\Gamma_{90} = 0.225$ and apparently moves towards the wall as Γ_{90} increases, reaching the wall at $\Gamma_{90} = 1.0$. Thereafter it moves out again towards its sharp corner position as Γ_{90} is further increased. This is rather surprising since one might expect to see a uni-directional movement of the zero point from its flat plate ($\Gamma_{90} = 0$) position on the wall to its sharp corner ($\Gamma_{90} = \infty$) position as Γ_{90} is increased from zero to infinity. Whether this behaviour of the zero point is a correct reflection of the physical situation or is an advanced warning of the difficulties, mentioned previously, in obtaining solutions for very small values of Γ_{90} cannot yet be decided.

Fig. (4.42) shows the symmetry plane profiles of the crossflow component v for different values of Γ_{90} . All the profiles for finite Γ_{90} clearly show the beginning of the algebraic decay with increasing ξ^2 as well as systematic change with Γ_{90} . The profile for $\Gamma_{90} = \infty$ obtained by Ghia is included in the figure (dotted line) and the family resemblance between this and the present results for finite Γ_{90} is remarkable. The exceptional profile in the figure

is the present result for $\Gamma_{90} = \infty$. This particular case has been discussed in association with Ghia's results in Section 4.2.2 (a). The essence of that discussion was that the boundary conditions should ideally be applied at $\zeta^2 = \infty$ as was done by Ghia, whereas in the present solution they were placed at $\zeta^2 = 16$ for reasons given. Any effect of this is certain to be most pronounced at $\Gamma_{\lambda c} = \infty$ and this is evidently so from the results. The correspondence between the finite Γ_{90} results here and Ghia's result suggests that applying the boundary conditions at $\zeta^2 = 16$ has negligible effect on the results for finite Γ_{90}. Yet even for $\Gamma_{90} = \infty$ where the effect is more pronounced, we have already seen that, probably because the difference is significant only at large ζ^2 where v and u are uncoupled, the effect on u is still negligible (see Fig. (4.2)).

The results of the $\Gamma_{90} = 3$ case are used as an example to show the variation of the crossflow velocities with ζ^3. Figures (4.43) and (4.44) pertain to the profiles of v and w respectively. The behaviour of these velocity profiles is remarkably similar to the corresponding profiles of the $\Gamma_{90} = \infty$ case.

b) $\underline{\Gamma_{270} = 3}$

Fig. (4.45) shows the crossflow velocity field for $\Gamma_{270} = 3$. Unlike the solution for $\Gamma_{270} = \infty$ the flow pattern is simple and there are no negative values of v or any sign of a closed vortex. The profiles of v and w at planes parallel to the symmetry plane are shown in figures (4.46) and (4.47). They are similar in general trend to those for $\Gamma_{270} = \infty$ already discussed, figures

(4.22) and (4.23).

c) $\underline{\Gamma_{45} = \Gamma_{135} = \Gamma_{225} = \Gamma_{315} = 3}$

The crossflow velocity field for these cases are shown in figures (4.48) to (4.51). The most interesting feature here is the evident existence of a closed vortex in the crossflow velocity field for $\Gamma_{315} = 3$, Fig. (4.51). The symmetry plane profiles for v in each of the above cases, together with those corresponding to $\Gamma_{90} = \Gamma_{270} = 3$ are shown in Fig. (4.52).

4.3.3. Wall shear stress

The wall shear stress is shown in Fig. (4.53a) for several values of Γ_{90}. Two features are of interest in this figure. One is confirmation of the change from zero wall shear stress at $\xi^3 = 0$ in the case $\Gamma_{90} = \infty$ to non-zero shear for all finite values of Γ_{90}. The other is the wall shear stress behaviour for $\Gamma_{90} \leqslant 0.5$ exemplified by the increase in the lateral extent of the corner effect. This behaviour is nevertheless in keeping with the fact that as Γ_{λ_c} decreases, the curvature variation extends to larger distances from the plane of symmetry, i.e. larger values of ξ^3, with the consequence of increasing the extent of the low wall shear stress. It appears that for rather large values of Γ_{90} (>1.0 approx.) the initial higher shear at the symmetry plane dominates the tendency for increasing lateral extent with reducing curvature and for such values the wall shear stress is everywhere greater than that for the sharp corner. For lower values, e.g. $\Gamma_{90} = 0.25$, we find the slower variation in curvature

resulting in the much slower approach to the flat plate wall shear stress as shown. Apart from these features the behaviour is unremarkable, the shear stress varying with Γ_{90} in an expected fashion.

The variation of the wall shear stress at $\xi^3 = 0$ with Γ_{90} is also shown in Fig. (4.53a). The wall shear stress is seen to vary exponentially from the flat plate value towards that of the sharp corner case.

The wall shear stress for $\Gamma_{\lambda_c} = 3$ is plotted for several values of λ_c, Fig. (4.53b). An interesting phenomenon is displayed in the curves for $\lambda_c > 180^o$ where the shear stress initially increases with ξ^3 near the symmetry plane before eventually falling rapidly to values somewhat lower than those for a flat plate. Thereafter the shear asymptotes slowly to the flat plate value. There is no reason to doubt that this is anything but a correct representation of the physical situation. Another interesting and possibly important feature is the small negative shear stress near $\xi^3 = 0$ for the $\Gamma_{45} = 3$ case. This corresponds to the results shown in Fig. (4.27).

A summary of the effects of a radiused corner and of the corner angle is offered in Fig. (4.54) where the results for the shear stress and the streamwise velocity in the symmetry plane are compared for $\Gamma_{\lambda_c} = 3$ and $\Gamma_{\lambda_c} = \infty$.

4.4. Sharp-profiled corner

Two particular additional examples of corner geometry are introduced here primarily to illustrate the generality of application of the theory in this respect. The examples

chosen are shown in the adjacent sketch. Each is the mirror image of the other and correspond to $\lceil_{90,60,3} = 0.5$ and $\lceil_{270,300,3} = 0.5$ (for notation see p. 110). The geometry of the first case may be described as a semi-infinite sharp rectangular corner each of whose walls constitutes a non-symmetrical external corner, the geometry as a whole exhibiting symmetry about the corner line. The other will have a complementary description.

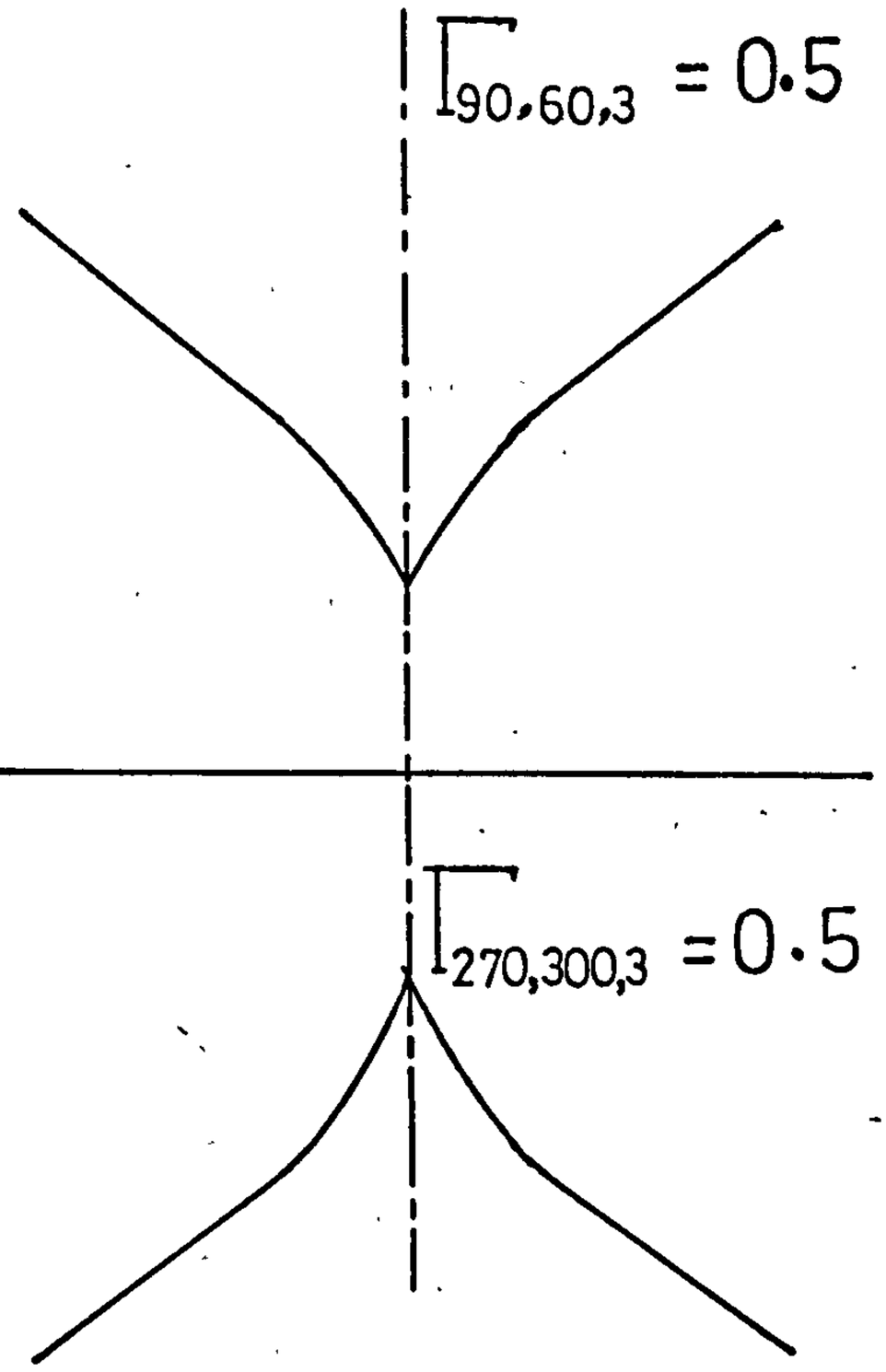

The results are computed from the same formulation used for the sharp and radiused corner cases with the following values of the parameters introduced in the numerical scheme:

$$\zeta_{max} = 14.4$$
$$\xi^2_{max} = 16.0$$
$$h = 0.4$$
$$a = 0.58$$

4.4.1. Streamwise velocity

a) $\lceil_{90,60,3} = 0.5$

The results of the streamwise velocity u in planes parallel to the symmetry plane and the corresponding isovels are shown in figures (4.55) and (4.56). The most

obvious feature of these results is the bulge in the isovels of u [illegible] Fig. (4.56). Other points to note are the extent of the low shear region near the symmetry plane and the velocity undershoot with respect to the asymptotic velocity profile illustrated by the profile at $\xi^3 = 9.39$ plane. The undershoot is greatest in this plane (approx.) and this is seen in Fig. (4.61) where the wall shear stress ratio is shown as a function of ξ^3. All these aspects of the flow appear to be [illegible]y consistent with the geometry of the corner. The convex shape of the corner walls results in a reduction of the boundary layer thickness near the region of convexity whilst the overall concave form of the corner and the smallness of the corner angle at $\xi^3 = 0$ lead to a thick boundary layer in the symmetry plane thereby giving rise to the bulging appearance.

b) $\underline{\Gamma_{270,300,3} = 0.5}$

The results for this example are shown in figures (4.57) and (4.58). Of the many results presented in this work those shown in these two figures are surely the most surprising. In all of the results (for external corners) shown previously it has invariably been found that the corner layer in the symmetry plane is thinner than elsewhere. The new results presented in this section show quite the opposite behaviour. This implies a remarkable sensitivity of the flow to the corner wall shape.

4.4.2 Crossflow velocity field

Only the crossflow fields are presented here and these are shown in figures (4.59) and (4.60). The negative values

of v at or near the plane of symmetry observed in the sharp corner examples are absent here. A most interesting feature is the possible existence of a closed vortex near the convex part of the corner wall for $\Gamma_{90,60,3} = 0.5$ (Fig. (4.59)).

4.4.3. Wall shear stress

This is shown for both corner parameter cases in Fig. (4.61). A consequence of the bulging appearance in the streamwise velocity isovels for the external corner (Fig. (4.58)) is to produce the low shear near the wall as shown in Fig. (4.61). This is followed by a rapid rise overshooting the flat plate value giving the distribution a kind of a wave-like appearance. The strangeness of this behaviour is perhaps highlighted on noting that qualitatively the shear stress distribution is a reflection in the line $(\tau_{w_c}/\tau_{w_\infty}) = 1$ of the distribution for external corners, shown in Fig. (4.54).

The wall shear stress distribution for the internal corner example bears a rather closer resemblance to previous examples of this corner type except for the overshoot to higher shear stress values than for the flat plate.

Inset in Fig. (4.61) is a wall shear stress distribution obtained experimentally by Zamir and Young. This corresponds to a velocity profile which displayed the bulging appearance of the example being discussed here. While it is important not to confuse the probably different causes of the bulges it is interesting to note the correspondence between Zamir's experimental results and the theoretical results given here. Whether there is anything profound to be deduced from this, is another matter.

4.5. Experimental Results

The results are presented in the ξ^i coordinate system variables. Physical lengths were originally measured in British units and subsequently converted to metric units and as such they are tabled here. For comparing the velocity profiles in the symmetry plane and in the two-dimensional regions the coordinate $\xi^2 \cos\lambda$ has been used instead of ξ^2 alone. This effectively represents the profiles in planes normal to the wall and because the profiles, as will be shown, are not greatly different this avoids any confusion that might arise from the crossing of the two profiles as happens in the ξ^2 only coordinate.

Throughout the experimental work the corner was positioned at 0.16^o adverse incidence. Figures (4.62) and (4.63) show the results obtained sufficiently far away from the symmetry plane for a two-dimensional flow region to prevail. For comparison purposes the Blasius profile is included in these figures. Excellent agreement is evident for about $u < 0.7$ while thereafter the experimental results tend to lie 'below' the Blasius profile. Nevertheless the agreement overall is thought to justify the belief that the experimental situation adequately realizes the theoretical model and that the experimental results may properly be compared directly with those from theory. This is a fortunate circumstance since the several attempts to improve still further the agreement by small increases in the adverse incidence of the corner invariably resulted in the onset of turbulence.

The velocity profiles in the symmetry plane and in the two-dimensional flow region are presented in figures (4.64) to (4.71) with the corresponding isovels shown in figures (4.72) to (4.75). The collected symmetry plane results, Fig. (4.76), show little of the anticipated systematic variation with Γ_{90} . Only the profile for the largest value, Γ_{90} = 0.53, is distinguishable from the others all of which could well be presented by a single curve. The only thing that can be deduced from these results is that the relative positions of the profiles for Γ_{90}= 0.53 and for other Γ_{90} values are qualitatively in agreement with the theory, which is hardly surprising on physical grounds. The apparent insensitivity of the flow to variation in Γ_{90} is to some extent in conflict with the theory. Unfortunately the large Γ_{90} values necessary to clarify the dependence experimentally were unobtainable for reasons mentioned in Section 3.2.1.

The agreement between theory and experiment is somewhat poorer than might be desired and without further experimentation the cause will remain uncertain. Meanwhile one observation worthmaking is that El-Gamal [4] encountered a similar circumstance between experiment and theory for the sharp 90^{o} corner (i.e. $\Gamma_{90} = \infty$). This is shown in Fig. (4.4), the theory being that introduced in this work and the experimental results referred to being those obtained by El-Gamal. There may also be some consideration to be given to the fact that it is not altogether an easy matter experimentally to distinguish profiles which are in truth rather close together.

The present results are somewhat limited in extent by

the largeness of the radius used and there is a corresponding limitation in the range of conclusions to be drawn from them. What is shown by the results is that for $\Gamma_{90} \leqslant 0.5$ approximately, the flow is only a little different from that on a flat plate at the same Reynolds number. This is of some importance since consideration of radiused corner flow situations in practice suggests that small values of Γ_{90} will be the dominant feature of the flow. Nevertheless it is desirable to have a larger experimental range for Γ_{90} and for this we must look to corners having a smaller radius r_o. Perhaps r_o = 2.5 mm would be optimum for a working streamwise length of approximately 1.0 m as is available in the wind-tunnel used here.

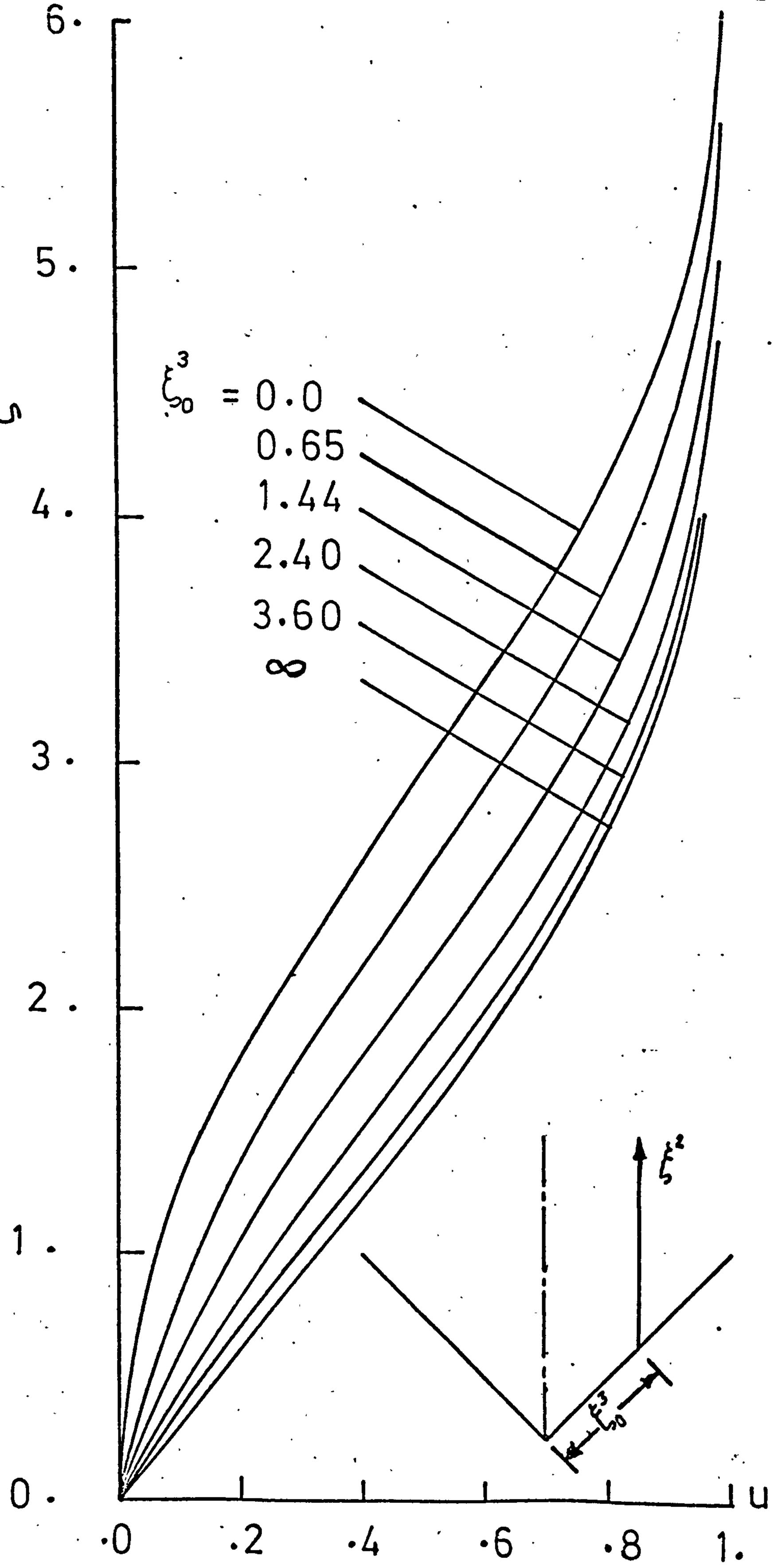

Fig.(4.1) Streamwise velocity u in planes parallel to the symmetry plane , $\sqrt{}_{90} = \infty$.

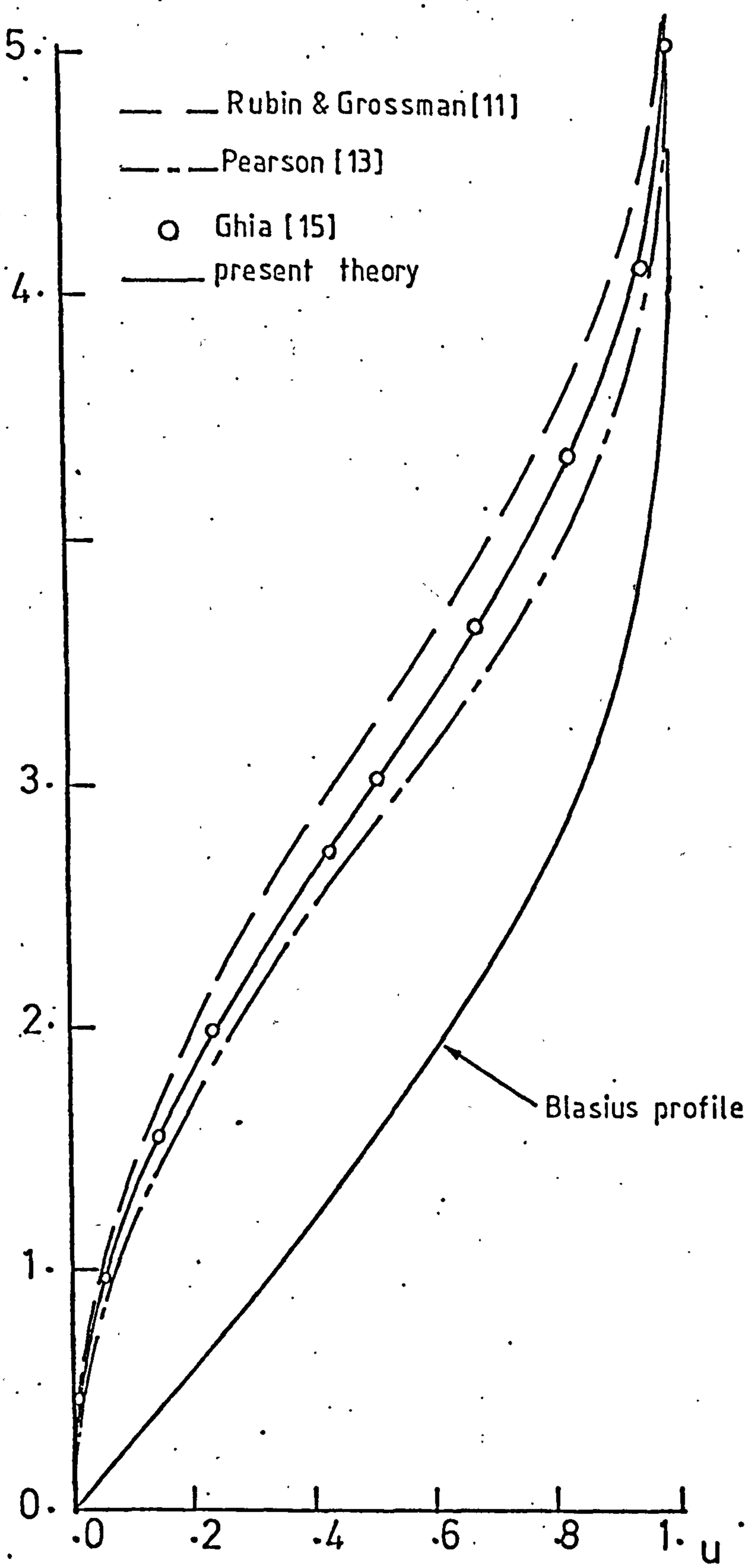

Fig.(4.2) Streamwise velocity u in symmetry plane , $\Gamma_{90} = \infty$.

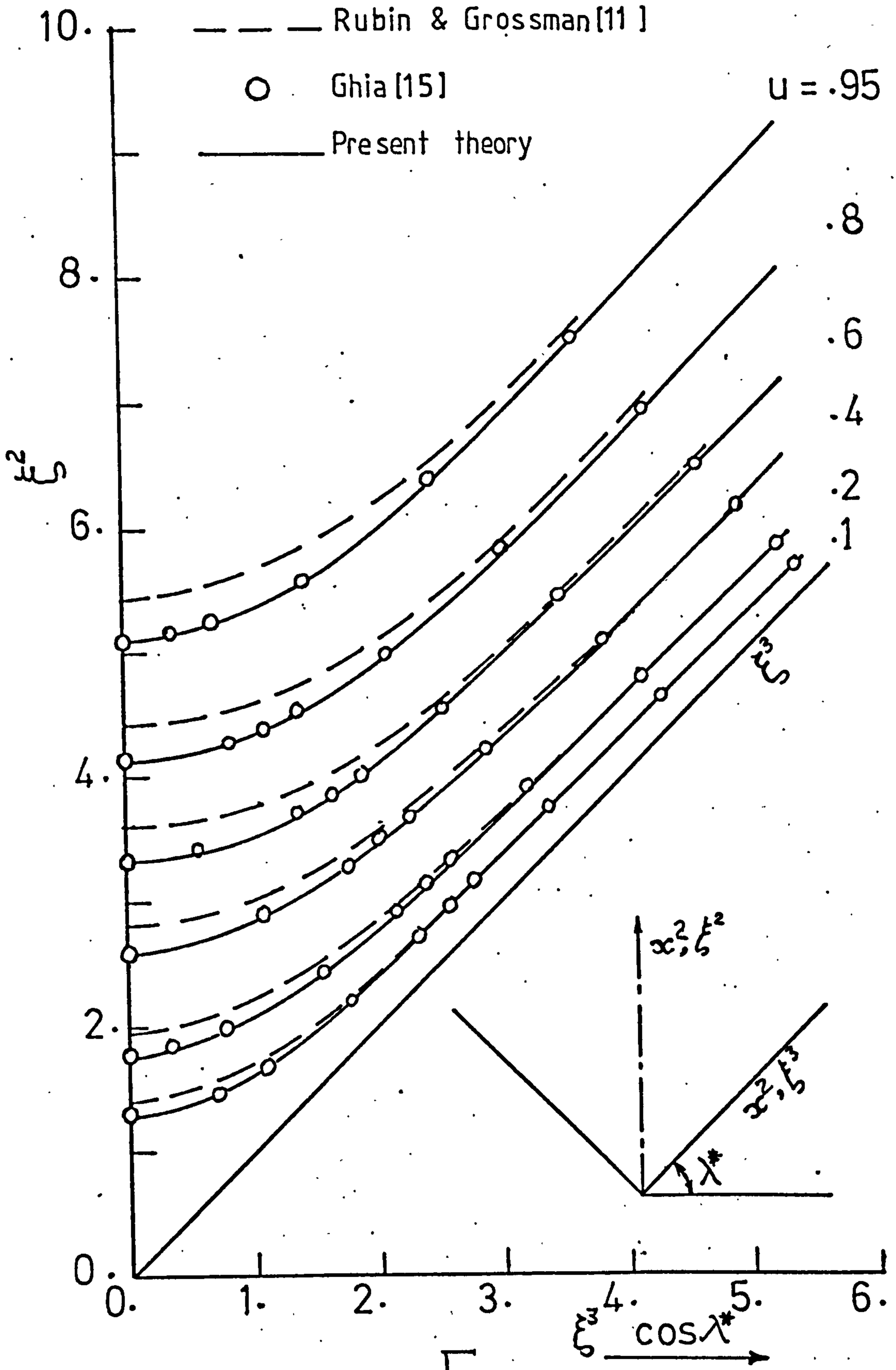

Fig.(4.3) Streamwise isovels , $\Gamma_{90} = \infty$.

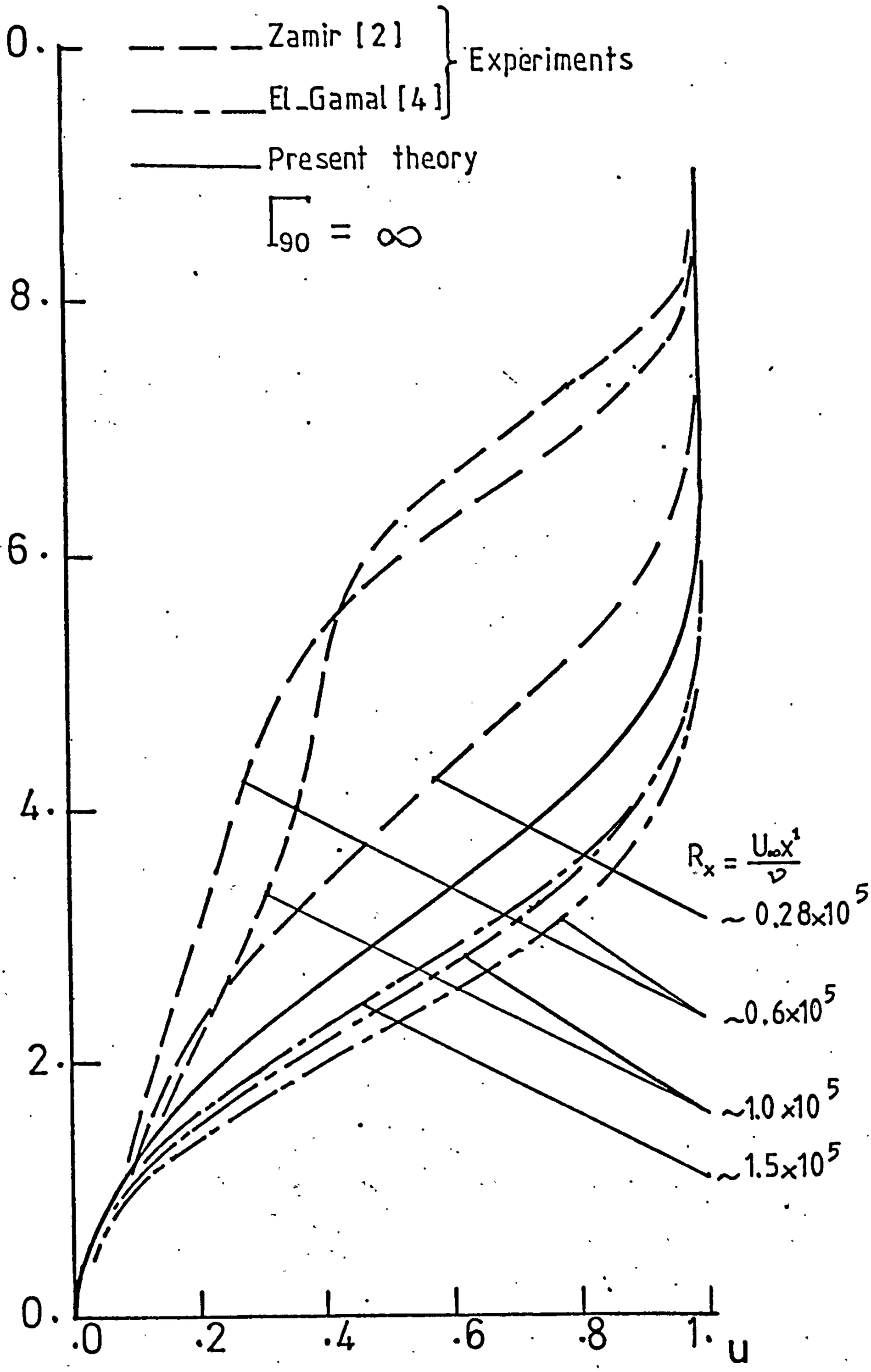

Fig.(4.4) Comparison between the solution for u in the symmetry plane and previously obtained experimental results .

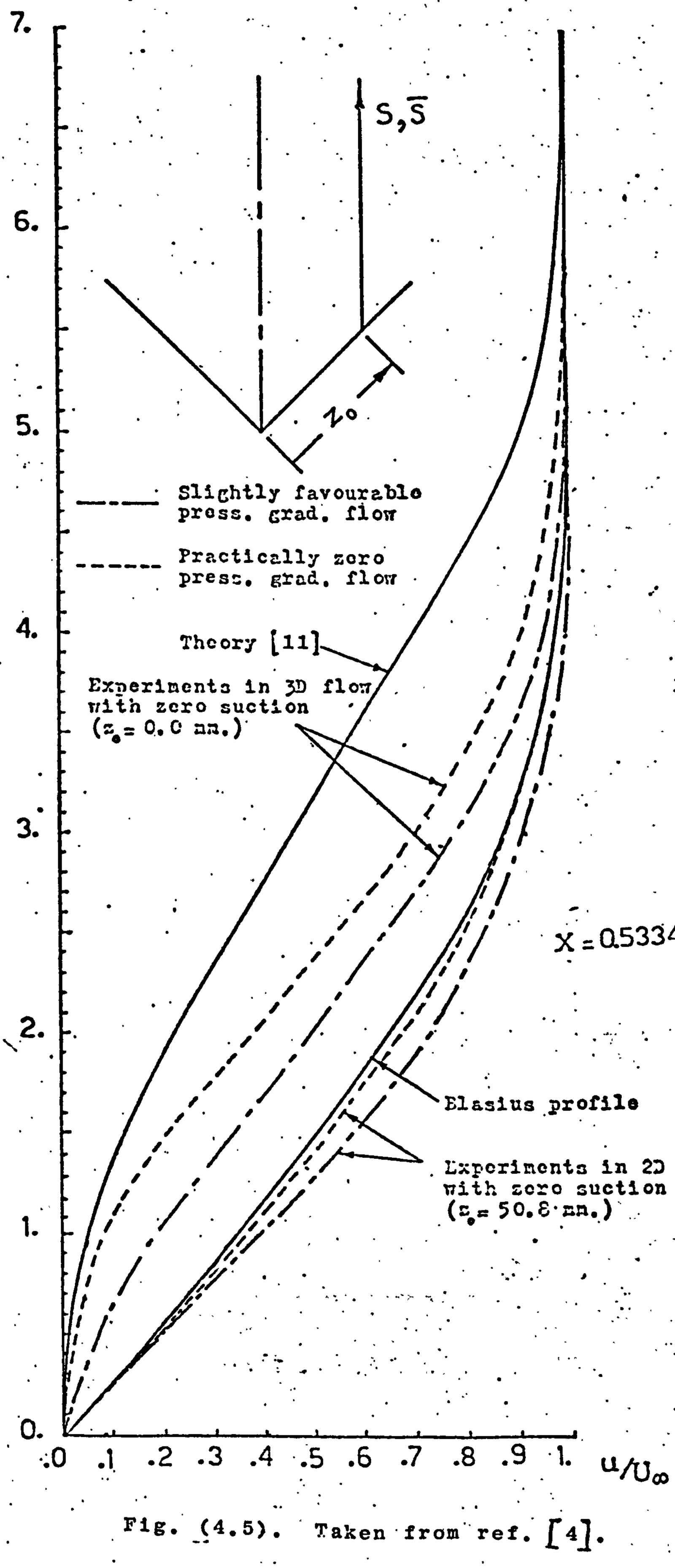

Fig. (4.5). Taken from ref. [4].

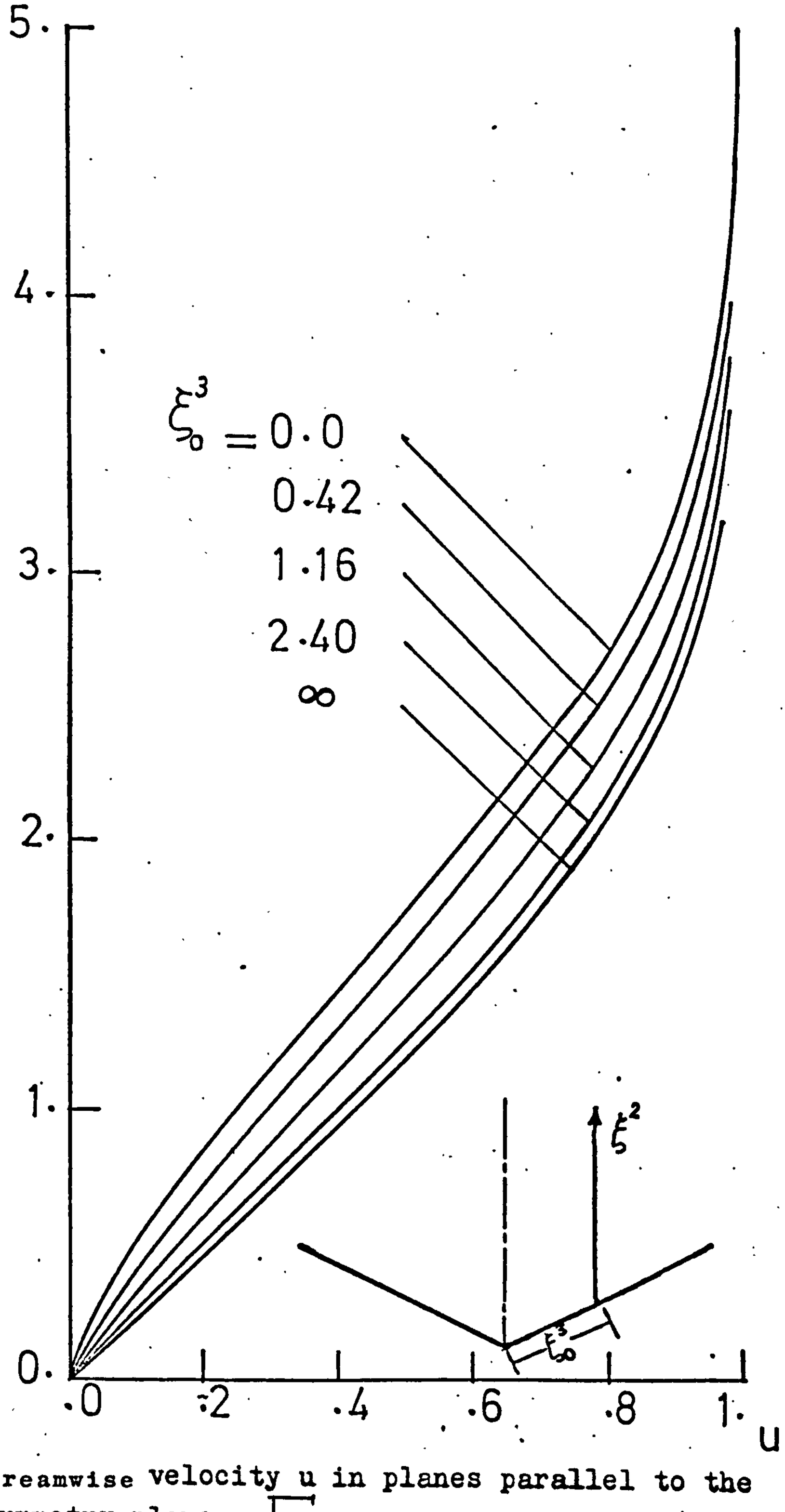

Fig.(4.6) Streamwise velocity u in planes parallel to the symmetry plane, $\Gamma_{135} = \infty$.

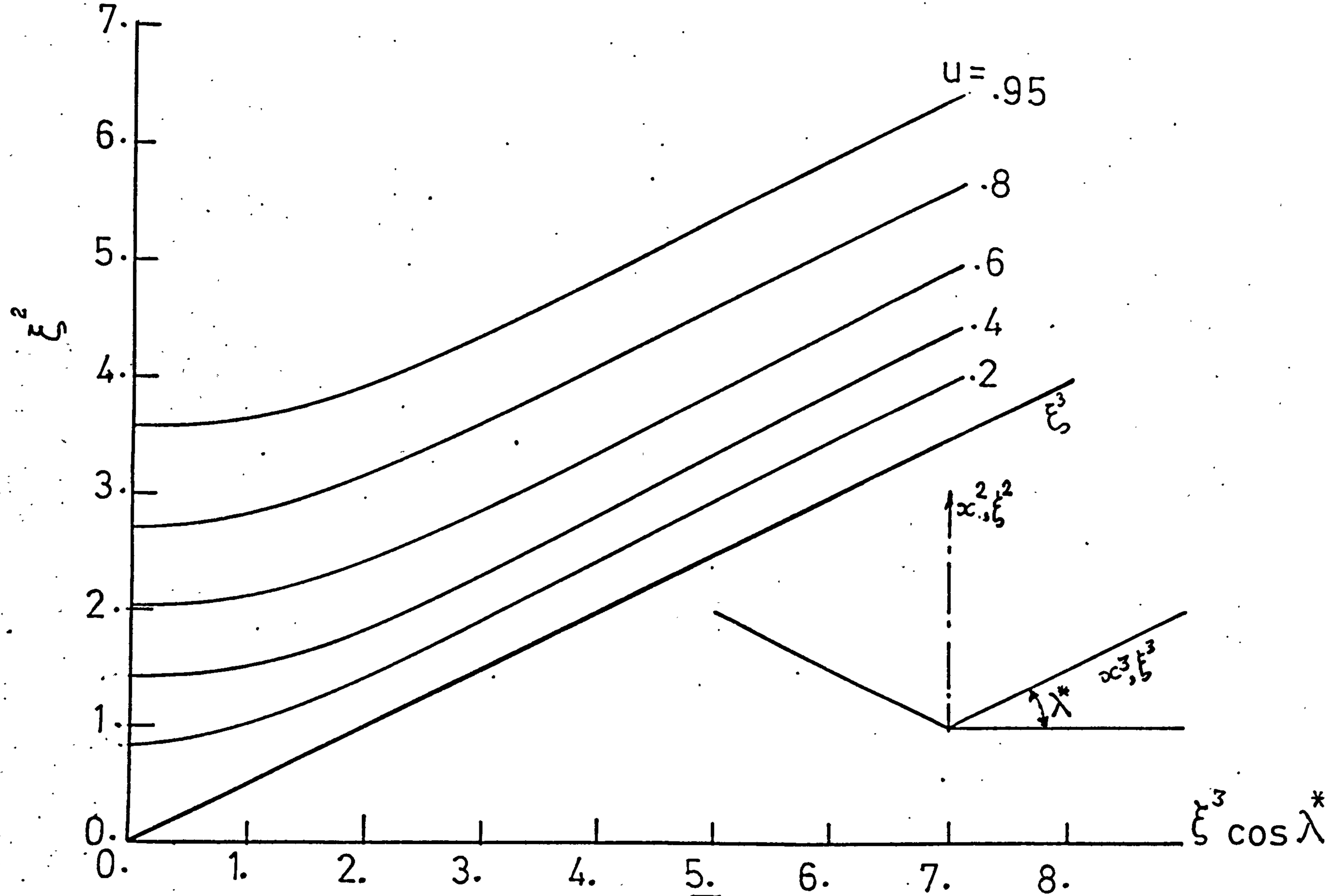

Fig.(4.7) Streamwise isovels, $\Gamma_{135} = \infty$.

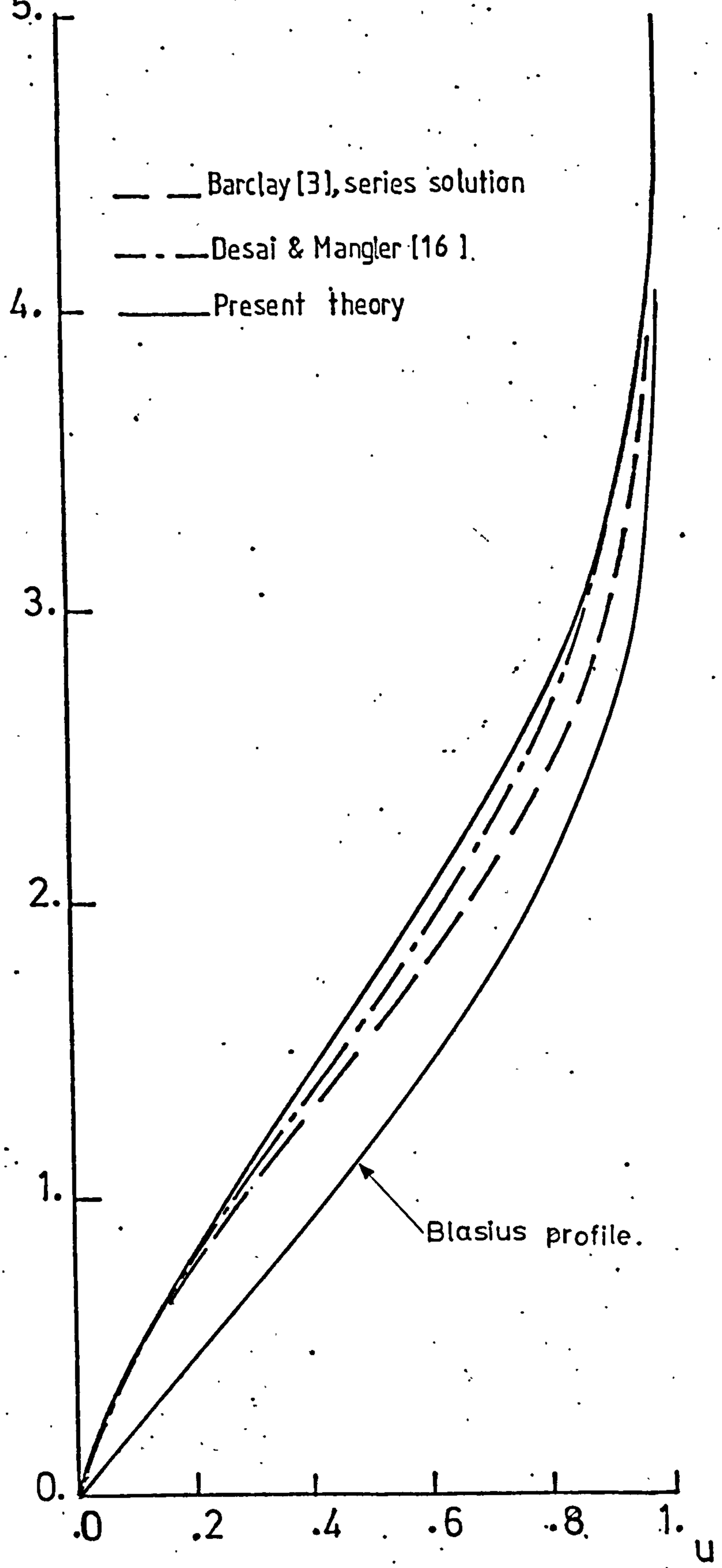

Fig.(4.8) Streamwise velocity u in symmetry plane, $\Gamma_{135} = \infty$.

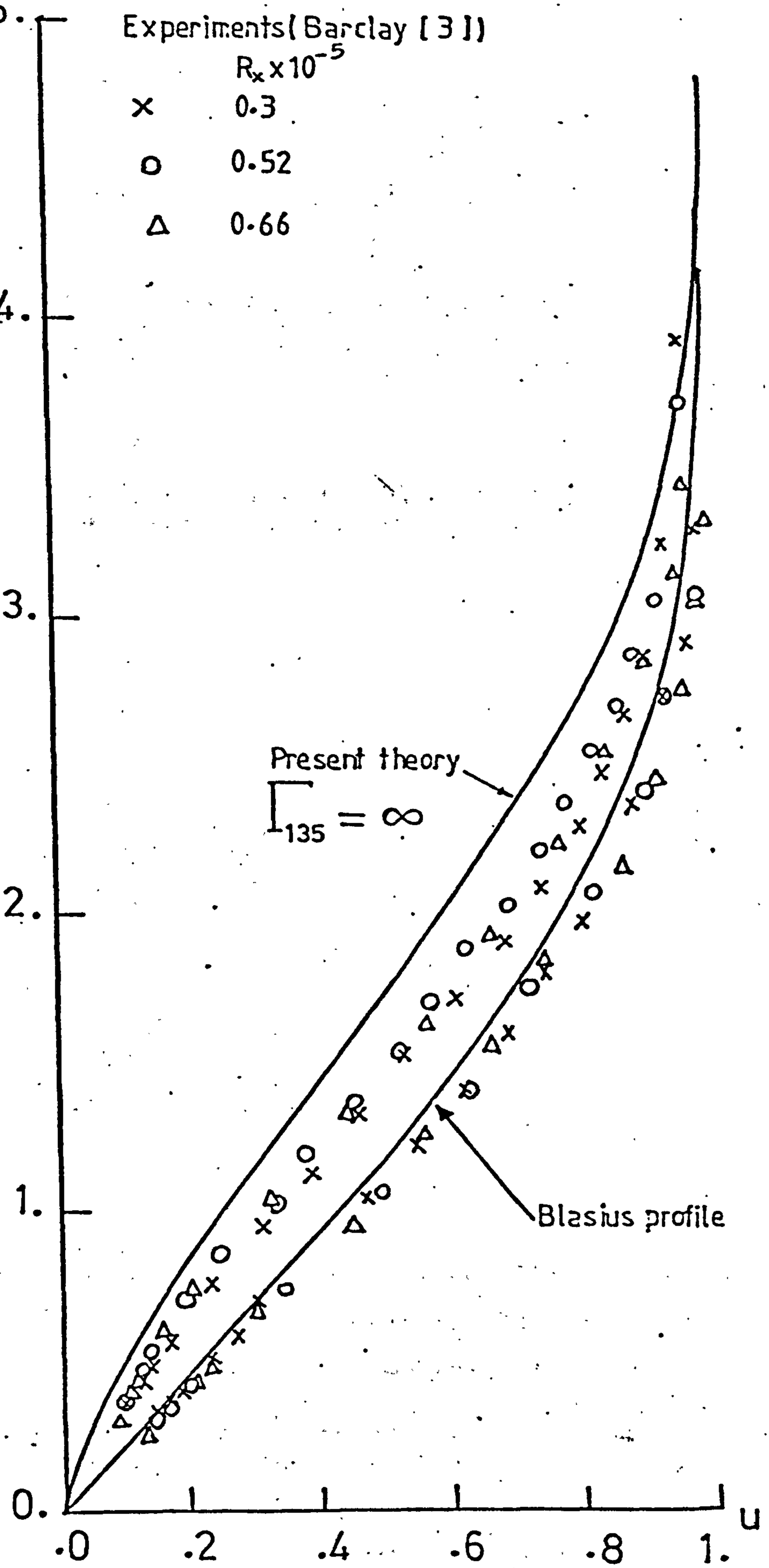

Fig.(4.9) Comparison between the solution for u in the symmetry plane with previously obtained experimental results.

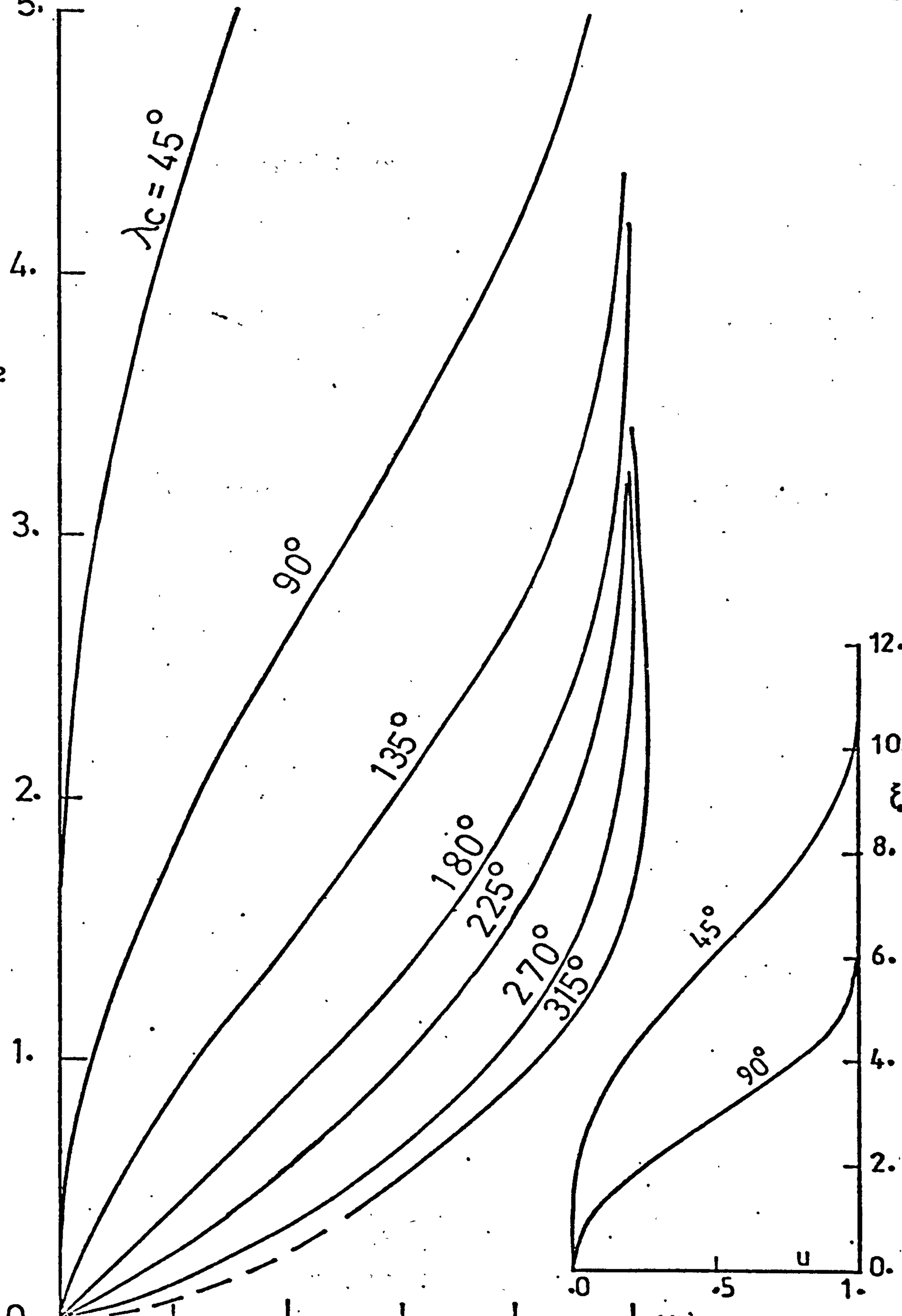

Fig.(4.10) Variation of streamwise velocity u (in symmetry plane) with corner angle λ_c for $\lambda_c = \infty$.

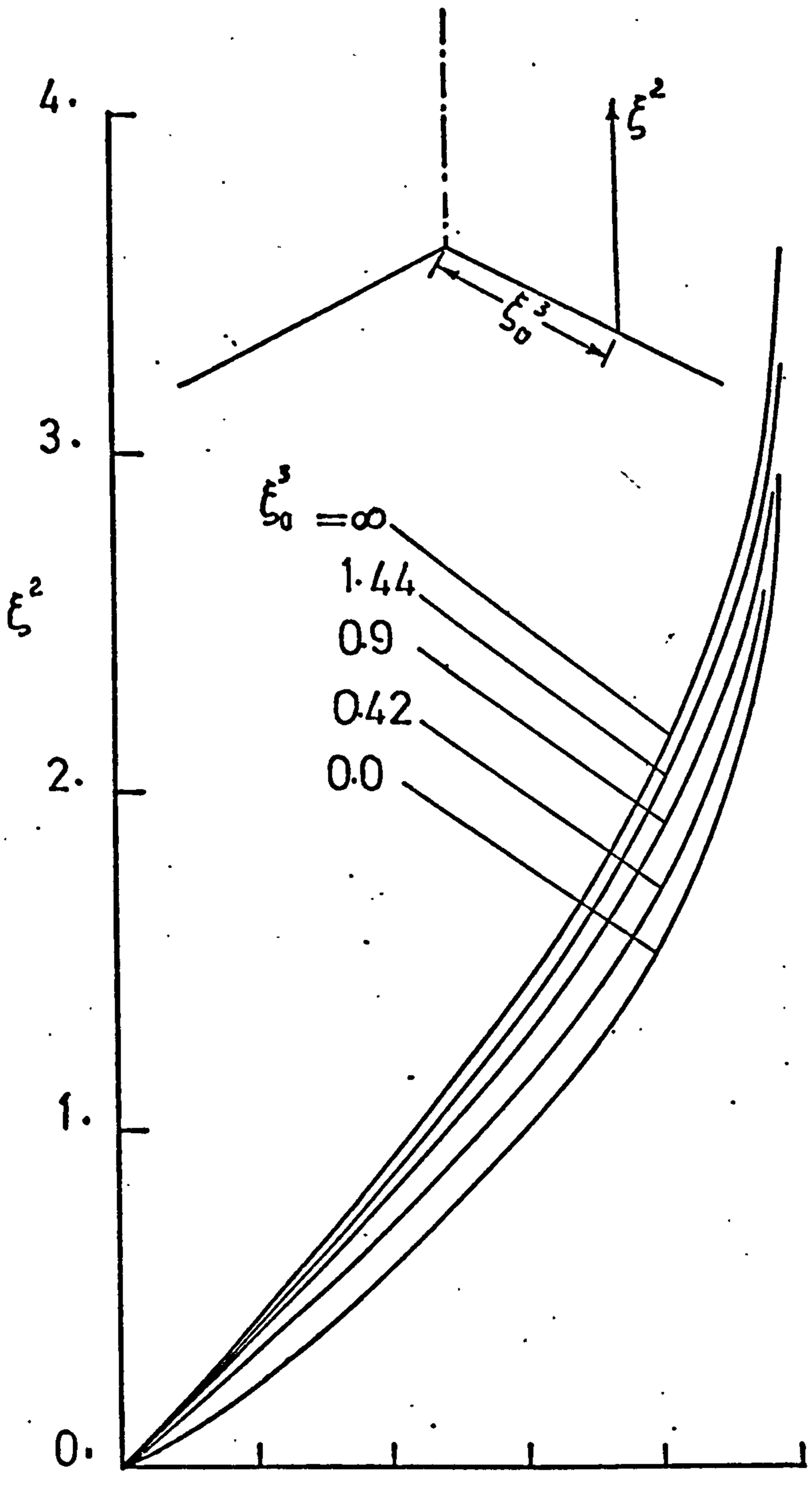

Fig.(4.11) Streamwise velocity in planes parallel to the symmetry plane , $\Gamma_{225} = \infty$.

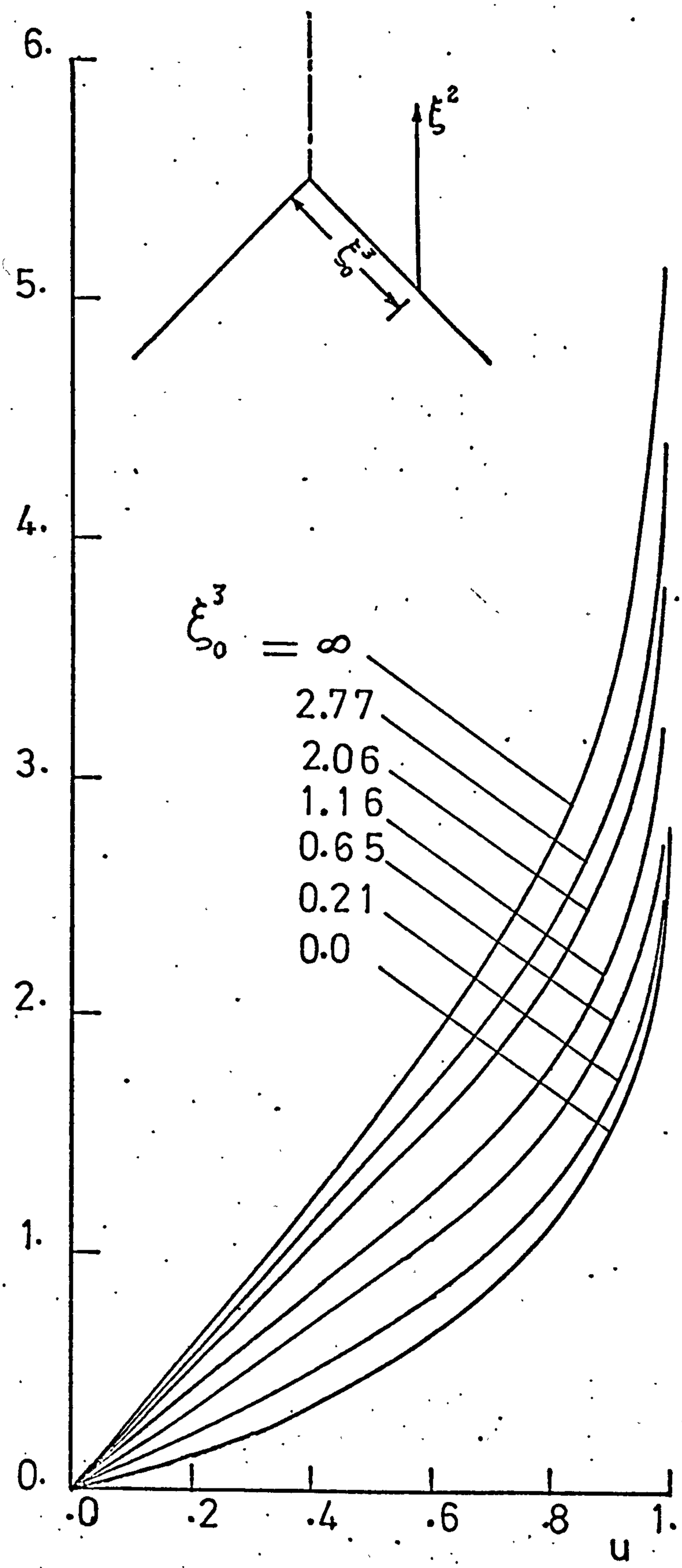

Fig.(4.12) Streamwise velocity in planes parallel to the symmetry plane , $\Gamma_{270} = \infty$.

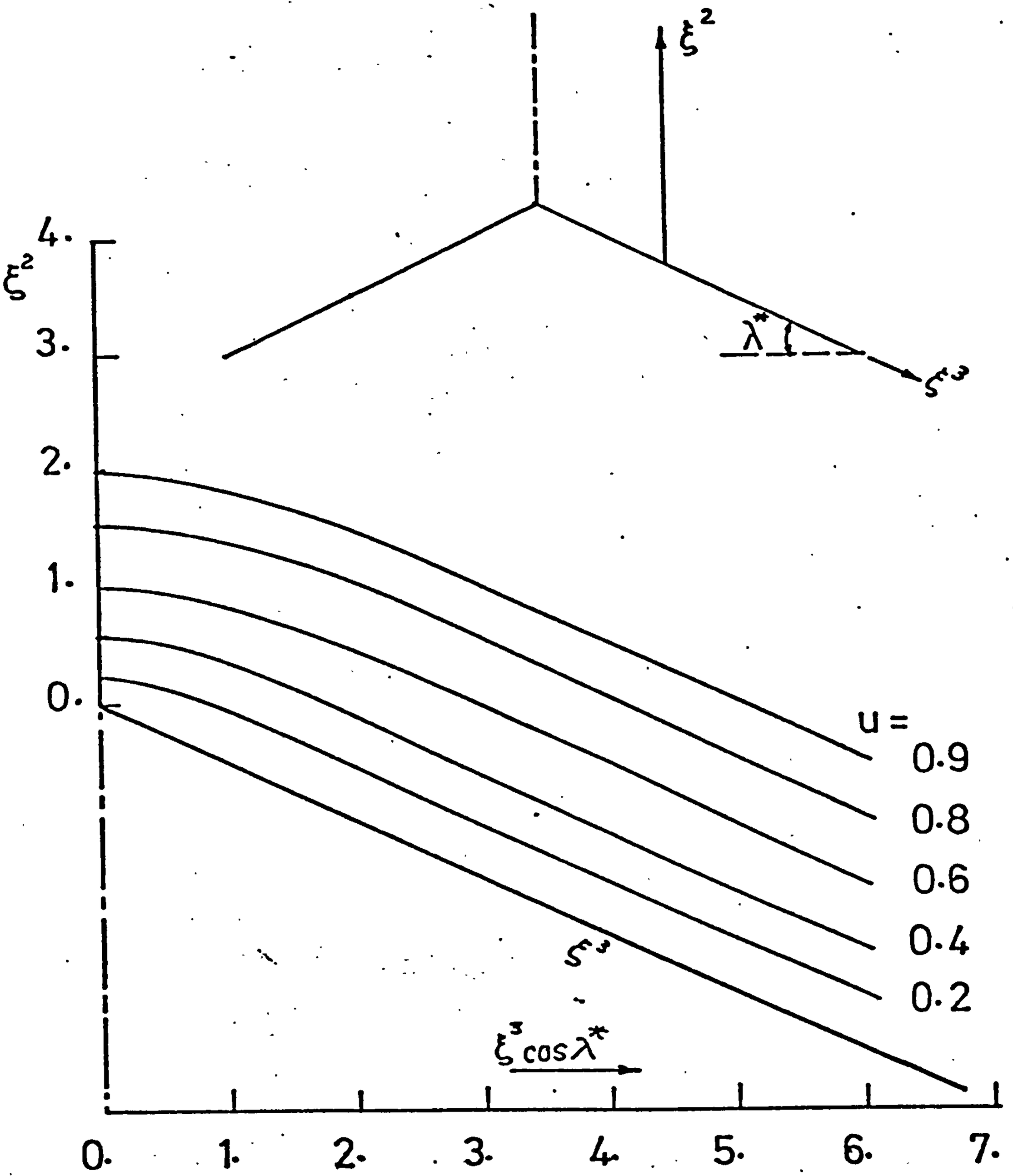

Fig.(4.13) Streamwise isovels , $\Gamma_{225} = \infty$.

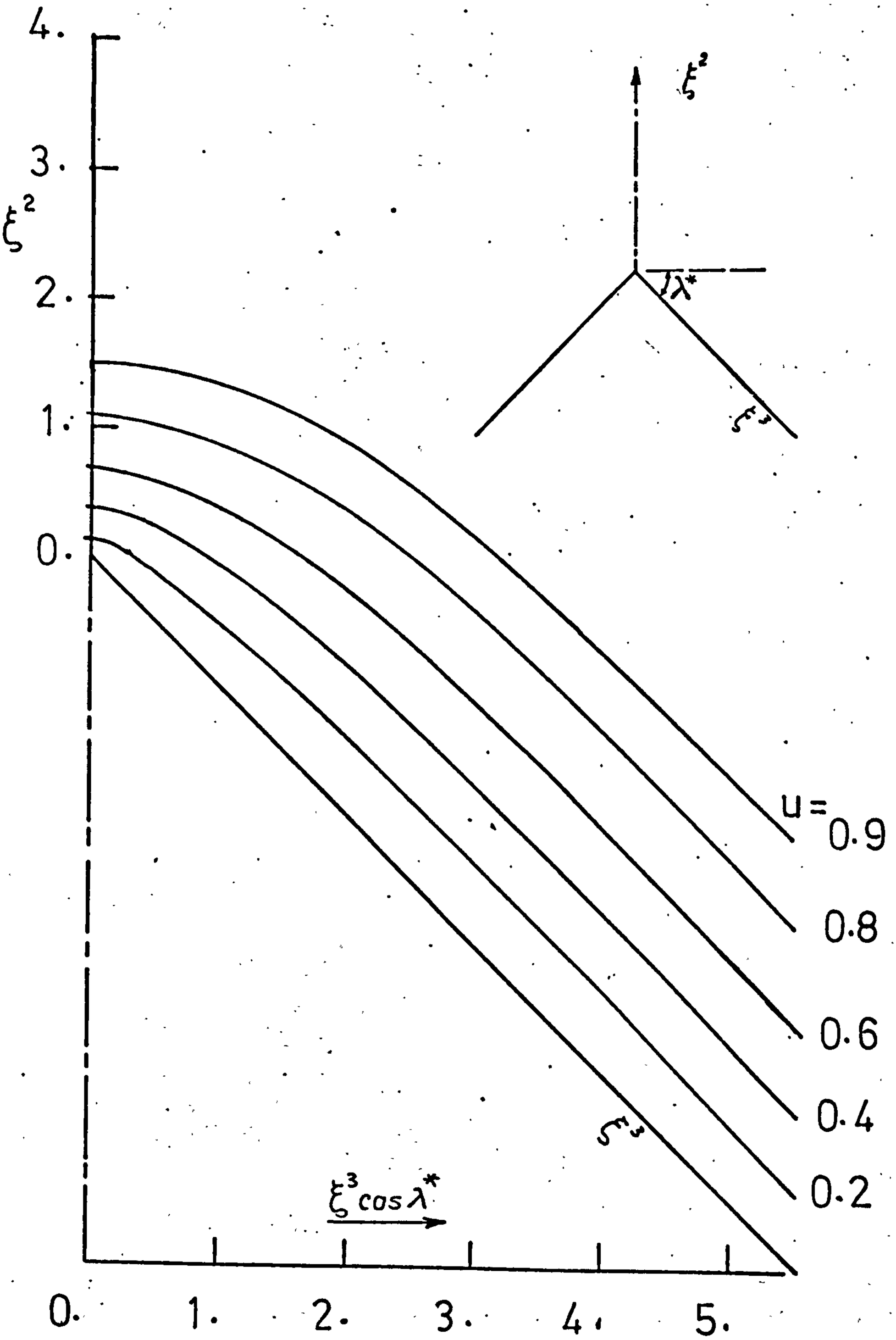

Fig.(4.13a) Streamwise isovels , $\Gamma_{270} = \infty$.

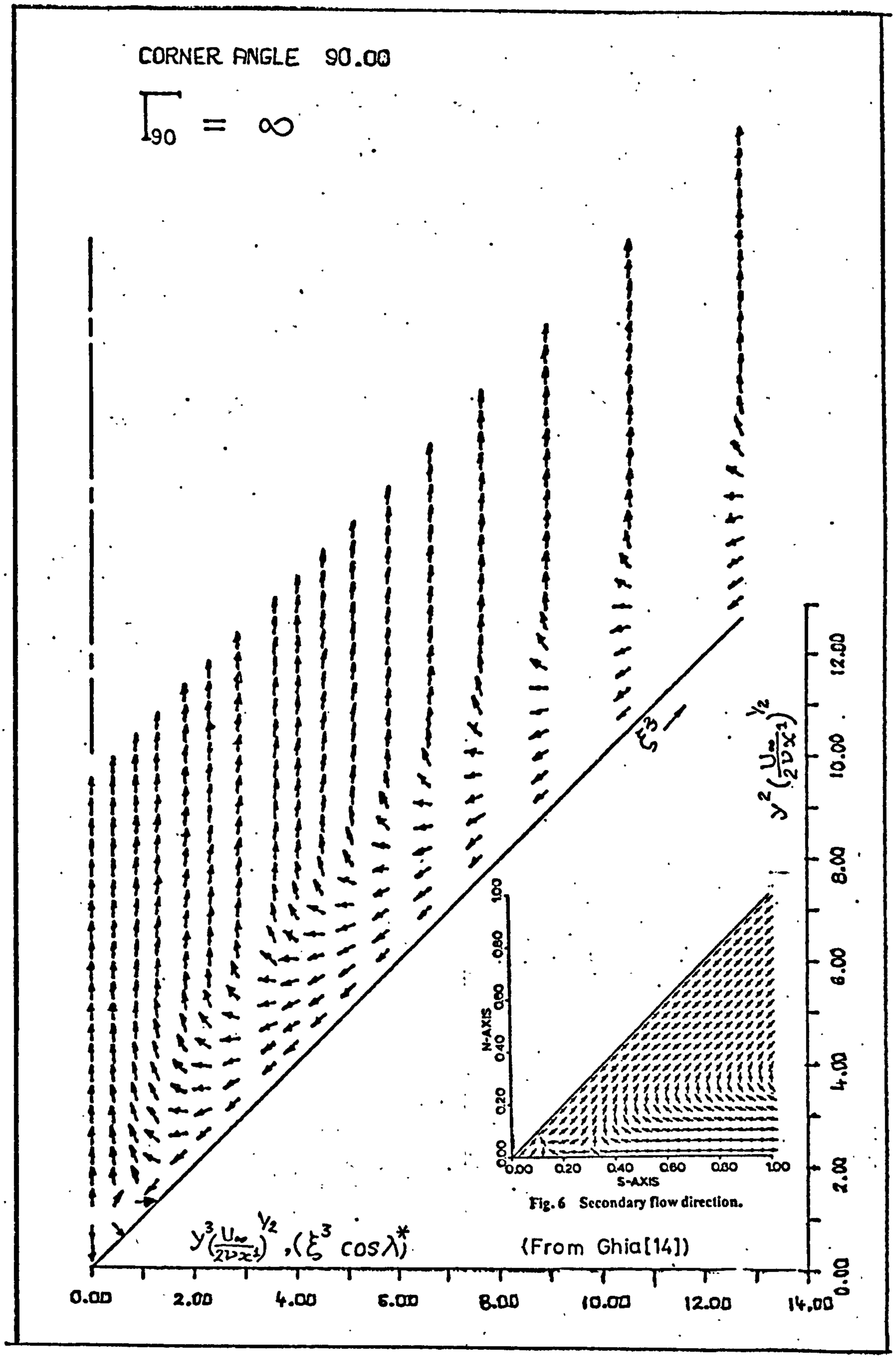

Fig. 6 Secondary flow direction.

Fig. (4.14) Crossflow direction.

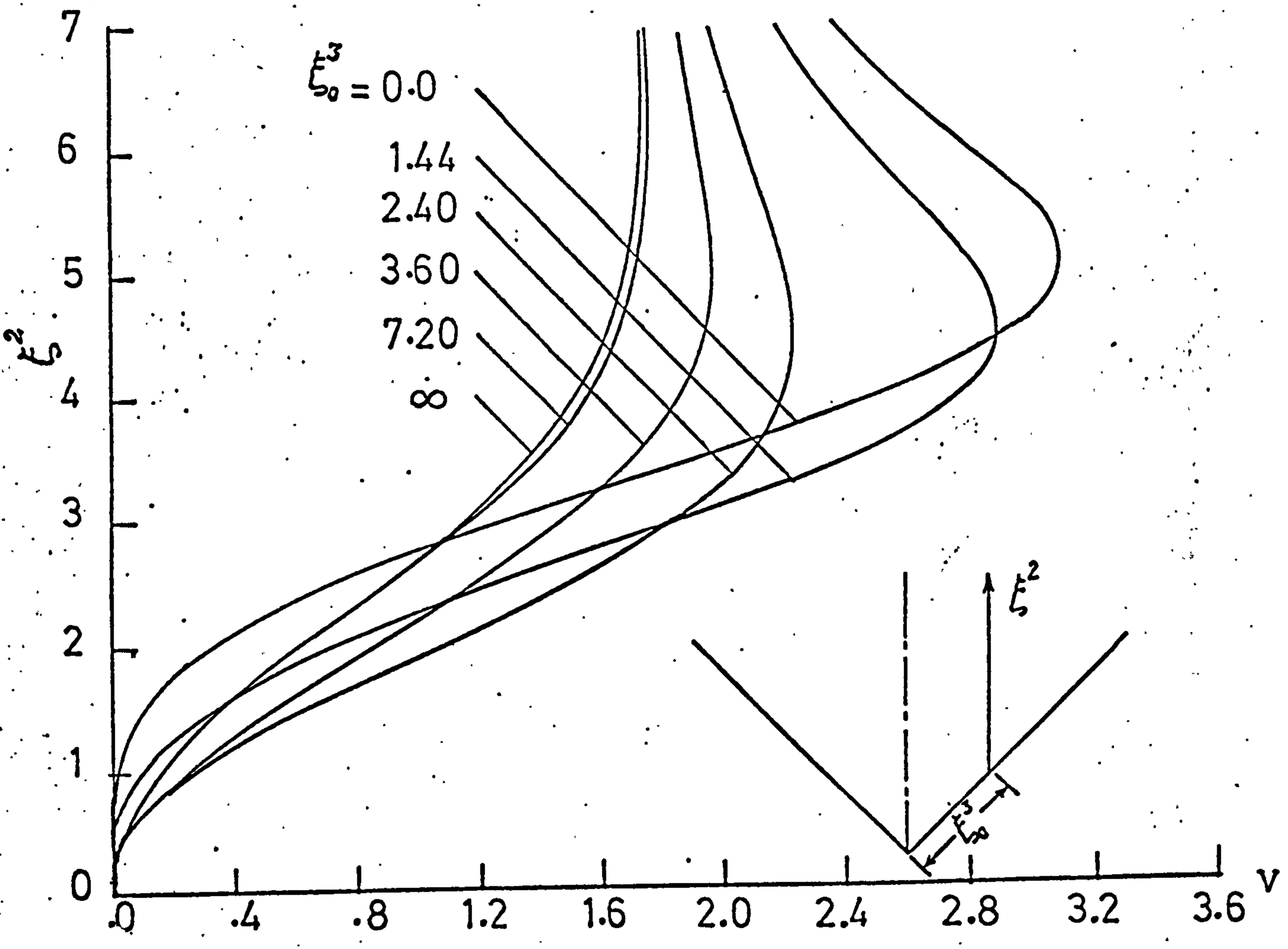

Fig.(4.15) Crossflow velocity component v in planes parallel to the symmetry plane, $\Gamma_{90} = \infty$.

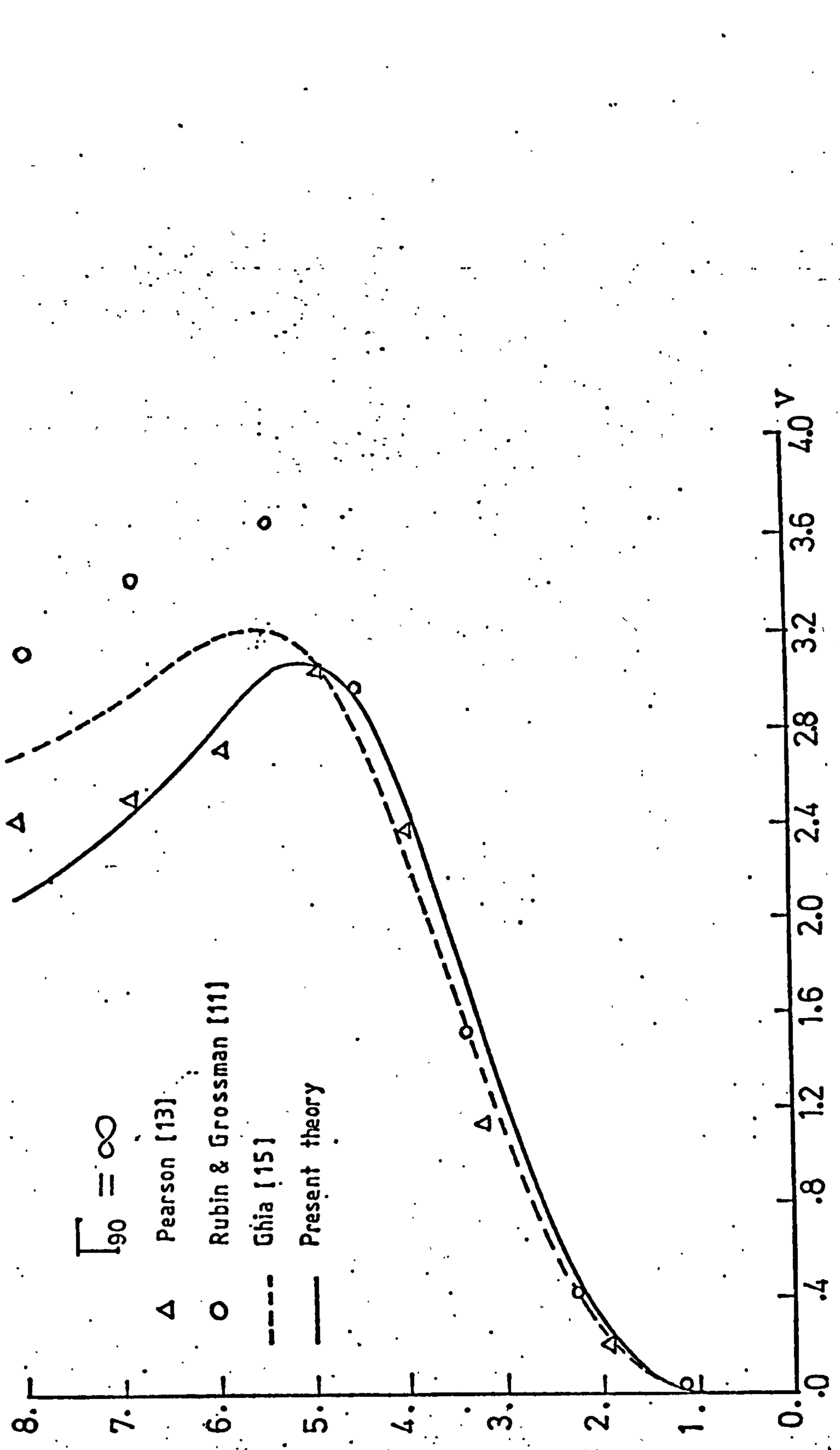

Fig.(4.16) Crossflow velocity component v in symmetry plane •

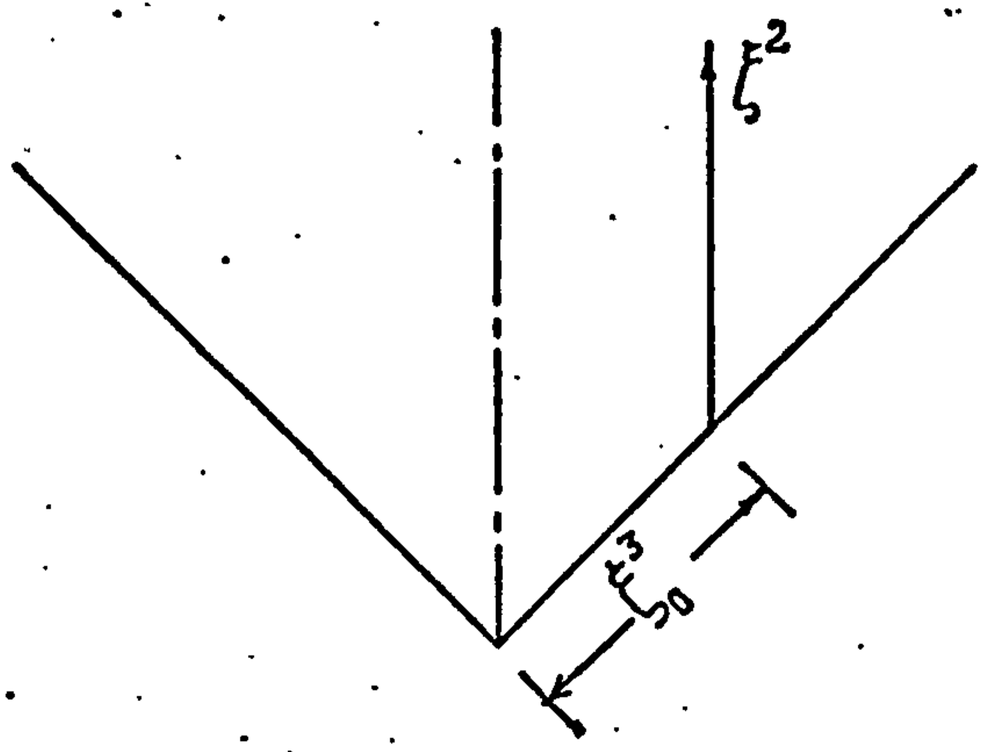

Curve	ζ^3_{50}
1	0.0
2	0.9
3	2.06
4	3.6
5	8.05
6	16.36
7	∞

Fig.(4.17) Crossflow velocity component w at planes parallel to the symmetry plane , $\Gamma_{90} = \infty$.

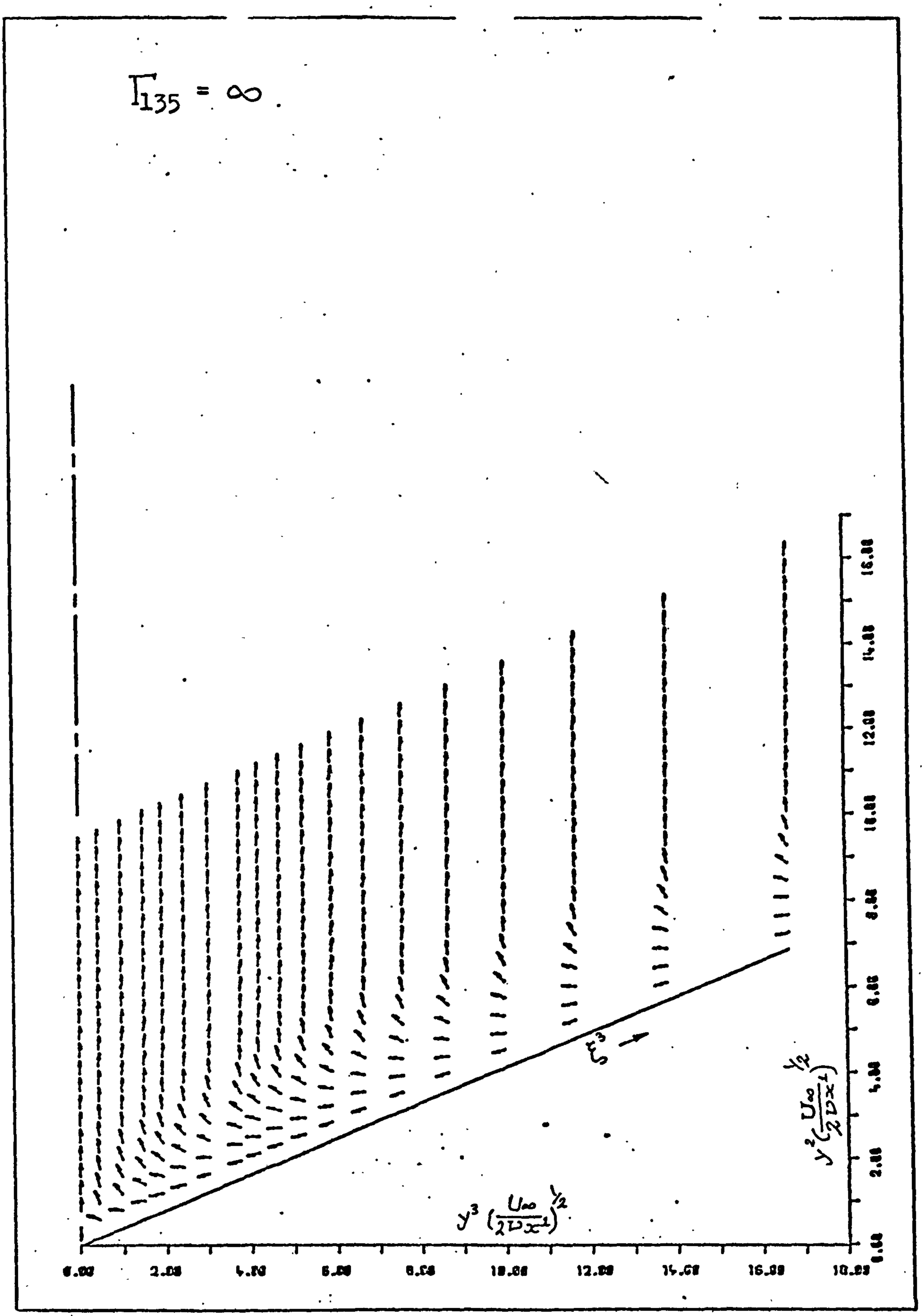

Fig.(4.18) Crossflow direction .

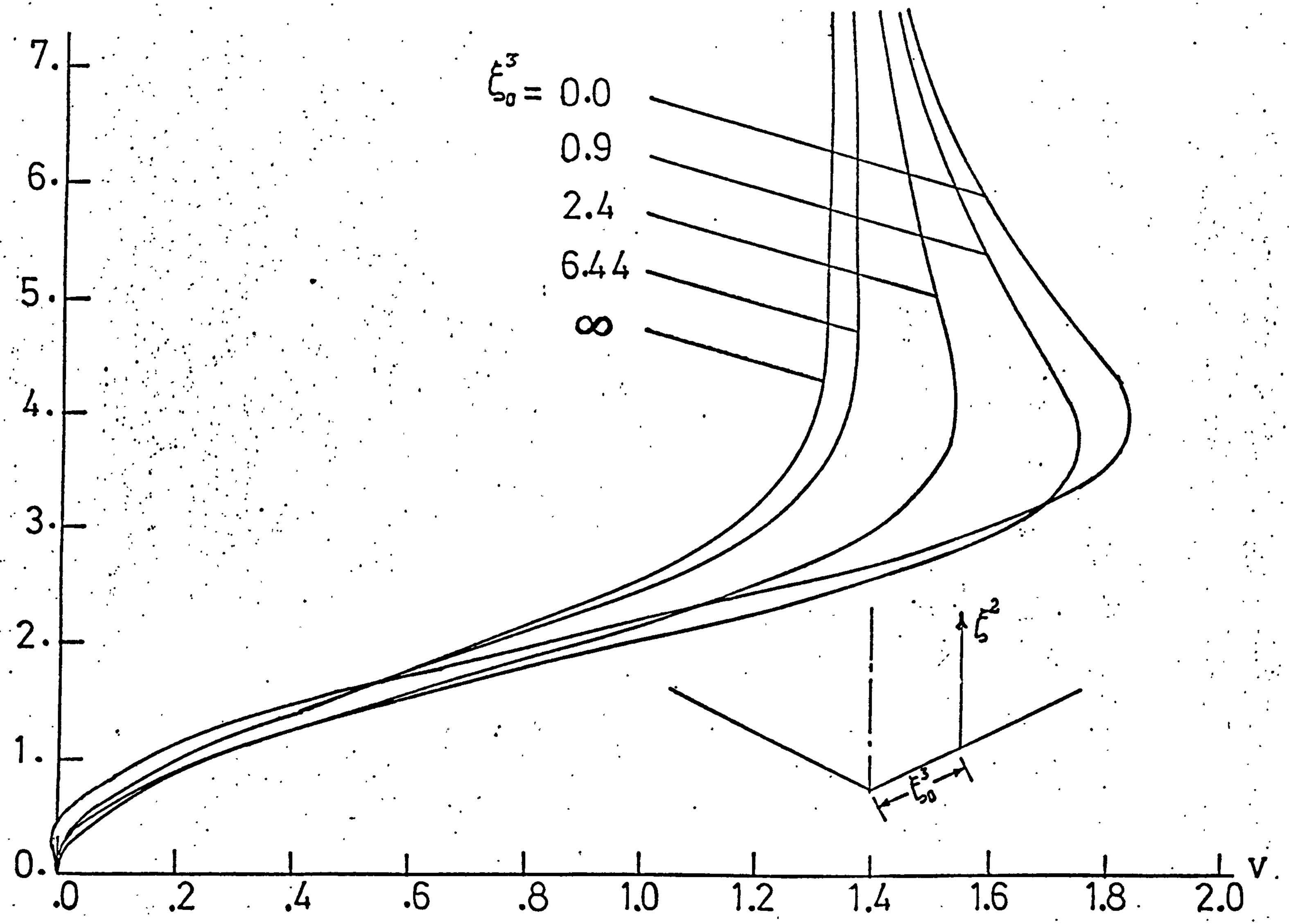

Fig.(4.19) Crossflow velocity component v in planes parallel to the symmetry plane , $\Gamma_{135} = \infty$.

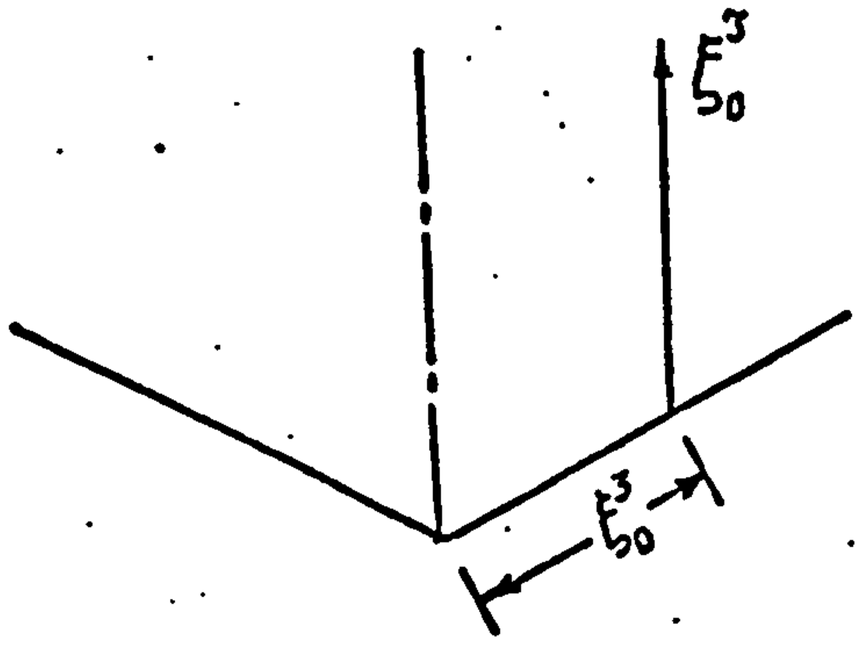

Curve	ξ_0^3
1	0.0
2	0.66
3	2.06
4	3.6
5	∞

Fig.(4.20) Crossflow velocity component w at planes parallel to the symmetry planes, $\Gamma_{135} = \infty$.

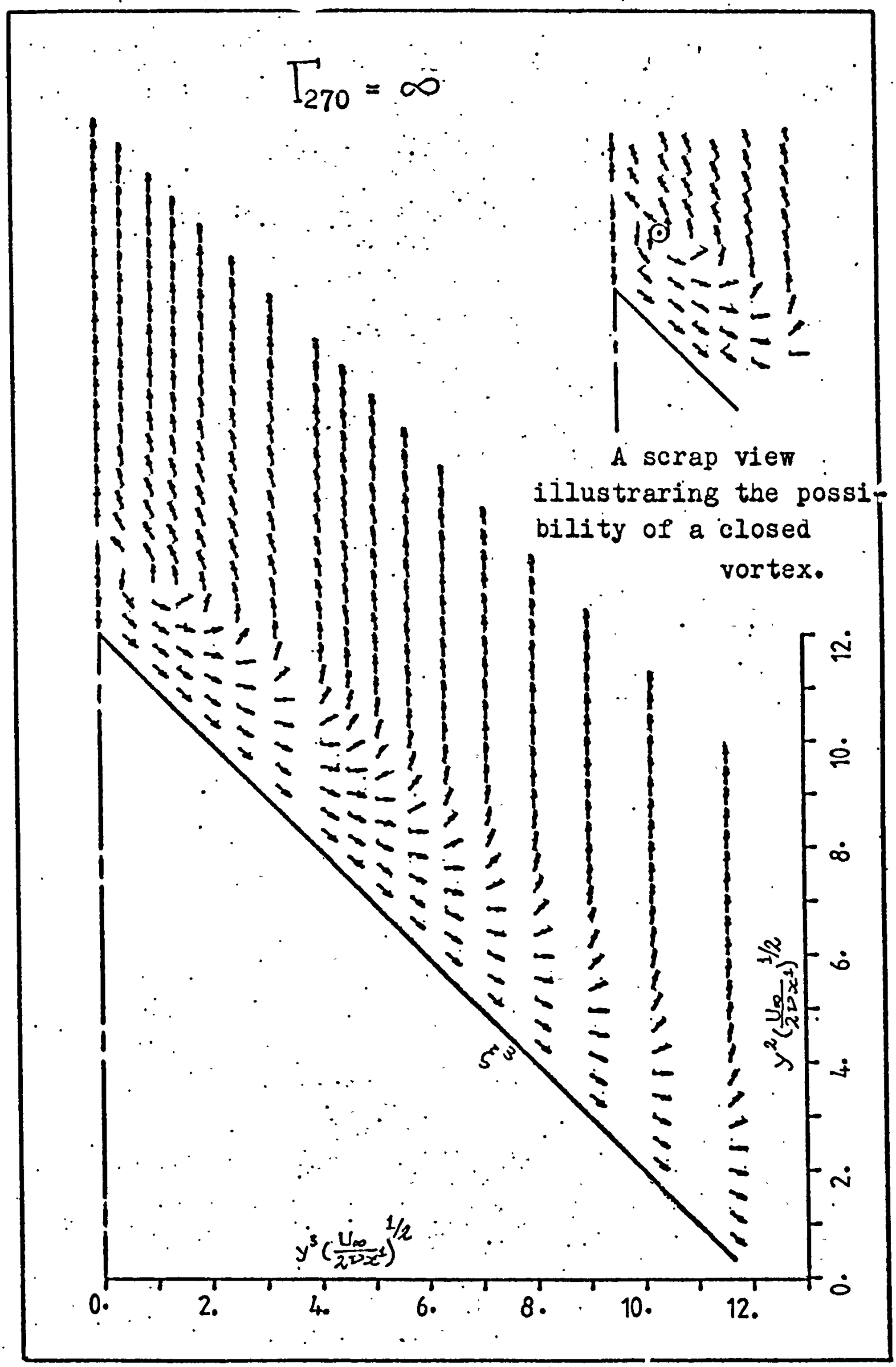

Fig.(4.21) Crossflow direction .

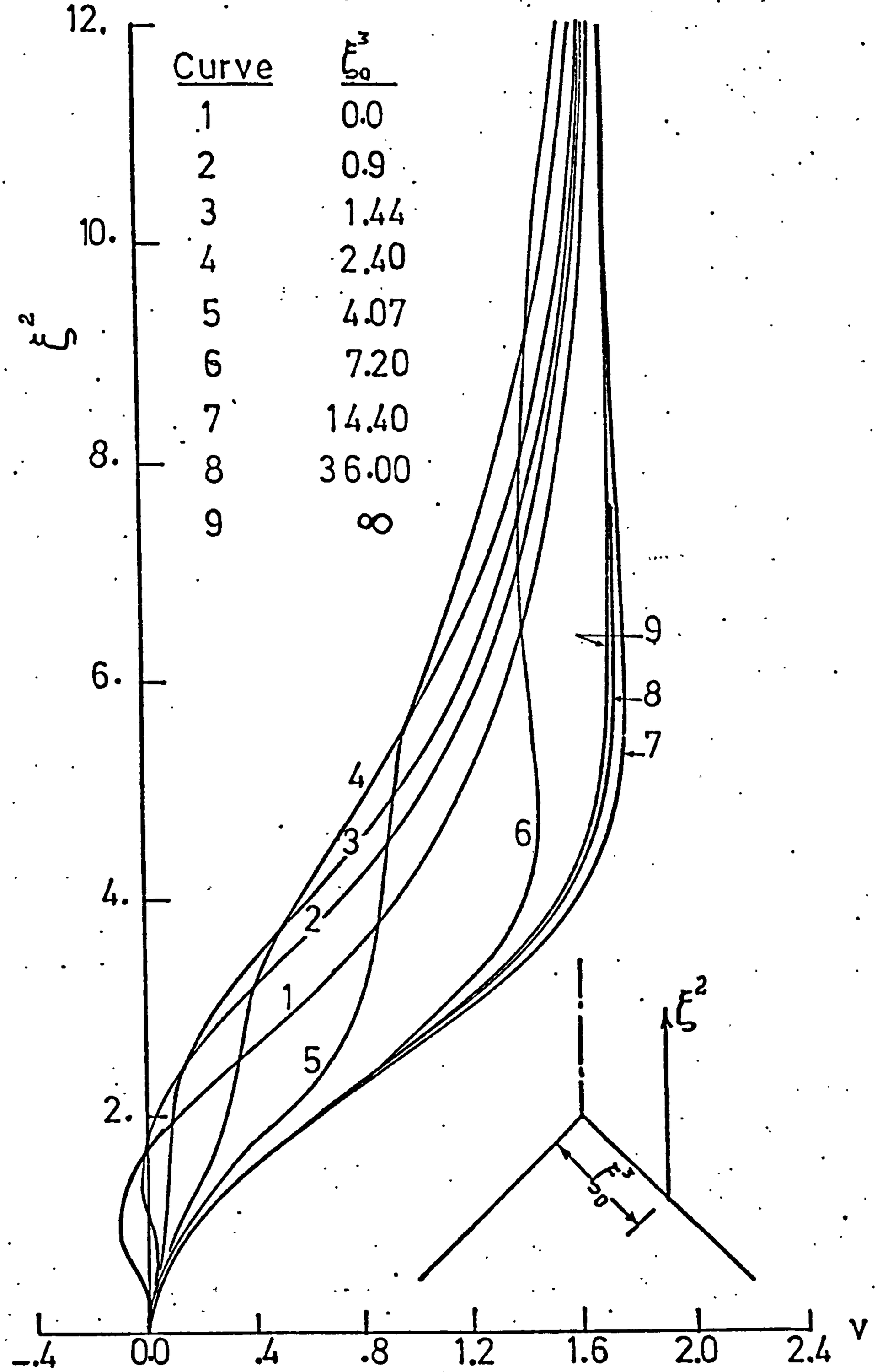

Fig.(4.22) Crossflow velocity component v in planes parallel to the symmetry plane, $\Gamma_{270} = \infty$.

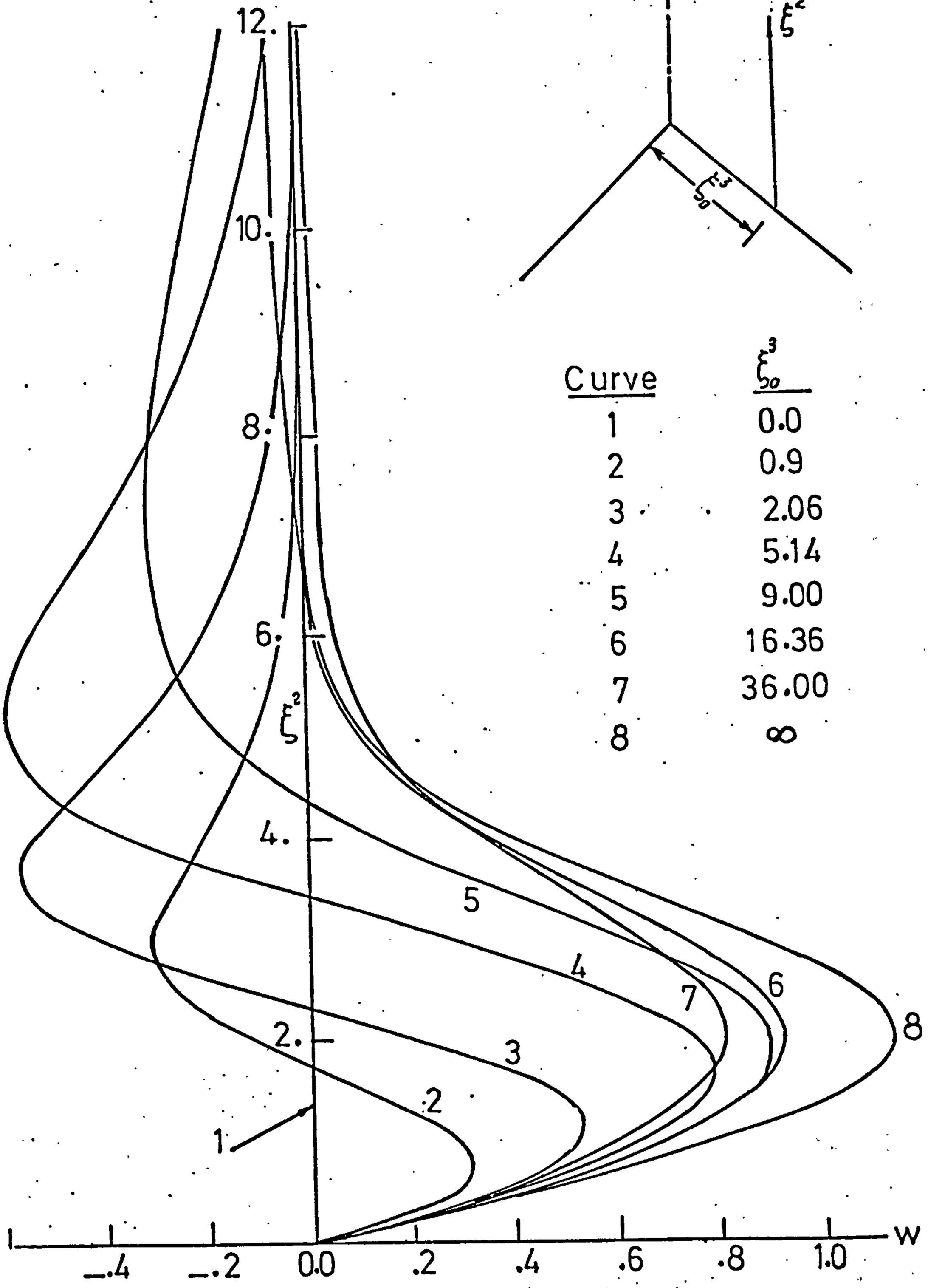

Curve	ξ^3_0
1	0.0
2	0.9
3	2.06
4	5.14
5	9.00
6	16.36
7	36.00
8	∞

Fig.(4.23) Crossflow velocity component w at planes parallel to the symmetry plane, $\Gamma_{270} = \infty$.

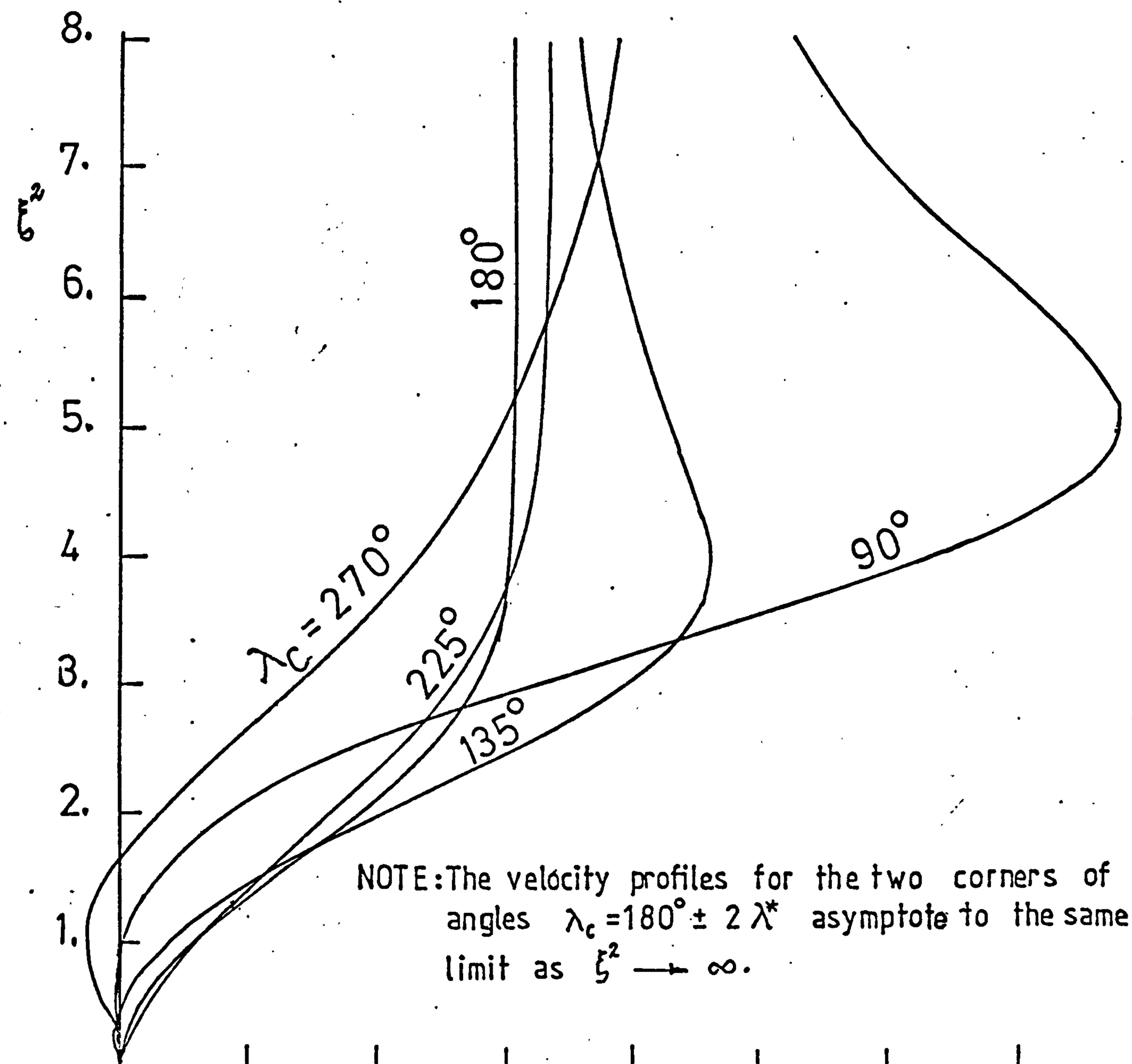

Fig.(4.24) Variation of velocity v, at $\xi^3 = 0$, with corner angle λ_c.

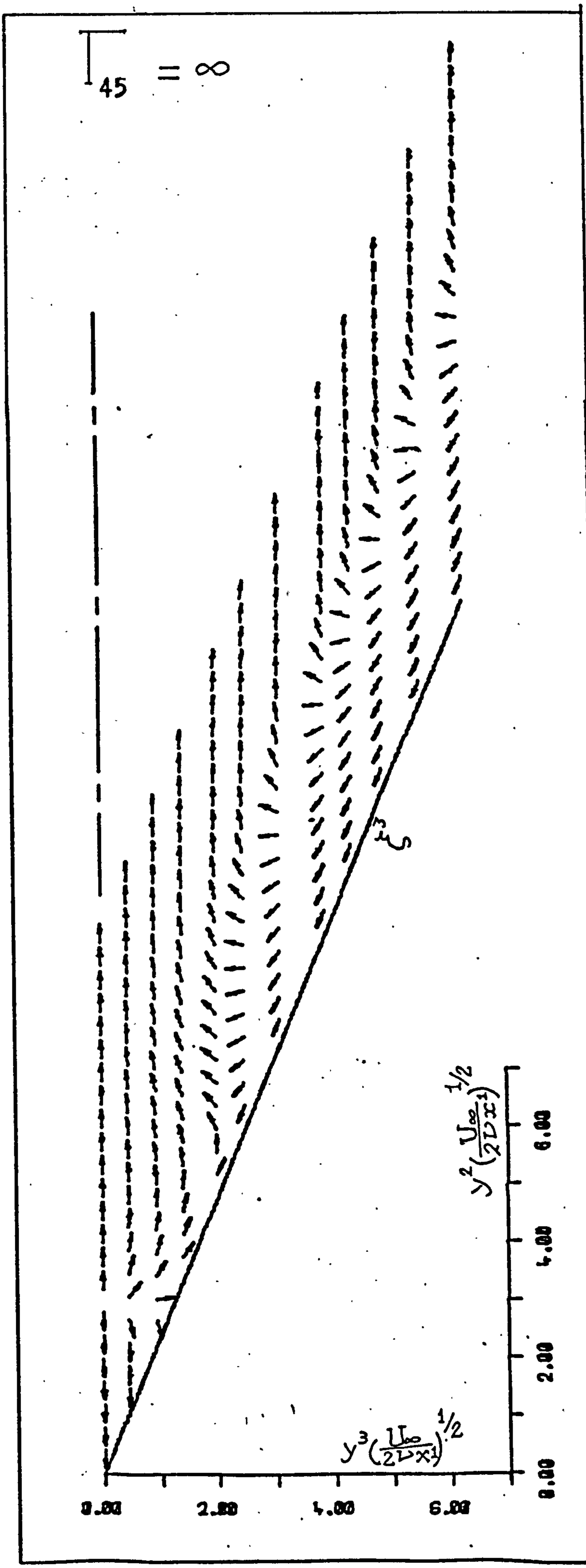

Fig.(4.25)
Crossflow
direction.

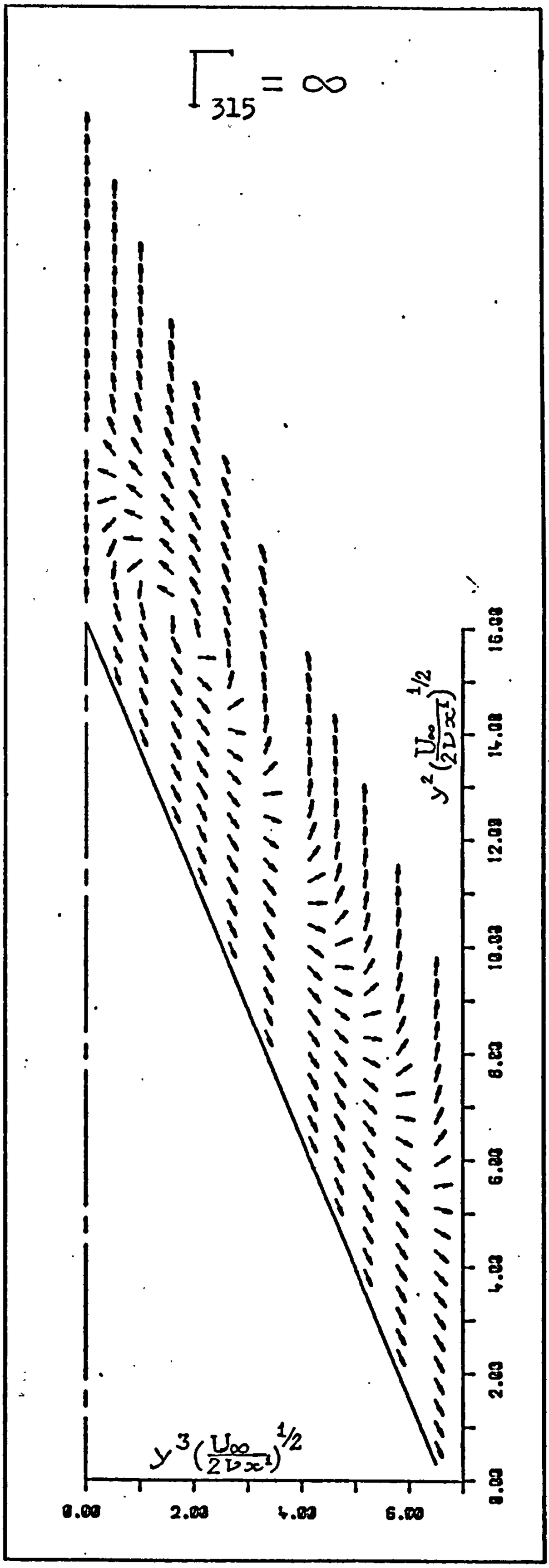

Fig.(4.26) Crossflow direction.

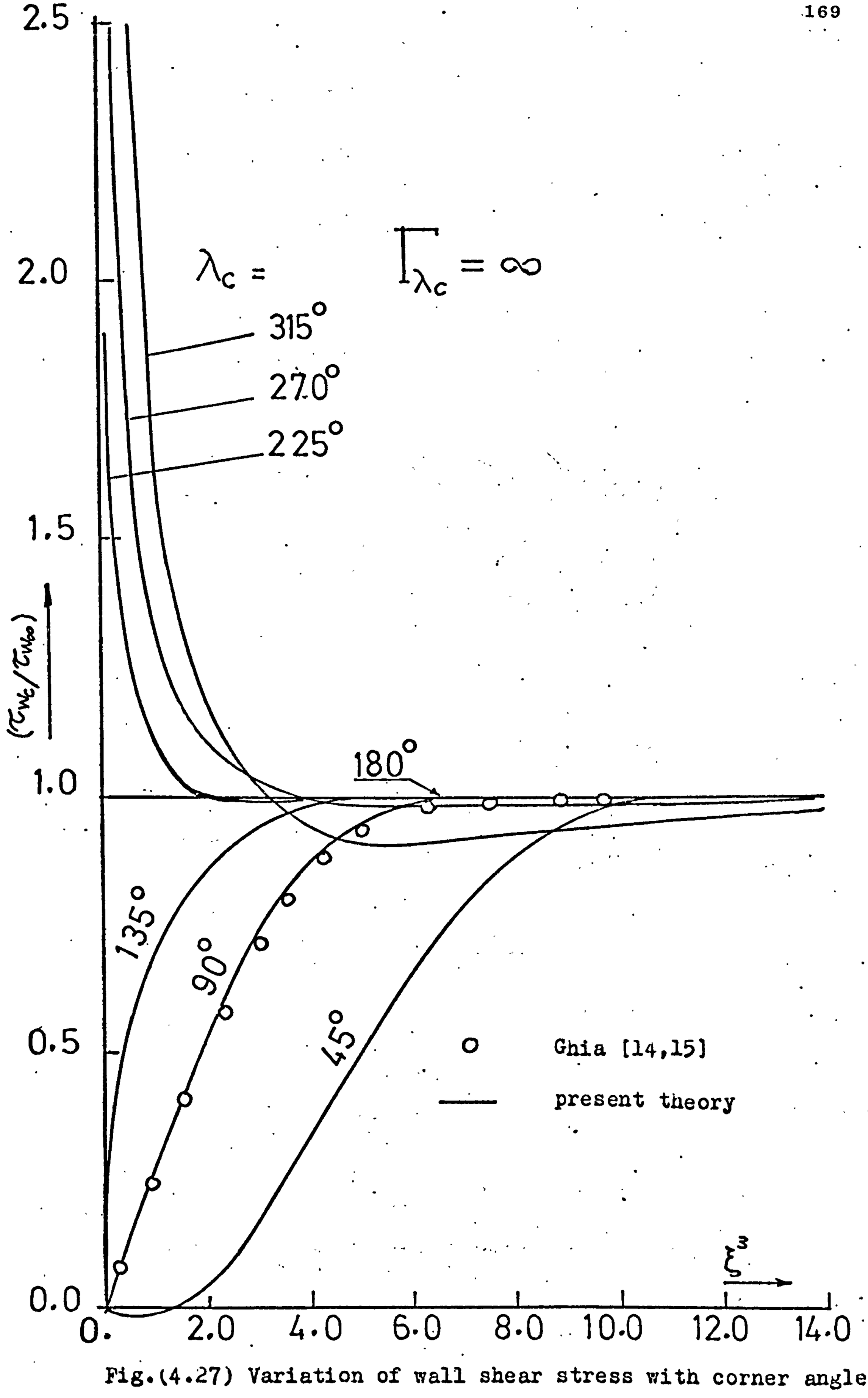

Fig.(4.27) Variation of wall shear stress with corner angle.

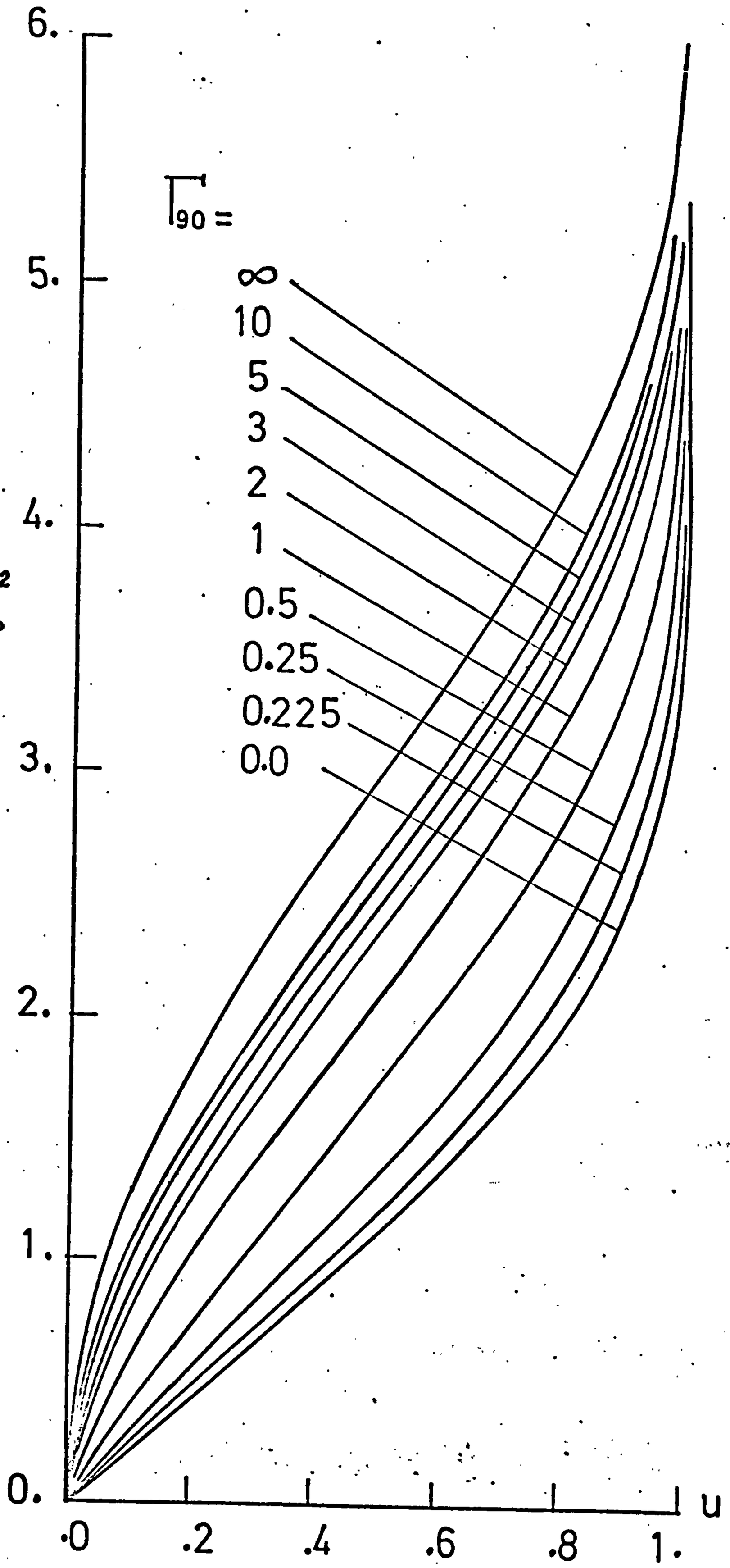

Fig.(4.28) Streamwise velocity in symmetry plane.

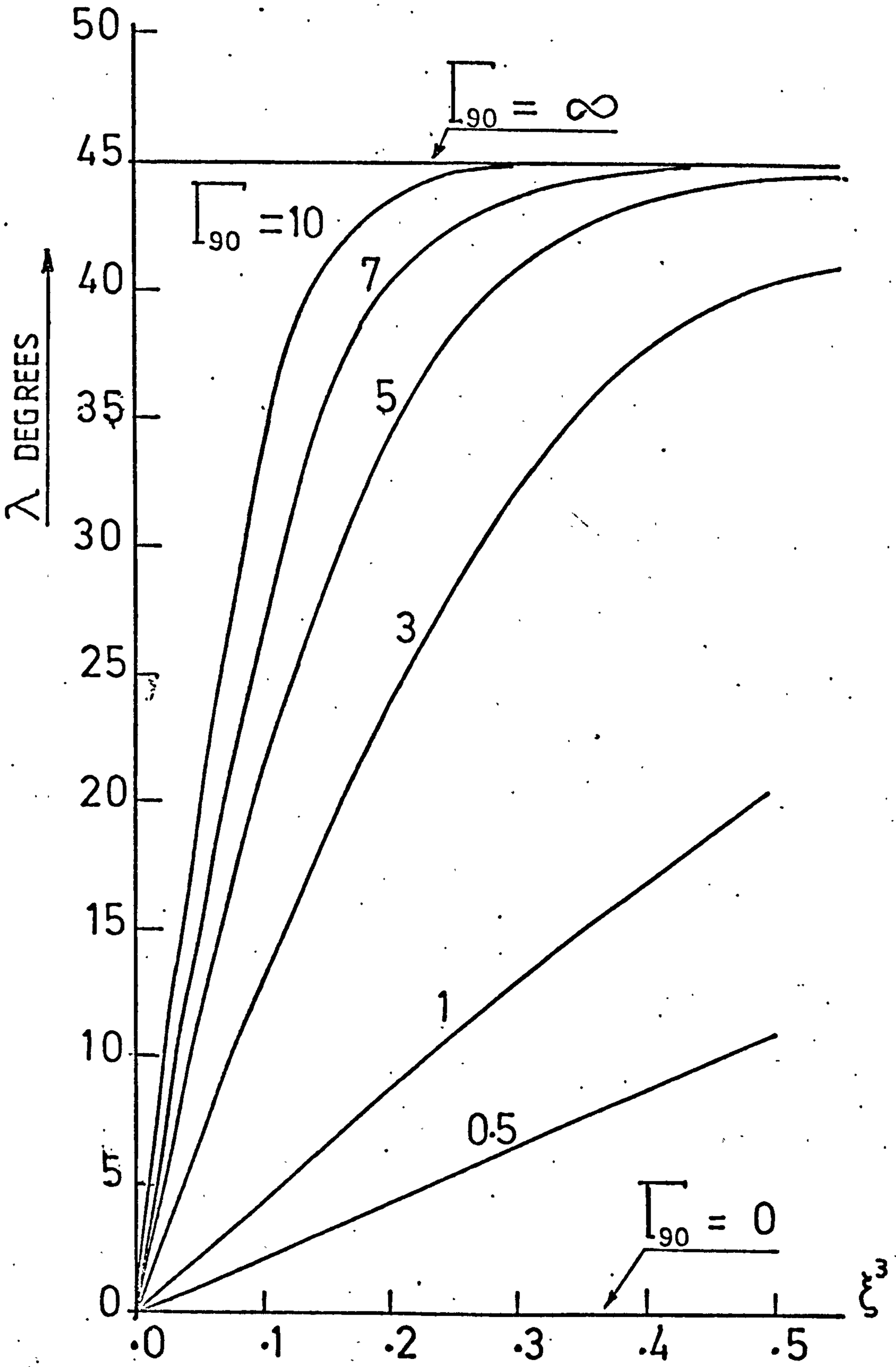

Fig.(4.29) Variation of the local angle λ with distance from the plane of symmetry.

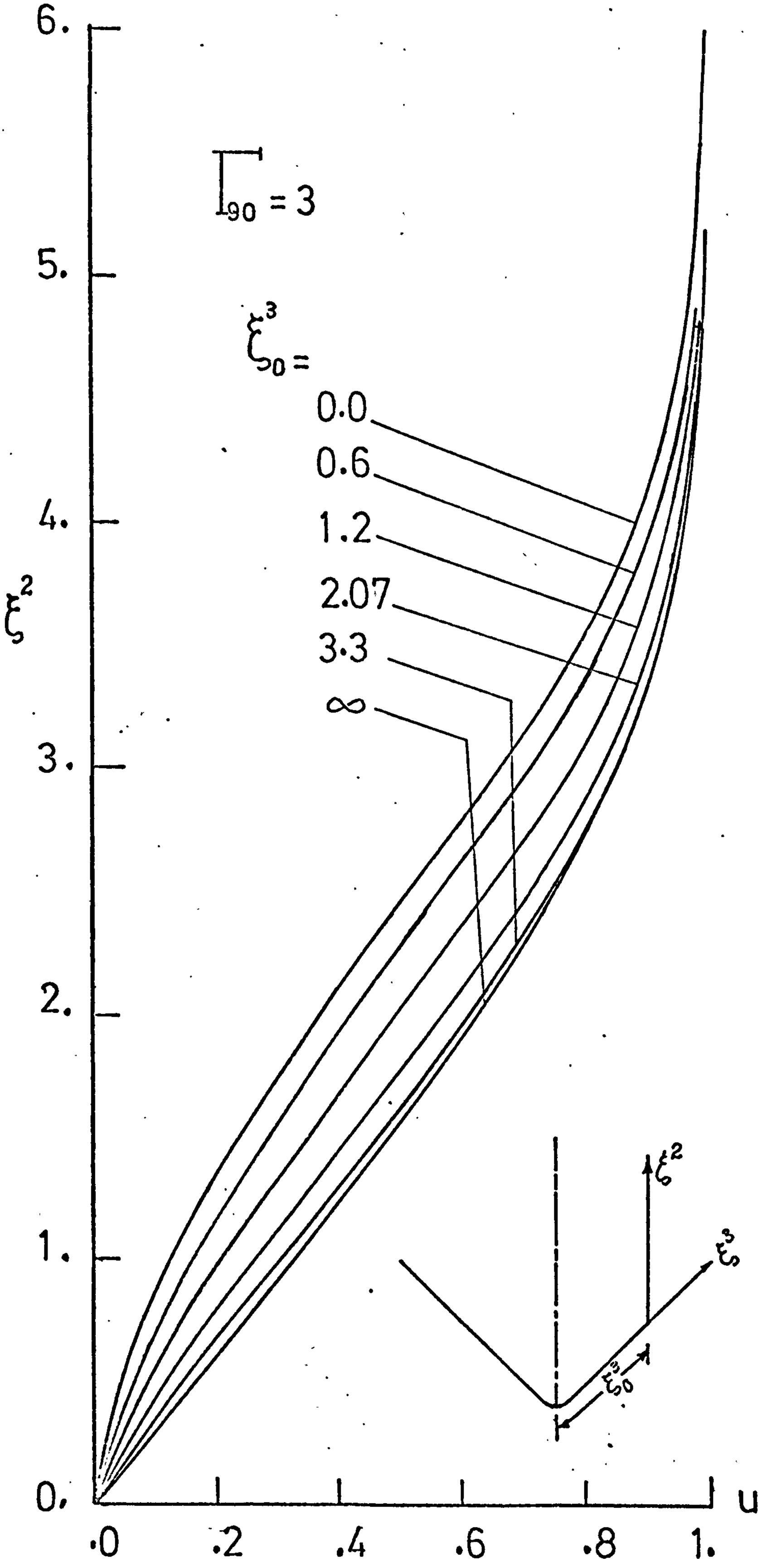

Fig.(4.30) Streamwise velocity u in planes parallel to the symmetry plane :

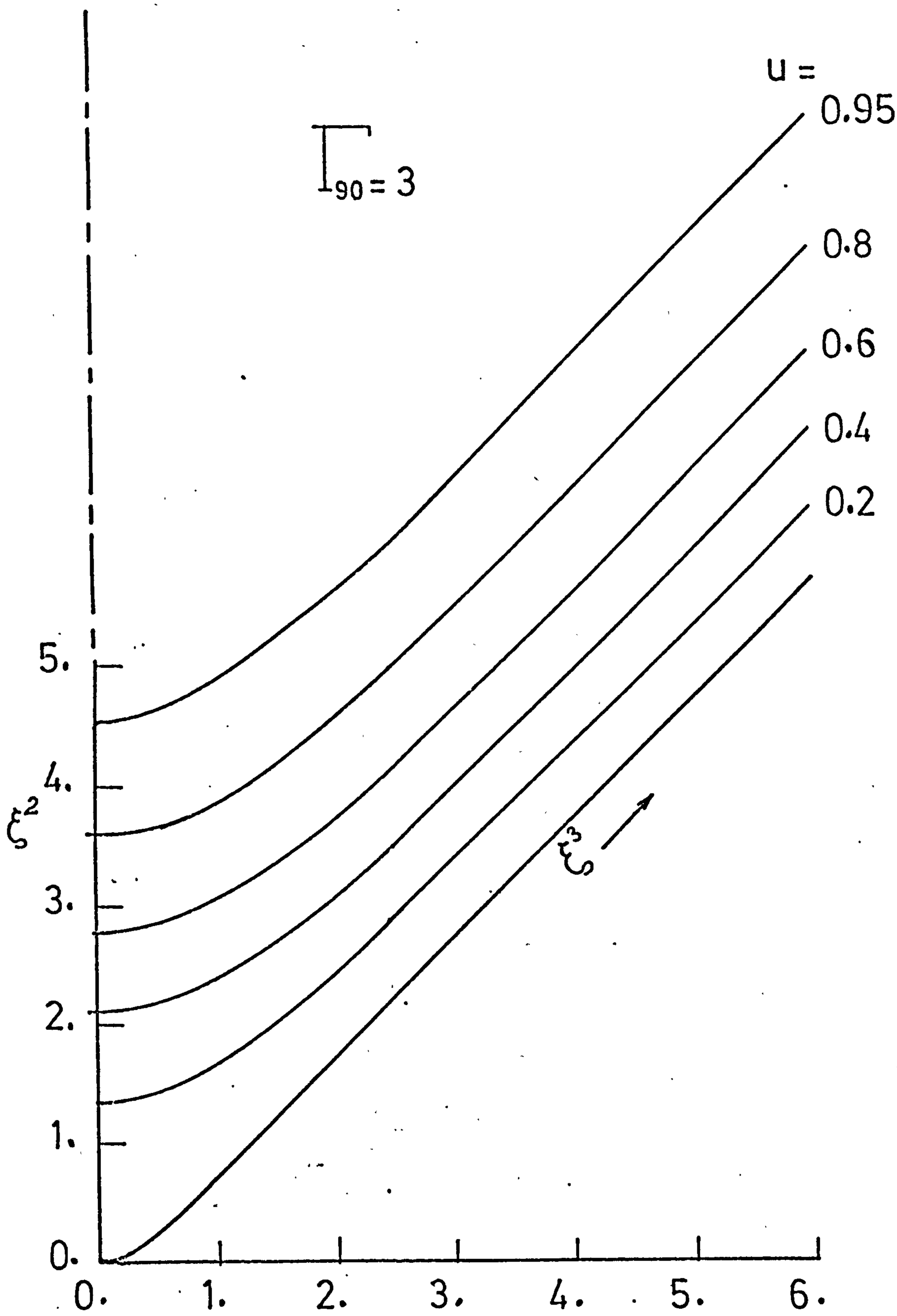

Fig.(4.31) Streamwise isovels .

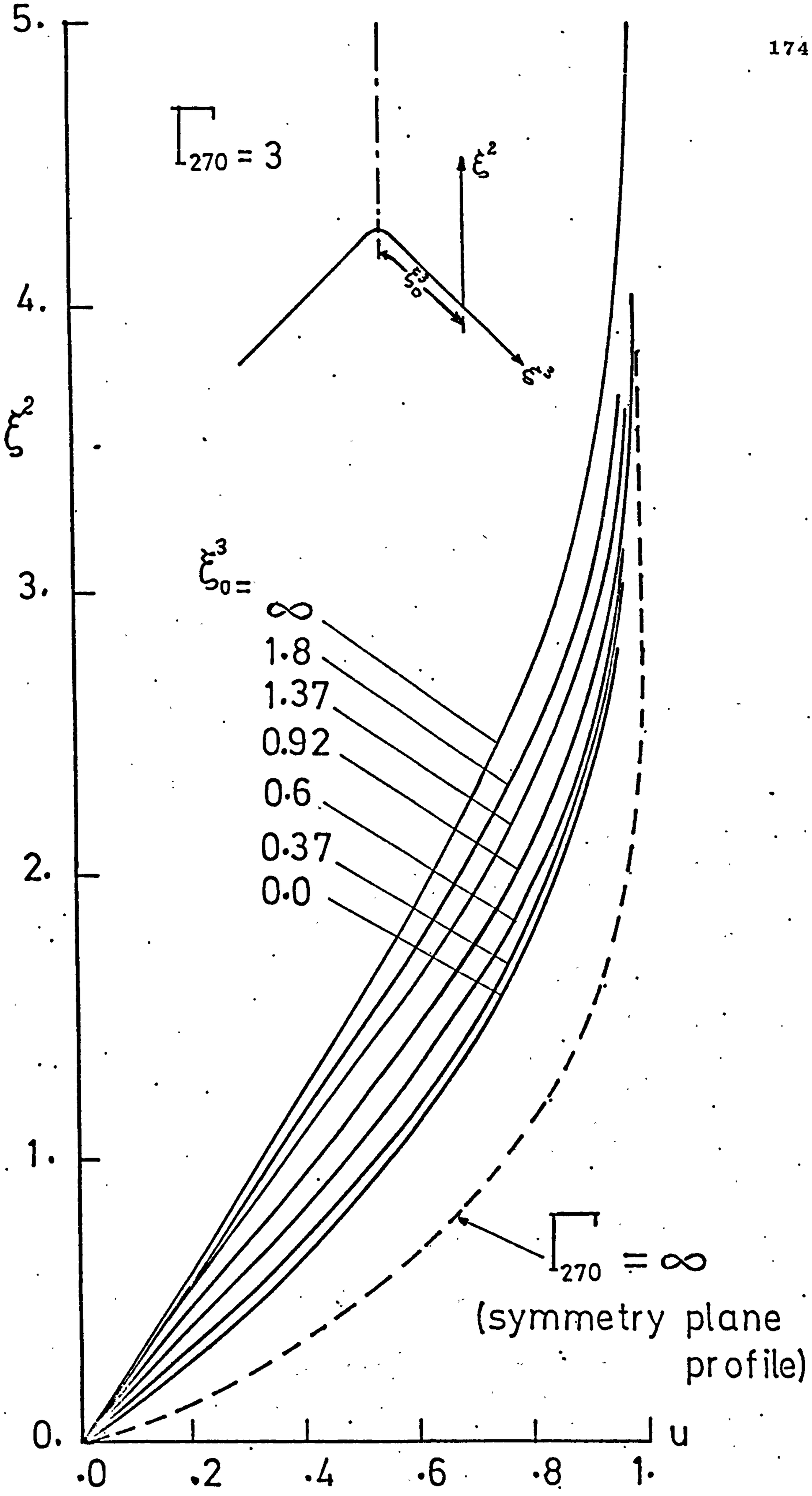

Fig.(4.32) Streamwise velocity u in ξ^3 = const. planes .

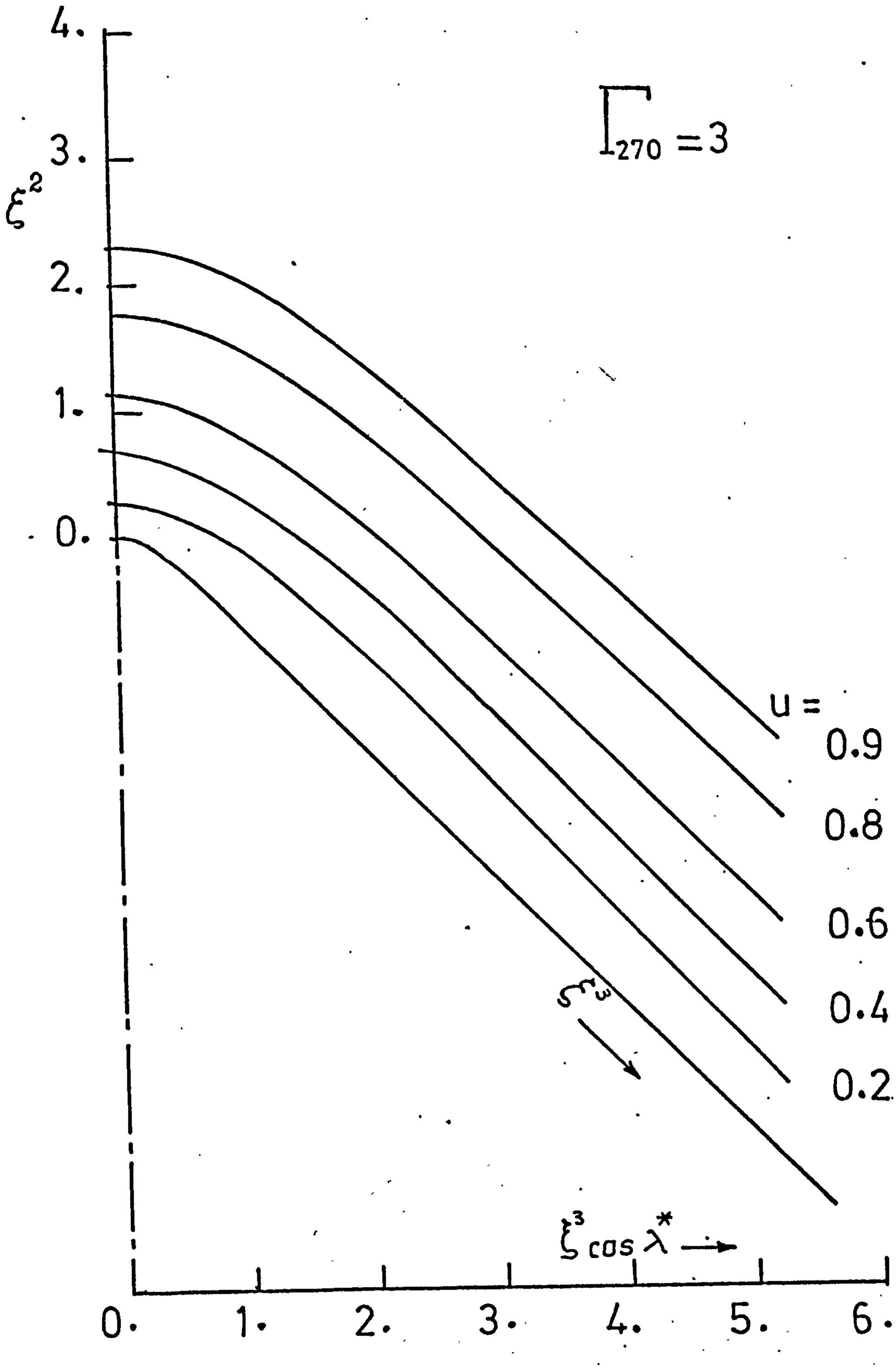

Fig.(4.33) Streamwise isovels.

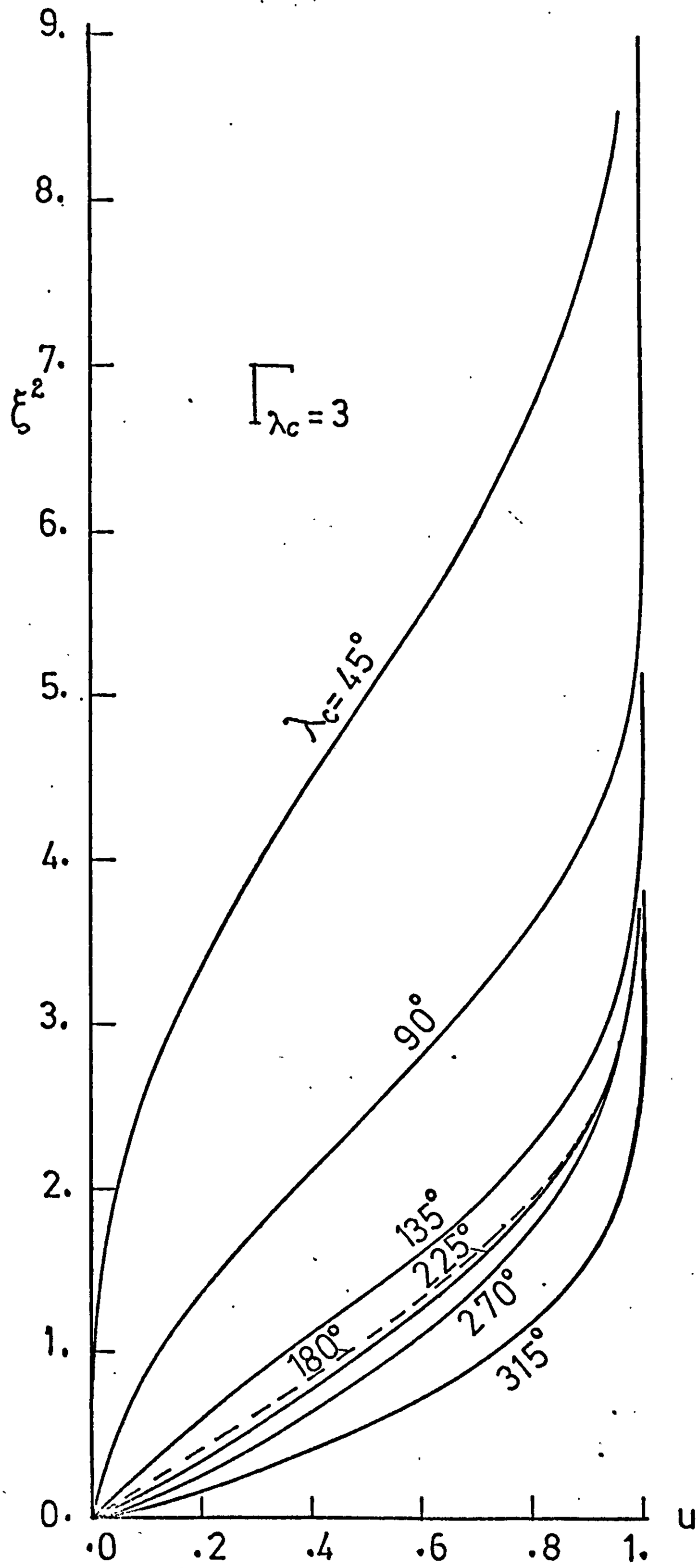

Fig.(4.34) Variation of velocity u ,in symmetry plane, with corner angle .

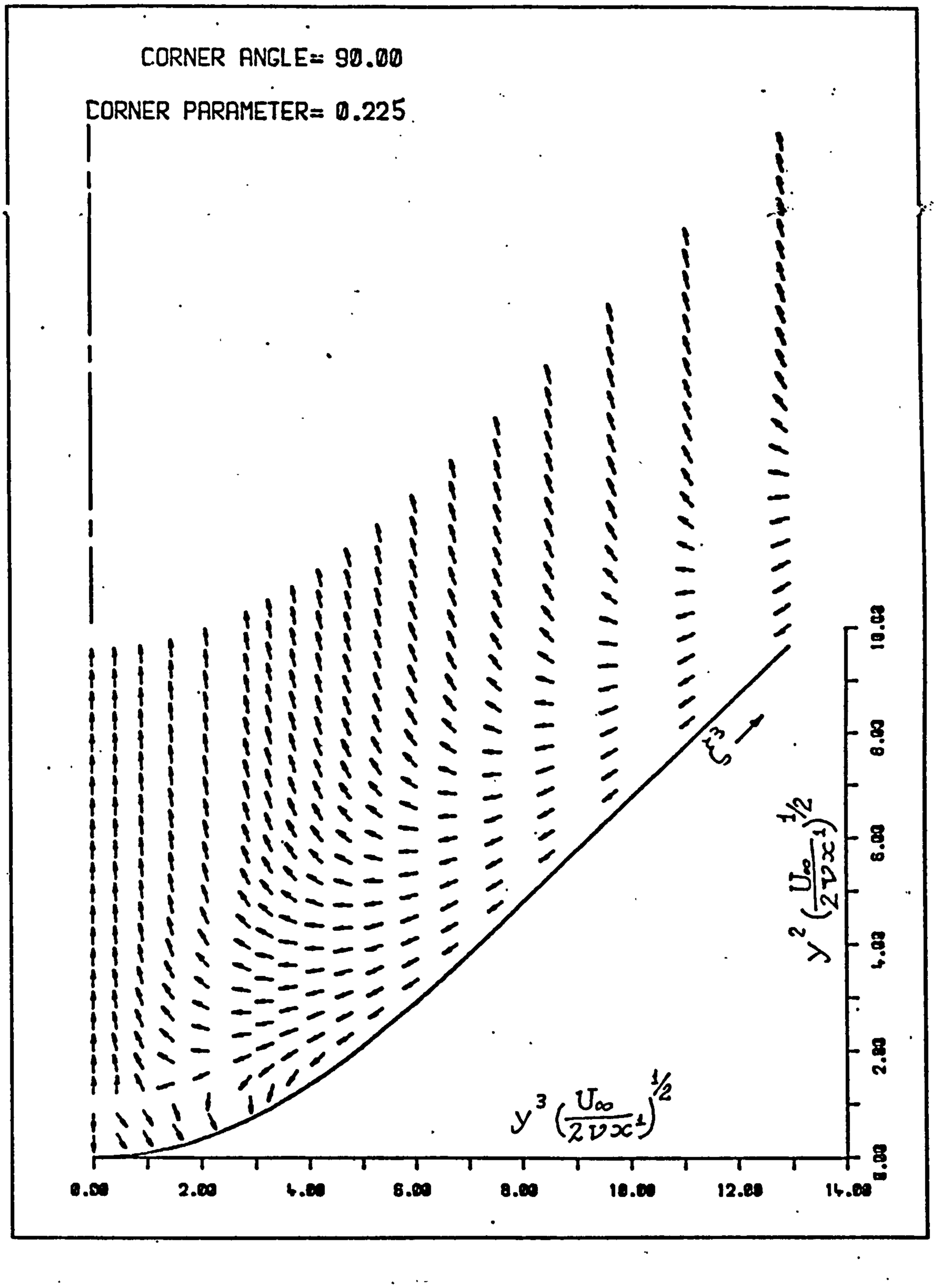

Fig.(4.35) Crossflow direction.

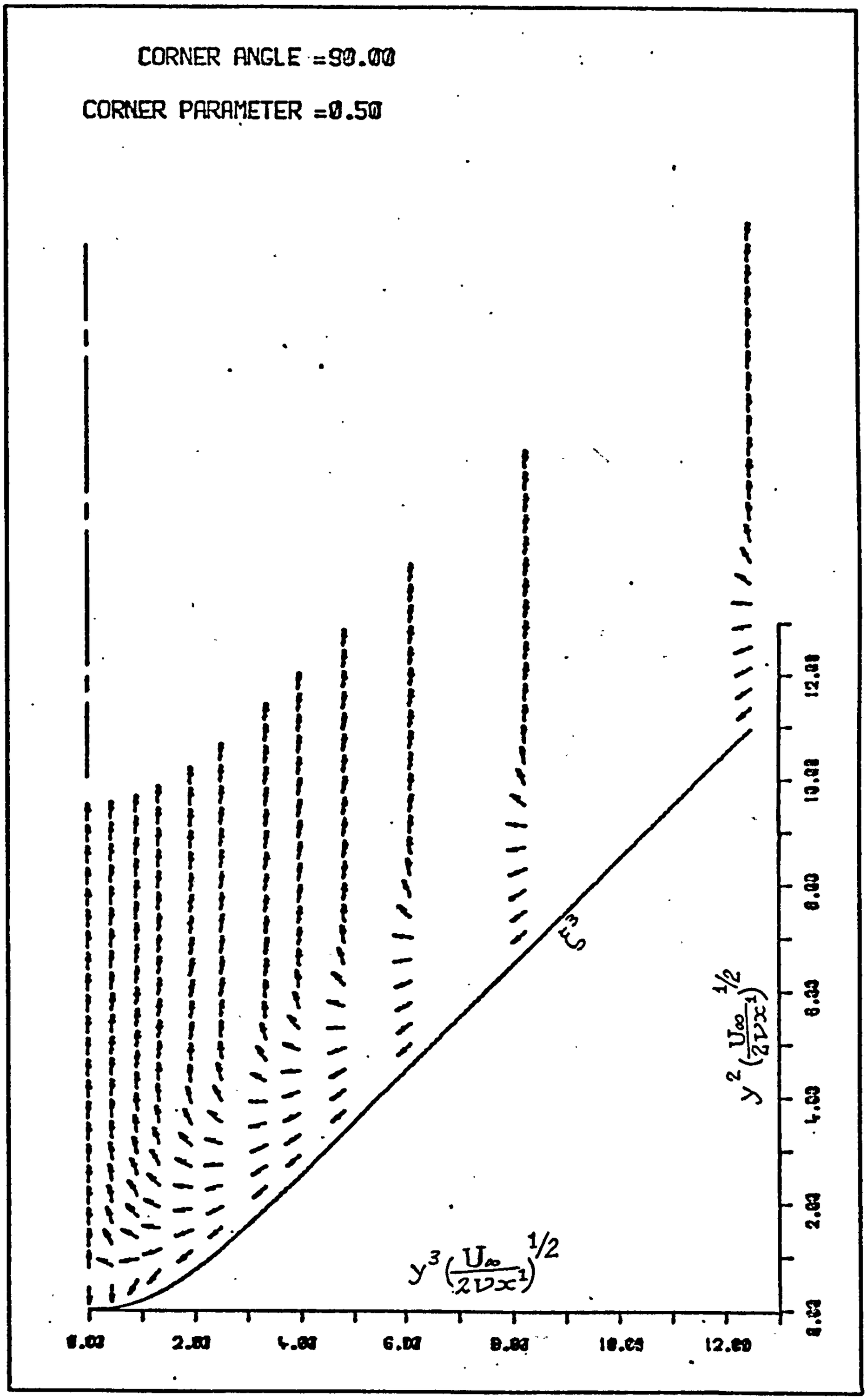

Fig.(4.36) Crossflow direction .

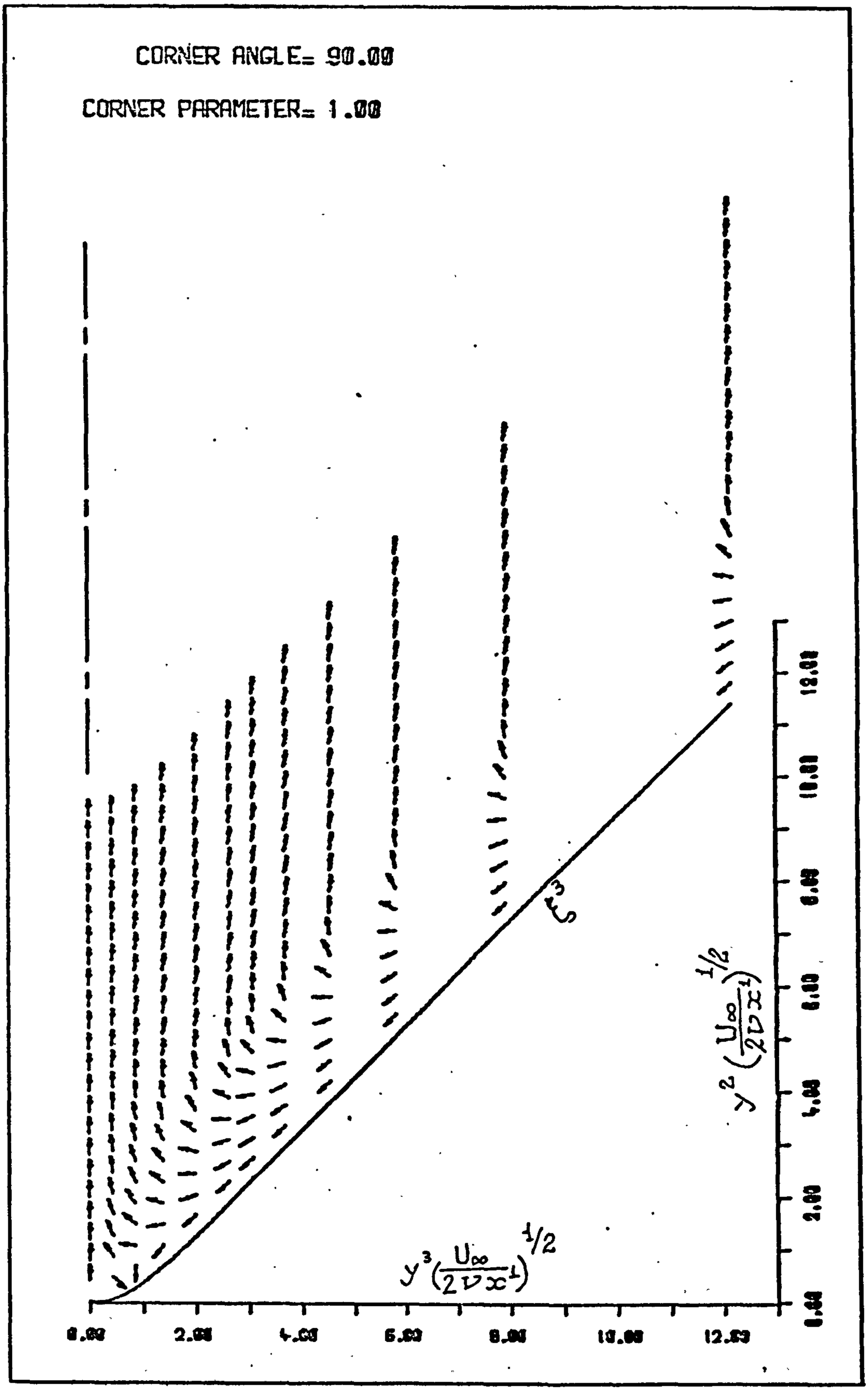

Fig.(4.37) Crossflow direction .

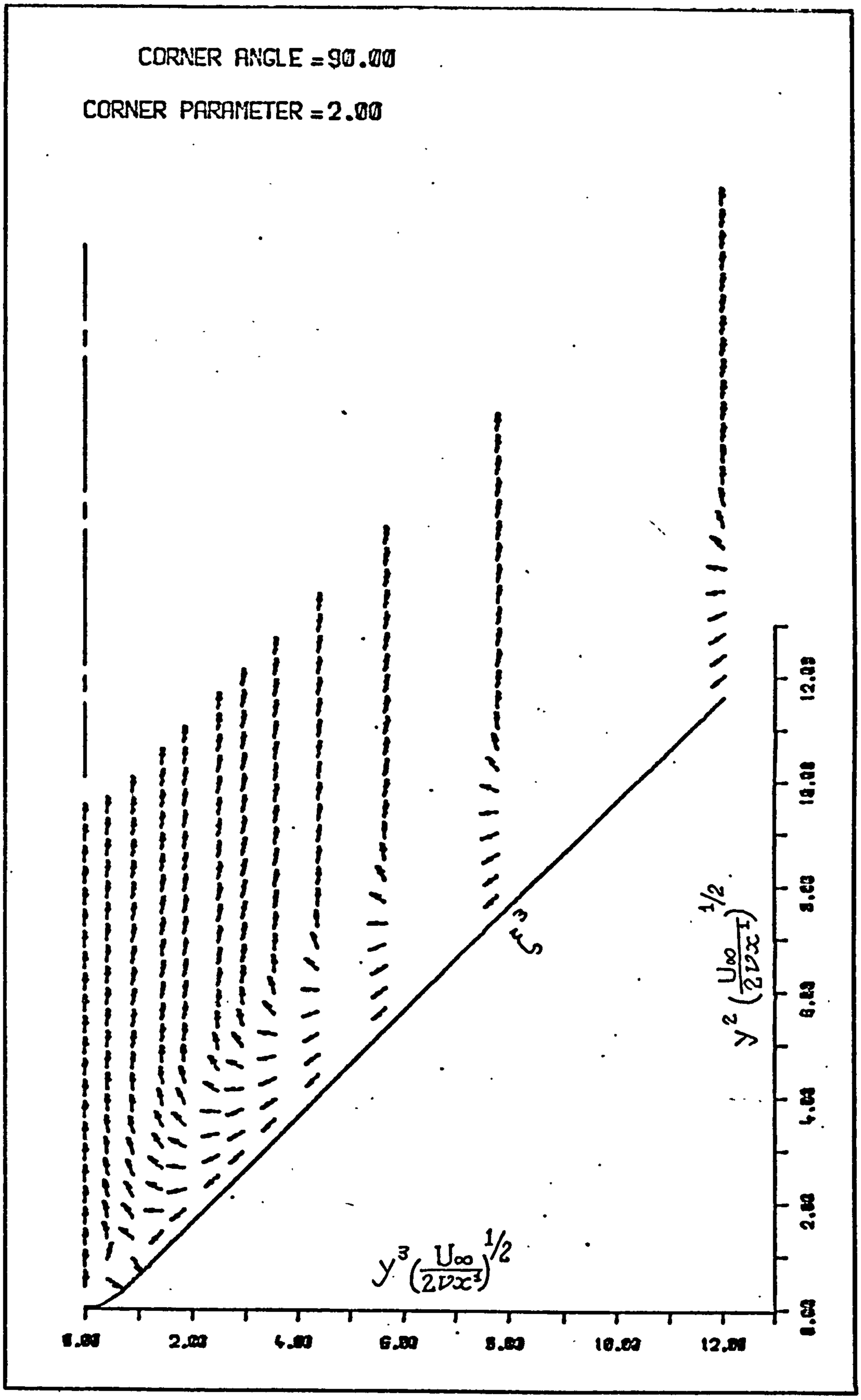

Fig.(4.38) Crossflow direction .

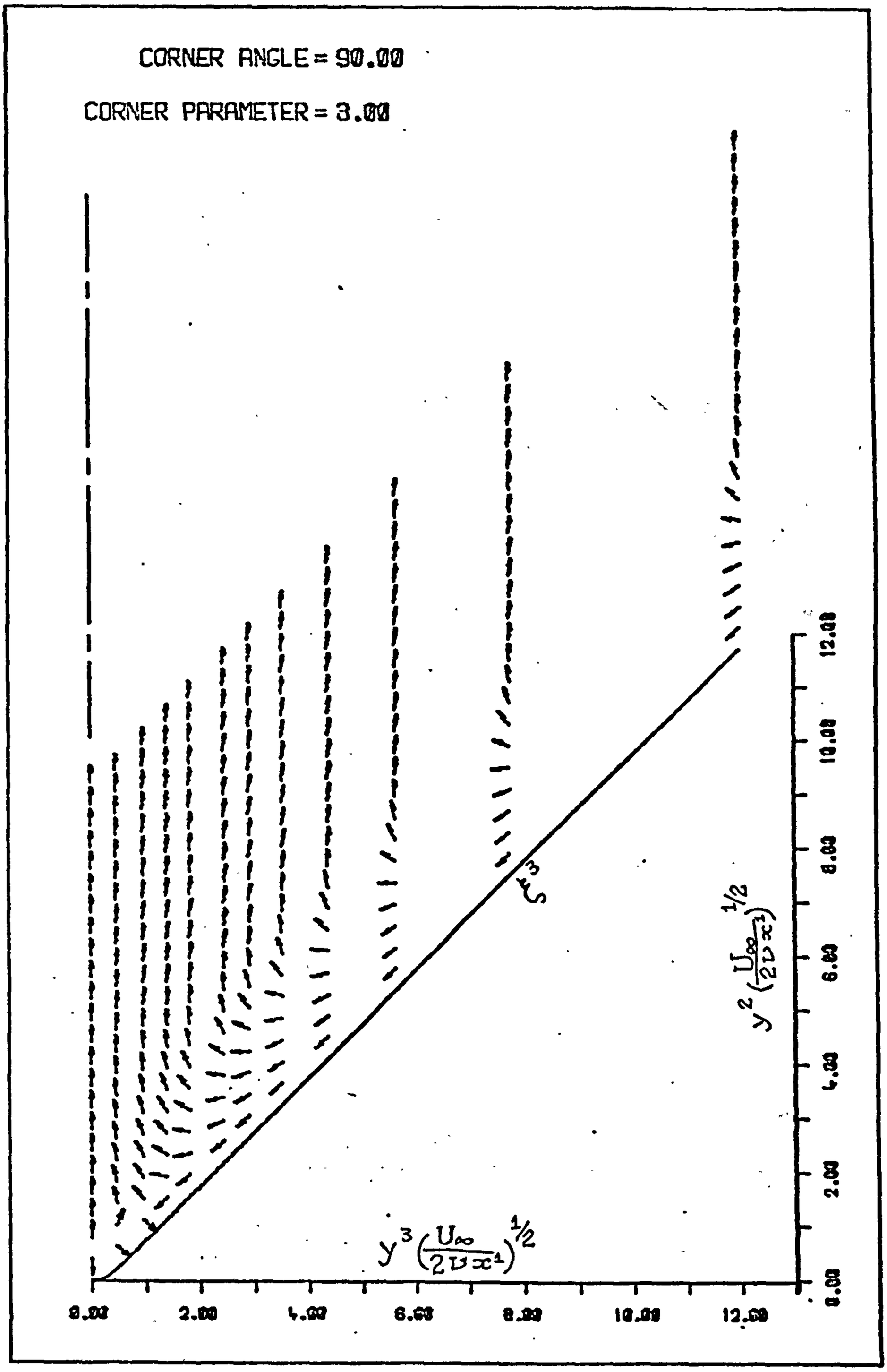

Fig.(4.39) Crossflow direction.

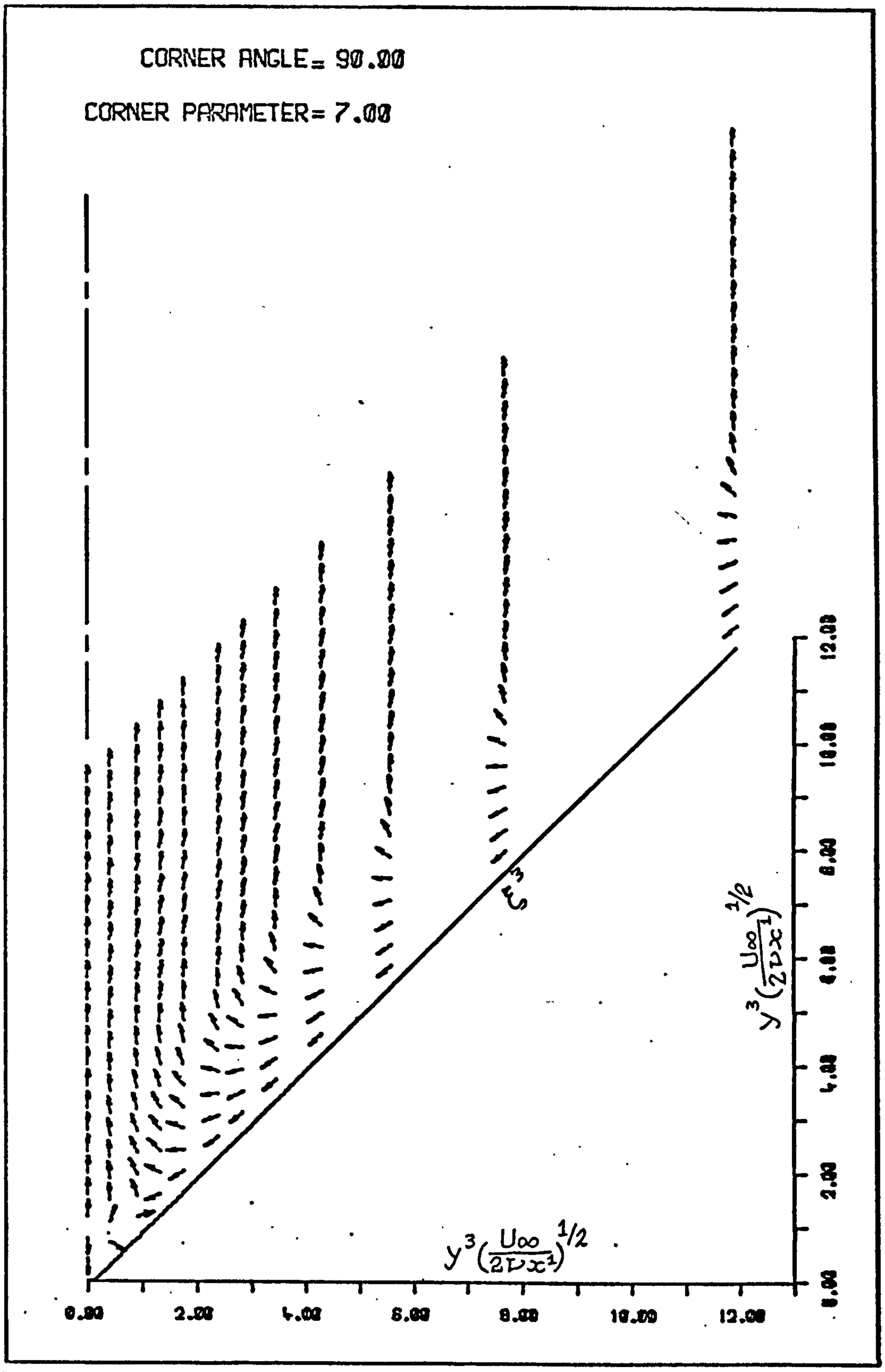

Fig.(4.40) Crossflow direction .

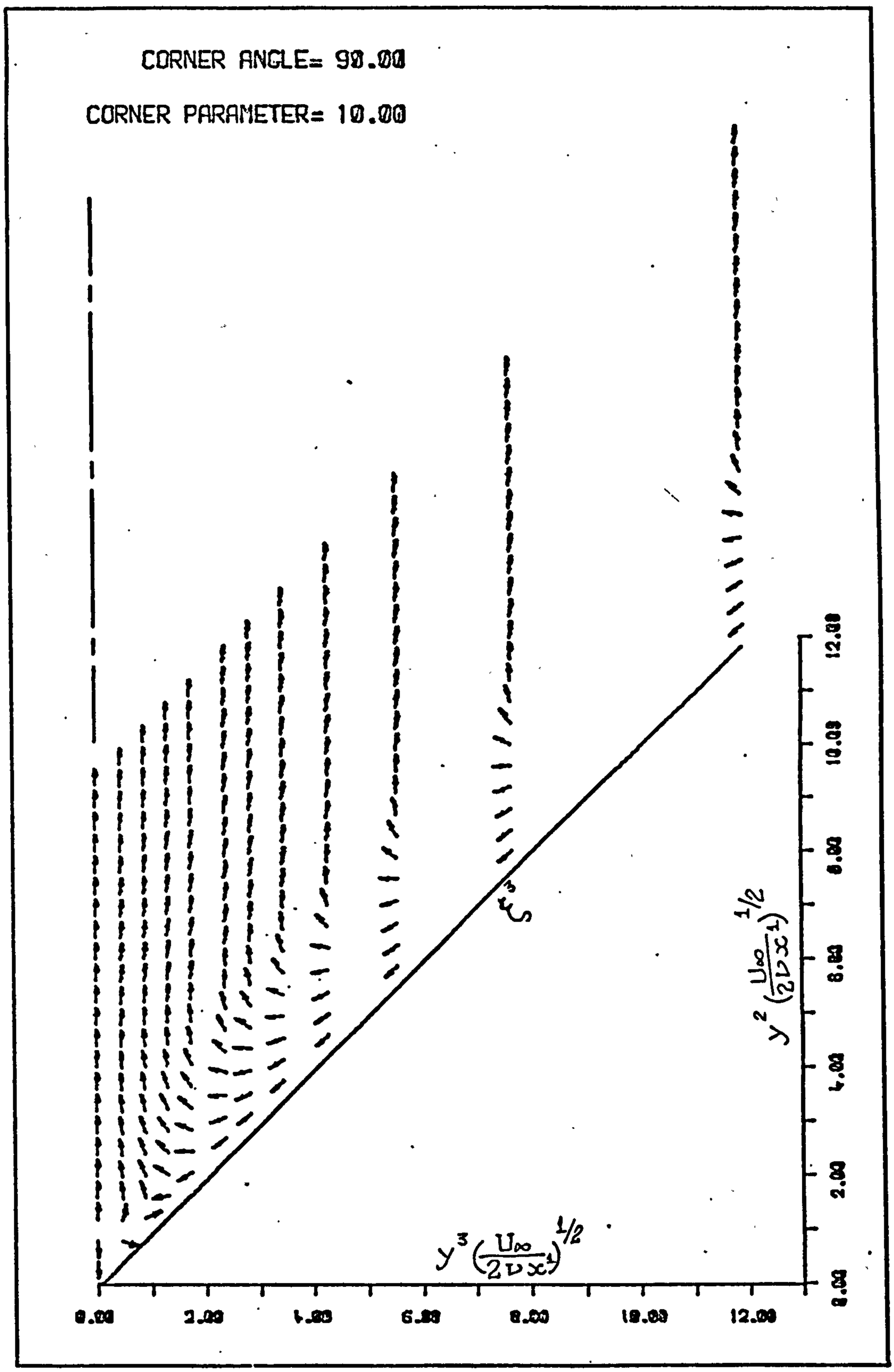

Fig.(4.41) Crossflow direction .

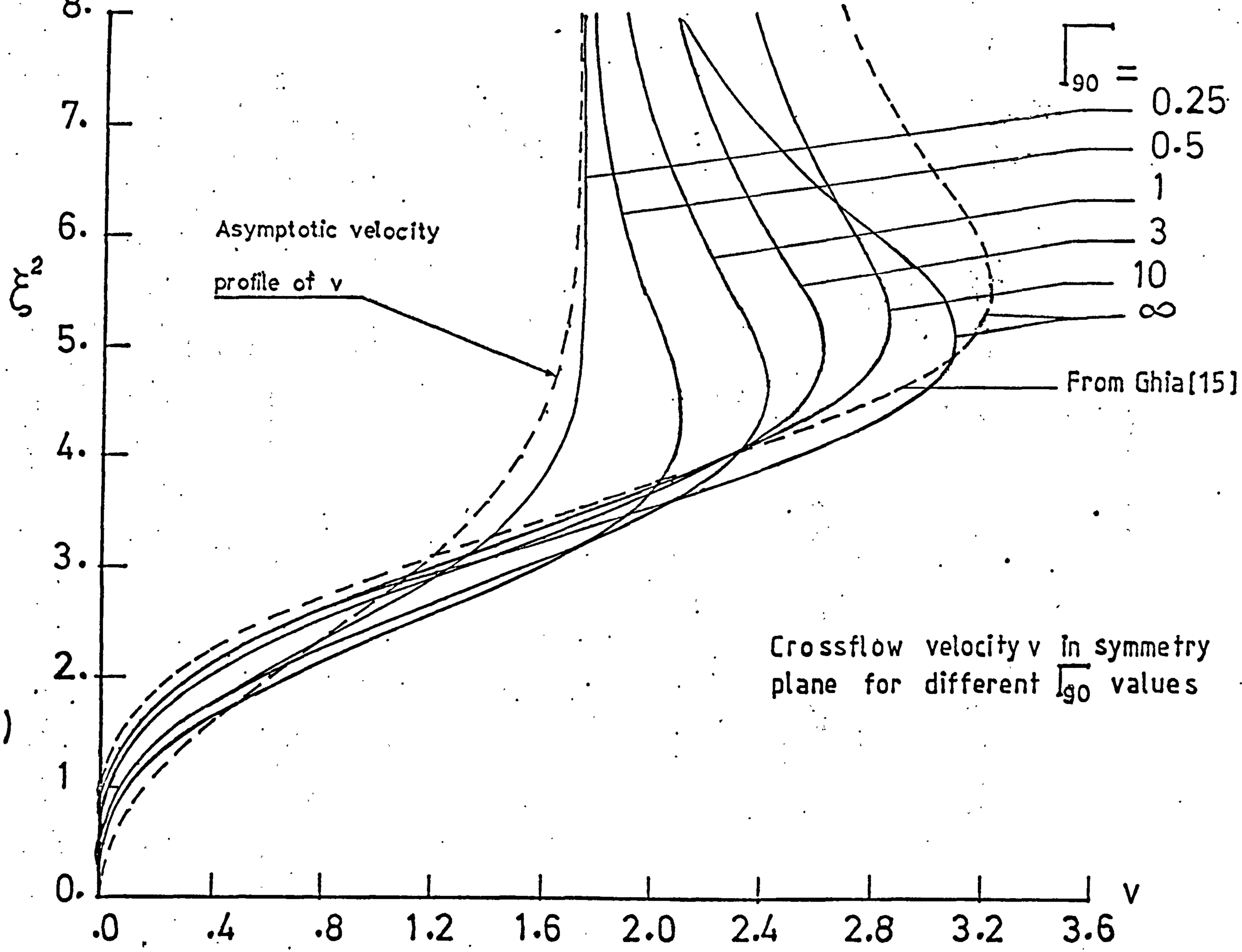

Crossflow velocity v in symmetry plane for different Γ_{90} values

Fig(4.42)

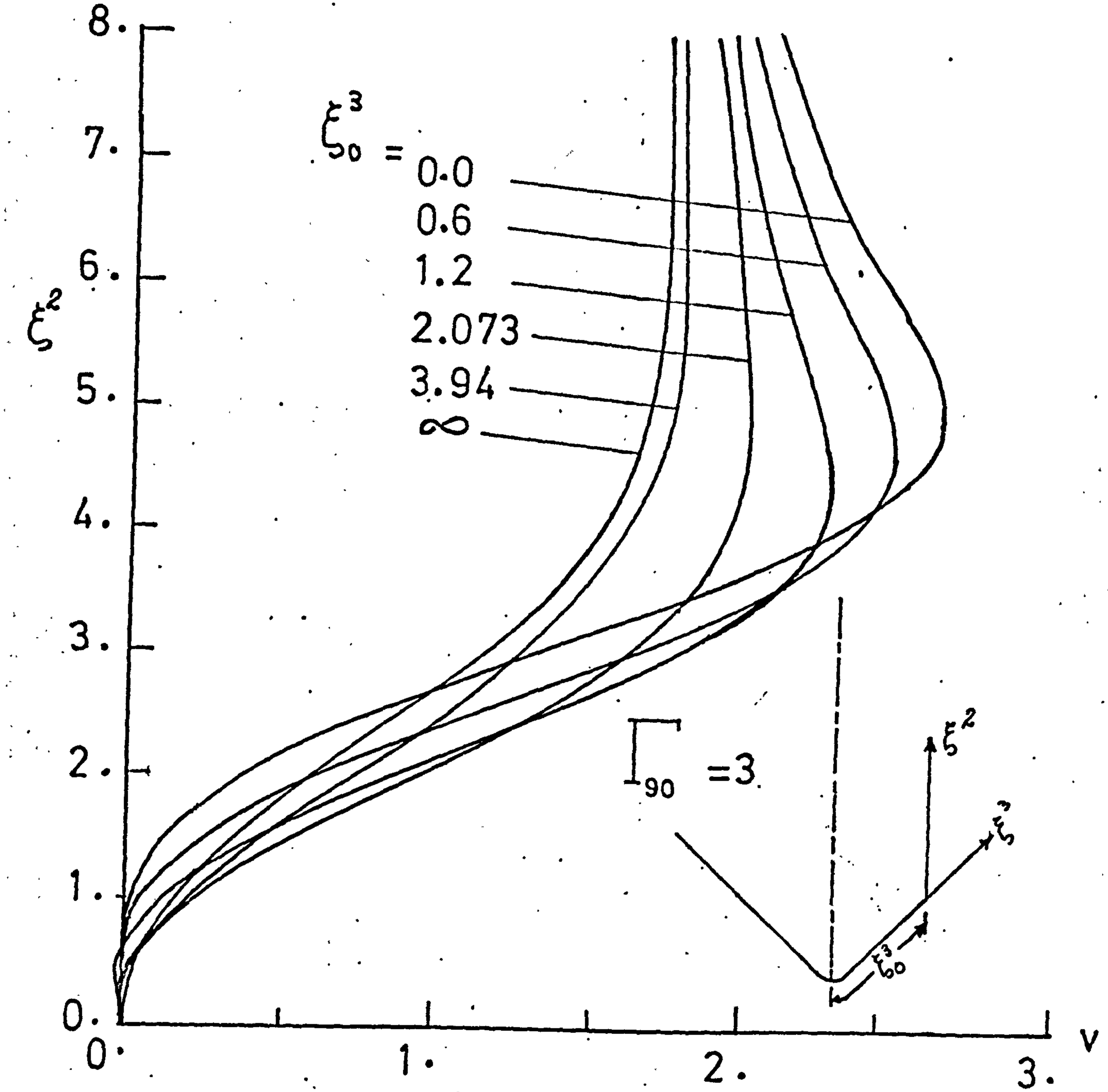

Fig (4.43) Crossflow velocity v in ξ^3 = const. planes.

$\Gamma_{90} = 3$

curve	ξ_o^3
1	0.0
2	0.6
3	2.4
4	6.0
5	34.8
6	∞

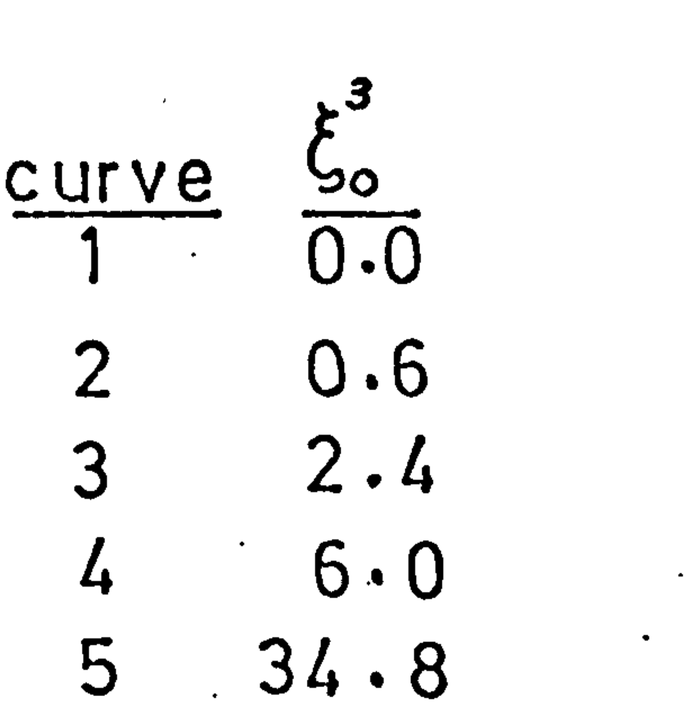

Fig.(4.44) Crossflow velocity w at ξ^3 = const. planes .

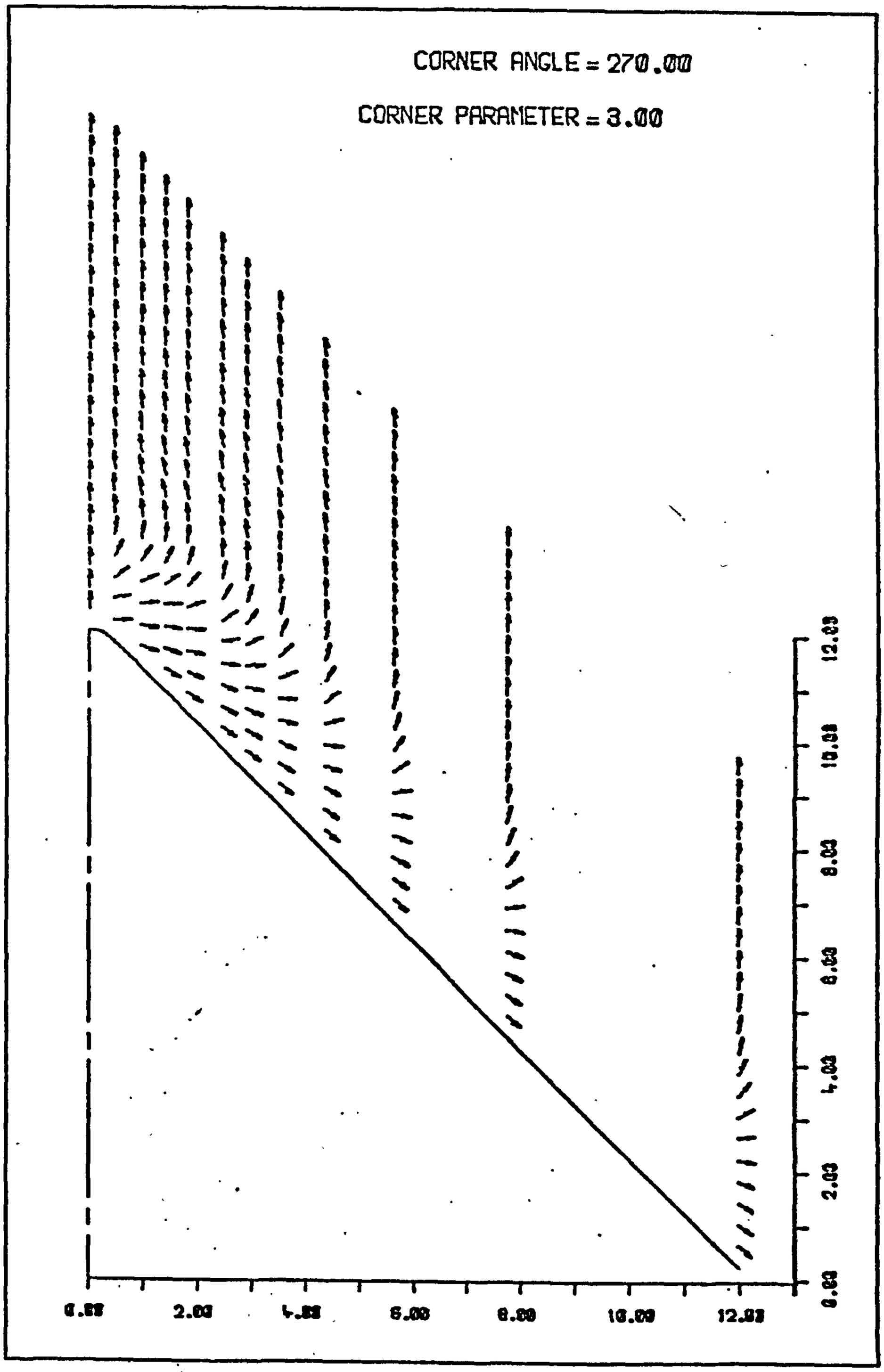

Fig.(4.45) Crossflow direction .

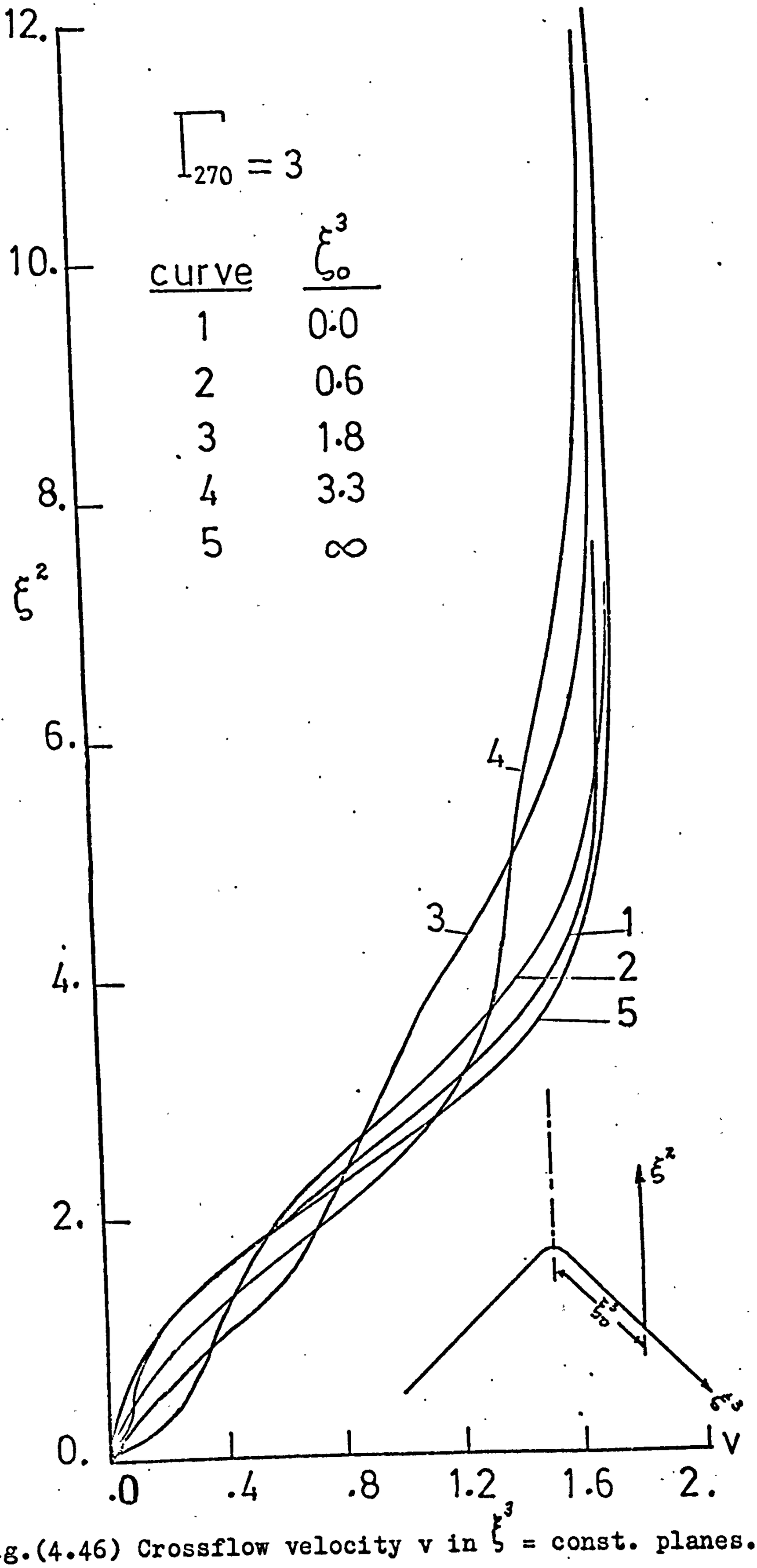

Fig.(4.46) Crossflow velocity v in ξ^3 = const. planes.

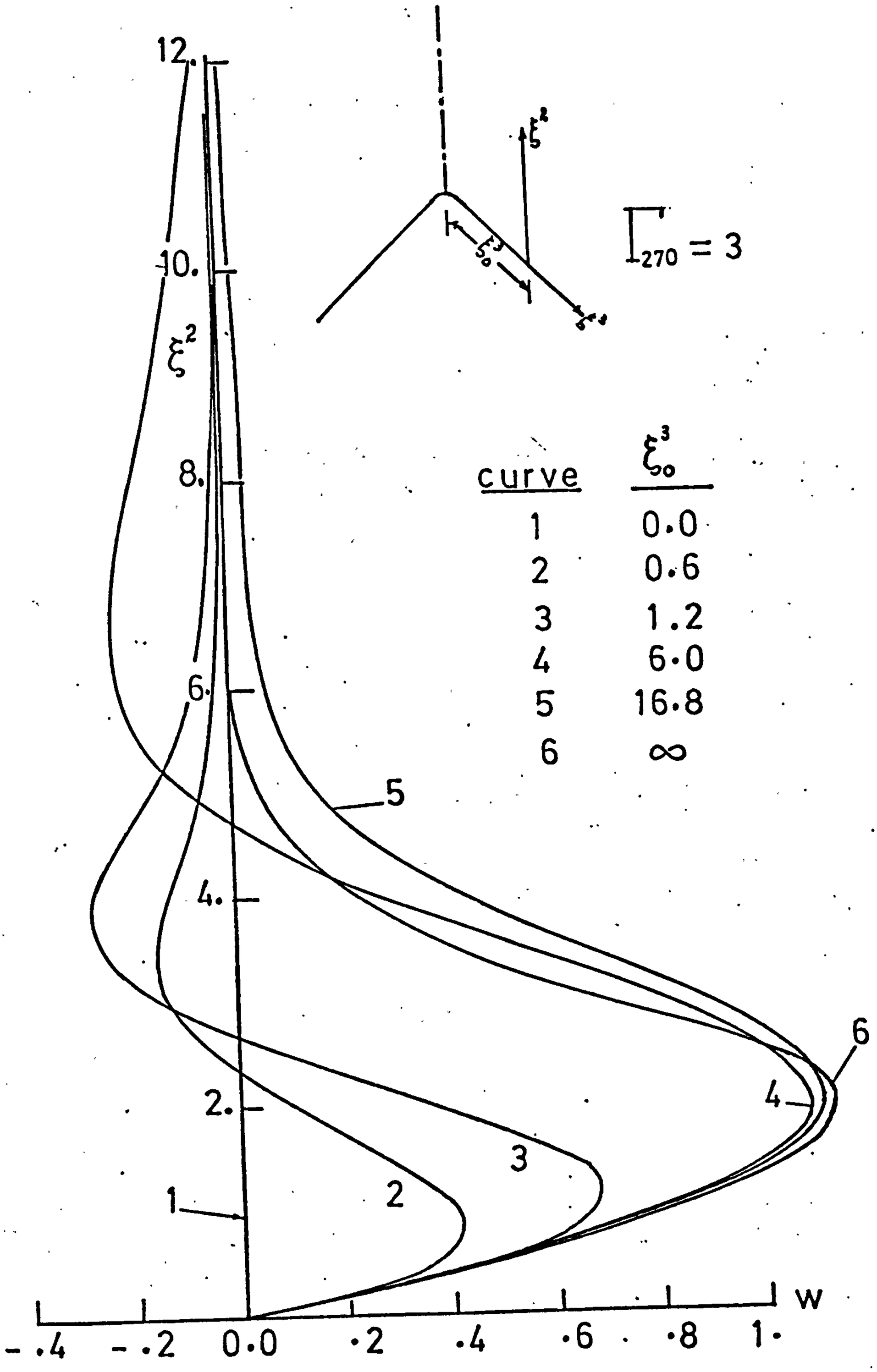

curve	ξ^3_o
1	0.0
2	0.6
3	1.2
4	6.0
5	16.8
6	∞

Fig.(4.47) Cross flow velocity w at ξ^3 = const. planes.

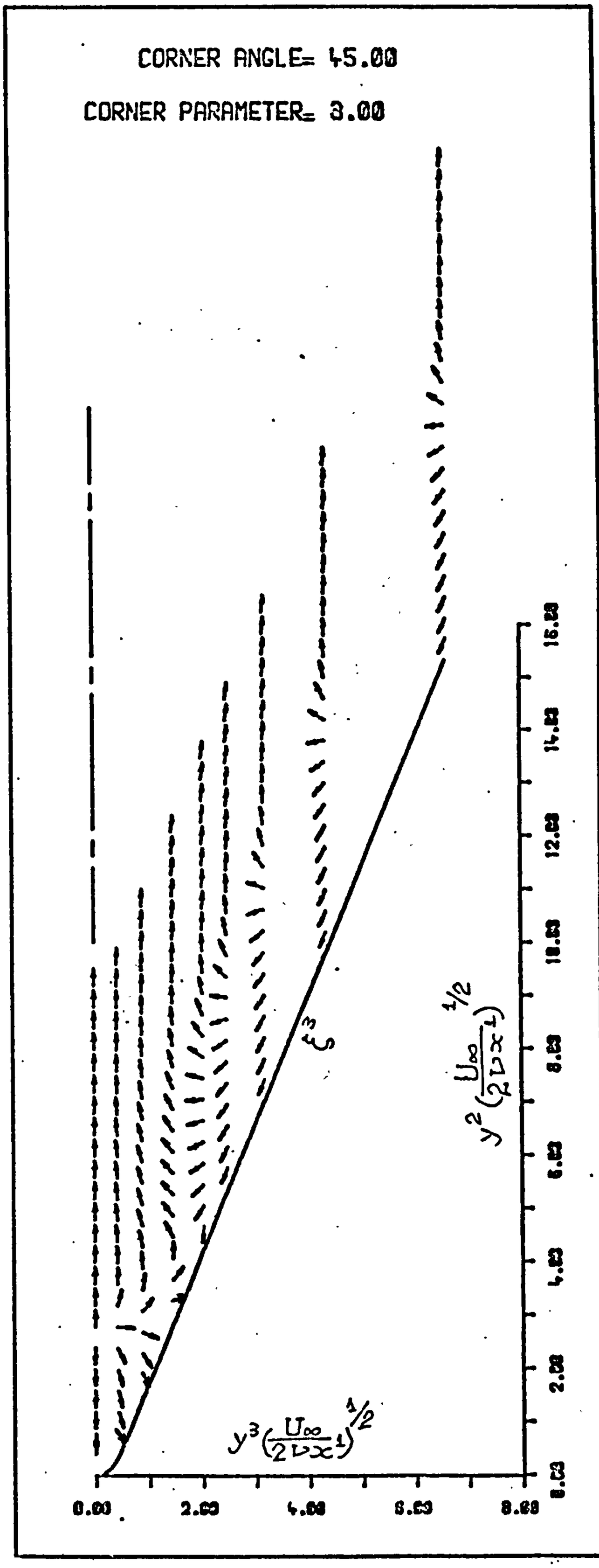

Fig.(4.48) Crossflow direction.

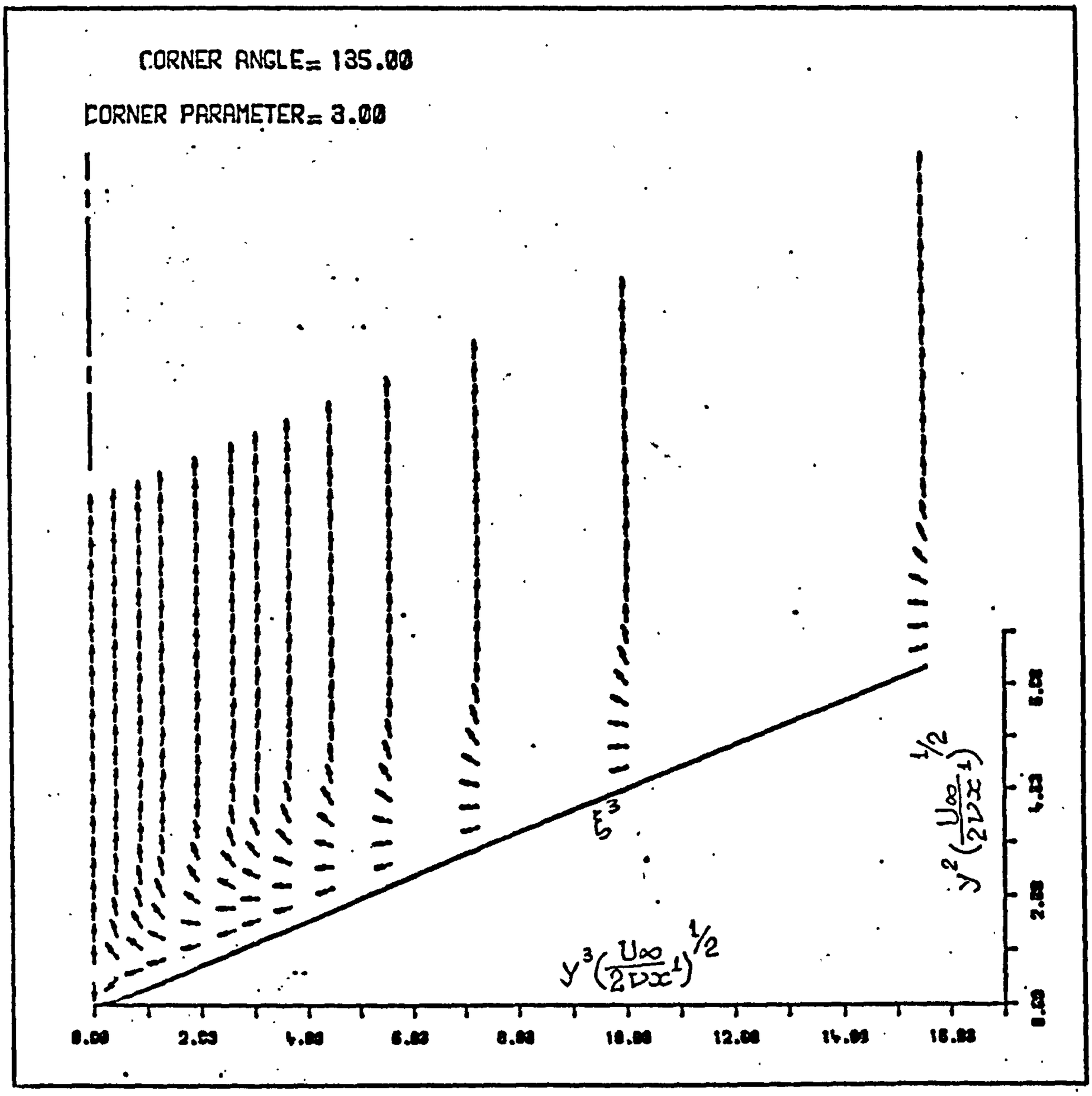

Fig.(4.49) Crossflow direction .

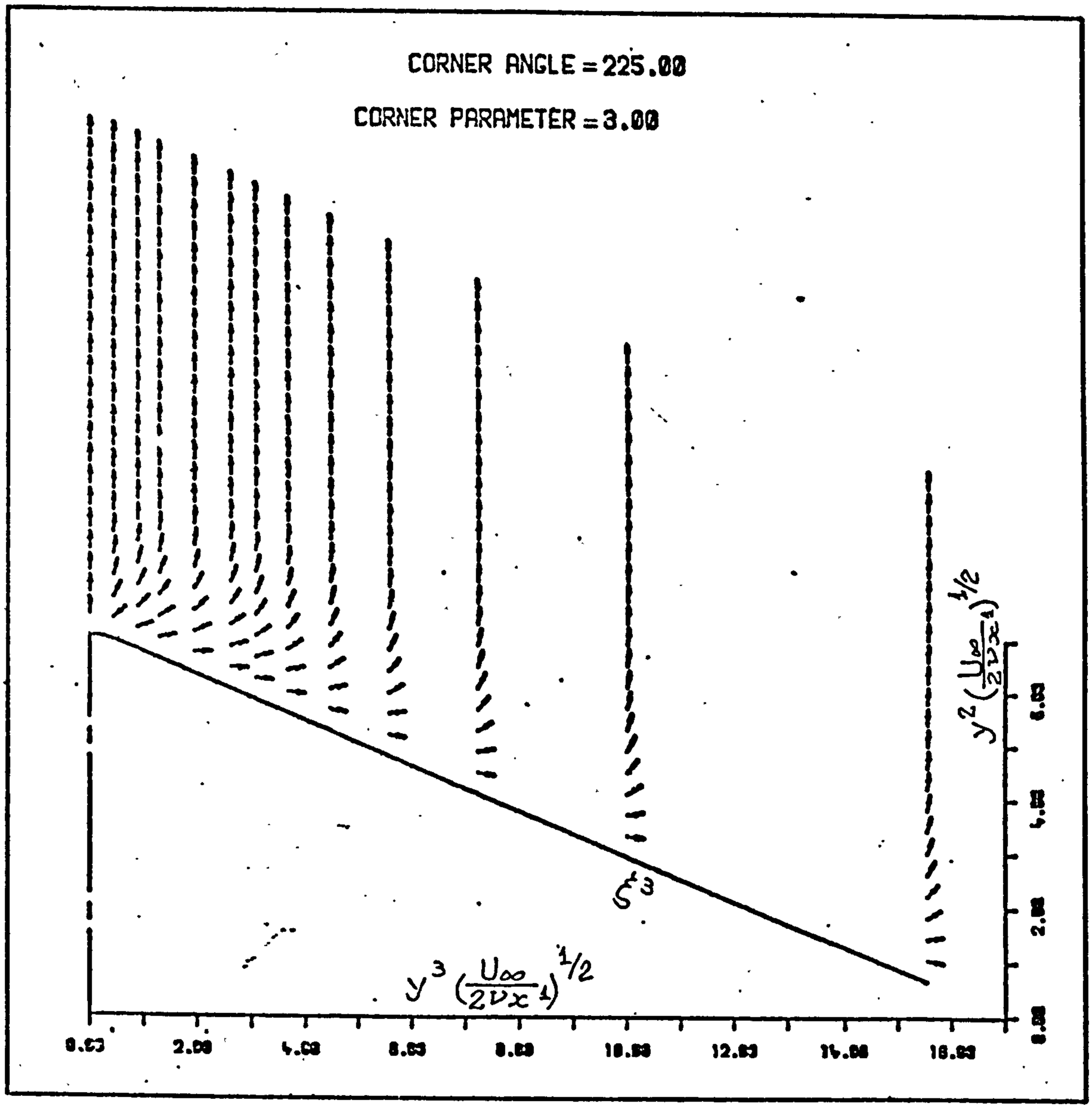

Fig.(4.50) Crossflow direction .

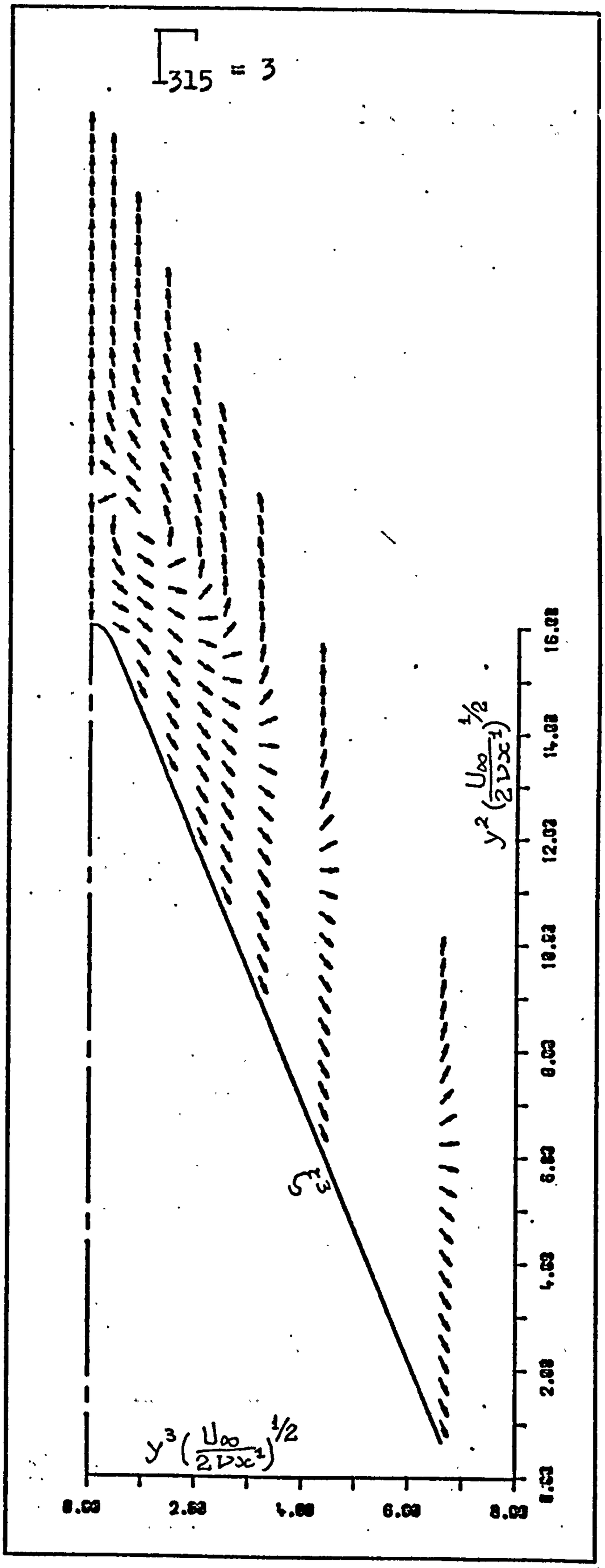

Fig.(4.51)
Crossflow
direction.

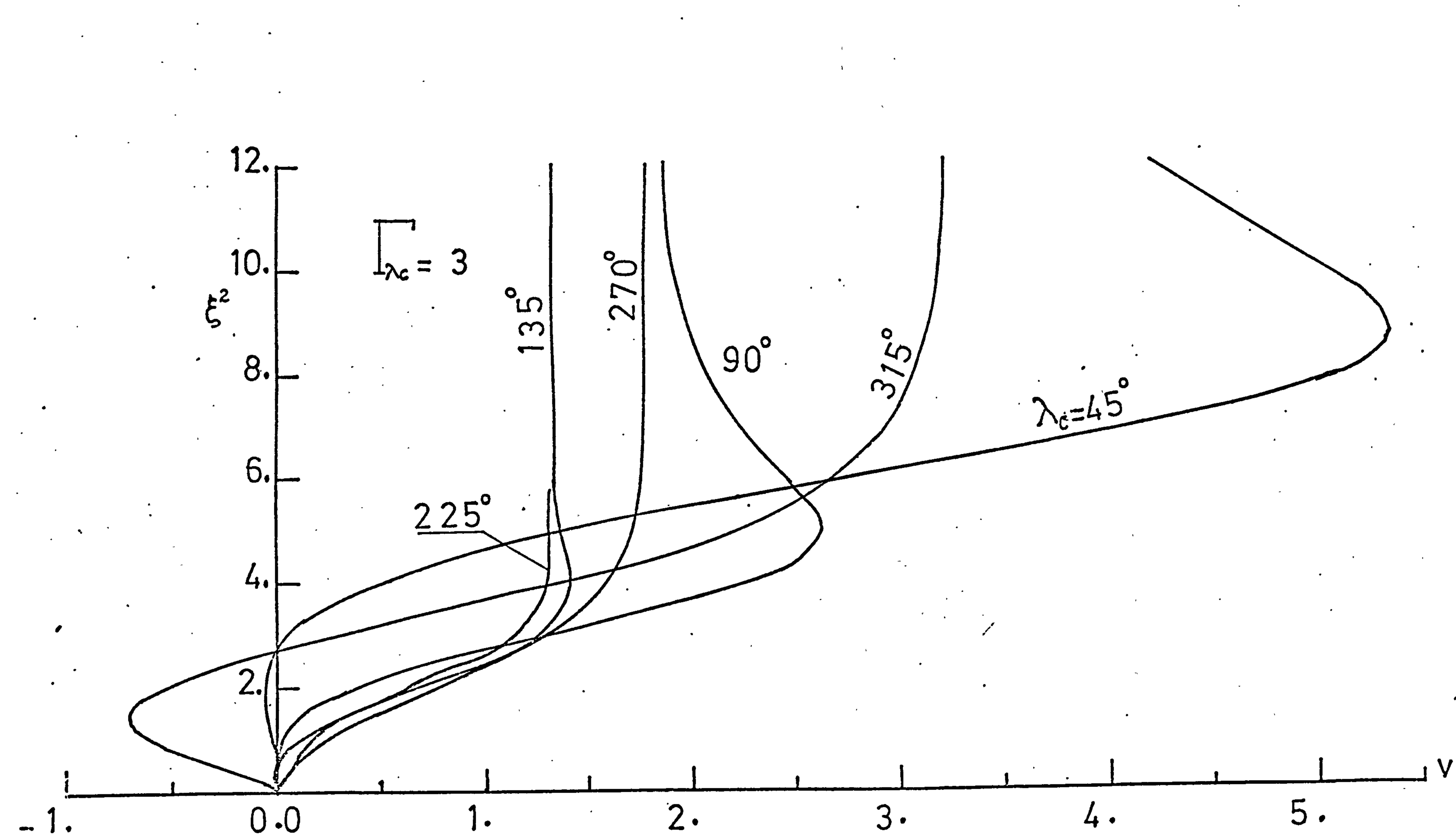

Fig.(4.52) Variation of crossflow velocity v, in symmetry plane, with corner angle.

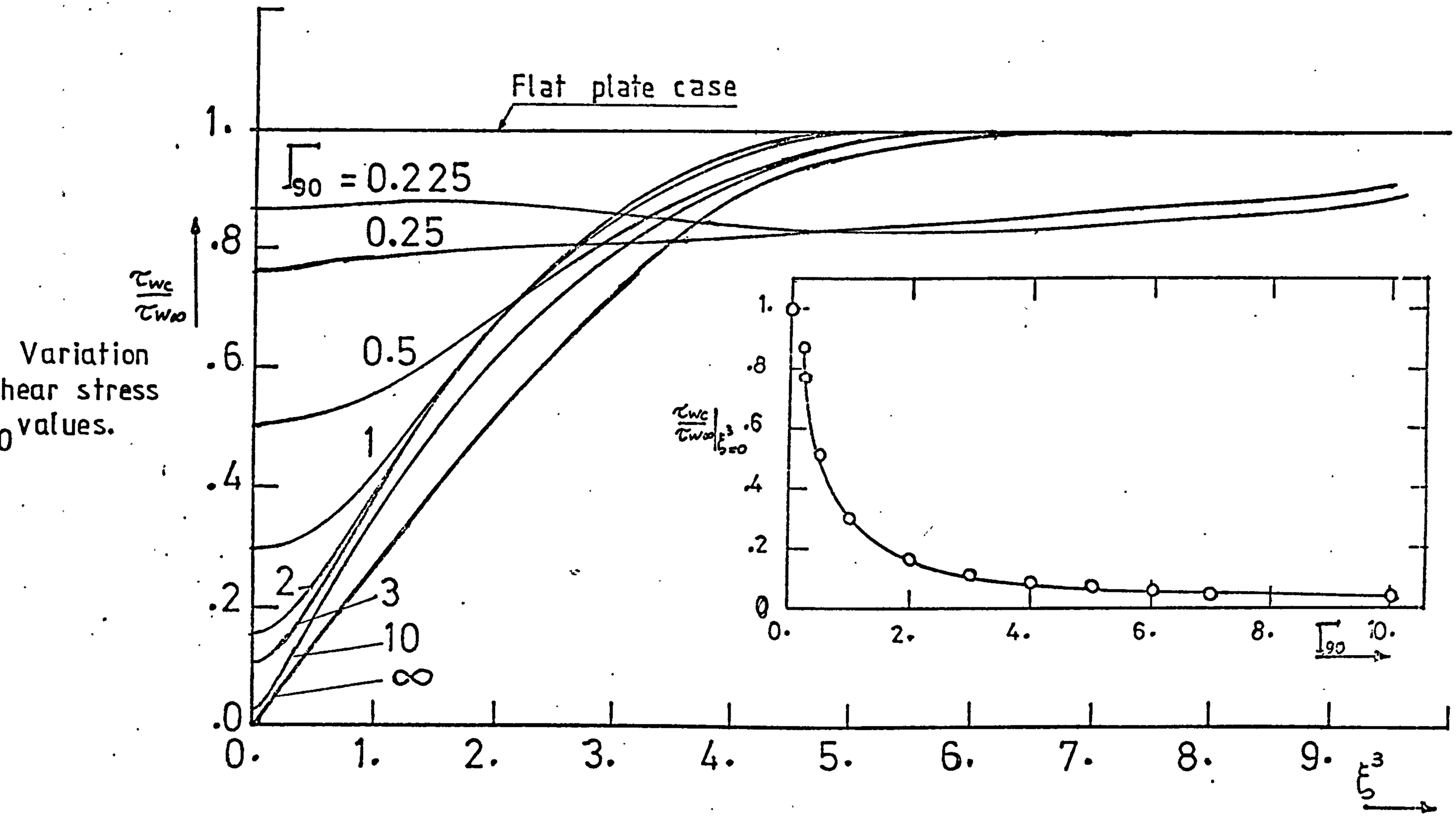

Fig.(4.53a) Variation of wall shear stress with Γ_{90} values.

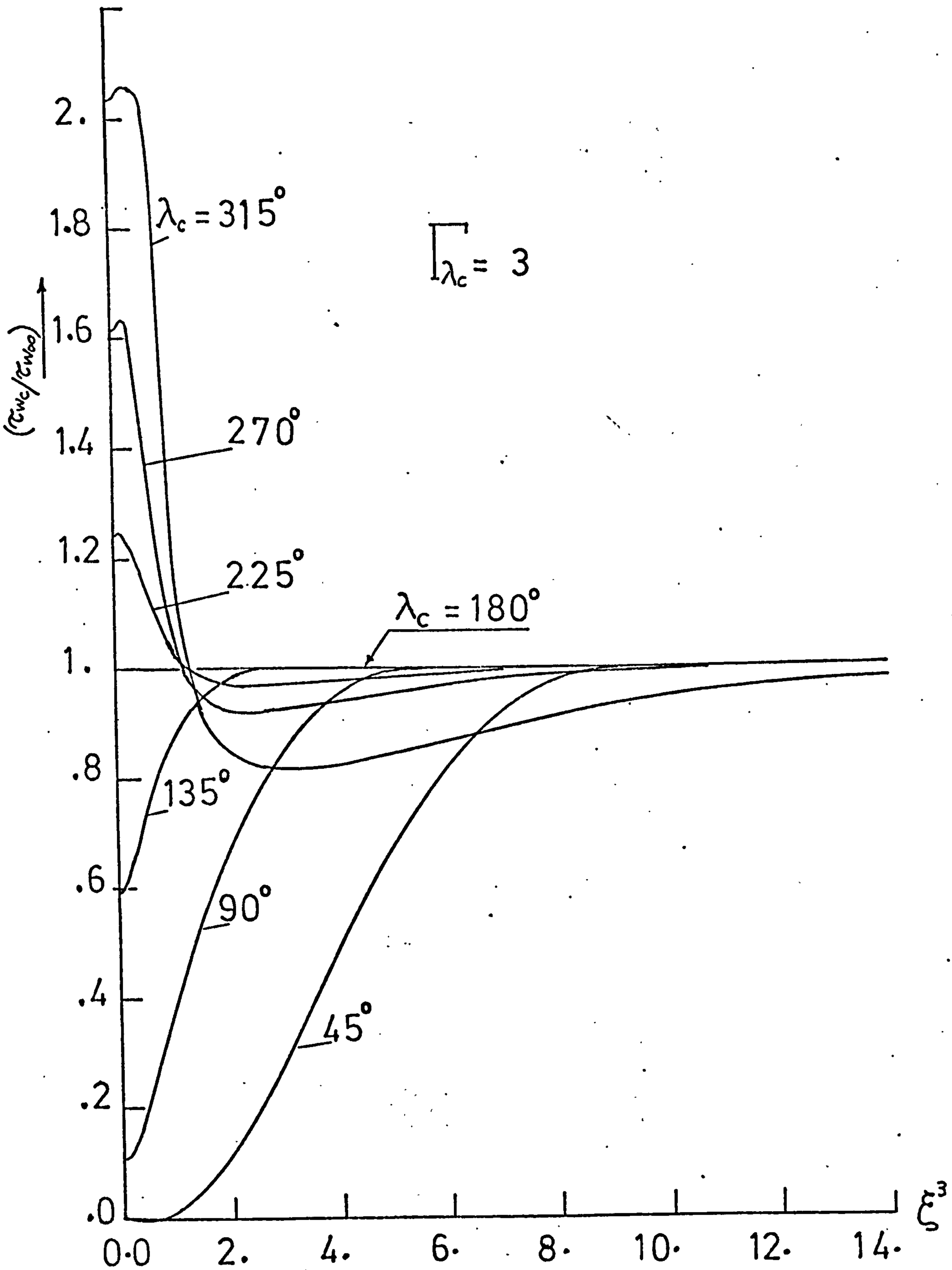

Fig.(4.53b) Variation of wall shear stress with corner angle.

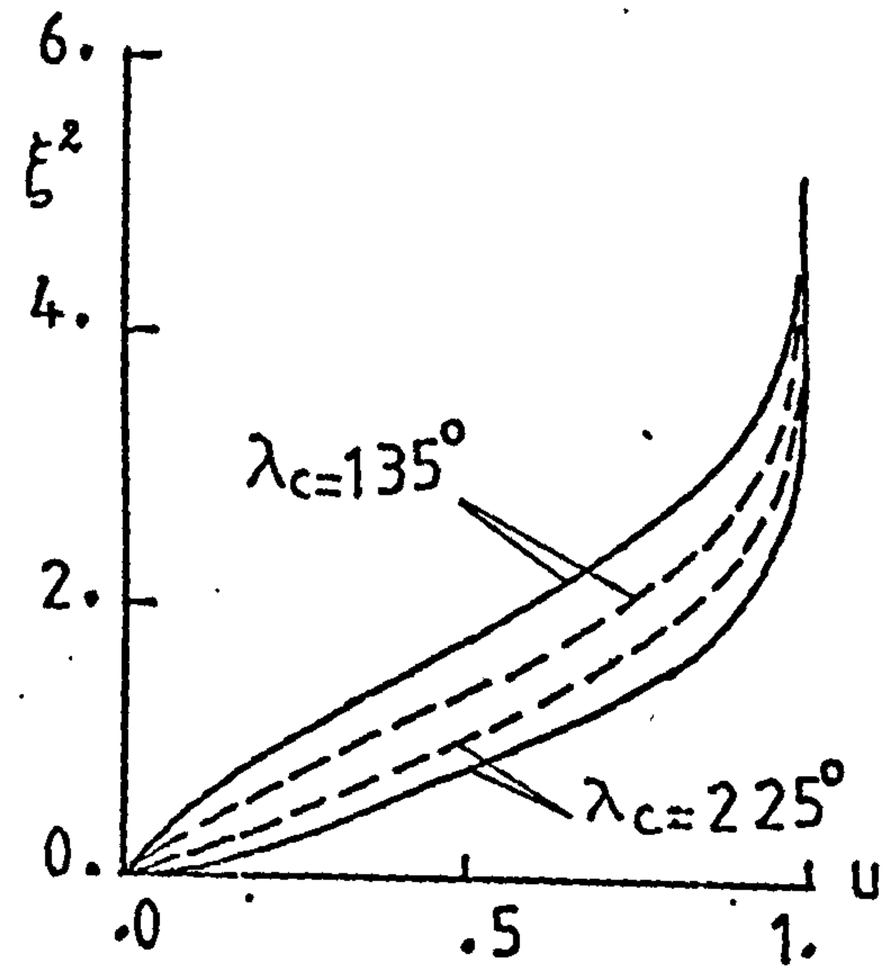

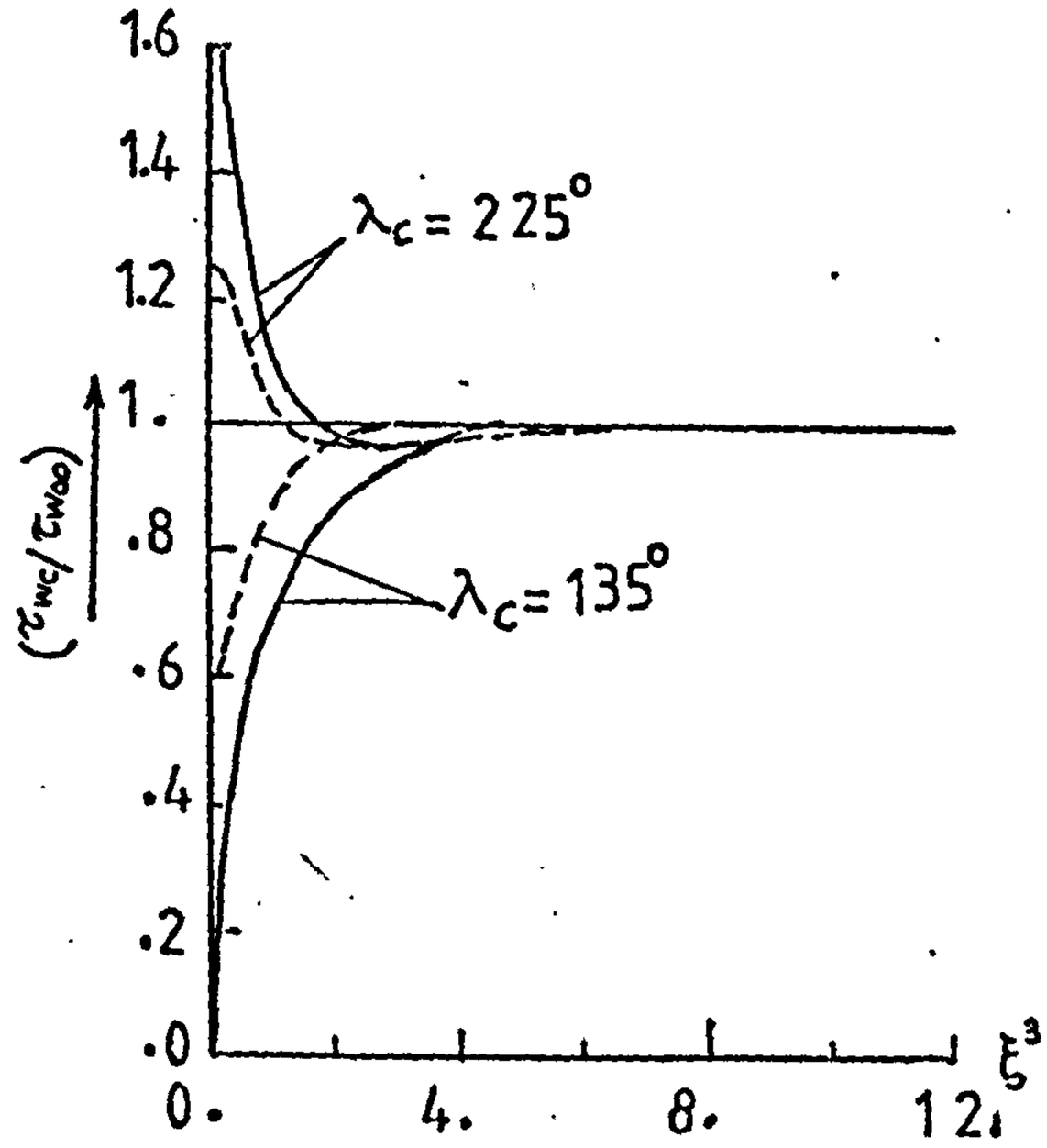

——— $\lambda_c = \infty$

- - - - $\lambda_c = 3$

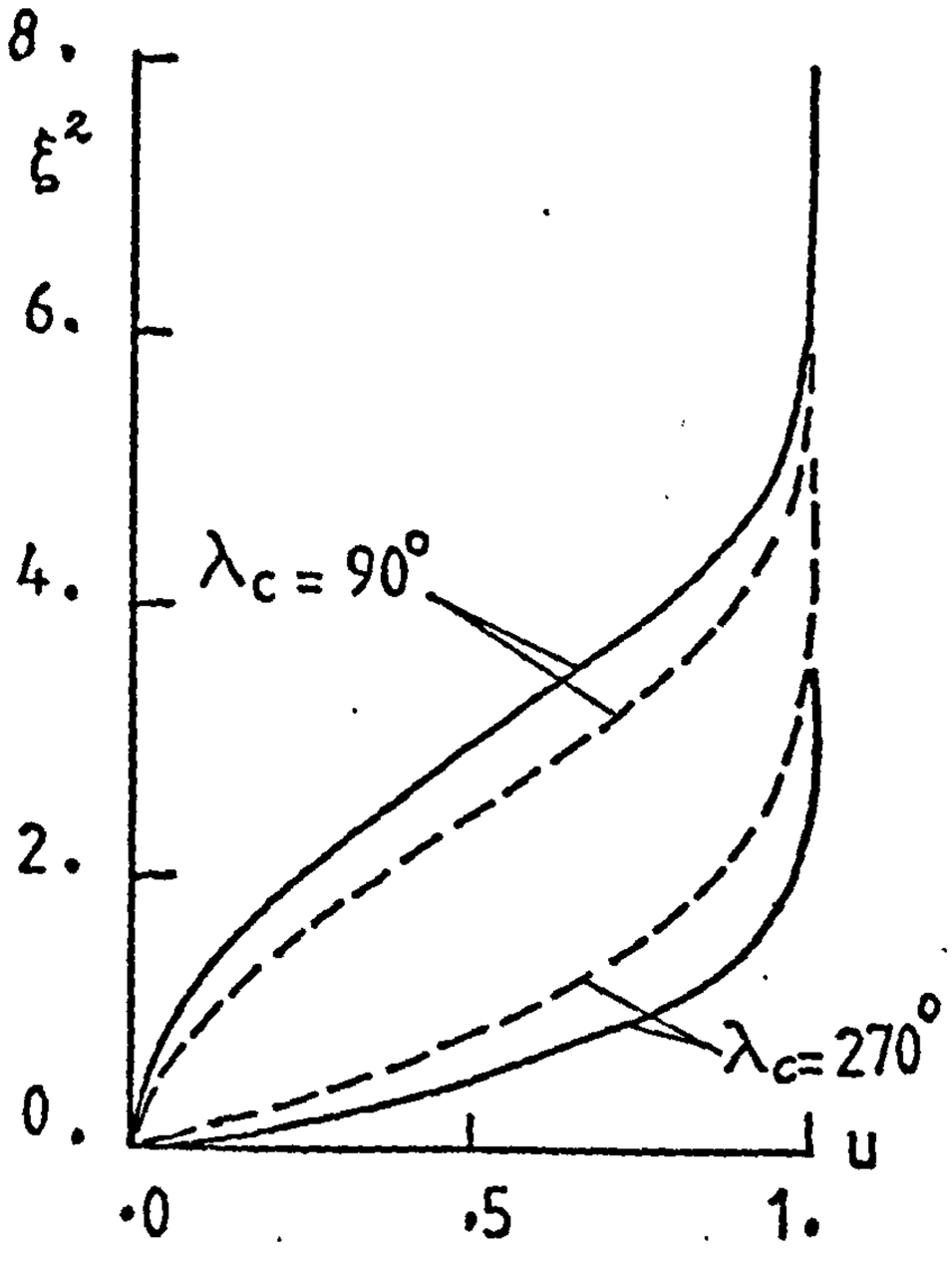

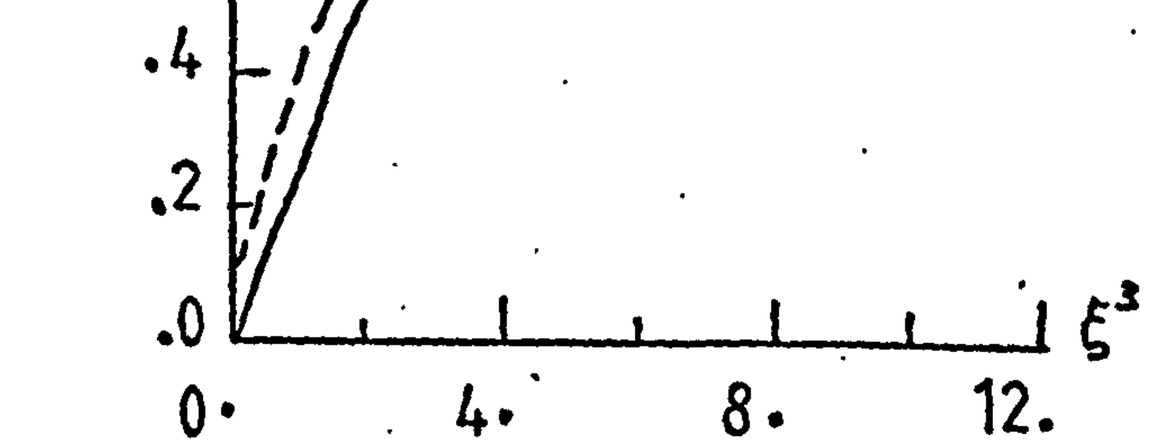

Fig.(4.54)

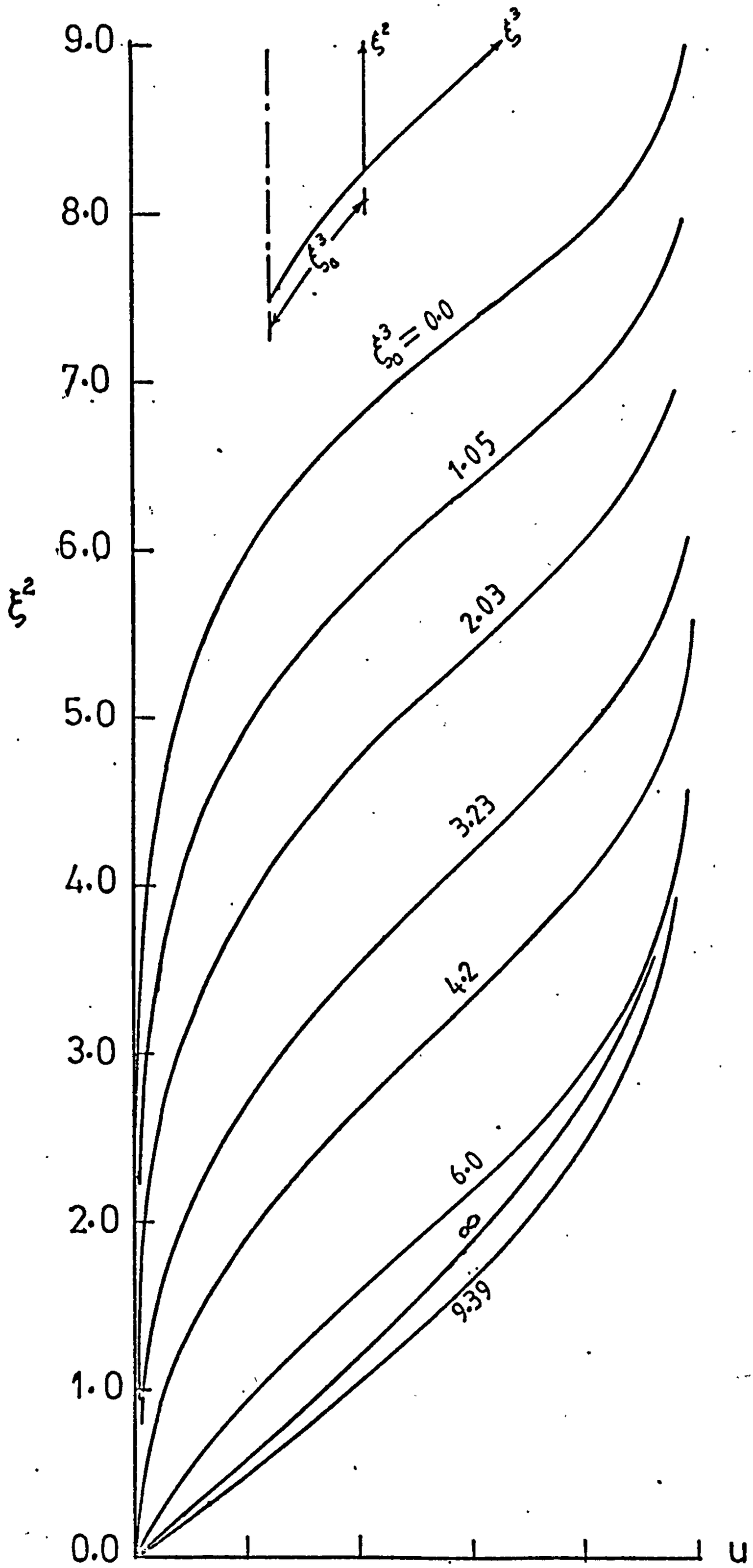

Fig.(4.55) Streamwise velocity u in ξ^3 = const. planes,

$\Gamma_{90,60,3} = 0.5$.

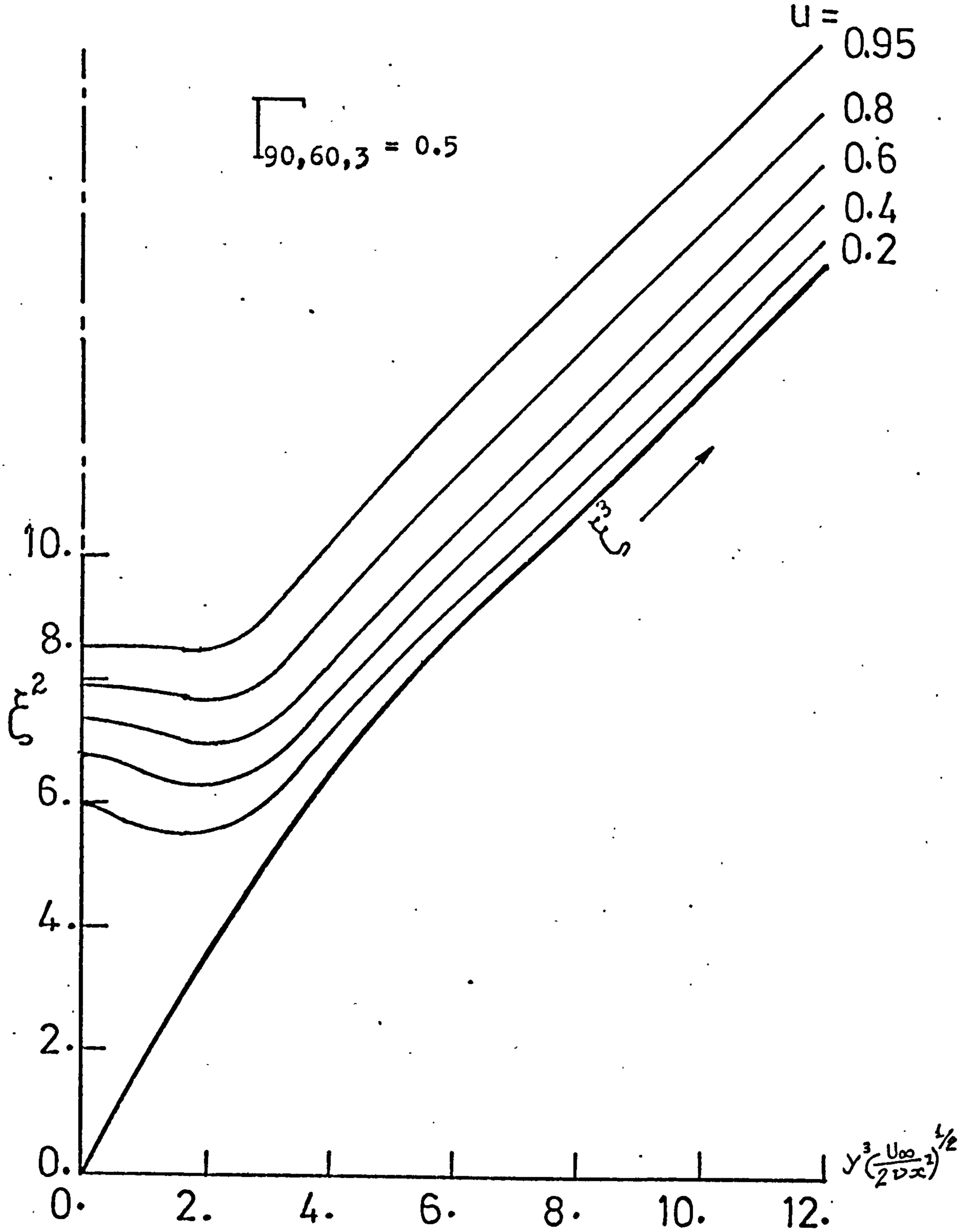

Fig.(4.56) Streamwise isovels.

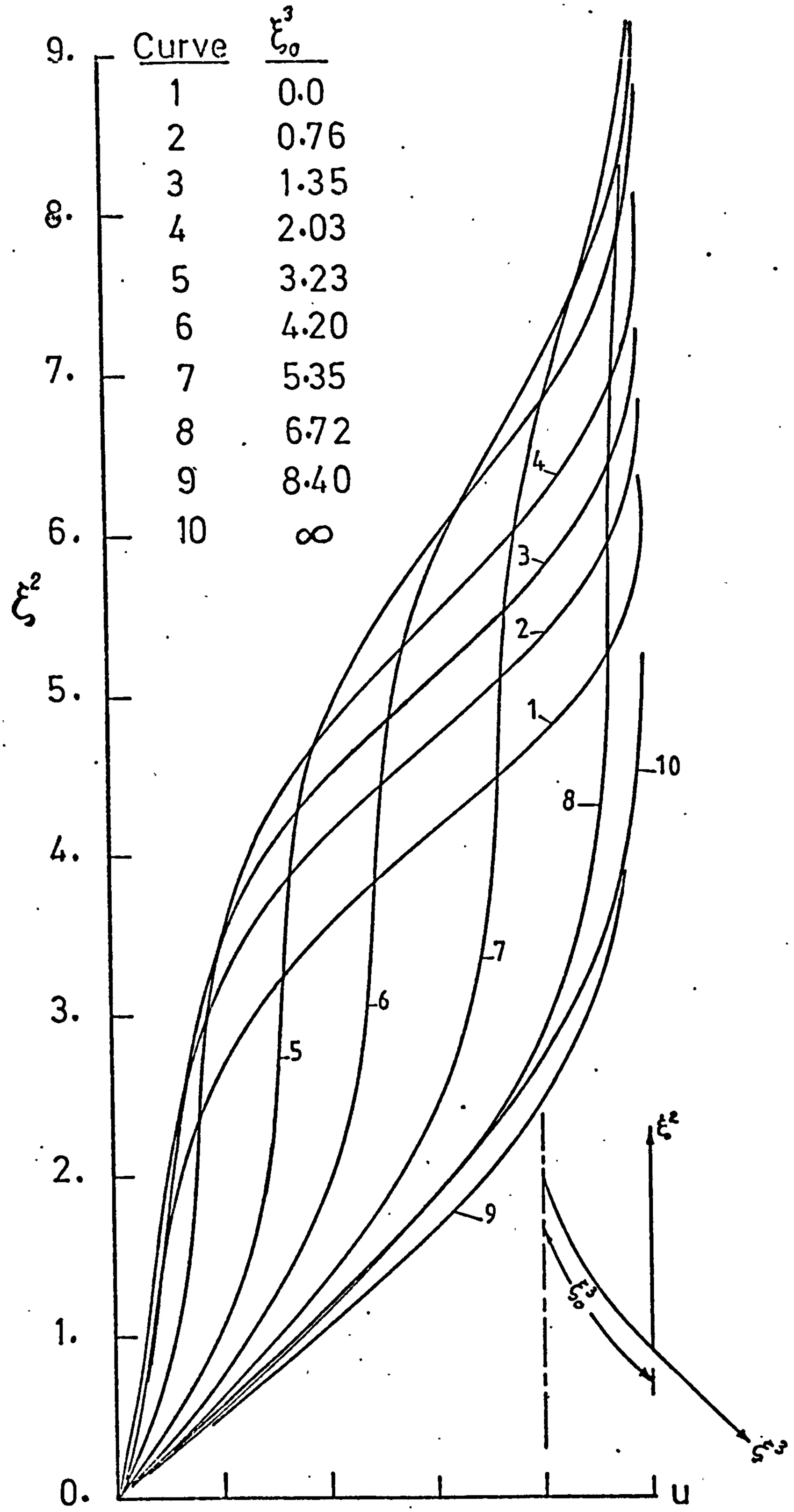

Fig.(4.57) Streamwise velocity u in ξ^3 = const. planes , $\lceil_{270,300,3} = 0.5$.

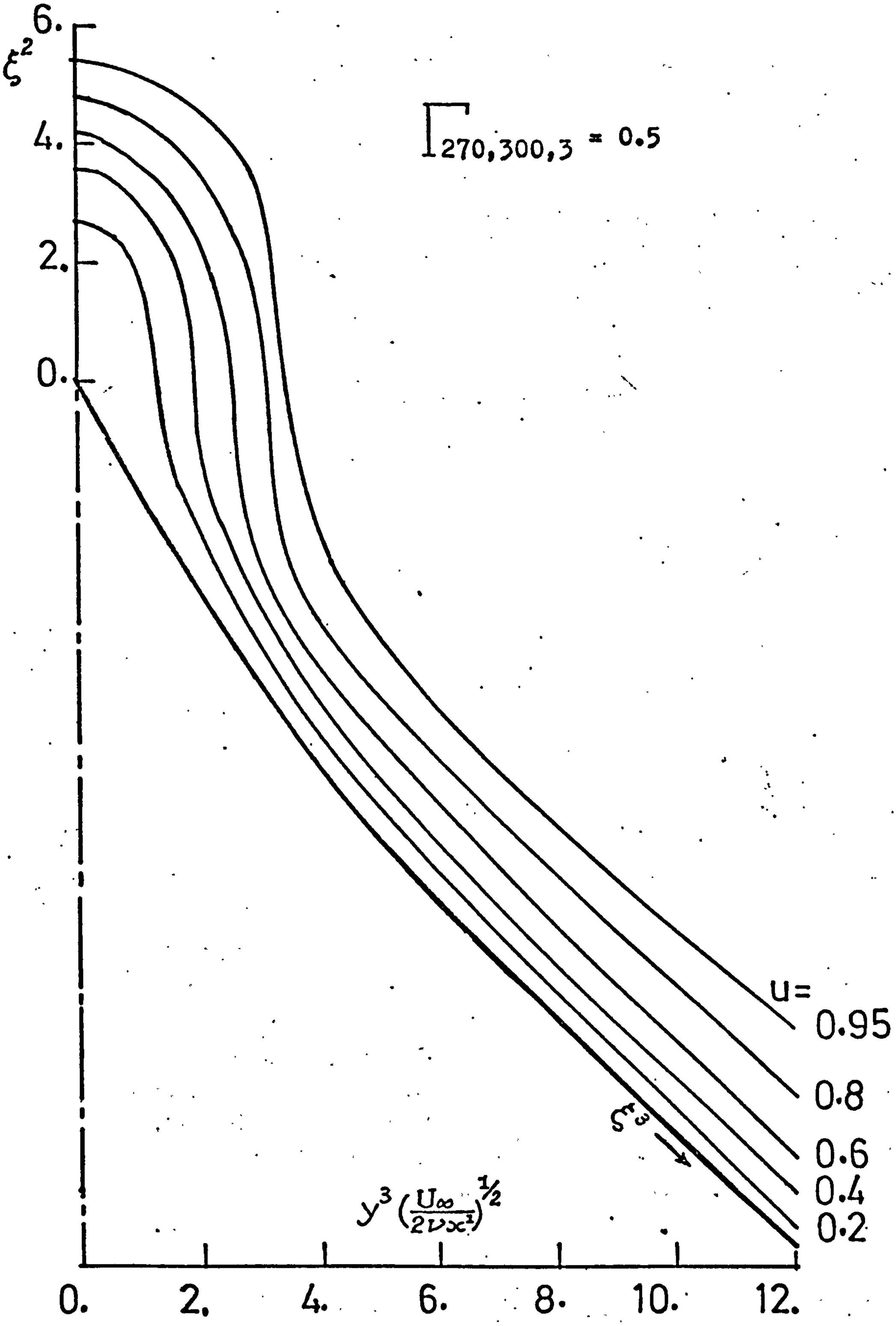

Fig.(4.58) Streamwise isovels.

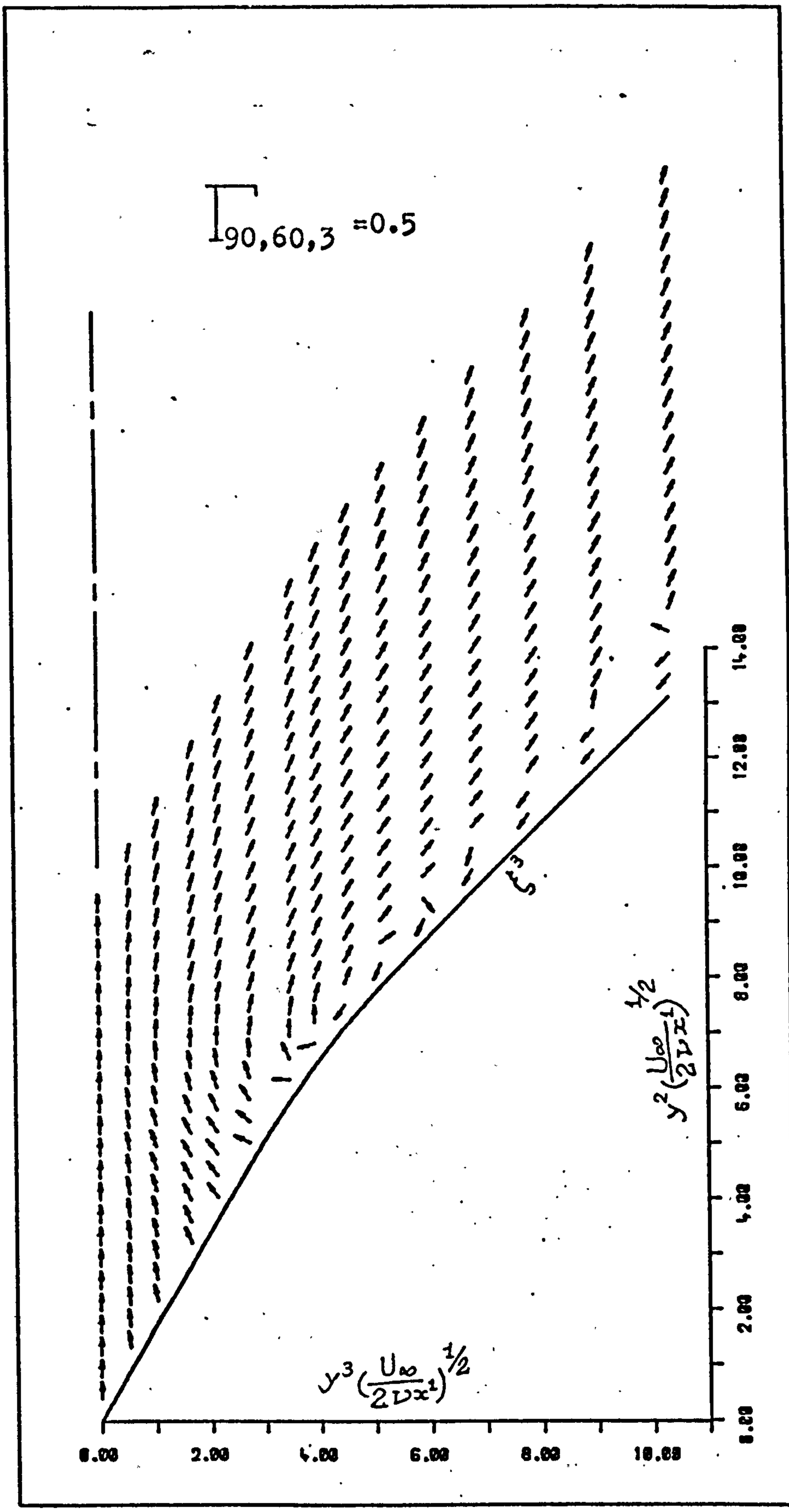

Fig.(4.59) Crossflow direction .

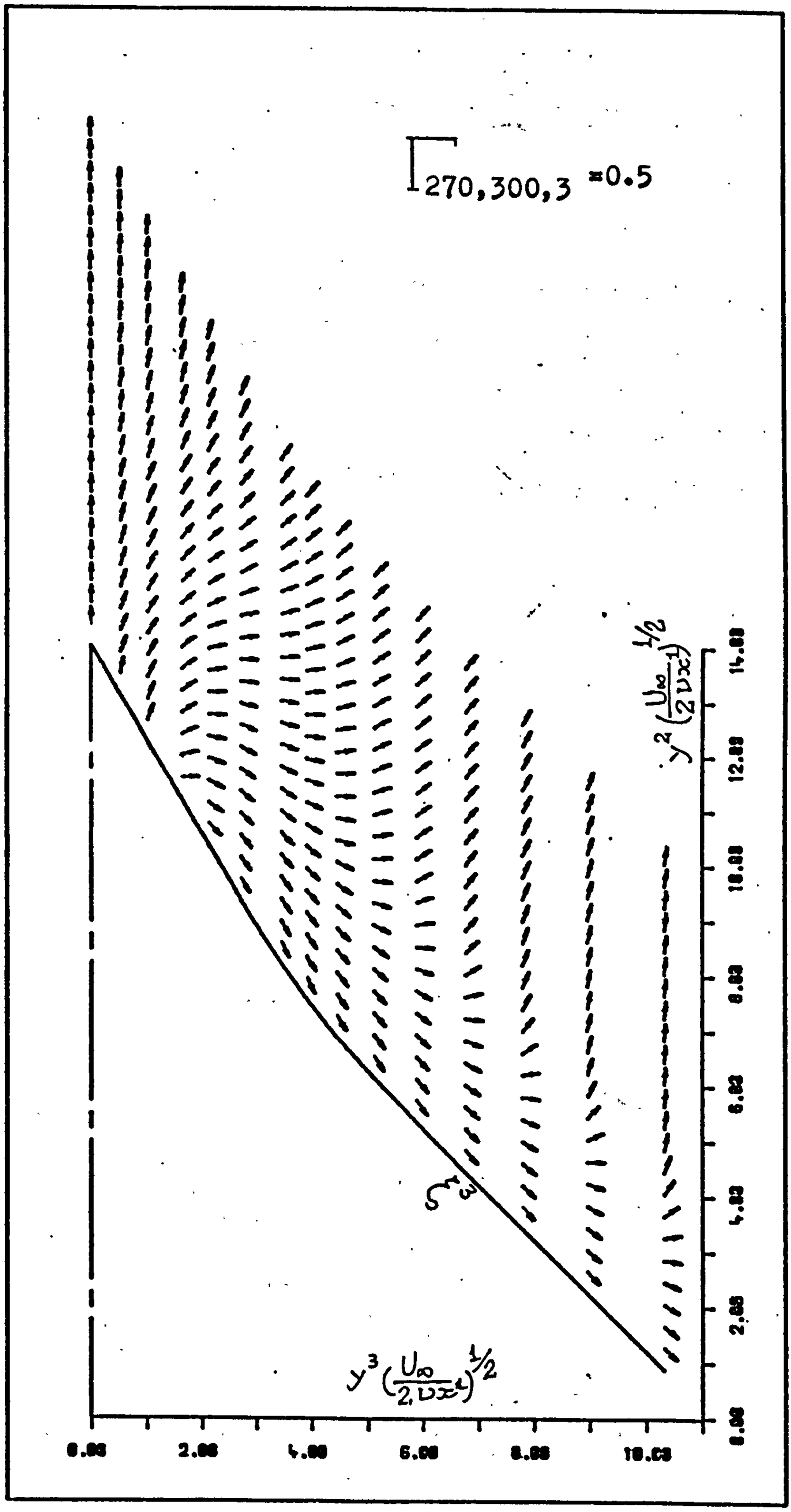

Fig.(4.60) Crossflow direction .

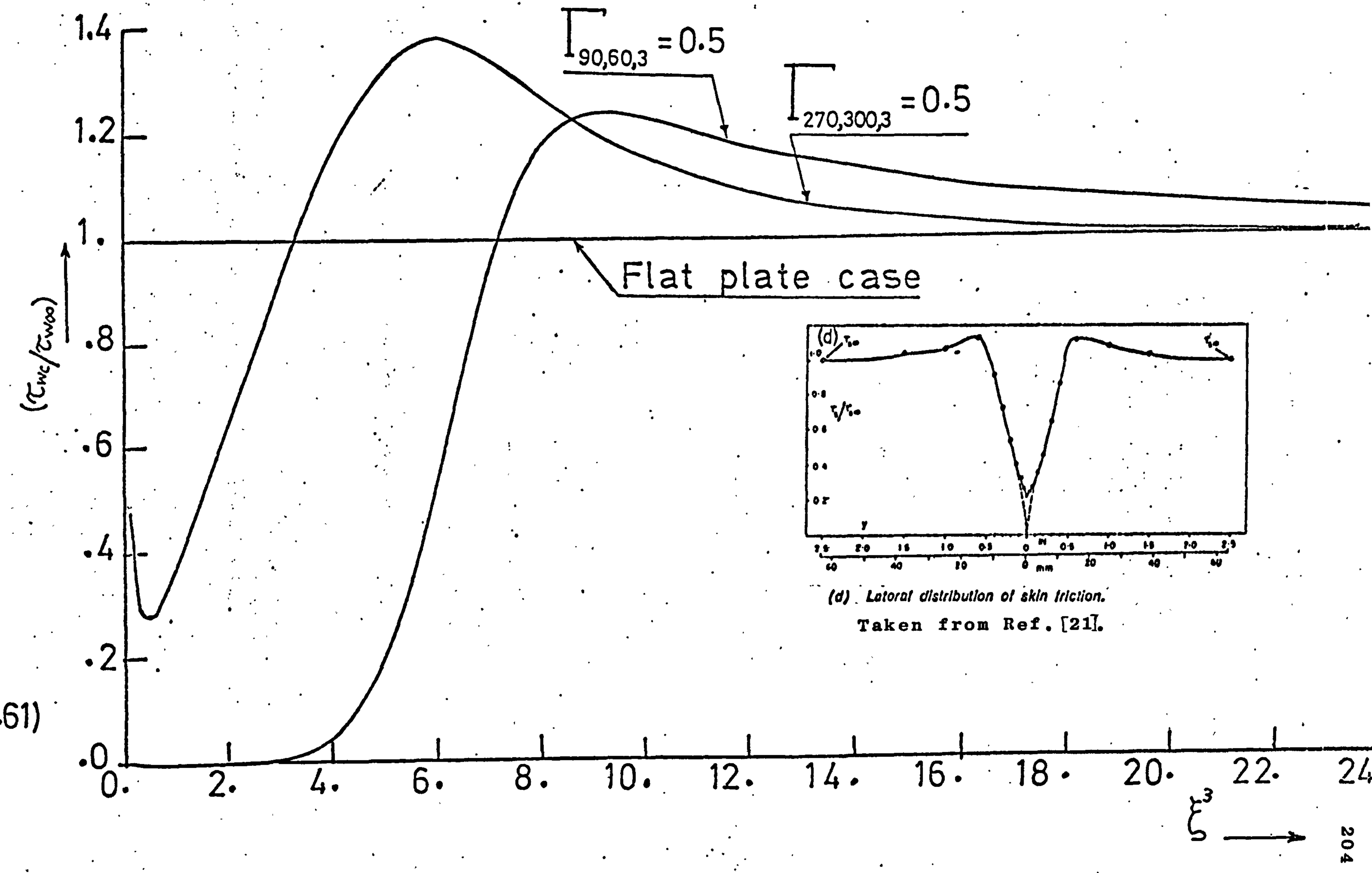

(d) Lateral distribution of skin friction.

Taken from Ref. [21].

Fig.(4.61)

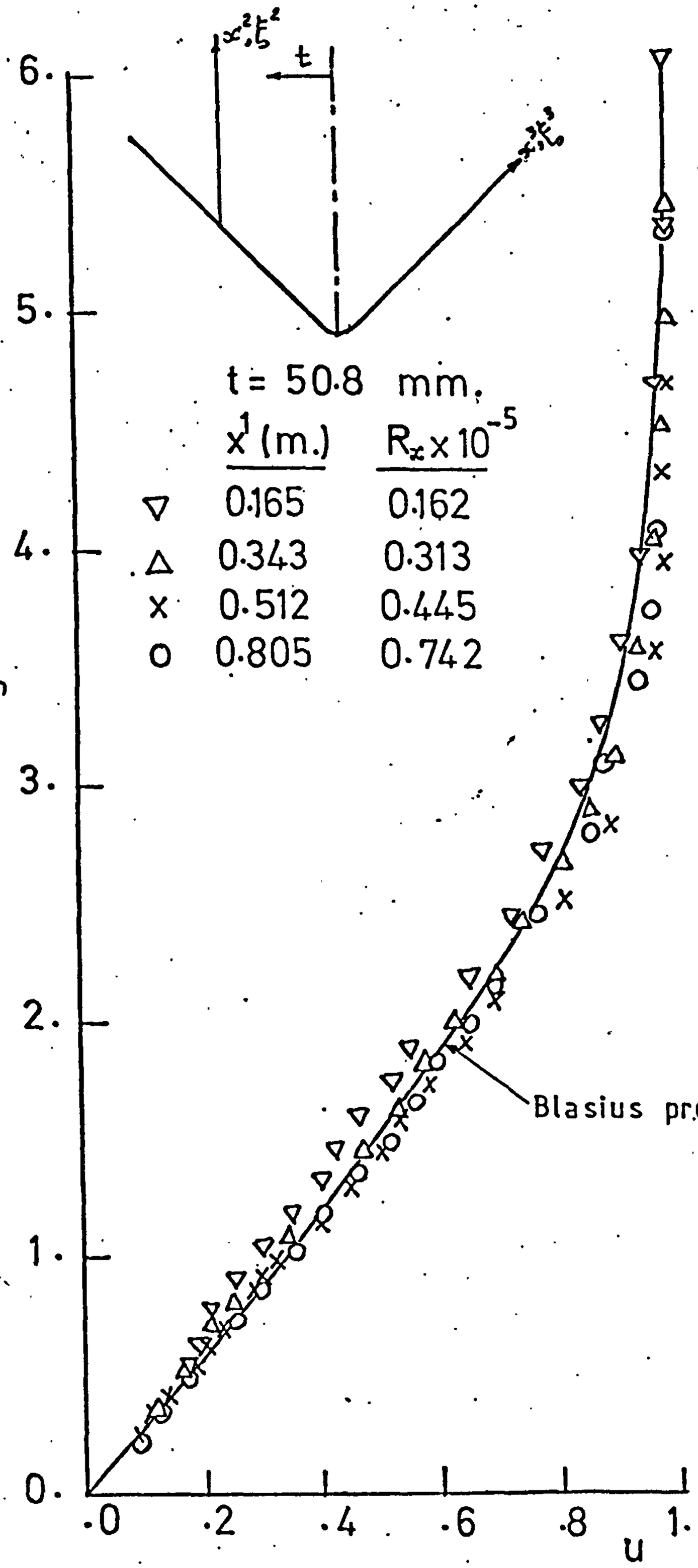
x^2,ξ^2
t
x^3,ξ^3
t = 50.8 mm.
x^1 (m.) $R_x \times 10^{-5}$
▽ 0.165 0.162
△ 0.343 0.313
x 0.512 0.445
o 0.805 0.742
ξ_2
Blasius profile
6.
5.
4.
3.
2.
1.
0.
.0
.2
.4
.6
.8
1.
u

Fig.(4.62)

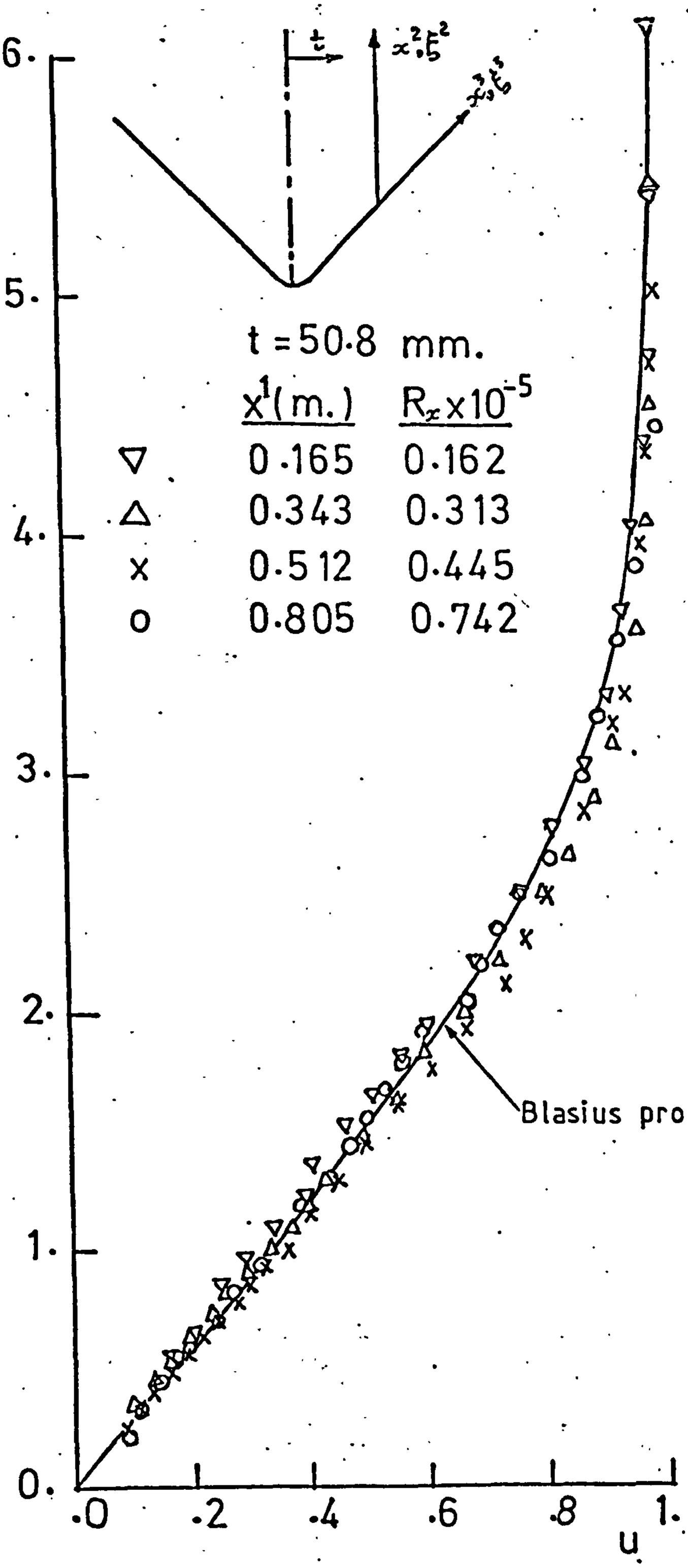
$\frac{1}{t}$
$x^2.5^2$
$x^3.5^3$
t = 50.8 mm.
x¹(m.) $R_x \times 10^{-5}$
▽ 0.165 0.162
△ 0.343 0.313
x 0.512 0.445
o 0.805 0.742
ξ5
6.
5.
4.
3.
2.
1.
0.
.0
.2
.4
.6
.8
1.
u
Blasius profile

Fig.(4.63)

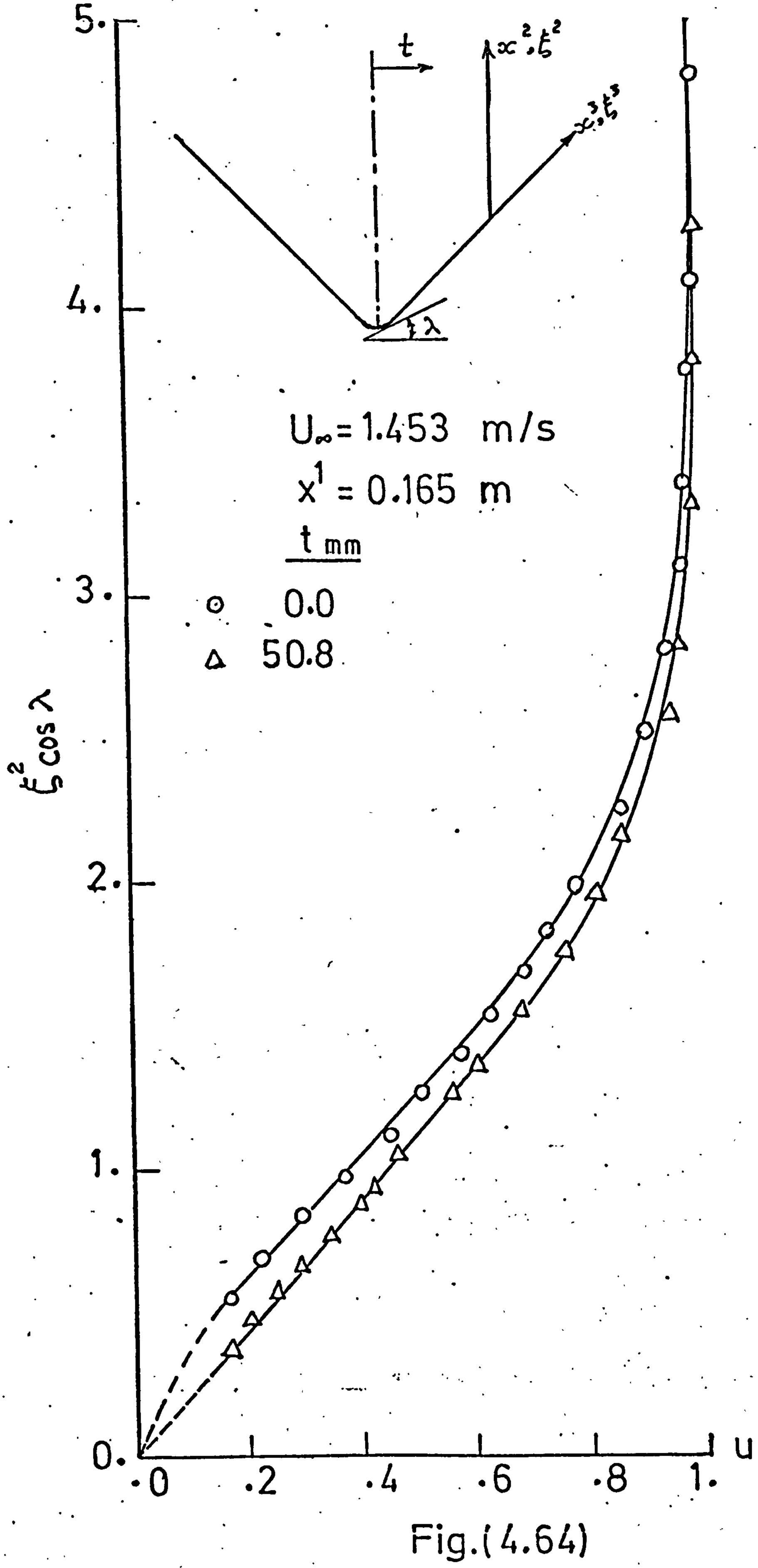
5.
4.
3.
2.
1.
0.
t
x^2, ξ^2
x^3, ξ^3
$\frac{1}{2}\lambda$
$U_\infty = 1.453$ m/s
$x^1 = 0.165$ m
t_{mm}
0.0
50.8
$\xi^2 \cos\lambda$
.0
.2
.4
.6
.8
1.
u

Fig.(4.64)

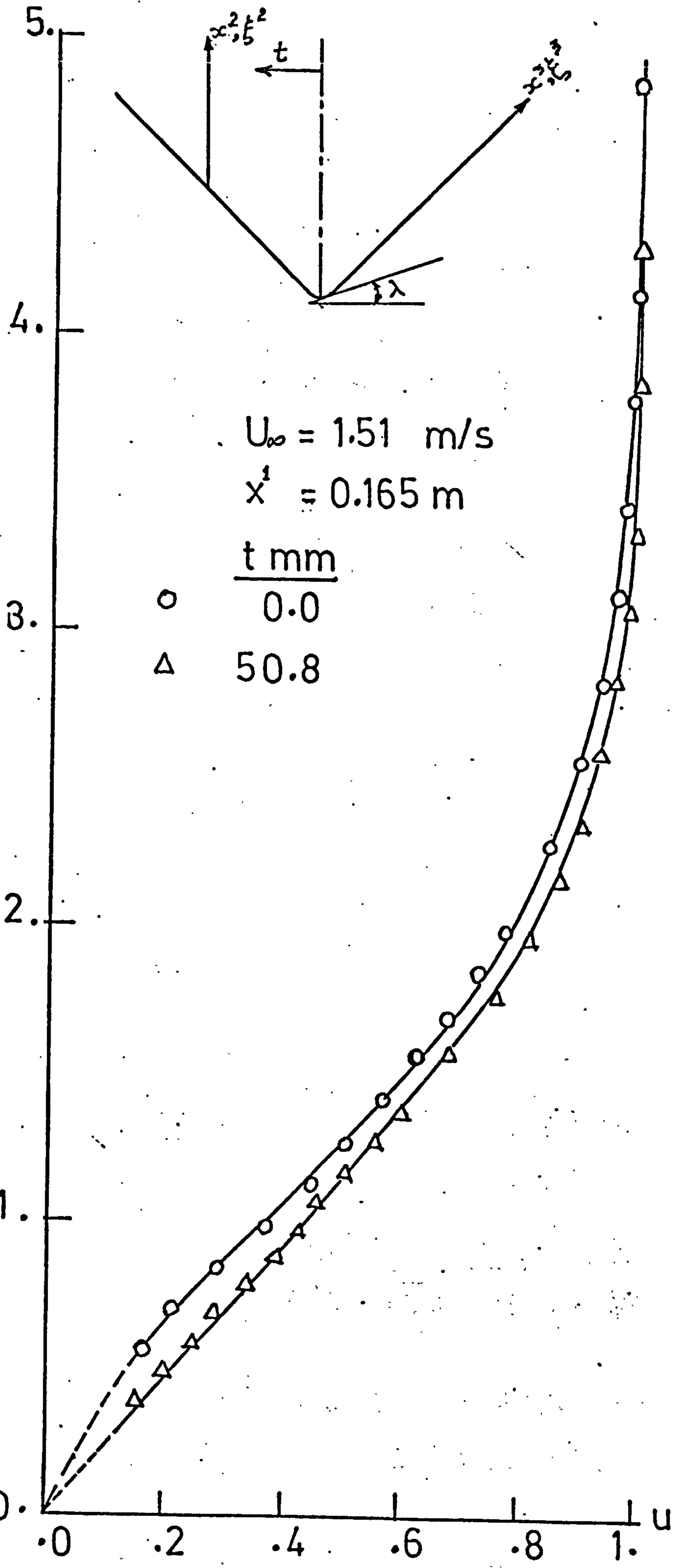
x^2, ξ^2
t
x^3, ξ^3
λ
U_∞ = 1.51 m/s
x^1 = 0.165 m
t mm
○ 0.0
△ 50.8
$\xi^2 \cos\lambda$
5.
4.
3.
2.
1.
0.
·0
·2
·4
·6
·8
1.
u

Fig.(4.65)

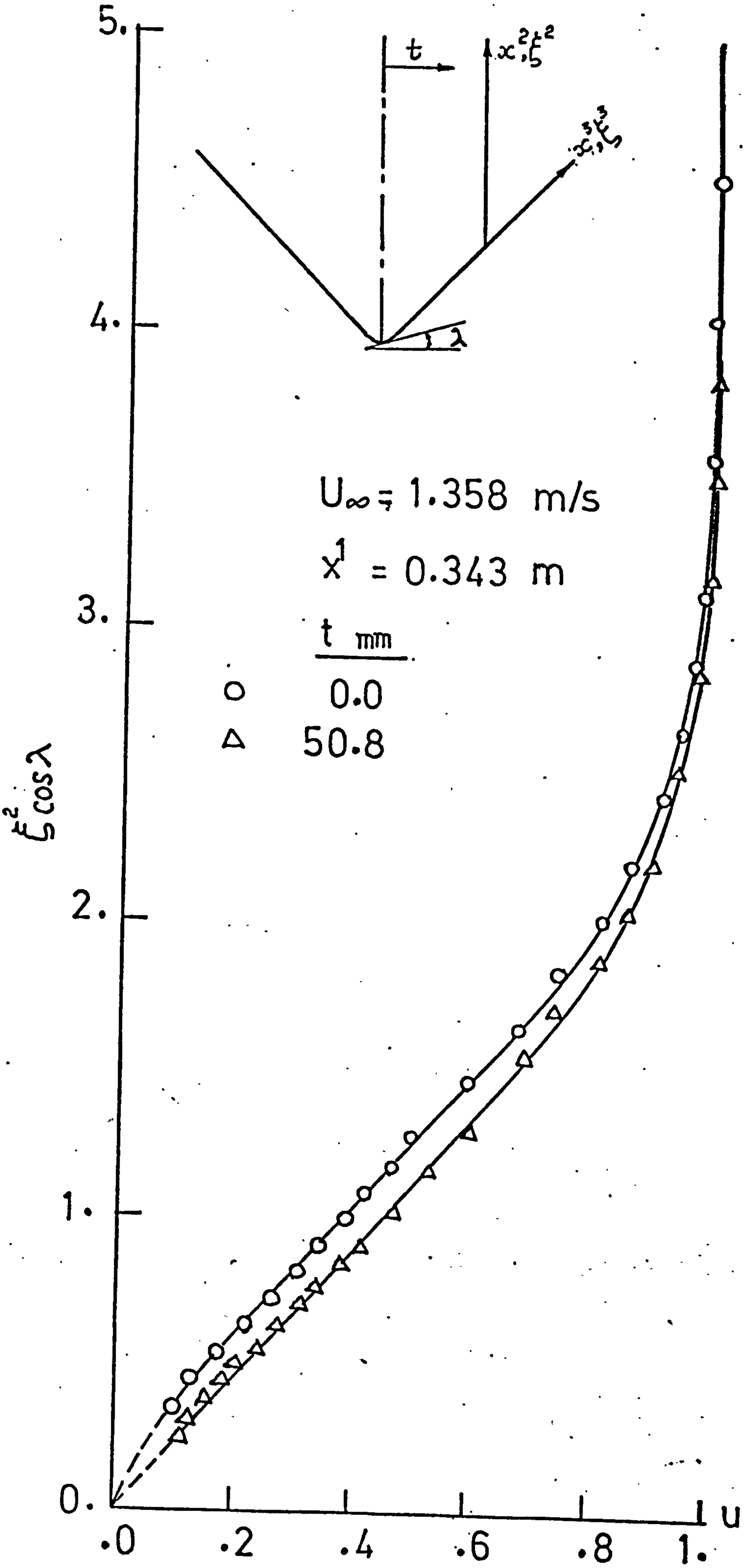
5.
4.
3.
2.
1.
0.
$\xi^2\cos\lambda$
t
x^2,ξ^2
x^3,ξ^3
λ
$U_\infty = 1.358$ m/s
$x^1 = 0.343$ m
t mm
○ 0.0
△ 50.8
.0
.2
.4
.6
.8
1.
u

Fig.(4.66)

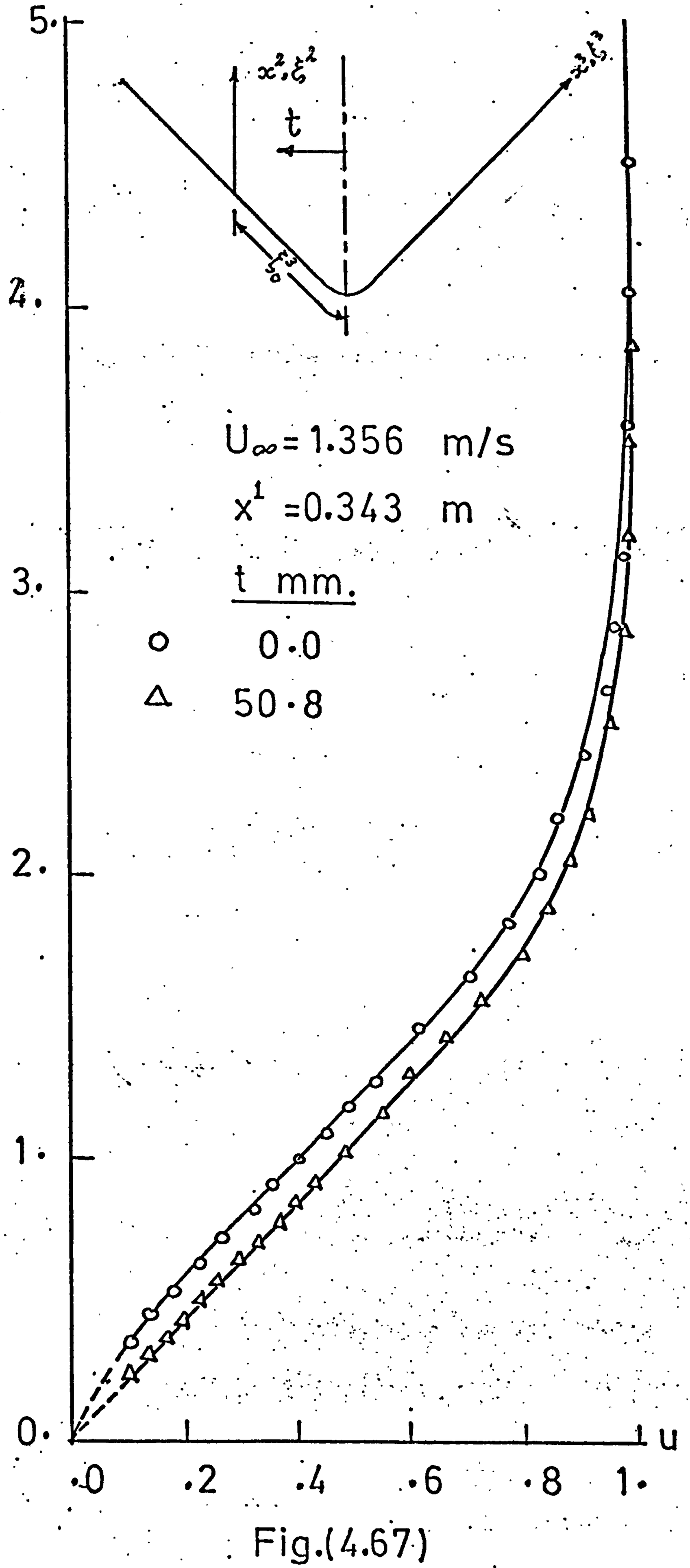
x^2, ξ^2
x^3, ξ^3
t
ξ_0^3
$U_\infty = 1.356$ m/s
$x^1 = 0.343$ m
t mm.
o 0.0
Δ 50.8
$\xi^2 \cos\lambda$
5.
4.
3.
2.
1.
0.
.0
.2
.4
.6
.8
1.
u

Fig.(4.67)

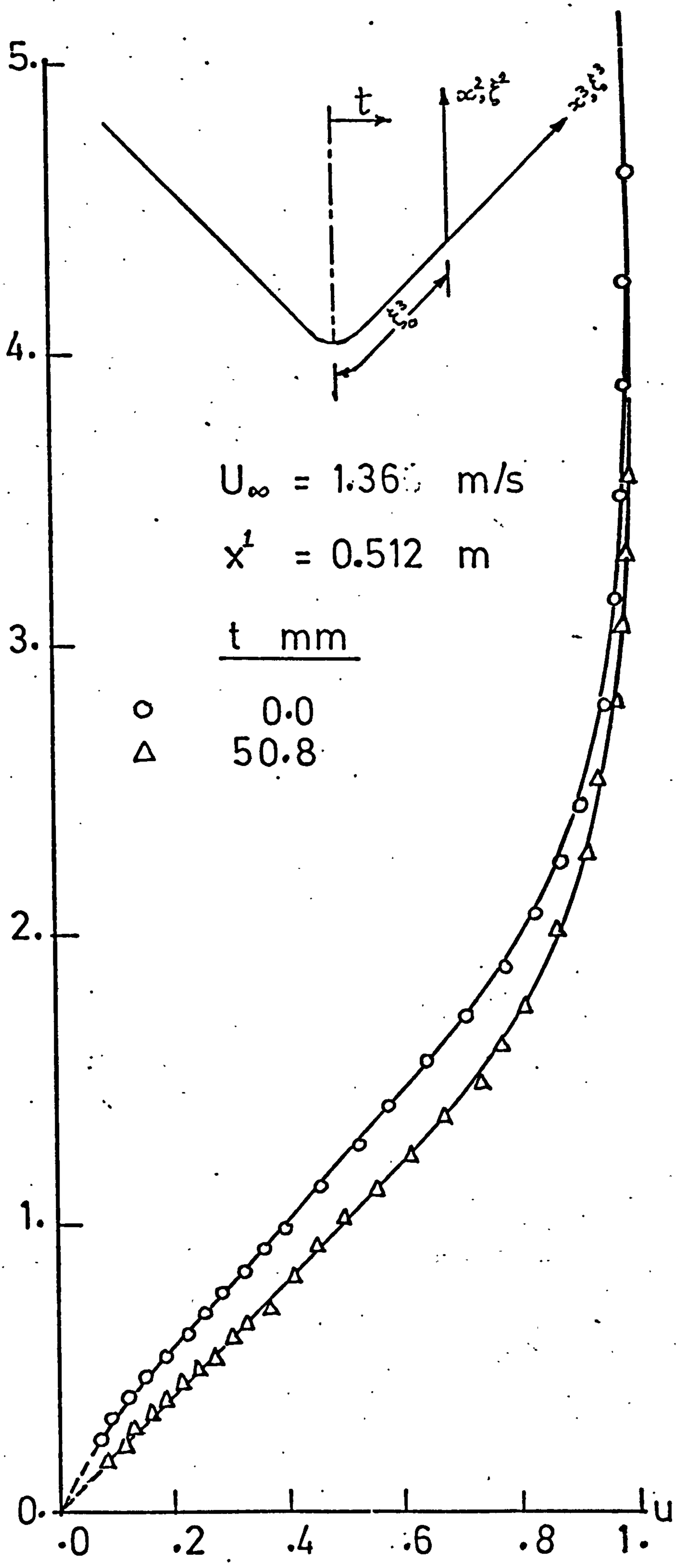
5.
4.
3.
2.
1.
0.
$\xi^2 \cos\lambda$
t
x^2, ξ^2
x^3, ξ^3
ξ^3_{50}
U_∞ = 1.36 m/s
x^1 = 0.512 m
t mm
o 0.0
Δ 50.8
.0
.2
.4
.6
.8
1.
u

Fig.(4.68)

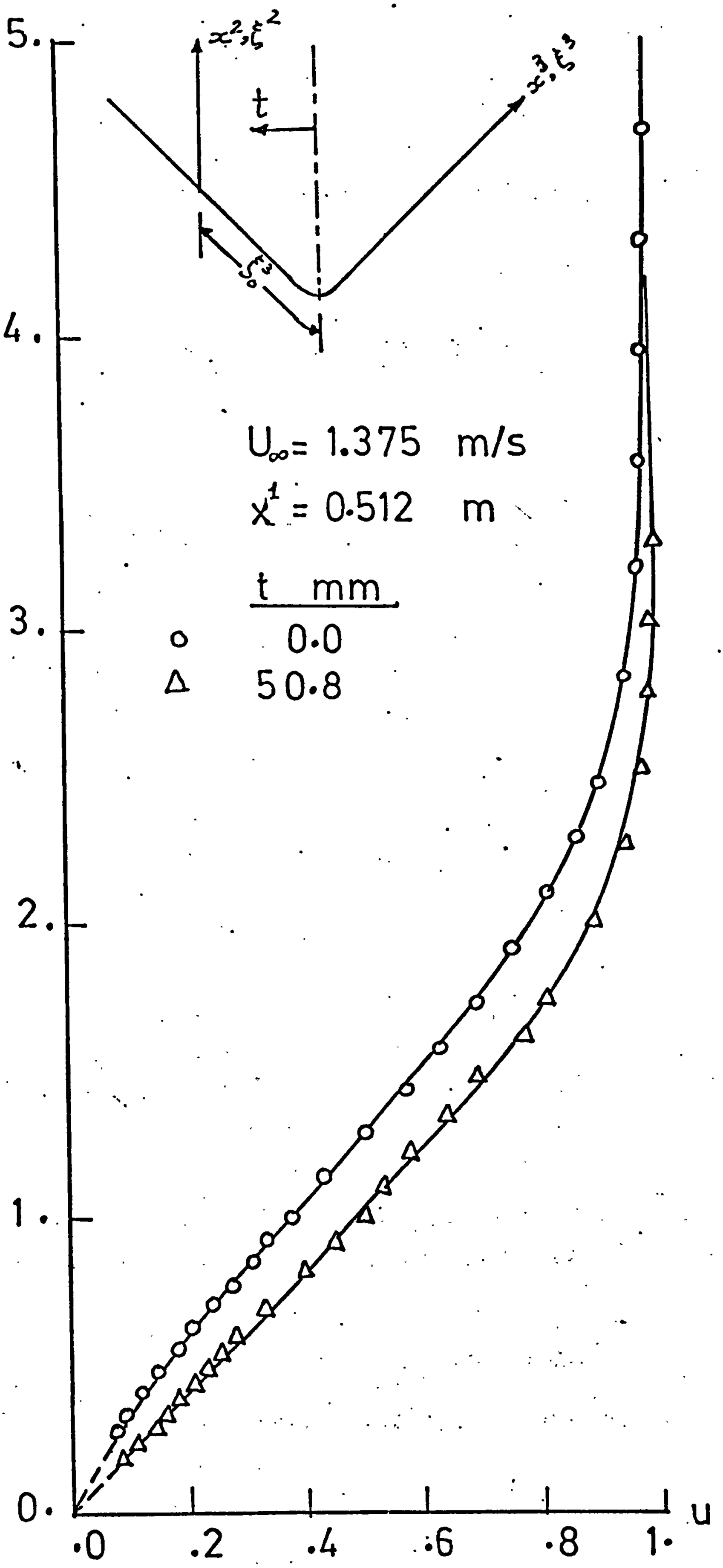
x^2, ξ^2
x^3, ξ^3
t
ξ_0^3
U_∞= 1.375 m/s
x^1 = 0.512 m
t mm
o 0.0
Δ 50.8
$\xi^2 \cos\lambda$
5.
4.
3.
2.
1.
0.
.0
.2
.4
.6
.8
1.
u

Fig.(4.69)

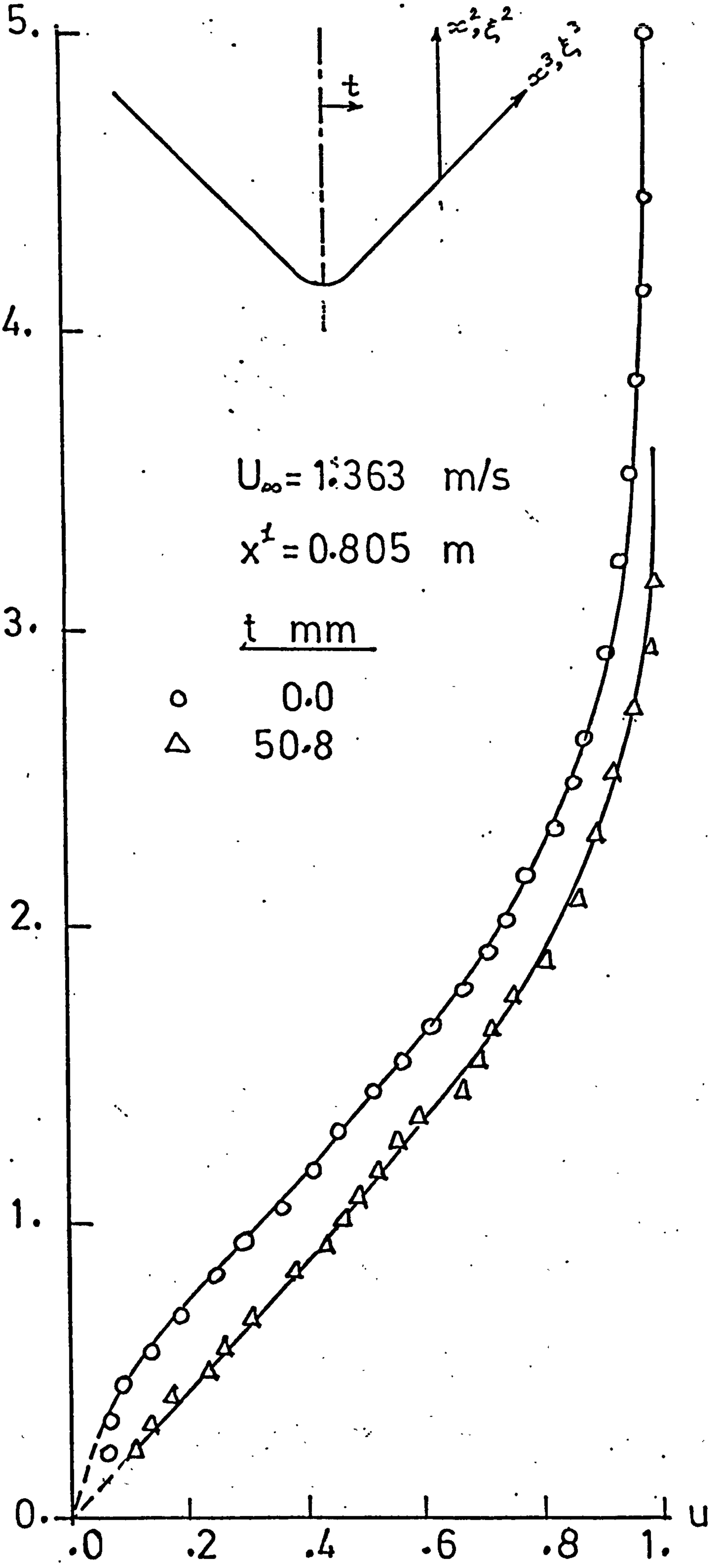
5.
4.
3.
2.
1.
0.
.0
.2
.4
.6
.8
1.
u
$\xi \cos\lambda$
t
x^2, ξ^2
x^3, ξ^3
U_∞= 1.363 m/s
x^1= 0.805 m
t mm
o 0.0
Δ 50.8

Fig.(4.70)

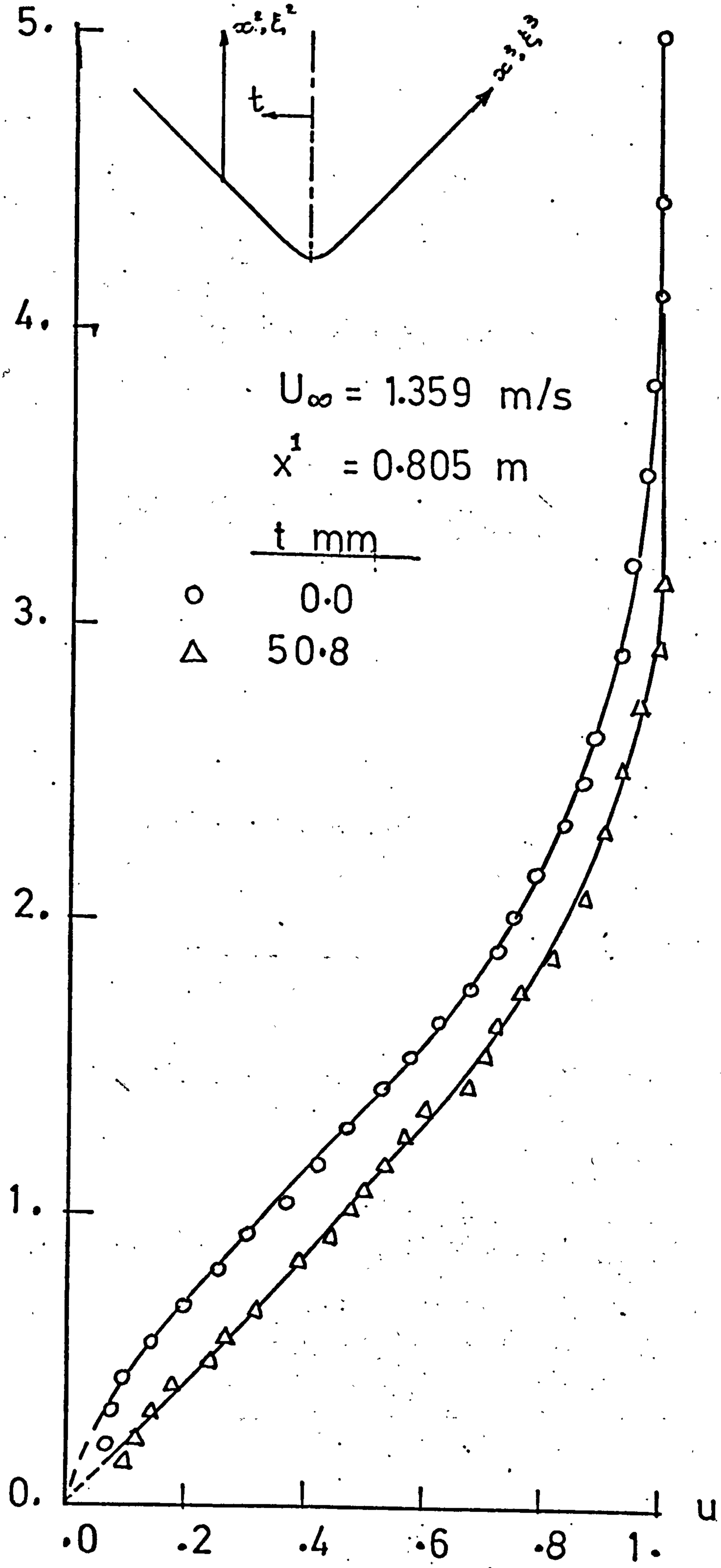
x^2, ξ^2
x^3, ξ^3
t
U_∞ = 1.359 m/s
x^1 = 0.805 m
t mm
○ 0.0
△ 50.8
$\xi^3 \cos\lambda$
u
0.
1.
2.
3.
4.
5.
.0
.2
.4
.6
.8
1.

Fig.(4.71)

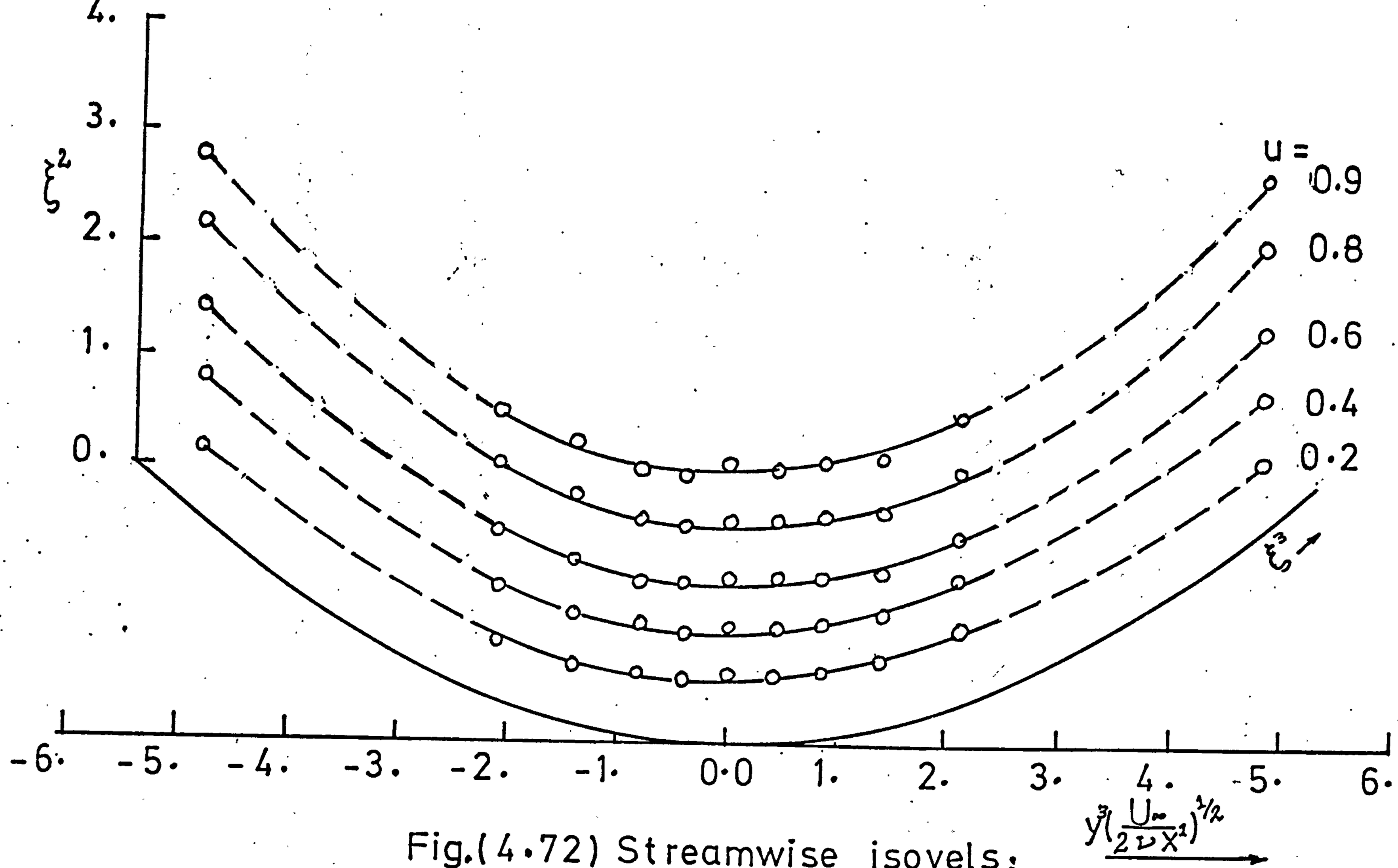

Fig.(4.72) Streamwise isovels;
x^1 = 0.165 m, Γ_{90} = 0.23.

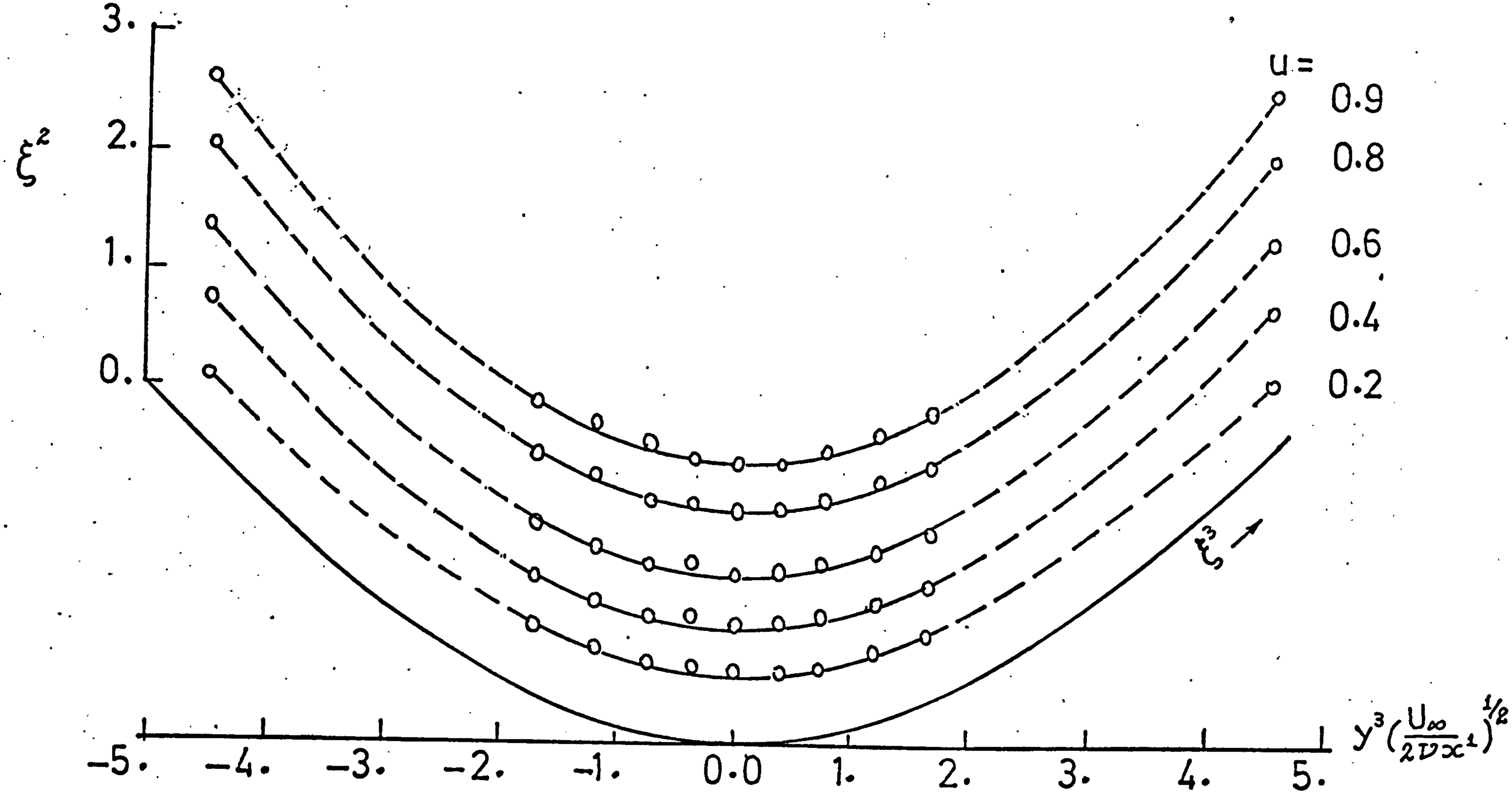

Fig (4.73) Streamwise isovels;

$x^1 = 0.343$ m , $\Gamma_{90} = 0.35$.

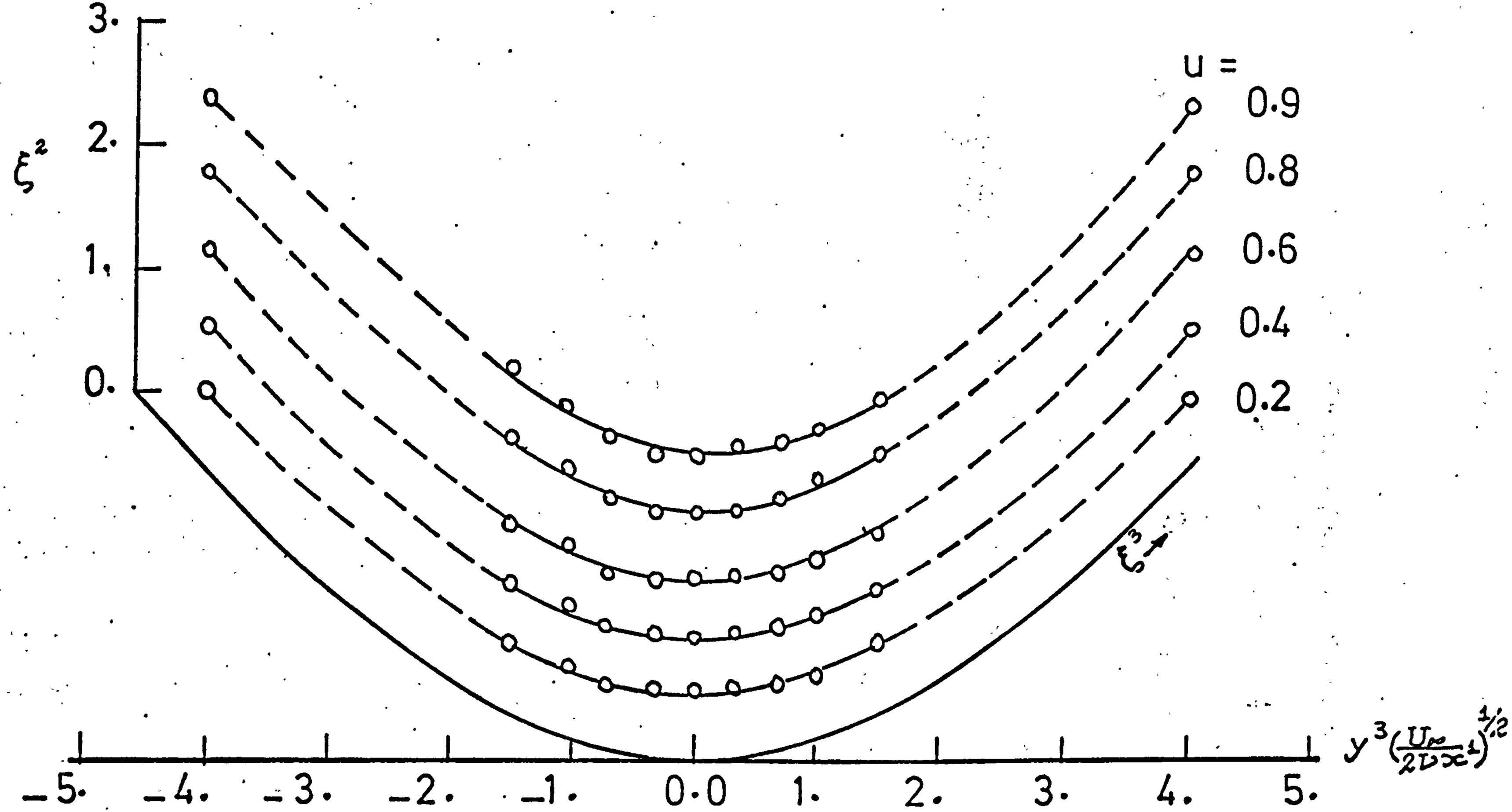

Fig.(4.74) Streamwise isovels;
$x^1 = 0.512$ m, $\Gamma_{90} = 0.44$.

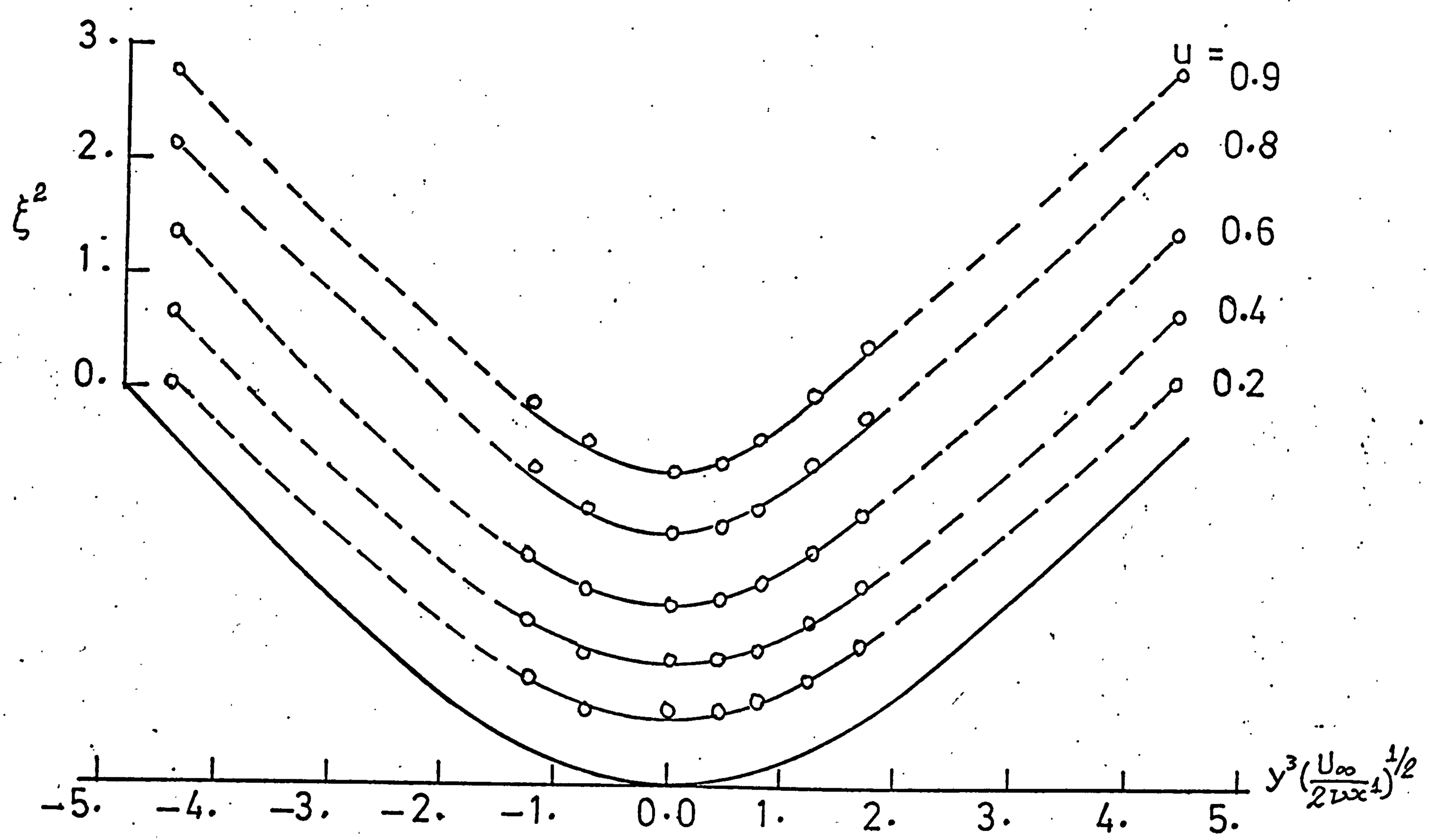

Fig.(4.75) Streamwise isovels;
$x^1 = 0.805$ m, $\Gamma_{90} = 0.53$.

Experimental results, ($\xi^3 = 0$):

symbol	x^1 m	$R_x \times 10^{-5}$	Γ_{90}
▽	0.165	0.162	0.233
x	0.343	0.313	0.35
△	0.510	0.445	0.44
o	0.805	0.742	0.53

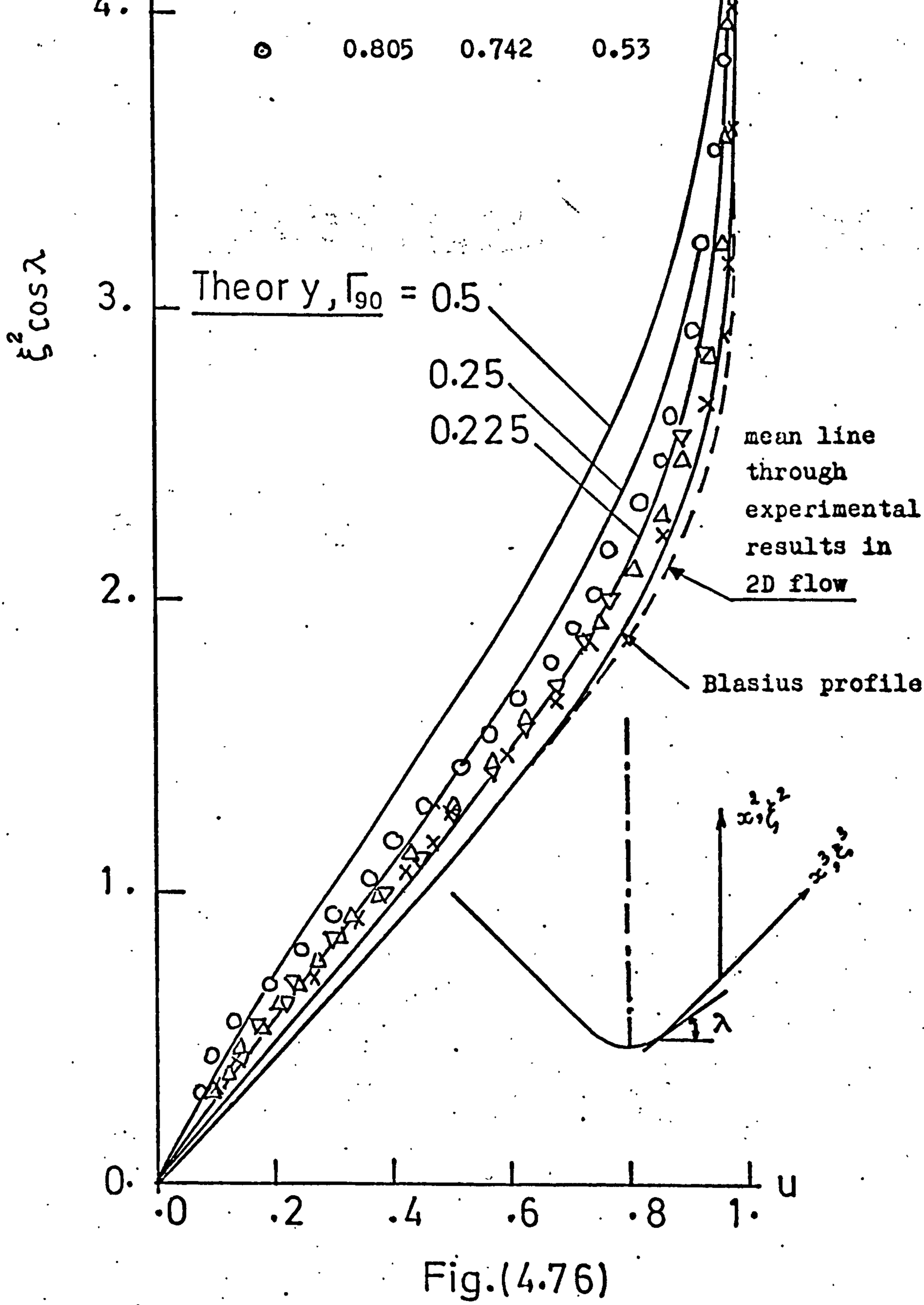

Fig.(4.76)

Table (2) Streamwise velocity u , $\Gamma_{\infty} = \infty$.

ξ^2 \ ξ^3	0.0	0.21	0.42	0.65	0.90	1.16	1.44	1.74	2.06	2.40	2.77
0.0	0.0	0.0	0.0	0.0	0.0	0.0	0.0	0.0	0.0	0.0	0.0
0.4	0.010	0.018	0.026	0.034	0.042	0.051	0.060	0.070	0.079	0.088	0.097
0.8	0.041	0.056	0.071	0.087	0.104	0.121	0.138	0.155	0.173	0.190	0.207
1.2	0.092	0.114	0.136	0.159	0.182	0.206	0.231	0.255	0.280	0.303	0.325
1.6	0.161	0.189	0.217	0.246	0.275	0.305	0.336	0.366	0.395	0.423	0.448
2.0	0.246	0.279	0.312	0.345	0.380	0.414	0.448	0.482	0.514	0.543	0.568
2.4	0.343	0.379	0.416	0.453	0.490	0.527	0.563	0.598	0.629	0.657	0.679
2.8	0.449	0.486	0.525	0.563	0.601	0.639	0.674	0.706	0.734	0.757	0.775
3.2	0.558	0.596	0.634	0.671	0.708	0.742	0.773	0.801	0.823	0.840	0.853
3.6	0.665	0.701	0.736	0.770	0.802	0.831	0.855	0.876	0.891	0.902	0.910
4.0	0.764	0.796	0.826	0.854	0.879	0.900	0.917	0.929	0.939	0.945	0.949
4.4	0.849	0.875	0.898	0.918	0.934	0.947	0.957	0.964	0.968	0.971	0.973
4.8	0.915	0.932	0.948	0.960	0.969	0.976	0.980	0.983	0.985	0.986	0.987
5.2	0.958	0.969	0.977	0.984	0.988	0.990	0.992	0.993	0.993	0.994	0.994
5.6	0.983	0.988	0.992	0.994	0.996	0.997	0.997	0.997	0.997	0.997	0.998
6.0	0.994	0.996	0.998	0.998	0.999	0.999	0.999	0.999	0.999	0.999	0.999
6.4	0.998	0.999	0.999	1.000	1.000	1.000	1.000	1.000	1.000	1.000	1.000
6.8	1.000	1.000	1.000	1.000	1.000	1.000	1.000	1.000	1.000	1.000	1.000

Table (2) (continued)

ξ^2 \ ξ^3	3.17	3.60	4.07	4.58	5.14	5.76	6.44	∞
0.0	0.0	0.0	0.0	0.0	0.0	0.0	0.0	0.0
0.4	0.106	0.114	0.120	0.125	0.129	0.131	0.133	0.133
0.8	0.222	0.235	0.246	0.254	0.259	0.263	0.265	0.265
1.2	0.345	0.361	0.373	0.382	0.389	0.393	0.395	0.394
1.6	0.469	0.485	0.498	0.507	0.513	0.517	0.519	0.518
2.0	0.588	0.603	0.614	0.622	0.627	0.630	0.633	0.631
2.4	0.696	0.709	0.717	0.723	0.728	0.730	0.732	0.730
2.8	0.788	0.798	0.804	0.808	0.811	0.813	0.815	0.813
3.2	0.861	0.867	0.872	0.874	0.876	0.878	0.879	0.878
3.6	0.915	0.919	0.921	0.923	0.924	0.925	0.926	0.925
4.0	0.951	0.953	0.955	0.956	0.957	0.957	0.957	0.957
4.4	0.974	0.975	0.976	0.976	0.977	0.977	0.977	0.977
4.8	0.987	0.988	0.988	0.988	0.989	0.989	0.989	0.989
5.2	0.994	0.994	0.995	0.995	0.995	0.995	0.995	0.995
5.6	0.998	0.998	0.998	0.998	0.998	0.998	0.998	0.998
6.0	0.999	0.999	0.999	0.999	0.999	0.999	0.999	0.999
6.4	1.000	1.000	1.000	1.000	1.000	1.000	1.000	1.000
6.8	1.000	1.000	1.000	1.000	1.000	1.000	1.000	1.000
∞	1.000	1.000	1.000	1.000	1.000	1.000	1.000	1.000

Table (3) Crosswise velocity v , $\Gamma_{90} = \infty$.

ξ^2 \ ξ^3	0.0	0.206	0.424	0.655	0.900	1.161	1.440	1.738	2.057	2.400	2.769
0.0	0.0	0.0	0.0	0.0	0.0	0.0	0.0	0.0	0.0	0.0	0.0
0.4	-0.008	-0.012	-0.015	-0.013	-0.002	-0.004	-0.008	-0.013	0.019	0.025	0.029
0.8	-0.015	-0.011	-0.001	0.007	0.030	0.069	0.092	0.116	0.138.	0.156	0.167
1.2	0.038	0.063	0.094	0.132	0.176	0.225	0.277	0.324	0.363	0.388	0.396
1.6	0.134	0.188	0.253	0.327	0.408	0.491	0.569	0.634	0.679	0.697	0.688
2.0	0.325	0.417	0.522	0.635	0.750	0.860	0.952	1.019	1.050	1.046	1.008
2.4	0.629	0.761	0.902	1.047	1.183	1.301	1.387	1.432	1.432	1.390	1.319
2.8	1.045	1.207	1.372	1.528	1.663	1.763	1.818	1.820	1.775	1.692	1.588
3.2	1.540	1.715	1.880	2.023	2.128	2.185	2.187	2.136	2.044	1.925	1.800
3.6	2.059	2.222	2.361	2.461	2.513	2.509	2.452	2.351	2.221	2.083	1.950
4.0	2.527	2.654	2.743	2.783	2.770	2.705	2.597	2.461	2.314	2.171	2.043
4.4	2.877	2.951	2.978	2.954	2.883	2.771	2.633	2.484	2.338	2.205	2.090
4.8	3.064	3.080	3.050	2.977	2.867	2.734	2.590	2.448	2.316	2.201	2.101
5.2	3.086	3.055	2.986	2.886	2.764	2.633	2.502	2.379	2.268	2.171	2.086
5.6	2.982	2.922	2.836	2.732	2.620	2.506	2.397	2.297	2.206	2.126	2.055
6.0	2.808	2.739	2.655	2.563	2.469	2.378	2.292	2.212	2.140	2.074	2.015
6.4	2.619	2.553	2.481	2.406	2.332	2.261	2.194	2.132	2.074	2.021	1.972
6.8	2.445	2.388	2.330	2.271	2.215	2.160	2.108	2.059	2.013	1.970	1.930
7.2	2.297	2.251	2,205	2.160	2.116	2.073	2.032	1.994	1.957	1.923	1.891
7.6	2.177	2.140	2.103	2.067	2.033	1.999	1.967	1.937	1.908	1.881	1.855
8.0	2.079	2.049	2.019	1.991	1.963	1.937	1.912	1.888	1.865	1.844	1.824
∞	1.721	1.721	1.721	1.721	1.721	1.721	1.721	1.721	1.721	1.721	1.721

Table (3) (continued)

ξ^2 \ ξ^3	3.168	3.600	4.070.	4.582	5.143	5.760	6.442	7.200	36.000	∞
0.0	0.0	0.0	0.0	0.0	0.0	0.0	0.0	0.0	0.0	0.0
0.4	0.032	0.033	0.031	0.028	0.025	0.021	0.019	0.017	0.026	0.027
0.8	0.169	0.161	0.151	0.137	0.123	0.112	0.103	0.096	0.105	0.106
1.2	0.387	0.365	0.336	0.307	0.281	0.259	0.243	0.231	0.235	0.235
1.6	0.658	0.613	0.565	0.520	0.482	0.452	0.428	0.411	0.409	0.407
2.0	0.949	0.881	0.815	0.757	0.710	0.673	0.644	0.622	0.615	0.611
2.4	1.231	1.144	1.065	0.999	0.947	0.905	0.873	0.849	0.837	0.830
2.8	1.480	1.381	1.297	1.228	1.174	1.130	1.096	1.070	1.054	1.045
3.2	1.682	1.581	1.497	1.429	1.374	1.330	1.296	1.269	1.251	1.240
3.6	1.833	1.736	1.656	1.590	1.537	1.494	1.460	1.433	1.413	1.400
4.0	1.935	1.845	1.770	1.709	1.658	1.616	1.583	1.558	1.535	1.522
4.4	1.993	1.912	1.843	1.786	1.738	1.699	1.667	1.643	1.620	1.606
4.8	2.016	1.943	1.881	1.828	1.784	1.748	1.719	1.696	1.673	1.659
5.2	2.012	1.948	1.893	1.845	1.805	1.773	1.746	1.726	1.703	1.690
5.6	1.992	1.936	1.887	1.846	1.811	1.781	1.758	1.740	1.719	1.706
6.0	1.962	1.914	1.873	1.837	1.806	1.781	1.760	1.744	1.726	1.714
6.4	1.928	1.888	1.853	1.823	1.797	1.775	1.758	1.744	1.729	1.718
6.8	1.894	1.861	1.832	1.807	1.786	1.768	1.753	1.742	1.730	1.719
7.2	1.862	1.835	1.812	1.791	1.774	1.759	1.748	1.739	1.730	1.719
7.6	1.832	1.811	1.793	1.777	1.763	1.751	1.742	1.735	1.729	1.720
8.0	1.806	1.790	1.776	1.763	1.752	1.744	1.737	1.731	1.729	1.720
∞	1.721	1.721	1.721	1.721	1.721	1.721	1.721	1.721	1.721	1.721

Table (4) Crossflow velocity w , $\Gamma_{90} = \infty$.

ξ^2 \ ξ^3	0.0	0.206	0.424	0.655	0.900	1.161	1.440	1.738	2.057	2.400	2.769	3.168
0.0	0.0	0.0	0.0	0.0	0.0	0.0	0.0	0.0	0.0	0.0	0.0	0.0
0.4	0.0	0.002	0.006	0.012	0.017	0.019	0.016	0.006	-0.014	-0.043	-0.079	-0.121
0.8	0.0	0.006	0.013	0.017	0.014	0.003	-0.020	-0.057	-0.107	-0.168	-0.235	-0.302
1.2	0.0	0.007	0.007	-0.001	-0.023	-0.059	-0.112	-0.179	-0.256	-0.338	-0.419	-0.494
1.6	0.0	-0.002	-0.017	-0.047	-0.096	-0.161	-0.241	-0.329	-0.420	-0.505	-0.580	-0.642
2.0	0.0	-0.020	-0.059	-0.116	-0.191	-0.279	-0.374	-0.766	-0.549	-0.616	-0.665	-0.702
2.4	0.0	-0.046	-0.111	-0.192	-0.284	-0.379	-0.468	-0.542	-0.595	-0.627	-0.643	-0.650
2.8	0.0	-0.073	-0.195	-0.252	-0.343	-0.423	-0.484	-0.521	-0.533	-0.526	-0.510	-0.495
3.2	0.0	-0.092	-0.185	-0.270	-0.340	-0.386	-0.405	-0.397	-0.369	-0.332	-0.297	-0.272
3.6	0.0	-0.094	-0.174	-0.234	-0.266	-0.269	-0.245	-0.201	-0.148	-0.097	-0.057	-0.034
4.0	0.0	-0.076	-0.126	-0.147	-0.138	-0.103	-0.049	0.014	0.075	0.124	0.157	0.137
4.4	0.0	-0.041	-0.053	-0.035	0.007	0.066	0.133	0.197	0.251	0.290	0.313	0.323
4.8	0.0	-0.001	0.024	0.071	0.131	0.198	0.263	0.318	0.360	0.388	0.404	0.410
5.2	0.0	0.034	0.085	0.147	0.212	0.275	0.330	0.374	0.407	0.428	0.440	0.445
5.6	0.0	0.057	0.121	0.186	0.248	0.303	0.349	0.384	0.411	0.429	0.440	0.446
6.0	0.0	0.067	0.133	0.195	0.250	0.298	0.337	0.368	0.392	0.409	0.421	0.428
6.4	0.0	0.067	0.129	0.185	0.235	0.277	0.312	0.340	0.363	0.380	0.393	0.401
6.8	0.0	0.062	0.118	0.168	0.213	0.251	0.283	0.311	0.333	0.350	0.363	0.372
7.2	0.0	0.055	0.105	0.150	0.190	0.226	0.256	0.282	0.304	0.321	0.334	0.344
7.6	0.0	0.048	0.093	0.134	0.170	0.203	0.232	0.256	0.277	0.294	0.308	0.317
8.0	0.0	0.043	0.082	0.119	0.153	0.183	0.210	0.233	0.253	0.270	0.283	0.293
∞	0.0	0.0	0.0	0.0	0.0	0.0	0.0	0.0	0.0	0.0	0.0	0.0

Table (4) (continued)

ξ^2 \ ξ^3	3.600	4.070	4.582	5.143	5.760	6.442	7.200	8.047	9.000	10.080	16.364	∞
0.0	0.0	0.0	0.0	0.0	0.0	0.0	0.0	0.0	0.0	0.0	0.0	0.0
0.4	-0.164	-0.204	-0.241	-0.273	-0.300	-0.324	-0.345	-0.362	-0.376	-0.389	-0.434	-0.388
0.8	-0.367	-0.425	-0.476	-0.522	-0.563	-0.599	-0.630	-0.658	-0.683	-0.705	-0.796	-0.710
1.2	-0.559	-0.617	-0.669	-0.716	-0.760	-0.801	-0.838	-0.872	-0.904	-0.935	-1.071	-0.952
1.6	-0.693	-0.739	-0.782	-0.825	-0.866	-0.907	-0.947	-0.985	-1.024	-1.062	-1.239	-1.099
2.0	-0.731	-0.760	-0.792	-0.828	-0.866	-0.905	-0.946	-0.988	-1.031	-1.076	-1.283	-1.142
2.4	-0.659	-0.673	-0.696	-0.725	-0.760	-0.798	-0.839	-0.883	-0.929	-0.979	-1.204	-1.084
2.8	-0.489	-0.496	-0.513	-0.538	-0.570	-0.607	-0.648	-0.693	-0.741	-0.792	-1.022	-0.946
3.2	-0.262	-0.266	-0.282	-0.306	-0.336	-0.372	-0.412	-0.456	-0.503	-0.554	-0.777	-0.759
3.6	-0.026	-0.032	-0.047	-0.070	-0.099	-0.133	-0.172	-0.214	-0.259	-0.307	-0.516	-0.561
4.0	0.176	0.168	0.153	0.131	0.104	0.072	0.036	-0.003	-0.045	-0.090	-0.282	-0.381
4.4	0.322	0.313	0.299	0.278	0.254	0.225	0.192	0.156	0.117	0.075	-0.100	-0.238
4.8	0.408	0.400	0.387	0.369	0.347	0.321	0.291	0.258	0.223	0.185	0.024	-0.137
5.2	0.444	0.438	0.427	0.411	0.392	0.369	0.342	0.313	0.280	0.245	0.097	-0.073
5.6	0.446	0.442	0.433	0.421	0.404	0.384	0.360	0.333	0.303	0.271	0.134	-0.035
6.0	0.430	0.427	0.421	0.410	0.396	0.378	0.357	0.333	0.305	0.276	0.148	-0.016
6.4	0.404	0.404	0.399	0.390	0.378	0.363	0.344	0.321	0.297	0.269	0.151	-0.007
6.8	0.377	0.377	0.374	0.367	0.357	0.343	0.326	0.306	0.283	0.258	0.148	-0.003
7.2	0.349	0.351	0.349	0.344	0.335	0.323	0.307	0.289	0.268	0.245	0.143	-0.001
7.6	0.324	0.326	0.325	0.321	0.313	0.303	0.289	0.273	0.254	0.232	0.138	-0.001
8.0	0.300	0.303	0.303	0.299	0.293	0.284	0.271	0.256	0.239	0.220	0.133	-0.000
∞	0.0	0.0	0.0	0.0	0.0	0.0	0.0	0.0	0.0	0.0	0.0	0.0

Table (5) Streamwise velocity u, $\Gamma_{135} = \infty$

ξ^2 \ ξ^3	0.0	0.42	0.90	1.44	2.06	2.40	3.17	3.60	5.14	∞
0.0	0.0	0.0	0.0	0.0	0.0	0.0	0.0	0.0	0.0	0.0
0.4	0.073	0.102	0.124	0.140	0.153	0.159	0.167	0.169	0.173	0.173
0.8	0.184	0.225	0.259	0.288	0.311	0.320	0.334	0.338	0.344	0.345
1.2	0.313	0.361	0.402	0.438	0.468	0.479	0.495	0.500	0.507	0.509
1.6	0.450	0.500	0.545	0.584	0.615	0.627	0.642	0.647	0.653	0.656
2.0	0.586	0.635	0.678	0.715	0.743	0.753	0.766	0.770	0.775	0.778
2.4	0.713	0.755	0.793	0.823	0.845	0.852	0.861	0.864	0.867	0.870
2.8	0.819	0.852	0.881	0.902	0.916	0.920	0.926	0.928	0.930	0.932
3.2	0.899	0.922	0.940	0.953	0.960	0.962	0.965	0.966	0.967	0.968
3.6	0.951	0.965	0.974	0.980	0.984	0.985	0.986	0.986	0.987	0.987
4.0	0.980	0.987	0.991	0.993	0.994	0.995	0.995	0.995	0.995	0.996
4.4	0.993	0.996	0.997	0.998	0.998	0.998	0.998	0.999	0.999	0.999
4.8	0.998	0.999	0.999	1.000	1.000	1.000	1.000	1.000	1.000	1.000
5.2	1.000	1.000	1.000	1.000	1.000	1.000	1.000	1.000	1.000	1.000

Table (6) Cross flow velocity v, $\Gamma_{135} = \infty$

ξ^2 \ ξ^3	0.0	0.424	0.900	1.738	2.400	4.582	6.442	9.000	36.000	∞
0.0	0.0	0.0	0.0	0.0	0.0	0.0	0.0	0.0	0.0	0.0
0.4	-0.005	0.022	0.034	0.043	0.040	0.028	0.026	0.028	0.035	0.035
0.8	0.084	0.128	0.163	0.183	0.173	0 135	0.128	0.129	0.139	0.137
1.2	0.250	0.325	0.382	0.405	0.382	0.312	0.297	0.295	0.305	0.300
1.6	0.504	0.604	0.672	0.681	0.638	0.536	0.513	0.507	0.516	0.506
2.0	0.823	0.932	0.994	0.971	0.906	0.776	0.746	0.736	0.740	0.727
2.4	1.161	1.260	1.298	1.231	1.146	0.997	0.961	0.948	0.947	0.929
2.8	1.465	1.536	1.537	1.428	1.332	1.174	1.133	1.116	1.111	1.090
3.2	1.686	1.719	1.686	1.551	1.452	1.294	1.251	1.231	1.222	1.200
3.6	1.804	1.803	1.746	1.606	1.515	1.364	1.320	1.298	1.286	1.264
4.0	1.831	1.806	1.742	1.615	1.535	1.397	1.353	1.331	1.317	1.295
4.4	1.797	1.763	1.704	1.598	1.531	1.408	1.366	1.344	1.329	1.309
4.8	1.737	1.704	1.655	1.571	1.516	1.408	1.369	1.348	1.332	1.313
5.2	1.675	1.646	1.608	1.541	1.496	1.403	1.368	1.348	1.333	1.315
5.6	1.618	1.595	1.565	1.512	1.476	1.397	1.365	1.347	1.332	1.315
6.0	1.570	1.551	1.528	1.486	1.457	1.390	1.362	1.345	1.331	1.315
6.4	1.530	1.514	1.495	1.462	1.438	1.383	1.359	1.344	1.330	1.315
6.8	1.495	1.482	1.467	1.441	1.422	1.376	1.355	1.342	1.329	1.315
7.2	1.465	1.455	1.443	1.422	1.407	1.369	1.352	1.340	1.329	1.316
7.6	1.440	1.431	1.421	1.405	1.393	1.363	1.348	1.338	1.328	1.316
8.0	1.418	1.411	1.403	1.390	1.381	1.357	1.345	1.337	1.327	1.316

Table (7) Cross flow velocity w, $\Gamma_{135} = \infty$ -

ξ^2 \ ξ^3	0.0	0.655	1.161	1.440	1.738	2.400	3.168	3.600	4.070	∞
0.0	0.0	0.0	0.0	0.0	0.0	0.0	0.0	0.0	0.0	0.0
0.4	0.0	-0.016	-0.049	-0.070	-0.093	-0.137	-0.173	-0.187	-0.201	-0.205
0.8	0.0	-0.054	-0.118	-0.154	-0.191	-0.258	-0.313	-0.337	-0.360	-0.360
1.2	0.0	-0.097	-0.182	-0.226	-0.267	-0.339	-0.399	-0.428	-0.457	-0.452
1.6	0.0	-0.127	-0.217	-0.257	-0.294	-0.355	-0.411	-0.440	-0.472	-0.471
2.0	0.0	-0.130	-0.203	-0.231	-0.255	-0.295	-0.341	-0.369	-0.400	-0.422
2.4	0.0	-0.101	-0.140	-0.151	-0.159	-0.177	-0.211	-0.235	-0.263	-0.326
2.8	0.0	-0.047	-0.047	-0.042	-0.037	-0.039	-0.063	-0.082	-0.105	-0.221
3.2	0.0	0.012	0.044	0.059	0.071	0.079	0.063	0.048	0.029	-0.129
3.6	0.0	0.058	0.106	0.126	0.141	0.152	0.141	0.130	0.116	-0.065
4.0	0.0	0.082	0.133	0.153	0.168	0.181	0.175	0.167	0.157	-0.029
4.4	0.0	0.086	0.134	0.152	0.165	0.179	0.179	0.174	0.166	-0.011
4.8	0.0	0.079	0.121	0.137	0.150	0.165	0.168	0.165	0.160	-0.004
5.2	0.0	0.068	0.105	0.119	0.131	0.147	0.153	0.152	0.149	-0.001
5.6	0.0	0.058	0.090	0.104	0.115	0.132	0.139	0.140	0.139	-0.000
6.0	0.0	0.050	0.079	0.091	0.102	0.118	0.127	0.129	0.129	0.000
6.4	0.0	0.044	0.069	0.081	0.091	0.107	0.117	0.120	0.121	0.000
6.8	0.0	0.039	0.062	0.073	0.082	0.098	0.109	0.112	0.113	0.0
7.2	0.0	0.035	0.056	0.066	0.075	0.090	0.101	0.105	0.107	0.0
7.6	0.0	0.031	0.051	0.060	0.069	0.084	0.094	0.098	0.101	0.0
8.0	0.0	0.029	0.047	0.055	0.064	0.078	0.088	0.092	0.095	0.0
∞	0.0	0.0	0.0	0.0	0.0	0.0	0.0	0.0	0.0	0.0

Table (8) Streamwise velocity u, $\Gamma_{270} = \infty$

ξ^2 \ ξ^3	0.0	0.21	0.42	1.44	2.06	2.77	3.17	3.60	4.07	∞
0.0	0.0	0.0	0.0	0.0	0.0	0.0	0.0	0.0	0.0	0.0
0.4	0.428	0.329	0.265	0.166	0.150	0.140	0.137	0.135	0.133	0.133
0.8	0.667	0.596	0.526	0.349	0.309	0,285	0.277	0.272	0.267	0.265
1.2	0.831	0.783	0.729	0.532	0.471	0.431	0.418	0.408	0.401	0.394
1.6	0.926	0.898	0.863	0.696	0.625	0.573	0.555	0.540	0.530	0.517
2.0	0.974	0.959	0.941	0.823	0.756	0.701	0.680	0.662	0.649	0.631
2.4	0.993	0.987	0.979	0.908	0.857	0.807	0.786	0.768	0.754	0.730
2.8	0.999	0.998	0.994	0.959	0.925	0.887	0.869	0.854	0.839	0.813
3.2	1.000	1.000	0.999	0.984	0.966	0.940	0.927	0.914	0.903	0.878
3.6	1.000	1.000	1.000	0.995	0.986	0.972	0.964	0.955	0.947	0.925
4.0	1.000	1.000	1.000	0.999	0.996	0.989	0.984	0.979	0.973	0.957
4.4	1.000	1.000	1.000	1.000	0.999	0.996	0.994	0.991	0.988	0.977
4.8	1.000	1.000	1.000	1.000	1.000	0.999	0.998	0.997	0.995	0.989
5.2	1.000	1.000	1.000	1.000	1.000	1.000	1.000	0.999	0.998	0.995
5.6	1.000	1.000	1.000	1.000	1.000	1.000	1.000	1.000	1.000	0.998
6.0	1.000	1.000	1.000	1.000	1.000	1.000	1.000	1.000	1.000	0.999
6.4	1.000	1.000	1.000	1.000	1.000	1.000	1.000	1.000	1.000	1.000

Table (9) Cross flow velocity v, $\Gamma_{270} = \infty$.

ξ^2 \ ξ^3	0.0	0.424	0.900	1.440	2.400	4.070	7.200	14.400	36.000	∞
0.0	0.0	0.0	0.0	0.0	0.0	0.0	0.0	0.0	0.0	0.0
0.4	-0.014	0.009	0.028	0.024	0.021	0.030	0.033	0.030	0.026	0.027
0.8	-0.088	-0.045	0.021	0.058	0.080	0.105	0.117	0.115	0.106	0.106
1.2	-0.089	-0.081	-0.005	0.078	0.159	0.219	0.248	0.250	0.237	0.235
1.6	-0.016	-0.057	-0.015	0.085	0.236	0.360	0.419	0.430	0.411	0.407
2.0	0.118	0.031	0.019	0.096	0.295	0.508	0.617	0.643	0.618	0.611
2.4	0.291	0.173	0.105	0.132	0.335	0.644	0.825	0.871	0.840	0.831
2.8	0.478	0.347	0.238	0.207	0.367	0.751	1.023	1.095	1.058	1.046
3.2	0.655	0.527	0.400	0.322	0.407	0.822	1.192	1.298	1.255	1.240
3.6	0.810	0.697	0.070	0.465	0.470	0.860	1.322	1.466	1.417	1.401
4.0	0.942	0.845	0.730	0.618	0.559	0.879	1.406	1.593	1.541	1.523
4.4	1.051	0.970	0.871	0.764	0.665	0.892	1.450	1.680	1.626	1.607
4.8	1.143	1.075	0.991	0.895	0.778	0.913	1.463	1.733	1.679	1.660
5.2	1.221	1.163	1.092	1.008	0.888	0.944	1.455	1.763	1.710	1.691
5.6	1.288	1.238	1.177	1.104	0.990	0.987	1.438	1.776	1.726	1.707
6.0	1.345	1.302	1.249	1.186	1.081	1.038	1.419	1.779	1.733	1.715
6.4	1.395	1.357	1.311	1.256	1.161	1.093	1.402	1.777	1.736	1.718
6.8	1.438	1.405	1.365	1.316	1.231	1.150	1.390	1.773	1.737	1.720
7.2	1.475	1.446	1.411	1.369	1.292	1.205	1.384	1.767	1.737	1.720
7.6	1.508	1.482	1.452	1.414	1.345	1.257	1.384	1.761	1.737	1.720
8.0	1.536	1.514	1.487	1.454	1.392	1.306	1.389	1.754	1.736	1.720
∞	1.721	1.721	1.721	1.721	1.721	1.721	1.721	1.721	1.721	1.721

Table (10) Cross flow velocity w, $\Gamma_{270} = \infty$.

ξ^2 \ ξ^3	0.0	0.655	1.161	2.057	2.769	5.143	9.000	16.364	36.000	∞
0.0	0.0	0.0	0.0	0.0	0.0	0.0	0.0	0.0	0.0	0.0
0.4	0.0	0.219	0.276	0.299	0.306	0.318	0.326	0.319	0.281	0.388
0.8	0.0	0.232	0.375	0.487	0.521	0.564	0.590	0.581	0.511	0.710
1.2	0.0	0.131	0.309	0.531	0.617	0.726	0.780	0.775	0.681	0.952
1.6	0.0	-0.009	0.135	0.423	0.576	0.789	0.887	0.892	0.784	1.099
2.0	0.0	-0.132	-0.074	0.196	0.400	0.744	0.903	0.926	0.816	1.142
2.4	0.0	-0.210	-0.249	-0.080	0.131	0.599	0.834	0.884	0.784	1.084
2.8	0.0	-0.234	-0.351	-0.328	-0.164	0.376	0.694	0.780	0.700	0.946
3.2	0.0	-0.217	-0.375	-0.491	-0.414	0.116	0.512	0.638	0.586	0.759
3.6	0.0	-0.180	-0.344	-0.553	-0.573	-0.136	0.318	0.486	0.462	0.561
4.0	0.0	-0.140	-0.287	-0.534	-0.631	-0.345	0.138	0.345	0.345	0.381
4.4	0.0	-0.106	-0.227	-0.469	-0.610	-0.489	-0.010	0.229	0.246	0.238
4.8	0.0	-0.080	-0.175	-0.388	-0.543	-0.567	-0.121	0.142	0.171	0.137
5.2	0.0	-0.061	-0.135	-0.312	-0.460	-0.590	-0.198	0.083	0.118	0.073
5.6	0.0	-0.047	-0.104	-0.248	-0.379	-0.575	-0.248	0.045	0.084	0.035
6.0	0.0	-0.036	-0.081	-0.197	-0.309	-0.537	-0.278	0.022	0.063	0.016
6.4	0.0	-0.028	-0.064	-0.157	-0.251	-0.488	-0.295	0.007	0.051	0.007
6.8	0.0	-0.021	-0.050	-0.125	-0.204	-0.436	-0.303	-0.003	0.045	0.003
7.2	0.0	-0.016	-0.039	-0.100	-0.166	-0.384	-0.305	-0.011	0.041	0.001
7.6	0.0	-0.012	-0.030	-0.080	-0.135	-0.336	-0.303	-0.017	0.040	0.001
8.0	0.0	-0.009	-0.023	-0.063	-0.109	-0.291	-0.296	-0.023	0.039	0.000
∞	0.0	0.0	0.0	0.0	0.0	0.0	0.0	0.0	0.0	0.0

Table (11) Streamwise velocity u, $\Gamma_{225} = \infty$

ξ^2 \ ξ^3	0.0	0.21	0.42	0.65	0.90	1.16	1.44	1.74	2.06	∞
0.0	0.0	0.0	0.0	0.0	0.0	0.0	0.0	0.0	0.0	0.0
0.4	0.295	0.254	0.227	0.209	0.196	0.187	0.180	0.176	0.172	0.174
0.8	0.505	0.470	0.439	0.413	0.392	0.375	0.362	0.352	0.345	0.345
1.2	0.678	0.649	0.621	0.595	0.572	0.552	0.535	0.521	0.510	0.509
1.6	0.809	0.787	0.766	0.744	0.723	0.704	0.687	0.672	0.660	0.656
2.0	0.898	0.884	0.869	0.853	0.838	0.822	0.808	0.795	0.784	0.778
2.4	0.952	0.944	0.935	0.925	0.915	0.904	0.894	0.885	0.876	0.870
2.8	0.980	0.976	0.972	0.966	0.961	0.955	0.949	0.943	0.937	0.932
3.2	0.993	0.991	0.989	0.987	0.984	0.981	0.978	0.975	0.972	0.968
3.6	0.998	0.997	0.997	0.996	0.995	0.993	0.992	0.991	0.989	0.987
4.0	1.000	0.999	0.999	0.999	0.998	0.998	0.998	0.997	0.997	0.996
4.4	1.000	1.000	1.000	1.000	1.000	1.000	0.999	0.999	0.999	0.999
4.8	1.000	1.000	1.000	1.000	1.000	1.000	1.000	1.000	1.000	1.000

Table (12) Cross flow velocity v, $\Gamma_{225} = \infty$.

ξ^2 \ ξ^3	0.0	0.206	0.655	1.440	2.400	3.600	5.760	9.000	14.400	∞
0.0	0.0	0.0	0.0	0.0	0.0	0.0	0.0	0.0	0.0	0.0
0.4	0.064	0.050	0.044	0.049	0.049	0.046	0.041	0.037	0.036	0.035
0.8	0.160	0.141	0.123	0.143	0.158	0.160	0.153	0.146	0.142	0.137
1.2	0.304	0.277	0.255	0.280	0.318	0.333	0.329	0.319	0.312	0.300
1.6	0.479	0.448	0.419	0.448	0.510	0.547	0.551	0.538	0.526	0.506
2.0	0.663	0.632	0.598	0.629	0.712	0.772	0.787	0.772	0.756	0.726
2.4	0.835	0.807	0.773	0.800	0.896	0.977	1.006	0.988	0.968	0.929
2.8	0.980	0.956	0.924	0.946	1.042	1.137	1.178	1.161	1.136	1.090
3.2	1.092	1.073	1.045	1.058	1.144	1.242	1.294	1.277	1.251	1.199
3.6	1.173	1.159	1.136	1.140	1.208	1.299	1.357	1.344	1.316	1.263
4.0	1.231	1.220	1.201	1.198	1.247	1.324	1.384	1.375	1.347	1.295
4.4	1.271	1.263	1.248	1.240	1.271	1.332	1.389	1.385	1.359	1.308
4.8	1.298	1.292	1.280	1.271	1.288	1.333	1.385	1.385	1.361	1.313
5.2	1.315	1.311	1.303	1.294	1.302	1.334	1.379	1.382	1.361	1.314
5.6	1.326	1.323	1.317	1.310	1.313	1.334	1.372	1.378	1.359	1.315
6.0	1.332	1.330	1.326	1.321	1.321	1.335	1.366	1.373	1.356	1.315
6.4	1.334	1.333	1.331	1.328	1.327	1.336	1.361	1.369	1.354	1.315
6.8	1.334	1.334	1.333	1.331	1.331	1.337	1.356	1.365	1.352	1.315
7.2	1.333	1.334	1.334	1.333	1.333	1.338	1.353	1.361	1.350	1.315
7.6	1.332	1.332	1.333	1.334	1.334	1.338	1.349	1.357	1.348	1.315
8.0	1.330	1.330	1.331	1.333	1.334	1.337	1.347	1.354	1.346	1.316
∞	1.317	1.317	1.317	1.317	1.317	1.317	1.317	1.317	1.317	1.317

Table (13) Cross flow velocity w, $\Gamma_{225} = \infty$

ξ^2 \ ξ^3	0.0	0.206	0.900	2.400	3.600	4.582	6.442	9.000	11.314	∞
0.0	0.0	0.0	0.0	0.0	0.0	0.0	0.0	0.0	0.0	0.0
0.4	0.0	0.024	0.084	0.119	0.112	0.105	0.089	0.066	0.047	0.205
0.8	0.0	0.026	0.106	0.178	0.175	0.165	0.139	0.098	0.064	0.360
1.2	0.0	0.015	0.084	0.177	0.185	0.178	0.149	0.100	0.056	0.452
1.6	0.0	-0.000	0.032	0.123	0.149	0.150	0.128	0.080	0.036	0.471
2.0	0.0	-0.016	-0.030	0.036	0.079	0.094	0.088	0.053	0.017	0.422
2.4	0.0	-0.026	-0.082	-0.058	-0.003	0.027	0.043	0.028	0.008	0.326
2.8	0.0	-0.029	-0.111	-0.133	-0.075	-0.034	0.004	0.012	0.008	0.221
3.2	0.0	-0.027	-0.114	-0.174	-0.124	-0.078	-0.025	0.002	0.011	0.129
3.6	0.0	-0.022	-0.100	-0.182	-0.147	-0.104	-0.043	-0.005	0.012	0.065
4.0	0.0	-0.016	-0.080	-0.167	-0.149	-0.112	-0.053	-0.009	0.011	0.029
4.4	0.0	-0.011	-0.059	-0.140	-0.137	-0.109	-0.056	-0.011	0.010	0.011
4.8	0.0	-0.008	-0.042	-0.111	-0.118	-0.099	-0.053	-0.011	0.011	0.004
5.2	0.0	-0.005	-0.029	-0.085	-0.097	-0.085	-0.048	-0.008	0.013	0.001
5.6	0.0	-0.003	-0.020	-0.063	-0.077	-0.071	-0.041	-0.004	0.017	0.000
6.0	0.0	-0.002	-0.013	-0.045	-0.059	-0.056	-0.033	0.001	0.021	0.000
6.4	0.0	-0.001	-0.008	-0.031	-0.043	-0.043	-0.025	0.005	0.025	0.000
6.8	0.0	-0.000	-0.004	-0.020	-0.030	-0.031	-0.017	0.009	0.028	0.000
7.2	0.0	0.000	-0.001	-0.011	-0.019	-0.020	-0.010	0.014	0.031	0.000
7.6	0.0	0.000	0.001	-0.005	-0.010	-0.010	-0.003	0.017	0.034	0.000
8.0	0.0	0.001	0.002	0.000	-0.003	-0.004	0.003	0.021	0.036	0.000
∞	0.0	0.000	0.000	0.000	0.000	0.000	0.000	0.000	0.000	0.000

Table (14) Streamwise velocity u, $\Gamma_{90} = 3.0$.

ξ^2 \ ξ^3	0.0	0.60	1.20	1.80	2.07	2.80	3.30	3.94	∞
0.0	0.0	0.0	0.0	0.0	0.0	0.0	0.0	0.0	0.0
0.4	0.032	0.047	0.070	0.089	0.097	0.112	0.120	0.127	0.133
0.8	0.088	0.117	0.159	0.193	0.206	0.233	0.246	0.257	0.265
1.2	0.065	0.206	0.263	0.308	0.325	0.359	0.375	0.388	0.394
1.6	0.261	0.311	0.378	0.429	0.448	0.485	0.501	0.513	0.517
2.0	0.371	0.426	0.497	0.550	0.569	0.604	0.619	0.629	0.630
2.4	0.486	0.543	0.613	0.664	0.681	0.711	0.723	0.731	0.730
2.8	0.601	0.655	0.720	0.764	0.778	0.801	0.809	0.815	0.812
3.2	0.709	0.757	0.812	0.845	0.855	0.871	0.876	0.880	0.877
3.6	0.803	0.842	0.884	0.906	0.913	0.922	0.925	0.927	0.924
4.0	0.878	0.907	0.934	0.948	0.951	0.956	0.957	0.958	0.957
4.4	0.932	0.951	0.967	0.973	0.975	0.977	0.977	0.978	0.977
4.8	0.967	0.977	0.985	0.987	0.988	0.989	0.989	0.989	0.989
5.2	0.986	0.990	0.993	0.994	0.995	0.995	0.995	0.995	0.995
5.6	0.995	0.996	0.997	0.998	0.998	0.998	0.998	0.998	0.998
6.0	0.998	0.999	0.999	0.999	0.999	0.999	0.999	0.999	0.999
6.4	0.999	0.999	1.000	1.000	1.000	1.000	1.000	1.000	1.000
6.8	1.000	1.000	1.000	1.000	1.000	1.000	1.000	1.000	1.000

Table (15) Crossflow velocity v, $\Gamma_{90} = 3.0$

ξ^2 \ ξ^3	0.0	0.300	0.600	0.918	1.200	2.073	3.943	∞
0.0	0.0	0.0	0.0	0.0	0.0	0.0	0.0	0.0
0.4	-0.001	-0.011	-0.016	-0.015	-0.012	0.007	0.022	0.025
0.8	0.002	0.000	0.010	0.032	0.057	0.124	0.124	0.103
1.2	0.050	0.065	0.110	0.173	0.228	0.339	0.286	0.231
1.6	0.171	0.213	0.309	0.418	0.501	0.623	0.489	0.403
2.0	0.387	0.460	0.608	0.754	0.851	0.938	0.715	0.606
2.4	0.700	0.800	0.986	1.146	1.235	1.245	0.945	0.825
2.8	1.092	1.207	1.401	1.542	1.600	1.509	1.163	1.041
3.2	1.523	1.632	1.797	1.890	1.901	1.714	1.355	1.236
3.6	1.937	2.018	2.122	2.148	2.110	1.855	1.510	1.398
4.0	2.276	2.315	2.341	2.301	2.224	1.940	1.626	1.521
4.4	2.501	2.494	2.448	2.357	2.259	1.982	1.704	1.606
4.8	2.602	2.558	2.460	2.343	2.242	1.995	1.750	1.660
5.2	2.599	2.534	2.412	2.291	2.198	1.988	1.774	1.692
5.6	2.531	2.460	2.336	2.225	2.146	1.970	1.783	1.709
6.0	2.437	2.369	2.255	2.159	2.093	1.947	1.784	1.717
6.4	2.340	2.280	2.181	2.101	2.046	1.923	1.781	1.721
6.8	2.252	2.202	2.119	2.050	2.004	1.901	1.776	1.723
7.2	2.179	2.137	2.066	2.008	1.969	1.880	1.771	1.723
7.6	2.118	2.083	2.023	1.973	1.940	1.863	1.766	1.724
8.0	2.068	2.040	1.988	1.944	1.915	1.848	1.762	1.724
∞	1.721	1.721	1.721	1.721	1.721	1.721	1.721	1.721

Table (16) Crossflow velocity w, $\Gamma_{90} = 3.0$

ξ^2 \ ξ^3	0.0	0.300	0.600	1.200	2.073	3.300	6.000	16.800	∞
0.0	0.0	0.0	0.0	0.0	0.0	0.0	0.0	0.0	-0.0 -0.388
0.4	0.0	0.010	0.013	0.008	-0.051	-0.186	-0.324	-0.378	-0.710
0.8	0.0	0.006	0.004	-0.038	-0.181	-0.392	-0.578	-0.676	-0.952
1.2	0.0	-0.007	-0.032	-0.133	-0.344	-0.567	-0.746	-0.884	-1.099
1.6	0.0	-0.032	-0.090	-0.251	-0.488	-0.665	-0.812	-0.993	-1.142
2.0	0.0	-0.065	-0.158	-0.355	-0.561	-0.658	-0.772	-0.995	-1.082
2.4	0.0	-0.096	-0.214	-0.406	-0.531	-0.544	-0.635	-0.899	-0.946
2.8	0.0	-0.114	-0.235	-0.377	-0.397	-0.349	-0.432	-0.726	-0.759
3.2	0.0	-0.109	-0.205	-0.265	-0.192	-0.117	-0.199	-0.511	-0.561
3.6	0.0	-0.080	-0.129	-0.099	0.031	0.105	0.023	-0.293	-0.381
4.0	0.0	-0.033	-0.027	0.074	0.223	0.283	0.205	-0.104	-0.238
4.4	0.0	0.019	0.072	0.214	0.355	0.401	0.332	0.038	-0.137
4.8	0.0	0.061	0.146	0.299	0.422	0.462	0.405	0.131	-0.073
5.2	0.0	0.086	0.186	0.332	0.438	0.478	0.435	0.181	-0.035
5.6	0.0	0.096	0.196	0.328	0.423	0.465	0.437	0.203	-0.016
6.0	0.0	0.093	0.187	0.304	0.392	0.437	0.421	0.206	-0.007
6.4	0.0	0.085	0.169	0.274	0.356	0.404	0.398	0.201	-0.003
6.8	0.0	0.075	0.149	0.243	0.320	0.369	0.372	0.192	-0.001
7.2	0.0	0.065	0.130	0.215	0.287	0.336	0.346	0.182	-0.001
7.6	0.0	0.056	0.114	0.190	0.258	0.306	0.321	0.172	-0.000
8.0	0.0	0.049	0.100	0.169	0.232	0.279	0.298	0.161	-0.0
∞	0.0	0.0	0.0	0.0	0.0	0.0	0.0	0.0	0.0

Table (17) Streamwise velocity u, $\Gamma_{270} = 3.0$.

ξ^2 \ ξ^3	0.0	0.37	0.60	0.92	1.37	1.80	3.30	7.80	34.80
0.0	0.0	0.0	0.0	0.0	0.0	0.0	0.0	0.0	0.0
0.4	0.270	0.228	0.191	0.158	0.136	0.128	0.124	0.130	0.133
0.8	0.471	0.430	0.384	0.331	0.285	0.263	0.247	0.260	0.265
1.2	0.632	0.598	0.557	0.501	0.440	0.405	0.370	0.387	0.394
1.6	0.758	0.733	0.700	0.651	0.589	0.545	0.491	0.508	0.518
2.0	0.851	0.834	0.810	0.772	0.719	0.675	0.606	0.621	0.632
2.4	0.915	0.904	0.888	0.863	0.822	0.785	0.711	0.720	0.731
2.8	0.956	0.949	0.940	0.924	0.897	0.869	0.802	0.804	0.813
3.2	0.979	0.976	0.971	0.962	0.946	0.928	0.874	0.870	0.878
3.6	0.991	0.990	0.987	0.983	0.974	0.964	0.926	0.919	0.925
4.0	0.997	0.996	0.995	0.993	0.989	0.984	0.961	0.953	0.957
4.4	0.999	0.999	0.998	0.997	0.996	0.994	0.981	0.974	0.977
4.8	1.000	0.999	0.999	0.999	0.999	0.998	0.992	0.987	0.989
5.2	1.000	1.000	1.000	1.000	1.000	0.999	0.997	0.994	0.995
5.6	1.000	1.000	1.000	1.000	1.000	1.000	0.999	0.997	0.998
6.0	1.000	1.000	1.000	1.000	1.000	1.000	1.000	0.999	0.999
6.4	1.000	1.000	1.000	1.000	1.000	1.000	1.000	1.000	1.000

Table (18) Crossflow velocity v, $\Gamma_{270} = 3.0$.

ξ^2 \ ξ^3	0.0	0.300	0.600	1.200	1.800	2.400	3.300	6.000	16.800	∞
0.0	0.0	0.0	0.0	0.0	0.0	0.0	0.0	0.0	0.0	0.0
0.4	0.072	0.149	0.226	0.178	0.109	0.082	0.066	0.042	0.027	0.026
0.8	0.119	0.207	0.334	0.367	0.282	0.221	0.183	0.139	0.108	0.105
1.2	0.226	0.288	0.400	0.504	0.467	0.403	0.347	0.286	0.239	0.234
1.6	0.401	0.422	0.481	0.595	0.627	0.596	0.545	0.478	0.414	0.407
2.0	0.627	0.606	0.599	0.668	0.747	0.772	0.756	0.702	0.621	0.611
2.4	0.874	0.821	0.753	0.747	0.835	0.912	0.957	0.940	0.843	0.830
2.8	1.114	1.042	0.932	0.845	0.907	1.012	1.123	1.173	1.062	1.046
3.2	1.319	1.244	1.116	0.967	0.979	1.081	1.242	1.380	1.260	1.240
3.6	1.477	1.410	1.287	1.104	1.062	1.136	1.316	1.545	1.423	1.401
4.0	1.587	1.534	1.429	1.244	1.160	1.190	1.355	1.660	1.548	1.522
4.4	1.657	1.619	1.537	1.370	1.264	1.253	1.377	1.728	1.634	1.607
4.8	1.700	1.673	1.612	1.475	1.365	1.323	1.396	1.756	1.689	1.660
5.2	1.726	1.707	1.663	1.554	1.454	1.395	1.421	1.757	1.721	1.691
5.6	1.741	1.728	1.696	1.612	1.527	1.464	1.453	1.743	1.738	1.707
6.0	1.751	1.742	1.717	1.652	1.583	1.523	1.490	1.722	1.747	1.715
6.4	1.757	1.751	1.732	1.681	1.626	1.572	1.528	1.701	1.751	1.718
6.8	1.761	1.757	1.742	1.701	1.657	1.612	1.564	1.684	1.753	1.720
7.2	1.764	1.761	1.749	1.716	1.680	1.642	1.596	1.671	1.754	1.720
7.6	1.766	1.764	1.755	1.726	1.698	1.666	1.623	1.664	1.754	1.721
8.0	1.768	1.767	1.759	1.735	1.711	1.684	1.646	1.660	1.754	1.721
∞	1.721	1.721	1.721	1.721	1.721	1.721	1.721	1.721	1.721	1.721

Table (19) Crossflow velocity w, $\Gamma_{270} = 3.0$.

ξ^2 \ ξ^3	0.0	0.300	0.600	1.200	1.800	2.400	3.300	6.000	16.800	∞
0.0	0.0	0.0	0.0	0.0	0.0	0.0	0.0	0.0	0.0	0.0
0.4	0.0	0.195	0.343	0.395	0.365	0.355	0.358	0.369	0.370	0.388
0.8	0.0	0.201	0.419	0.633	0.656	0.646	0.648	0.675	0.680	0.710
1.2	0.0	0.156	0.364	0.681	0.811	0.841	0.856	0.905	0.917	0.952
1.6	0.0	0.093	0.248	0.578	0.801	0.904	0.962	1.047	1.066	1.099
2.0	0.0	0.026	0.112	0.380	0.644	0.819	0.949	1.091	1.119	1.142
2.4	0.0	-0.028	-0.013	0.149	0.390	0.607	0.813	1.037	1.077	1.084
2.8	0.0	-0.062	-0.012	-0.058	0.110	0.319	0.578	0.900	0.959	0.946
3.2	0.0	-0.074	-0.145	-0.200	-0.131	0.027	0.292	0.707	0.792	0.759
3.6	0.0	-0.069	-0.148	-0.265	-0.288	-0.208	0.014	0.490	0.609	0.561
4.0	0.0	-0.056	-0.127	-0.265	-0.353	-0.351	-0.206	0.281	0.441	0.381
4.4	0.0	-0.041	-0.098	-0.228	-0.344	-0.402	-0.345	0.103	0.303	0.238
4.8	0.0	-0.030	-0.072	-0.178	-0.296	-0.384	-0.402	-0.032	-0.203	-0.137
5.2	0.0	-0.021	-0.052	-0.133	-0.235	-0.331	-0.397	-0.125	0.137	0.073
5.6	0.0	-0.016	-0.038	-0.098	-0.179	-0.267	-0.357	-0.180	0.097	0.035
6.0	0.0	-0.012	-0.029	-0.074	-0.136	-0.209	-0.303	-0.209	0.074	0.016
6.4	0.0	-0.010	-0.023	-0.057	-0.104	-0.162	-0.248	-0.218	0.062	0.007
6.8	0.0	-0.008	-0.018	-0.045	-0.080	-0.126	-0.201	-0.216	0.055	0.003
7.2	0.0	-0.006	-0.015	-0.036	-0.063	-0.099	-0.161	-0.205	0.050	0.001
7.6	0.0	-0.005	-0.012	-0.029	-0.051	-0.079	-0.130	-0.191	0.047	0.001
8.0	0.0	-0.004	-0.010	-0.023	-0.041	-0.063	-0.105	-0.174	0.044	0.000
∞	0.0	0.0	0.0	0.0	0.0	0.0	0.0	0.0	0.0	0.0

1.445	1.435	1,432	1.50	1.512	U_∞ m/s	1.55	1.544	1.55	1.476	1.476	1.466
50.8	3.81	1.524	0.762	0.0	$-y^3$ mm | y^3 mm	0.0	0.762	1.524	2.54	3.81	50.8
u = v(1)/U_∞					x^2 mm	u = v(1)/U_∞					
0.165	0.165	0.167	0.193	0.169	0.994	0.166	0.179	0.191	0.189	0.172	0.154
0.233	0.232	0.241	0.254	0.220	1.248	0.220	0.226	0.247	0.234	0.209	0.204
0.243	0.308	0.317	0.321	0.292	1.502	0.293	0.296	0.321	0.303	0.275	0.247
0.290	0.386	0.395	0.393	0.369	1.756	0.375	0.364	0.391	0.384	0.340	0.284
0.344	0.450	0.467	0.460	0.450	2.010	0.449	0.420	0.468	0.465	0.400	0.340
0.397	0.513	0.520	0.526	0.509	2.264	0.508	0.481	0.536	0.526	0.467	0.395
0.421	0.579	0.584	0.580	0.581	2.518	0.572	0.559	0.596	0.600	0.531	0.421
0.464	0.639	0.641	0.650	0.629	2.772	0.632	0.619	0.637	0.647	0.605	0.460
0.512	0.688	0.700	0.717	0.694	3.026	0.680	0.685	0.693	0.728	0.650	0.509
0.566	0.746	0.758	0.761	0.730	3.280	0.732	0.729	0.735	0.748	0.705	0.562
0.607	0.791	0.791	0.798	0.780	3.534	0.776	0.773	0.791	0.798	0.751	0.604
0.688	0.867	0.867	0.870	0.860	4.042	0.852	0.855	0.861	0.859	0.843	0.685
0.770	0.917	0.923	0.920	0.902	4.550	0.899	0.902	0.903	0.907	0.888	0.760
0.820	0.944	0.954	0.947	0.938	5.058	0.935	0.938	0.939	0.941	0.917	0.817
0.873	0.971	0.971	0.968	0.965	5.566	0.962	0.962	0.965	0.972	0.958	0.871
0.910	0.978	0.982	0.978	0.975	6.074	0.976	0.982	0.982	0.989	0.979	0.907
0.940	0.992	0.989	0.992	0.989	6.709	0.988	0.986	0.986	0.992	0.989	0.937
0.960	0.996	0.996	0.996	0.996	7.344	0.996	0.989	0.993	0.996	0.996	0.958
0.985	1.000	1.000	1.000	1.000	8.614	1.000	0.996	0.996	1.000	1.000	0.982
0.994					9.884		1.000	1.000			0.992
0.997					11.154						0.996
1.000											1.000

Table (20) Measurements in the corner flow
(x^1 = 0.165 m)

1.348	1.349	1.350	1.351	1.350	1.348	U m/s	1.349	1.351	1.352	1.350	1.351	1.349
50.8	4.572	3.302	2.032	1.016	0.0	$-y^3$ mm | y^3 mm	0.0	1.016	2.032	3.302	4.572	50.8
		u = v(1)/U∞				x^2 mm			u = v(1)/U∞			
0.116	0.105	0.105	0.104	0.099	0.100	0.968	0.103	0.099	0.104	0.104	0.097	0.096
0.125	0.126	0.133	0.140	0.128	0.133	1.222	0.132	0.138	0.139	0.137	0.137	0.130
0.156	0.158	0.171	0.178	0.170	0.177	1.476	0.177	0.180	0.182	0.180	0.181	0.163
0.182	0.204	0.204	0.222	0.208	0.223	1.730	0.222	0.223	0.228	0.222	0.222	0.190
0.205	0.253	0.247	0.259	0.251	0.263	1.984	0.266	0.272	0.265	0.264	0.264	0.228
0.246	0.293	0.294	0.295	0.299	0.324	2.238	0.313	0.307	0.311	0.316	0.308	0.256
0.274	0.338	0.343	0.343	0.344	0.356	2.492	0.347	0.362	0.358	0.362	0.358	0.295
0.306	0.386	0.393	0.396	0.382	0.402	2.746	0.392	0.405	0.401	0.392	0.400	0.330
0.340	0.432	0.449	0.441	0.435	0.457	3.000	0.423	0.450	0.450	0.432	0.439	0.368
0.386	0.477	0.479	0.477	0.470	0.492	3.254	0.470	0.481	0.483	0.472	0.518	0.398
0.415	0.505	0.509	0.519	0.489	0.540	3.508	0.507	0.526	0.528	0.507	0.604	0.432
0.475	0.583	0.595	0.592	0.575	0.615	4.016	0.600	0.611	0.600	0.595	0.687	0.489
0.534	0.663	0.681	0.662	0.673	0.709	4.524	0.687	0.690	0.678	0.680	0.756	0.554
0.579	0.719	0.741	0.718	0.735	0.771	5.032	0.748	0.751	0.751	0.751	0.812	0.600
0.632	0.789	0.794	0.789	0.804	0.831	5.540	0.815	0.815	0.804	0.815	0.845	0.665
0.694	0.841	0.829	0.840	0.862	0.859	6.048	0.865	0.868	0.851	0.848	0.894	0.728
0.740	0.880	0.877	0.894	0.912	0.911	6.683	0.917	0.923	0.912	0.900	0.944	0.799
0.812	0.933	0.924	0.924	0.947	0.950	7.318	0.944	0.953	0.953	0.932	0.966	0.845
0.859	0.957	0.954	0.960	0.972	0.965	7.953	0.969	0.975	0.972	0.966	0.978	0.885
0.900	0.969	0.969	0.972	0.981	0.981	8.588	0.981	0.987	0.984	0.981	0.990	0.917
0.941	0.990	0.987	0.990	0.993	0.993	9.858	0.993	0.993	0.993	0.993	0.996	0.962
0.975	0.996	0.996	0.996	0.996	0.996	11.128	0.996	0.996	0.996	0.996	1.000	0.981
0.990	1.000	1.000	1.000	1.000	1.000	12.398	1.000	1.000	1.000	1.000		0.993
0.996						13.669						0.996
1.000						14.939						1.000

Table (21) Measurements in the corner flow.
(x^1 = 0.343m)

1,374	1.370	1.378	1.378	1.374	1.374	U_∞ m/s	1.33	1.345	1.349	1.366	1.374	1.378
50.8	5.08	3.556	2.286	1.143	0.0	$-y^3$ mm / x^2 mm	0.0	1.143	2.286	3.556	5.08	50.8
		$u = v(1)/U_\infty$				y^3 mm			$u = v(1)/U_\infty$			
0.085	0.078	0.076	0.076	0.074	0.072	0.897	0.070	0.071	0.070	0.070	0.071	0.080
0.109	0.090	0.091	0.092	0.090	0.090	1.151	0.091	0.094	0.090	0.091	0.093	0.113
0.140	0.115	0,118	0.116	0.117	0.118	1.405	0.119	0.122	0.117	0.117	0.119	0.130
0.168	0.138	0.143	0.143	0.143	0.144	1.659	0.150	0.150	0.142	0.141	0.143	0.163
0.186	0.173	0.180	0.178	0.176	0.181	1.913	0.183	0.185	0.180	0.176	0.175	0.188
0.203	0.210	0.214	0.212	0.208	0.206	2.167	0.225	0.213	0.215	0.200	0.203	0.214
0.231	0.244	0.248	0.248	0.246	0.242	2.421	0.253	0.246	0.245	0.239	0.236	0.240
0.256	0.271	0.288	0.291	0.276	0.274	2.675	0.285	0.284	0.272	0.266	0.266	0.276
0.279	0.312	0.315	0.320	0.306	0.309	2.929	0.323	0.318	0.311	0.296	0.300	0.299
0.308	0.350	0.349	0.344	0.345	0.334	3.183	0.361	0.350	0.335	0.326	0.324	0.326
0.327	0.391	0.386	0.383	0.382	0.375	3.437	0.397	0.396	0.381	0.372	0.368	0.367
0.400	0.448	0.465	0.451	0.452	0.432	3.945	0.457	0.459	0.443	0.429	0.429	0.406
0.452	0.510	0.517	0.530	0.521	0.508	4.453	0.523	0.522	0.516	0.494	0.487	0.451
0.506	0.572	0.582	0.596	0.586	0.577	4.961	0.577	0.590	0.577	0.544	0.541	0.496
0.534	0.639	0.642	0.659	0.637	0.629	5.469	0.638	0.644	0.634	0.604	0.598	0.555
0.584	0.671	0.677	0.708	0.697	0.697	5.977	0.713	0.690	0.696	0.658	0.647	0.615
0.644	0.737	0.757	0.770	0.762	0.756	6.612	0.779	0.774	0.749	0.721	0.716	0.672
0.695	0.806	0.695	0.815	0.824	0.812	7.247	0.831	0.831	0.791	0.775	0.756	0.738
0.778	0.847	0.868	0.862	0.871	0.868	7.882	0.873	0.879	0.852	0.832	0.804	0.770
0.815	0.883	0.898	0.898	0.901	0.901	8.517	0.910	0.907	0.888	0.862	0.856	0.813
0.895	0.929	0.942	0.945	0.948	0.945	9.787	0.954	0.951	0.938	0.910	0.904	0.871
0.951	0.964	0.967	0.967	0.967	0.970	11.057	0.970	0.977	0.970	0.948	0.935	0.920
0.974	0.987	0.986	0.980	0.983	0.980	12.327	0.986	0.983	0.986	0.970	0.964	0.942
0.990	0.993	0.990	0.986	0.986	0.986	13.597	0.990	0.993	0.993	0.977	0.977	0.974
0.993	0.996	0.993	0.993	0.993	0.993	14.867	0.996	0.996	0.996	0.983	0.990	0.986
1.000	1.000	0.996	0.996	0.996	0.996	16.137	1.000	1.000	1.000	0.993	0.993	0.993
		1.000	1.000	1.000	1.000	17.407				0.996	0.996	1.000
						18.677				1.000	1.000	

Table (22) Measurements in the corner flow.

(x^1 = 0.512 m)

1.367	1.364	1.361	1.345	U_∞ m/s		1.343	1.352	1.357	1.366	1.374	1.357
50.8	5.08	3.175	0.0	$-y^3$ mm	y^3 mm	0.0	1.524	3.175	5.08	6.985	50.8
		$u = v(1)/U_\infty$		x^2 mm				$u = v(1)/U_\infty$			
0.091	0.069	0.073	0.065	0.896		0.064	0.068	0.069	0.066	0.064	0.089
0.112	0.100	0.120	0.067	1.404		0.065	0.097	0.102	0.097	0.094	0.108
0.140	0.136	0.142	0.091	1.912		0.085	0.130	0.138	0.133	0.131	0.137
0.172	0.185	0.190	0.132	2.420		0.130	0.205	0.187	0.180	0.175	0.170
0.244	0.220	0.234	0.192	2.928		0.185	0.258	0.231	0.216	0.219	0.241
0.265	0.277	0.311	0.244	3.436		0.243	0.312	0.308	0.274	0.258	0.263
0.314	0.321	0.340	0.295	3.944		0.294	0.371	0.337	0.318	0.304	0.312
0.345	0.369	0.395	0.363	4.452		0.360	0.409	0.391	0.366	0.333	0.342
0.384	0.422	0.435	0.414	4.960		0.412	0.463	0.431	0.417	0.395	0.382
0.437	0.457	0.499	0.458	5.468		0.455	0.505	0.495	0.454	0.418	0.434
0.475	0.493	0.545	0.521	5.976		0.518	0.549	0.541	0.490	0.471	0.473
0.502	0.534	0.585	0.573	6.484		0.570	0.586	0.580	0.531	0.526	0.499
0.530	0.576	0.632	0.618	6.992		0.615	0.632	0.629	0.572	0.556	0.528
0.561	0.606	0.670	0.674	7.500		0.671	0.692	0.665	0.604	0.589	0.560
0.599	0.659	0.710	0.716	8.008		0.713	0.717	0.707	0.656	0.642	0.596
0.672	0.703	0.738	0.748	8.516		0.744	0.745	0.735	0.700	0.656	0.669
0.698	0.724	0.768	0.779	9.151		0.774	0.809	0.764	0.718	0.691	0.694
0.726	0.752	0.821	0.833	9.786		0.829	0.826	0.818	0.749	0.734	0.722
0.759	0.786	0.842	0.862	10.421		0.860	0.856	0.838	0.783	0.762	0.756
0.812	0.820	0.870	0.881	11.056		0.878	0.885	0.867	0.816	0.814	0.810
0.870	0.882	0.900	0.919	12.326		0.916	0.917	0.896	0.879	0.847	0.867
0.899	0.911	0.931	0.940	13.596		0.937	0.947	0.926	0.908	0.885	0.896
0.929	0.939	0.953	0.963	14.866		0.959	0.956	0.950	0.935	0.920	0.926
0.965	0.974	0.971	0.977	16.136		0.974	0.965	0.968	0.971	0.944	0.962
0.997	0.984	0.992	0.994	17.406		0.990	0.978	0.978	0.981	0.968	0.993
1.000	0.996	0.999	0.996	18.676		0.993	0.990	0.987	0.993	0.990	1.000
	1.000	1.000	0.999	21.216		0.996	1.000	0.996	1.000	1.000	
			1.000	23.756		1.000		1.000			

Table (23) Measurements in the corner flow.

(x^1 = 0.805 m)

CHAPTER 5

CONCLUSIONS

The analysis of the flow along a radiused streamwise corner presented here offers a useful extension to the range of corner configurations so far treated theoretically. The new method contains the sharp corner solution as a special case. The treatment is confined to corners having a transverse cross-section which is invariant in the streamwise direction. The flow non-similarity which this implies is reflected in the solutions.

The algebraic decay previously known to exist in a sharp rectangular corner, has been shown to be present also in corners of all angles whether sharp or radiused. In the latter case the algebraic behaviour of the crossflow is dependent on the curvature distribution as well as on the angle. By contrast the asymptotic boundary conditions (at the potential region and at the side-edges) can be prescribed without reference to the curvature of the corner surface.

In the special case of a rectangular sharp corner, excellent agreement exists between the present solution and Ghia's solution [14, 15] which is arguably the best available.

For radiused corners no other solutions are known to the author with which to compare the present theory. However, confidence in the theory is encouraged by the agreement for the special case already noted and the smooth and systematic variation of the solution with curvature

between the two reliable extremes of flat plate and sharp corner.

The crossflow as viewed in transverse planes, is complex and in some cases streamwise closed vortices are evident.

A surprising feature of the solution is the marked differences in the results for two sharp corners when one of them has slightly curved walls in the vicinity of the symmetry plane. In the two cases dealt with, the external corner has small concave curvature on its walls and conversely for the internal corner.

Three independently obtained sets of experimental data have been used to test the theory. Two sets pertain to sharp corners and the experimental results obtained in the course of the present work are for a radiused corner. All of these show a similar relation to the corresponding theoretical solutions, the experimental streamwise velocities being significantly higher than predicted. The experimental results therefore, although qualitatively similar to theory, do not entirely vindicate the analysis. However there is some likelihood that the difficulty in realizing experimentally the model which the theory attempts to represent is to a large extent responsible for the differences. This emphasizes the need for further careful and extensive experimentations before drawing firm conclusions from the comparison. The shortage of experimental data is primarily due to the extremely tedious,time consuming nature of the work which so far has been done manually. What is required, and this has been pointed by previous workers, is an automatic

traversing and data collection and processing system. This would permit much more exhaustive traverses to be made with perhaps statistical treatment of the results to improve confidence.

There is no shortage of corner flow problems remaining to be dealt with. Of those amenable to treatment the most important are probably flows with non-zero pressure gradient and flows where compressibility is significant. It is suggested that such studies are conveniently pursued by the approach developed here.

APPENDIX A

On the asymptotic boundary conditions derived by Desai and Mangler [16]

To derive the correct asymptotic boundary conditions in the formulation by Desai and Mangler only the necessary details need be given. The governing equations of the corner boundary layer as derived by Desai and Mangler are

$$\Delta u - \varphi u_{,2} + (\gamma_{22,3} - \gamma_{23,2} - \psi) u_{,3} = 0 \qquad \text{(A1a)}$$

$$\Delta A - \varphi A_{,2} + (\gamma_{22,3} - \gamma_{23,2} - \psi) A_{,3} + (u J_0) A = j_{11,2} u u_{,3} - j_{11,3} u u_{,2} \qquad \text{(A1b)}$$

$$\varphi_{,2} + \psi_{,3} = -J_0 u \qquad \text{(A1c)}$$

$$\gamma_{33} \psi_{,2} - \gamma_{22} \varphi_{,3} + \gamma_{23} (\varphi_{,2} - \psi_{,3}) - (\gamma_{22,3} - \gamma_{23,2}) \varphi = J_0 A \qquad \text{(A1d)}$$

with

$$\Delta = \gamma_{33} \frac{\partial^2}{(\partial \xi^2)^2} - 2 \gamma_{23} \frac{\partial^2}{\partial \xi^2 \partial \xi^3} + \gamma_{22} \frac{\partial^2}{(\partial \xi^3)^2}$$

where $\gamma_{ij\,(i,j=1,2,3)}$ are functions of ξ^2 and ξ^3 only,

$$J_0 = \sqrt{j_{22} j_{33} - j_{23}^2} \qquad (j_{ij} = J_0 \gamma_{ij})$$

and a comma before a subscript i denotes differentiation with respect to ξ^i. The non-dimensional dependent variables are:

u streamwise velocity,

A a quantity related to the streamwise covariant component of vorticity,

φ, ψ quantities related to the contravariant velocity components in the ξ^2 and ξ^3 directions respectively.

The physical velocity components v(2) and v(3) along x^2 and x^3 are related to u, φ and ψ by

$$\left.\begin{aligned} v(2) &= \left[\sigma_1^2 u + \frac{\sigma_2^2}{J_o}\varphi\right] U_\infty \sqrt{\frac{\nu}{U_\infty x}} = v U_\infty \sqrt{\frac{\nu}{U_\infty x}} \\ v(3) &= \left[\sigma_1^3 u + \frac{\sigma_2^3}{J_o}\varphi + \frac{\sigma_3^2}{J_o}\psi\right] U_\infty \sqrt{\frac{\nu}{U_\infty x}} = w U_\infty \sqrt{\frac{\nu}{U_\infty x}} \end{aligned}\right\} \quad (A2)$$

where σ_i^j (i,j=1,2,3)are functions of ξ^2 and ξ^3 only. As remarked in Chapter 1 Desai and Mangler assumed that as $\xi^3 \longrightarrow \infty$, the crossflow velocity vector approaches a constant value to $O(R_e^{-\frac{1}{2}})$, whence

$$v_{,3} = 0 \text{ and } w_{,3} = 0$$

which from equations (A2) resulted in

$$\left.\begin{aligned} \varphi_{,3} &= \frac{J_{o,3}}{J_o} \\ \text{and} \quad \psi_{,3} &= -\tfrac{1}{2} J_o u - \frac{\sigma_{2,3}^3}{\sigma_3^3}\varphi \qquad \text{for } \xi^3 \longrightarrow \infty \end{aligned}\right\} \quad (A3)$$

according to their coordinate system, equation (1.2).

The correct boundary conditions may be obtained as follows. If $\bar{v}$ and $\bar{w}$ are the non-dimensional physical components of the velocity vector along the ξ^2 and ξ^3 coordinates and A is the streamwise vorticity, then the continuity equation and vorticity definition, in terms of Desai and Mangler's notation, are

$$-\tfrac{1}{2}(\xi^2 u_{,2} + \xi^3 u_{,3}) + (\sigma_3^3 \bar{v})_{,2} + (\sigma_2^2 \bar{w})_{,3} = 0 \quad (A4)$$

$$\left[\left(\frac{\sigma_2^3 \sigma_3^3}{\sigma_2^2}\right)\bar{v} + \sigma_3^3 \bar{w}\right]_{,2} - \left[\sigma_2^2 \bar{v} + \sigma_2^3 \bar{w}\right]_{,3} = J_o \bar{A} \quad (A5)$$

For $\xi^3 \longrightarrow \infty$; $u \sim 1$, $\bar{A} \sim 0$

$$\bar{v}_{,3} = 0 \quad , \quad \bar{w}_{,3} = 0$$

which when substituted in equation (A4) gives

$$(\sigma_3^3 \bar{v})_{,2} = 0 \text{ since } \sigma_2^2 = \text{const.}$$

i.e. $\lim_{\xi^3 \to \infty} (\sigma_3^3 \bar{v}) = \text{const.}$

From symmetry $\bar{v} = 0$ at $\xi^2 = 0$ and since $\sigma_3^3 \neq 0$ (or infinite) in the limit then

$$\lim_{\xi^3 \to \infty} \bar{v} = 0 \quad \text{for all } \xi^2 .$$

Similarly, from the continuity definition we have

$$\lim_{\xi^3 \to \infty} \left[\sigma_3^3 \bar{w}_{,2} + (\sigma_{3,2}^3 - \sigma_{2,3}^3) \bar{w} \right] = 0 \qquad \text{(A6)}$$

In Desai and Mangler's coordinate system $\sigma_{3,2}^3 - \sigma_{2,3}^3 = 0$, which from (A6) leads to

$$\lim_{\xi^3 \to \infty} \bar{w}_{,2} = 0$$

or

$$\lim_{\xi^3 \to \infty} \bar{w} = \text{const.} = \beta_0 \text{ say.}$$

It can be shown that these results are equivalent to

$$\left.\begin{aligned} v &= 0 \\ w &= \beta_\sigma \end{aligned}\right\} \quad \xi^3 \longrightarrow \infty \qquad \text{(A7)}$$

and when substituted in equation (A2) lead to the required boundary conditions on φ and ψ as $\xi^3 \longrightarrow \infty$,

$$\left.\begin{aligned} \varphi &= -\sigma_1^2\,\sigma_3^3 \\ \psi &= \sigma_2^2\,\beta_0 + (\sigma_2^3\sigma_1^2 - \sigma_1^3\sigma_2^2) \end{aligned}\right\} \xi^3 \longrightarrow \infty \qquad \text{(A8)}$$

The asymptotic boundary conditions as $\xi^2 \longrightarrow \infty$ for the flow variables can be obtained from the asymptotic series for large ξ^2 used by Desai and Mangler. (This series is similar to that used by Pal and Rubin [10]).

$$\left.\begin{aligned} u &= \sum_{n=0}^{\infty} (\xi^2)^{-n}\; u_n(\xi^3) \\ A &= \sum_{n=0}^{\infty} (\xi^2)^{-n+1}\; A_n(\xi^3) \\ \varphi &= \sum_{n=0}^{\infty} (\xi^2)^{-n+1}\; \varphi_n(\xi^3) \\ \psi &= \sum_{n=0}^{\infty} (\xi^2)^{-n}\; \psi_n(\xi^3) \qquad \text{for } \xi^2/\xi^3 > 1 . \end{aligned}\right\} \qquad \text{(A9)}$$

Upon substituting series (A9) in equations (A1) the following solutions were obtained for the zeroth-order equations

$$\left.\begin{aligned} u_0 &= \frac{1}{\cos^2\beta}\,B' \quad , \qquad \psi_0 = -\frac{1}{2}\,B \\ \varphi_0 &= -\frac{1}{2}\,B' \quad , \qquad A_0 = \frac{1}{2\cos^4\beta}\,B'' \end{aligned}\right\} \qquad \text{(A10)}$$

where $B(\xi^3)$ is the Blasius function and is governed by

$$2B''' + \cos^2\beta \;\; BB'' = 0$$

subject to boundary conditions

$$B(0) = B'(0) = 0$$

$$B'(\infty) \longrightarrow \cos^2\beta$$

the prime denoting differentiation with respect to ξ^3.

Consistent with boundary conditions (A3) (or (A8)), the first order equations for u_1 and ψ_1 with their boundary conditions, have the solution

$$u_1(\xi^3) = \psi_1(\xi^3) = 0$$

as was shown by Desai and Mangler.

So far the analysis by Desai and Mangler is perfectly sound. It is when the solution of φ_1 and A_1 is sought that the boundary conditions (A3) together with the assumption that $\xi^2 \longrightarrow \infty$ corresponds to x^2 large affect the solution adversely. In Desai and Mangler's development the equation for φ_1 is

$$\frac{1}{\cos^2\beta}\varphi_1''' + \frac{1}{2}B\varphi_1'' + B'\varphi_1' + \frac{1}{2}B''\varphi_1$$

$$+\frac{1}{2}\xi^3 B'B''\sin\beta\cos\beta + \tan\beta\ B''' = 0 \quad \text{(A11)}$$

and the associated boundary conditions are

$$\varphi_1(0) = \underline{\varphi_1'(0)} = 0 \quad , \quad \varphi_1'(\infty) \longrightarrow -\frac{1}{2}\xi^3\cos^2\beta\ u_o' = 0 \quad \text{(A12)}$$

In contrast, from equations (A8) and series (A9) the correct boundary conditions are

$$\varphi_1(0) = 0 \quad , \quad \underline{\varphi_1(\infty)} = \varphi_1'(\infty) = 0 \ . \quad \text{(A13)}$$

The difference between the two sets of boundary conditions lies in the underlined terms. The underlined term in equation (A12) incorporates the assumption of strictly two-dimensional flow at $\xi^2 \longrightarrow \infty$, whereas the underlined condition in (A13) implies three-dimensionality in the same region. The solution of equation (A11) with conditions (A13) is

$$\varphi_1 = \underline{-\frac{1}{2}\sin\beta\cos\beta\,(\xi^3 B' - B)} + \\ + \frac{1}{2} B'' \sin\beta\cos\beta \int_0^{\xi^3} \frac{t\cos^2\beta - 2\beta_0\cos\beta}{B''(t)}\,dt \quad \text{(A14)}$$

where β_0 is obtained from (A2) and the zeroth order solutions

$$\beta_0 = \lim_{\xi^3\to\infty} w = \frac{1}{2\cos\beta} \lim_{\xi^3\to\infty} (\xi^3 B' - B) \quad .$$

A similar result can be obtained for A_1 from the relation

$$A_1 = -\frac{1}{\cos^4\beta}\,\varphi_1'$$

The underlined term in equation (A14) is the result obtained by Desai and Mangler for φ_1 according to conditions (A12).

It can be shown by redefining the variables on the R.H.S. of equations (A14) to suit a rectangular cartesian coordinate system where ξ^3 is taken normal to the wall, that this result is essentially the same as that obtained by Pal and Rubin [10] for the corresponding variables (see Ch. 2, Section 2.6 for similar example). Equation (A14) however is more general in that it is derived for an arbitrary angle.

APPENDIX B

Solution of equation (2.49)

Equation (2.49) is

$$\frac{1}{c^{*2}}\psi_1''' + f\psi_1'' + 2f'\psi_1' + f''\psi_1 = 2\frac{s^*}{c^*}f''' + 2c^*s^*\xi^2 f'f'' \qquad (1B)$$

and the appropriate boundary conditions are

$$\xi^2 = 0 \quad ; \qquad \psi_1 = 0$$

$$\xi^2 \longrightarrow \infty ; \qquad \psi_1 = 0$$

The solution of equation (1B) can take a closed integral form. Integrating equation (1B) once, we get

$$\frac{1}{c^{*2}}\psi_1'' + f\psi_1' + f'\psi_1 = c^*s^*\, f'(\xi^2 f' - f) + \frac{s^*}{c^*}f'' + C_1 \qquad (2B)$$

where C_1 is an integration constant found by using the boundary conditions $\psi_1''(\infty) = \psi_1'(\infty) = \psi_1(\infty = 0$ to be

$$C_1 = -c^*s^*\beta \ .$$

On integrating again equation (2B) becomes

$$\frac{1}{c^{*2}}\psi_1' + f\psi_1 = c^*s^*(\xi^2 f' - f)f + \frac{s^*}{c^*}\xi^2 f'' - c^*s^*\beta\xi^2 + C_2 \qquad (3B)$$

where C_2 is another integration constant and is similarly found to be

$$C_2 = c^*s^*\beta^2 \ .$$

Carrying out the following steps

(i) replace f by $-\frac{1}{c^{*2}}\frac{f'''}{f''}$ (from equation (2.44))

in the L.H.S. of equation (3B),

(ii) divide throughout by f'',

(iii) integrate between the limits of 0 and ξ^2, and

(iv) use $\psi(0) = 0$

the result is

$$\psi_1 = -c^{*3} s^* \beta f'' \int_0^{\xi^2} \frac{\eta-\beta}{f''(\eta)} d\eta + s^* c^* (\xi^2 f' - f) . \qquad (4B)$$

With the Blasius function f being known ψ_1 is evaluated numerically by using Simpson's rule with a step-size of 0.02 in ξ^2.

APPENDIX C

Numerical Solution of Equations (2.66)

Equations (2.66) are suited to numerical solution by the finite difference Gauss-Seidel iterative method. The domain of integration is divided into square grids each of mesh size h (see Fig. 1). At interior mesh points second-order central difference approximations are used to express the derivatives of the dependent variables. For example, at the grid point (i,j) the derivatives of u are approximated by

$$\left(\frac{\partial u}{\partial \xi^2}\right)_{i,j} = \frac{1}{2h}\left(u_{i,j+1} - u_{i,j-1}\right)$$

$$\left(\frac{\partial u}{\partial \zeta}\right)_{i,j} = \frac{1}{2h}\left(u_{i+1,j} - u_{i-1,j}\right)$$

$$\left(\frac{\partial^2 u}{\partial \zeta \partial \xi^2}\right)_{i,j} = \frac{1}{4h^2}\left(u_{i+1,j+1} - u_{i+1,j-1} - u_{i-1,j+1} + u_{i-1,j-1}\right)$$

$$\left(\frac{\partial^2 u}{(\partial \xi^2)^2}\right)_{i,j} = \frac{1}{h^2}\left(u_{i,j+1} - 2u_{i,j} + u_{i,j-1}\right)$$

$$\left(\frac{\partial^2 u}{\partial \zeta^2}\right)_{i,j} = \frac{1}{h^2}\left(u_{i+1,j} - 2u_{i,j} + u_{i-1,j}\right)$$

The suffixes i and j index the ξ^3 and ξ^2 coordinates as shown in Fig. 1. Second order three-point end-difference approximations are used to express derivatives at the boundaries of the integration domain, e.g.

$$\left(\frac{\partial u}{\partial \xi^2}\right)_{i,j} = \frac{1}{2h}\left(4u_{i,j+1} - 3u_{i,j} - u_{i,j+2}\right)$$

$$\left(\frac{\partial u}{\partial \zeta}\right)_{i,j} = \frac{1}{2h}\left(4u_{i+1,j} - 3u_{i,j} - u_{i+2,j}\right)$$

In these (finite-difference) approximations a comma separating i and j does not denote differentiation. Using such

approximations equations (2.66) at interior grid point (i,j) become

$$\frac{2}{h^2}\left[(1+\zeta_1^2)\right]_{i,j} u_{i,j} = \frac{1}{h^2}(u_{i,j+1} + u_{i,j-1}) + \frac{\zeta_1^2}{h^2}(u_{i+1,j} + u_{i-1,j}) + \left[(c\varphi - \frac{\kappa}{c})u_{,2}\right]_{i,j} + \left[(cD + \frac{\kappa s}{c}\zeta_1)u_{,\zeta}\right]_{i,j} - 2\left[s\zeta_1 u_{,2\zeta}\right]_{i,j} \quad , \quad (1C)$$

$$\left[\frac{2}{h^2}(1+\zeta_1^2) + c^2(2 + \xi^3(\ln c)_{,3})\right]_{i,j} \times \theta^*_{i,j}$$

$$=$$

$$\frac{1}{h^2}(\theta^*_{i,j+1} + \theta^*_{i,j+1}) + \frac{\zeta_1^2}{h^2}(\theta^*_{i+1,j} + \theta^*_{i-1,j}) + \left[(c\varphi - \frac{\kappa}{c})\theta^*_{,2}\right]_{i,j} + \left[(cD + \frac{\kappa s}{c}\zeta_1)\theta^*_{,\zeta}\right]_{i,j} - 2\left[s\zeta_1 u_{,2\zeta}\right]_{i,j} + \left[2c\zeta_1(\xi^2 + s\xi^3 - (\xi^3)^2 s_{,3})u_{,\zeta} - 2c(s\xi^2 + \xi^3)u_{,2} - c\xi^3(s_{,3} + \xi^3 s_{,33})u + c\kappa\xi^3(\zeta_1\psi^*_{,\zeta} - \varphi_{,2}) + c(\kappa + \xi^3\psi^*_{,3}) + cE\right]_{i,j} \times u_{i,j} + \left[\frac{c}{c^*}f''\psi^* + c(\frac{1}{c^*}\xi^3 f''' - \xi^3\kappa u_{,2})\varphi + cFu_{,\zeta} + \frac{1}{c}\xi^3\kappa(\zeta_1^2 u_{,\zeta\zeta} - u_{,22}) + cG\right]_{i,j} \quad , \quad (2C)$$

$$\left[\frac{2}{h^2}(1+\zeta_1^2) + (\frac{c_{,3}}{c})_{,3}\right]_{i,j} \times \varphi_{i,j}$$

$$=$$

$$\frac{1}{h^2}(\varphi_{i,j+1} + \varphi_{i,j-1}) + \frac{\zeta_1^2}{h^2}(\varphi_{i+1,j} + \varphi_{i-1,j}) - \left[s\zeta_1\varphi_{,2\zeta} + s_{,3}\varphi_{,2} + (\frac{c_{,3}}{c}\zeta_1 + \zeta_2)\varphi_{,\zeta} + \zeta_1(\frac{sc_{,3}}{c} - 2s_{,3})\psi^*_{,\zeta} + (\frac{sc_{,3}}{c} - 2s_{,3})_{,3}\psi^* + (2c + \xi^3 c_{,3})u_{,2} + (cs_{,3} + \xi^3(cs_{,3})_{,3})u - c^2\zeta_1\theta^*_{,\zeta} - 2cc_{,3}\theta^* + D^*\right]_{i,j} \quad , \quad (3C)$$

$$\frac{2}{h^2}\left[(1+\zeta_1^2)\right]_{i,j}\ \psi^*_{i,j} = \frac{1}{h^2}(\psi^*_{i,j+1}+\psi^*_{i,j-1}) + \frac{\zeta_1^2}{h^2}(\psi^*_{i+1,j} +$$

$$+\ \psi^*_{i-1,j}) + \Big[s\,\varphi_{,22} + \left(\frac{c_{,3}}{c}\right)\varphi_{,2} - s\,\zeta_1\,\psi^*_{,2\zeta} -$$

$$-\left(s_{,3} - 2\frac{c_{,3}}{c}\right)\psi^*_{,2} + c\,s_{,3}\,\xi^3 u_{,2} - \zeta_1(2c+\xi^3 c_{,3})\,u_{,\zeta} -$$

$$- \quad c^2\theta^*_{,2} + \zeta_2\,\psi^*_{,\zeta} - (3c_{,3} +$$

$$+\ \xi^3 c_{,33})u + E^*\Big]_{i,j} \quad . \qquad (4C)$$

In equations (1C) - (4C) all quantities in square brackets are evaluated at the grid point (i,j).

The dependent variables are evaluated at the boundaries of the integration domain by using the boundary conditions, equations (2.67), as follows:

(i) <u>Conditions on the wall, j=1 (ξ^2 =0)</u>:

$$u_{i,1} = \varphi_{i,1} = \psi^*_{i,1} = 0 \qquad i=1,2,-\ldots,M-1$$

$$\theta^*_{i,1} = \frac{1}{2h^2c^2}(4\psi^*_{i,2} - \psi^*_{i,3}) + \left[\xi^3\left(\frac{c^*}{c^2} - \frac{1}{c^*}\right)\right]_{i,1} f''(0)\,.$$

(ii) <u>Conditions on the symmetry plane, i=1 (ζ =0)</u>:

a) <u>Conditions for a sharp corner, Fig. (2.2b)</u>:

$$u_{1,j} = \frac{1}{3}(4u_{2,j} - u_{3,j}) - \frac{s}{3\zeta_1}(u_{1,j+1} - u_{1,j-1})\ ,$$

$$\theta^*_{1,j} = 0\ ,$$

$$\varphi_{1,j} = \frac{1}{3}(4\varphi_{2,j} - \varphi_{3,j}) - \frac{s}{3\zeta_1}(\varphi_{1,j+1} + \varphi_{1,j-1}) + \frac{2}{3}\,s\,\mathrm{sch}\,u_{1,j}\ ,$$

$$\psi^*_{1,j} = 0\ .$$

b) Conditions for a radiused corner:

The boundary conditions for u and φ at $\zeta = 0$ are strictly

$$u_{,\zeta} = \varphi_{,\zeta} = 0 \quad .$$

When used in their finite-difference form, these conditions were found to influence the solution upon changing the values of the constants a and b, equation (2.64), to an undesirable extent. Consequently the full equations of u and φ are used after applying these conditions directly and found to lead to satisfactory results. At the plane of symmetry equations (1C) and (3C) after applying the symmetry conditions, become

$$\frac{2}{h^2}\left[1+\zeta_1^2\right]_{1,j}\ u_{1,j} = \frac{1}{h^2}(u_{1,j+1} + u_{1,j-1}) + \frac{2\zeta_1^2}{h^2} u_{2,j} + \left[(c\varphi - \frac{\rho}{c})\, u_{,2}\right]_{1,j} \quad ,$$

$$\left[\frac{2}{h^2}(1+\zeta_1^2) + (\frac{c_{,3}}{c})\right]_{1,j}\ \varphi_{1,j} = \frac{1}{h^2}(u_{1,j+1} + u_{1,j-1}) + \frac{2\zeta_1^2}{h^2}\varphi_{2,j} - \left[s_{,3}\varphi_{,2} - 2\zeta_1 s_{,3}\psi^*_{,\zeta} + 2c\,u_{,2} + c\,s_{,3}\,u - c^2\zeta_1\,\theta^*_{,\zeta} + D^*\right]_{1,j} \quad .$$

with $(\frac{\partial\theta^*}{\partial\zeta})_{1,j}$ and $(\frac{\partial\psi^*}{\partial\zeta})_{1,j}$ becoming

$$(\frac{\partial\theta^*}{\partial\zeta})_{1,j} = \frac{1}{h}\theta^*_{2,j} \quad , \quad (\frac{\partial\psi^*}{\partial\zeta})_{1,j} = \frac{1}{h}\psi^*_{2,j} \quad .$$

The boundary conditions on θ^* and ψ^* at $\zeta = 0$ are as before, i.e.

$$\theta^*_{1,j} = \psi^*_{1,j} = 0 \quad .$$

c) Conditions for the example shown in Fig. (2.2a)

$$u_{1,j} = \frac{1}{3}\,(4u_{2,j} - u_{3,j}) - \frac{s}{\zeta_1}(u_{1,j+1} - u_{1,j-1}) \quad ,$$

$$\theta^*_{1,j} = 0 \quad ,$$

$$\varphi^*_{1,j} = \frac{\zeta_1(4\varphi_{2,j} - \varphi_{3,j}) - s(\varphi_{1,j+1} - \varphi_{1,j-1}) + 2h\,sc\,u_{1,j}}{\left[3\zeta_1 + 2h\,\frac{c_{,3}}{c}\right]_{1,j}} \quad ,$$

$$\psi^*_{1,j} = 0 \quad .$$

(iii) Conditions in the potential region, j=N

$$u_{i,N} = 1 \quad ,$$

$$\theta^*_{i,N} = 0 \quad ,$$

$$\varphi_{i,N} = [\,c\,(\xi^2 - \beta)]_{i,N} \quad ,$$

$$\psi^*_{i,N} = [\xi^3(c - c^*)]_{i,N} \quad .$$

(iv) Conditions at the side-edge of the corner layer, i=M

$$u_{M,j} = f'(\xi^2) \quad ,$$

$$\theta^*_{M,j} = -c^* s^* \beta \left[f''(\xi^2) \int_0^{\xi^2} \frac{\eta-\beta}{f''(\eta)}\,d\eta + (\xi^2-\beta)\right] + \frac{s^*}{c^*}\,\xi^2 f''(\xi^2) \quad ,$$

$$\varphi_{M,j} = c^* f(\xi^2) \quad ,$$

$$\psi^*_{M,j} = -c^{*3} s^* \beta\, f''(\xi^2) \int_0^{\xi^2} \frac{\eta-\beta}{f''(\eta)}\,d\eta + s^* c^* (\xi^2 f'(\xi^2) - f(\xi^2)) \, .$$

The iteration process commences with the following initial guess for u, θ^*, φ and ψ^* which satisfies all boundary conditions,

$$u_{i,j} = u_{M,j} \quad ,$$

$$\theta^*_{i,j} = \left(\frac{i-1}{M-1}\right) \times \theta^*_{M,j} \quad ,$$

$$\varphi_{i,j} = \varphi_{M,j} \quad ,$$

$$\psi^*_{i,j} = \left(\frac{i-1}{M-1}\right) \times \psi^*_{M,j} \quad .$$

After each iteration, the new value of any of the dependent variables is relaxed according to

$$X^{n}_{i,j} = \omega X^{n}_{i,j} + (1-\omega) X^{n-1}_{i,j}$$

where X represents u, θ^*, φ or ψ^*. ω is the relaxation factor and n is the number of iterations. The solution is considered to be satisfactory when the following condition was attained

$$\left| X^{n}_{i,j} - X^{n-1}_{i,j} \right| < 0.0005$$

for all the dependent variables at every grid point in the integration domain.

The choice of the size of the integration domain and the values of a and the step size are given for each corner configuration in Chapter 4.

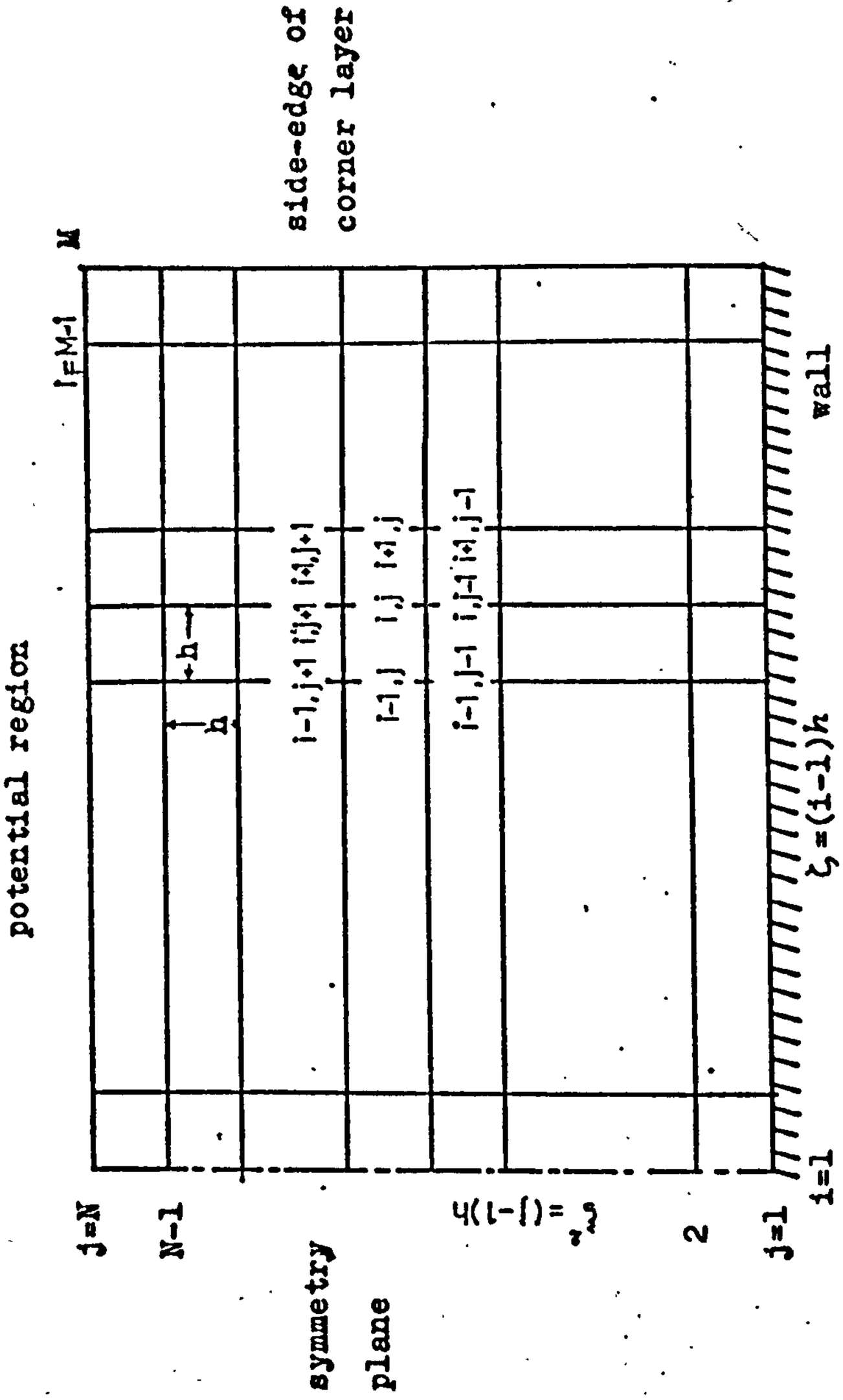

Fig. 1. Integration domain.

REFERENCES

1. Oman, R. 'The three-dimensional laminar layer along a corner'. Ph.D. Thesis, 1959, Dept. of Mechanical Engineering, M.I.T.

2. Zamir, M. 'Boundary layer flow in a streamwise corner'. Ph.D. Thesis, University of London, 1968.

3. Barclay, W. H. 'Laminar flow in a streamwise corner'. Ph.D. Thesis, 1971. University of London.

4. El-Gamal, H. 'Laminar flow along a corner with boundary layer suction'. Ph.D. Thesis, 1977, University of London.

5. Loitsianskii, L. G. 'Interference of boundary layers' - Central Aero-Hydrodynamical Institute. Moscow. Report No. 249, English translation: ARC Report 3186-FM 342.

6. Loitsianskii, L. G. & Bolshakov, V. P. 'On motion of fluid in boundary layer near line of intersection of two planes'. NACA TM 1308, 1951. (Translated from CAHI, Rep. No. 279, 1936, pp. 3-18).

7. Carrier, G. F. 'The boundary layer in a corner'. Quart. Appl. Math., Vol. 4, No. 4, 1947, pp. 367-370.

8. Dowdell, R. B. 'Incompressible boundary layer flow along interior corners'. 10th Midwestern Conference on Mechanics, 1967, pp. 1355-1378.

9. Rubin, S. G. 'Incompressible flow along a corner'. J. Fluid Mech., Vol. 26, Pt. 1, 1966, pp. 97-110.

10. Pal, A. & Rubin, S. G. 'Asymptotic features of viscous flow along a corner'. Quart. Appl. Math., Vol. 29, 1971, pp. 91-108.

11. Rubin, S. G. & Grossman, B. 'Viscous flow along a corner: Part II. Numerical solution of corner layer equations'. Quart. Appl. Math., Vol. 29, 1971, pp. 169-186.

12. Stewartson, K. 'Viscous flow past a quarter-infinite plate'. J. Aero. Sci., Vol. 28, pp. 1-9, 1961.

13. Pearson, J. R. A. 'Homogeneous turbulence and laminar viscous flow'. Ph.D. Thesis, 1957, Cambridge University.

14. Ghia, K. N. 'Incompressible streamwise flow along an unbounded corner'. AIAA Journal, Vol. 13, No. 7, 1975, pp. 902-907.

15. Ghia, K. N. Private communication, 1977.

16. Desai, S. S. & Mangler, K. W. 'Incompressible laminar boundary layer flow along a corner formed by two intersecting planes'. RAE. Tech. Rep. 74062, 1974, pp. 1-99.

17. Zamir, M. 'Boundary-layer theory and the flow in a streamwise corner'. The Aero. J. of the Royal Aero. Soc., Vol. 74, 1970, pp. 330-332.

18. Zamir, M. 'On the corner boundary layer with favourable pressure gradient'. Aero. Quart., Vol. 23, Pt. 2, 1972, pp. 161-168.

19. Zamir, M. 'Further solution of the corner boundary layer equations'. Aero. Quart., Vol. 24, Pt. 3, 1973, pp. 219-226.

20. Tokuda, N. 'Viscous flow near a corner in three dimensions'. J. Fluid Mech., Vol. 53, Pt. 1, 1972, pp. 129-148.

21. Zamir, M. & Young, A. D. 'Experimental investigation of the boundary layer in a streamwise corner'. Aero. Quart., Vol. 21, Pt. 4, 1970, pp. 313-339.

22. Weinberg, B. C. 'Compressible corner flow'. Ph.D. Thesis, Polytechnic Institute of Brooklyn, 1972.

23. Aris, R. 'Vectors, tensors and the basic equations of fluid Mechanics'. Prentice-Hall, London, 1962.

24. Rosenhead, L. (Editor) 'Laminar boundary layers' Clarendon Press, Oxford, 1963.

25. Stewartson, K. & Howarth, L. 'On the flow past a quarter infinite plate using Oseen's equations'. J. Fluid Mech., Vol. 7, Pt. 1, pp. 1-9, 1960.

26. Sills, J. A. 'Transformations for infinite Regions and their applications to flow problems'. AIAA Journal, Vol. 7, Jan. 1969, pp. 117-123.

27. Majola, O. O. 'Turbulent boundary layer along a streamwise corner'. Ph.D. Thesis, 1972, University of London.

28. Collis, D. C. & Williams, M. J. 'Two-dimensional convection from heated wires at low Reynolds numbers'. J. Fluid Mech., Vol. 6, 1959, pp. 357-384.

29. King, L. V. 'On the convection of heat from small cylinders in a stream of fluid'. Phil. Trans. Roy. Soc. A 214, 1914, p. 373.

30. Goldstein, S. (Editor) 'Modern developments in fluid dynamics', Vol. 1. Dover Publications, New York, 1965. (First published by Clarendon Press, Oxford, in 1938).

31. Barclay, W. H. 'Experimental investigation of the laminar flow along a straight 135° corner'. Aero. Quart., Vol. 24, Pt. 2, 1973, pp. 147-154.

32. Stewartson, K. & Williams, P. G. 'Self-induced separation'. Proc. Roy. Soc. A. 312, 1969, 181-206.

33. Schlichting, H. 'Boundary layer theory', 6th ed. McGraw Hill, New York, 1968.

34. Smith, G. D. 'Numerical solution of partial differential equations'. Oxford mathematical handbooks, Oxford University Press, 1971.